



PHD

**Integration of Advanced Techniques for The Optimisation of Energy Consumption and The Mitigation of Urban Heat Island
(Alternative Format Thesis)**

Ibrahim, Yasser

Award date:
2022

Awarding institution:
University of Bath

[Link to publication](#)

Alternative formats

If you require this document in an alternative format, please contact:
openaccess@bath.ac.uk

Copyright of this thesis rests with the author. Access is subject to the above licence, if given. If no licence is specified above, original content in this thesis is licensed under the terms of the Creative Commons Attribution-NonCommercial 4.0 International (CC BY-NC-ND 4.0) Licence (<https://creativecommons.org/licenses/by-nc-nd/4.0/>). Any third-party copyright material present remains the property of its respective owner(s) and is licensed under its existing terms.

Take down policy

If you consider content within Bath's Research Portal to be in breach of UK law, please contact: openaccess@bath.ac.uk with the details. Your claim will be investigated and, where appropriate, the item will be removed from public view as soon as possible.



Integration of Advanced Techniques for The Optimisation of Energy Consumption and The Mitigation of Urban Heat Island

Yasser Mahmoud Mohammed Ibrahim

A thesis submitted for the degree of Doctor of Philosophy

University of Bath

Faculty of Engineering & Design

Department of Architecture and Civil Engineering

Centre for Energy and the Design of Environments (EDEn)

September 2022

Supervisors

Dr Tristan Kershaw

University of Bath

Dr Paul Shepherd

University of Bath

Thesis Examiners

Prof Rohinton Emmanuel

Glasgow Caledonian University

Dr Sukumar Natarajan

University of Bath

Copyright

Attention is drawn to the fact that copyright of this thesis rests with the author and copyright of any previously published materials included may rest with third parties. A copy of this thesis has been supplied on condition that anyone who consults it understands that they must not copy it or use material from it except as licenced, permitted by law or with the consent of the author or other copyright owners, as applicable.

Author Declaration

I am the author of this thesis, and the material presented here for examination for the award of a higher degree by research has not been incorporated into a submission for another degree.

Abstract

Current global urbanisation rates highlight the need to reconsider our design practices to minimise the negative impacts of our built environments on natural resources and the health and well-being of urban residents. The debate on the sustainability of urban form started decades ago, underpinned by a set of environmental criteria, delineating the path for policy development to find the optimum balance between urban density and the thermal and energy performance. In developing countries, despite their anticipated share of global urban population, this balance is far from being realised. In Egypt, where massive construction projects are being carried out, the vulnerability of urban residents is mostly recognised by the gap between a drastic urban growth and its reflection on the local construction policies, which pay very little attention to the environmental implications of building new conurbations.

This thesis fills this gap by presenting quantitative scientific evidence on the relationship between urban form and both thermal comfort and energy performance in buildings, in Cairo, Egypt. In doing so, the thesis introduces a simulation workflow within the parametric design interface, Grasshopper for Rhino3D, to investigate the impact of various urban geometry configurations on different environmental performance criteria, studied within three key milestones. The performance criteria are outdoor thermal comfort, represented by the Universal Thermal Climate Index (UTCI), and the total energy loads in buildings. First, 7716 urban street canyon configurations are studied through varying their design parameters in three consecutive phases, to maximise outdoor thermal comfort. Simulations includes changing 12 heights of canyon's flanks simultaneously and separately, 11 street widths, and 12 different orientations of the street canyon. The results reveal new correlations between the design parameters and thermal comfort, showing the ability to reduce thermal stress beyond the design thresholds of local construction codes, which reaches up to 6° C, thus highlighting the need for climate-sensitive design regulations.

Second, 3430 typological and morphological design configurations are investigated on an urban block scale through varying their design parameters, to find the best typology and its associated density parameters which maximise outdoor thermal comfort and minimise energy loads.

Simulations includes changing 10 building heights, 7 different orientation of the urban block, and 7 street widths in each direction (NS and EW). The results show that compact and medium density urban configurations correspond to the best trade-off between the performance criteria, also indicating a relative outperformance of the courtyard typology.

Finally, the environmental performance of the courtyard block typology is revisited to investigate the potential improvements in outdoor thermal comfort and energy loads by changing the heights of individual buildings. Simulation included varying 3 street widths, 4 different orientations of the courtyard blocks, and 3 heights for each building within a single courtyard block. The results show that courtyard blocks perform best when they have minimum interspaces, orientated NE-SW or NW-SE, where their northern and southern buildings are relatively higher than the eastern and western buildings. The results also shows that vertically heterogeneous configurations have the potential to improve both performance criteria, as compared to conventional courtyard blocks, highlighting the need for deliberate passive solar design, as well as the need to bring vernacular design traditions back into practice.

The findings of this thesis can help shift the current design practices in Egypt towards achieving a climate-responsive urban form, in line with ambitious national goals - Egypt's Vision 2030. The thesis contributes to the scientific knowledge through defining design guidelines for urban built forms in extreme and typical hot-arid climate conditions, considering outdoor thermal comfort and energy loads, which are significantly correlated to the urban heat island mitigation. Also, the thesis contributes a methodology for modelling and simulating different performance criteria, which could be replicated in other climate contexts. Moreover, the implications drawn from this thesis pave the way for future studies on the passive solar design in hot-arid regions, and thus, this thesis serves as a future reference for both educational and research studies.

Acknowledgements

All praise to Allah, Lord of the World.

First and foremost, I would like to express my gratitude for my supervisor, Dr Tristan Kershaw for his consistent support, friendly guidance, and patience throughout my PhD journey. Under his supervision, I have learnt many lessons that extended from developing my research concepts to improving my writing skills.

My deepest gratitude also goes to my co-supervisor, Dr Paul Shepherd who introduced me to the field of parametric design, directed my enthusiasm to the right path, and astutely advised me on how to handle my research obstacles. Also, his influential contributions to writing up my research publications and my thesis are more than appreciated.

I would also like to express my sincere appreciation for the thesis examiners, Professor Rohinton Emmanuel, and Dr Sukumar Natarajan for their constructive feedback which is key for the completion of this work.

Big thanks are addressed to my local advisor, Dr Hesham Elkady for his administrative support and patience, and to Ibrahim Elwy in the Egypt-Japan University of Science and Technology, with whom I had meaningful discussions and consultations.

Thanks to all my colleagues at the Department, in 6-East and the Research Hub in 4-East South. Special thanks to Petros Ampatzidis for being a true friend, whose support during the hardest times of the COVID-19 lockdown is more than appreciated.

Finally, and most importantly, I am endlessly in debt to my parents who showed their unconditional moral and mental support throughout my journey; this thesis is dedicated to you. I am sincerely grateful to my brothers and sisters whose support in Egypt crossed the 'borders' and gave me company in the UK.

Yasser Ibrahim

September 2022

Contents

Abstract.....	IV
Acknowledgements	VII
Contents	IX
List of Figures.....	XI
List of Tables.....	XV
Abbreviations.....	XVI
Nomenclature.....	XIX
Dissemination.....	XX
1 Introduction	1
1.1 Global concerns and the need for sustainable urban development.....	1
1.2 Urban form: Analyses, approaches and recent advancements.....	9
1.3 The Egyptian context Urban and environmental insights.....	16
1.4 Motivation.....	22
1.5 Hypothesis, aims and objectives.....	22
1.6 Thesis outline	24
2 Literature review Climate and the Built Environment.....	28
2.1 Preface.....	28
2.2 Climate structures.....	29
2.3 Urban energy balance.....	30
2.4 Urban heat island	33
2.5 Thermal comfort.....	44
2.6 Urban climate modelling.....	52
2.7 Epilogue.....	56
3 Methodology	58
3.1 Preface.....	58
3.2 Experimental Approach.....	59
3.3 Grasshopper	62
3.4 Methods Ladybug-tools.....	62
3.5 Model verification	64
3.6 Model improvement.....	77
3.7 Model validation	85
3.8 References	86
3.9 Epilogue.....	88
4 Thermal Comfort Optimisation of Urban Canyon Geometries	90
4.1 Preface.....	90
4.2 Abstract	93
4.3 Introduction.....	93
4.4 Methodology	100
4.5 Results and discussion	111
4.6 Implications for urban design.....	123

4.7	Study limitations.....	126
4.8	Conclusion.....	127
4.9	References.....	128
4.10	Addendum.....	134
4.11	Epilogue.....	136
5	Urban Scale Multi-Objective Optimisation.....	138
5.1	Preface.....	138
5.2	Abstract.....	143
5.3	Introduction.....	143
5.4	Methodology.....	152
5.5	Results and Discussion.....	158
5.6	Selective Cases and Urban Design Implications.....	165
5.7	Conclusions.....	168
5.8	References.....	171
5.9	Epilogue.....	178
6	Courtyard Blocks Algorithmic Optimisation.....	180
6.1	Preface.....	180
6.2	Abstract.....	185
6.3	Introduction.....	185
6.4	Methodology.....	189
6.5	Results.....	197
6.6	Discussion.....	205
6.7	Conclusion.....	212
6.8	References.....	215
6.9	Addendum.....	220
6.10	Epilogue.....	221
7	Conclusions.....	223
7.1	Research findings.....	224
7.2	Interpretation of the findings: answers to research questions.....	226
7.3	Bringing all together.....	228
7.4	Contribution to knowledge.....	229
7.5	Research limitations.....	231
7.6	Future work.....	232
7.7	Concluding remarks.....	234
	References.....	235

List of Figures

Figure 1.1: Estimated and projected urban populations from 1950 to 2050.....	2
Figure 1.2: The 17 Sustainable Development Goals (SDGs).....	3
Figure 1.3: Howard's Garden City as a diagram (left), and Perry's Neighbourhood Unit (right).....	5
Figure 1.4: Plan Voisin by Le Corbusier in 1925	6
Figure 1.5: The Cornell New Urbanist community designed by Duany Plater-Zyberk.....	6
Figure 1.6: Siemens technology, Masdar City, UAE.....	8
Figure 1.7: Wikalat Al-Ghuri (Commercial caravanserai), originally built in 1504.....	10
Figure 1.8: General layout of New Gournia Village, Luxor, Egypt	10
Figure 1.9: Urban canyon proportions (left), Sky view factor for a point P (middle).....	11
Figure 1.10: Most common urban-scale design parameters.	12
Figure 1.11: Radiant temperature thermal map based on satellite-derived morphology	13
Figure 1.12: London's annual domestic heat density map as produced by the UEIB	14
Figure 1.13: Evolution of a block typology (K) by varying plot subdivision	15
Figure 1.14: Three building typologies studied and optimised	15
Figure 1.15: Thermal comfort-optimised building heights.....	15
Figure 1.16: Köppen-Geiger climate map, and Egypt's eight climatic zones.....	17
Figure 1.17: 1540's Amna bint Salim house.....	19
Figure 1.18: 1983 master plan of Cairo.....	19
Figure 1.19: General structure of the thesis.	26
Figure 2.1: PBL vertical structure within (a) mesoscale, (b) local scale, and (c) microscale.....	30
Figure 2.2: Surface energy balance during (a) daytime, and (b) night-time.....	32
Figure 2.3: Urban heat island causes	35
Figure 2.4: Heat exchange between a tree and urban form	42
Figure 2.5: Heat exchanges of the human body	47
Figure 2.6: Projected area exposed (A_p) as a function of solar altitude and azimuth	47
Figure 2.7: Components of MRT in an urban environment.....	49
Figure 2.8: The thermo-physiological model.....	50
Figure 3.1: General methodological approach used throughout the thesis.	61
Figure 3.2: Geometry configurations for the three layouts.....	69
Figure 3.3: 3D presentation for the three layouts (Exported from Rhino viewport).....	69
Figure 3.4: MRT comparison within the three layouts.....	73
Figure 3.5: Average UTCI comparison within the three layouts.....	74
Figure 3.6: UTCI thermal maps for each layout at 7 am, 12 pm and 5 pm.....	74
Figure 3.7: Model geometry and receptors of interest	79

Figure 3.8: MRT results at different receptors for the four scenarios.	81
Figure 3.9: Scatter plots for the average MRT values over the whole layout.....	84
Figure 3.10: Average UTCI for Cairo on 7 th June.....	84
Figure 4.1: Concept of the UTCI equivalent temperature	98
Figure 4.2: Schematic diagram showing the data streaming	104
Figure 4.3: Results for the average of all grid points	105
Figure 4.4: Site of measurements as shown (a) in Google Earth, (b) in the Rhino scene.....	105
Figure 4.5: Scattered plots showing the relationship between the measured parameters	107
Figure 4.6: Relationships between measured and simulated MRT.....	108
Figure 4.7: 3D view of the urban canyon simulated.....	110
Figure 4.8: Meteorological data in Cairo, on June 7 th	111
Figure 4.9: Coloured meshes showing the height-to-width based UTCI.....	113
Figure 4.10: H/W matrix as a product of all building heights and street widths in phase 1.	114
Figure 4.11: scattered plots for the correlation between UTCI and H/W	115
Figure 4.12: Clustered columns showing the relationship between building heights	117
Figure 4.13: Clustered columns showing the average UTCI for 6 heights of flank A.....	121
Figure 4.14: Scattered plots showing the correlation between UTCI	122
Figure 4.15: UTCI rose.....	125
Figure 4.16: Satellite images of a neighbourhood in Fez, Morocco.....	127
Figure 4.17: Cairo's hourly dry bulb temperatures as extracted from the IWEC file.....	134
Figure 4.18: MRT and UTCI absolute error	135
Figure 5.1: Generic urban forms (top), and their adapted version (bottom).....	140
Figure 5.2: Courtyard typology in Helwan University dorms (Google Earth).	140
Figure 5.3: Linear (left) and scattered (right) typologies in Alwafa' Wal Amal precinct.....	140
Figure 5.4: Three archetypes exemplified in this study	153
Figure 5.5: Simulation workflow showing the streaming of data	155
Figure 5.6: Average hourly air temperatures and direct normal radiation.....	158
Figure 5.7: Frequency distribution of (a) Av.UTCI, (b) max UTCI, (c) EUI.....	160
Figure 5.8: Performance evaluation of the three typologies in different orientations.....	161
Figure 5.9: Distances between buildings/blocks on the East-West axis.....	162
Figure 5.10: Trendlines of heights-based performance for the three typologies.....	163
Figure 5.11: Relationship between FAR and (a) Av.UTCI, and (b) EUI.....	164
Figure 5.12: Relationship between FAR, BCR and performance indicators	165
Figure 5.13: Parallel coordinates showing the selective cases for the minimum Av.UTCI.....	166
Figure 5.14: Parallel coordinates showing the selective cases for the minimum EUI.....	167
Figure 5.15: Selective cases for moderate heat stress Av.UTCI and the lowest 40% EUI.	168

Figure 6.1: Residential units under the solar envelope	181
Figure 6.2: The RSB Envelope applied in a Mediterranean Climate	181
Figure 6.3: Illustration of the basic fitness assignment.....	183
Figure 6.4: Types of courtyards investigated in this study.....	191
Figure 6.5: Graphical Abstract showing the simulation workflow	194
Figure 6.6: Cairo's weather data in the typical hot week (5 th - 11 th June).....	195
Figure 6.7: Solutions on the objective space for each courtyard type.....	197
Figure 6.8: Distribution of the Pareto front solutions	198
Figure 6.9: Frequency distribution of (a) interspaces, and (b) orientation	200
Figure 6.10: Performance of different courtyard types in different orientations	201
Figure 6.11: Performance of different courtyard types in different orientations	201
Figure 6.12: Frequency distribution of building heights in each direction of the courtyard.....	202
Figure 6.13: Frequency distribution of building heights in each direction of the courtyard.....	203
Figure 6.14: Frequency distribution of building heights in each direction of the courtyard.....	204
Figure 6.15: The best 12 cases of type A	206
Figure 6.16: The best 12 cases of type B.....	207
Figure 6.17: The best 12 cases of type C	208
Figure 6.18: Solar radiation analysis of (left) a selected case of type B.....	210
Figure 6.19: Range of building heights of the best 12 cases	210
Figure 6.20: Performance of different courtyard types in different orientations	220
Figure 7.1: Recommendations for using courtyard block types.....	229
Figure 7.2: Surface radiation analysis of nine design alternatives	233

List of Tables

Table 1.1: the 10 built-up Local Climate Zones (LCZ's).....	13
Table 2.1: Main characteristics and thermal scale of selected thermal comfort indices	52
Table 2.2: Capabilities of tools for evaluating the microclimate.....	55
Table 3.1: Declaration of authorship.....	65
Table 3.2: Construction materials input for both models.....	70
Table 3.3: Error calculations for MRT and UTCI.....	72
Table 3.4: Goodness of fit according to Guideline 14 (ASHRAE, 2014).....	77
Table 3.5: RMSE and R ² for the ladybug original and new models compared to ENVI-met.....	83
Table 3.6: Goodness of fit, in Cairo 7 th June scenario	85
Table 4.1: Declaration of authorship.....	92
Table 4.2: Thresholds and steps of the parameters simulated in all phases.....	102
Table 4.3: The parameters measured by the sensors and their corresponding range	106
Table 4.4: Physical and thermal properties of construction materials.....	109
Table 4.5: Upper and lower bounds for geometry parameters	115
Table 4.6: Minimum and maximum UTCI for orientations 0-30°.....	118
Table 4.7: Minimum and maximum UTCI for orientations 45-75°.....	119
Table 4.8: Minimum and maximum UTCI for orientations 90-120°.....	119
Table 4.9: Minimum and maximum UTCI for orientations 135-165°.....	120
Table 4.10: Minimum H/W thresholds for achieving the UTCI reduction benchmarks.....	123
Table 5.1: Declaration of Authorship.....	142
Table 5.2: Minimum, maximum and step size of each dynamic parameter simulated.....	153
Table 5.3: Fixed simulation parameters used in the study.....	157
Table 5.4: Correlation coefficients (R) between design parameters and performance criteria	160
Table 5.5: Correlation coefficients (R) between density parameters and performance Criteria ..	164
Table 5.6: Design recommendations for the optimum design thresholds in each typology.....	168
Table 6.1: Declaration of authorship.....	184
Table 6.2: Range, step size and number of iterations of each design parameter.....	190
Table 6.3: Correlation coefficients (R) of building heights	203
Table 6.4: Correlation coefficients (R) of building heights	204
Table 6.5: Correlation coefficients (R) of building heights	205
Table 6.6: Comparisons between the optimal solutions in each type	209
Table 6.7: Design guidelines for each courtyard type based on the results of the study.....	210

Abbreviations

IPCC	Intergovernmental Panel on Climate Change
SD	Sustainable Development
SDGs	Sustainable Development Goals
CoP	Conference of the Parties
CIAM	Congrès International d'Architecture Moderne
TND	Traditional Neighbourhood Development
TOD	Transit-Oriented Development
CNU	Congress for the New Urbanism
GNP	Gross National Product
LEED	Leadership in Energy and Environmental Design
BREEAM	Building Research Establishment Environmental Assessment Method
CASBEE	Comprehensive Assessment System for Building Environmental Efficiency
UHI	Urban Heat Island
SVF	Sky View Factor
OSR	Open Space Ratio
S/V	Surface-to-Volume ratio
FAR	Floor Area Ratio
BCR	Building Coverage Ratio
LCZ	Local Climate Zone
WUDAPT	The World Urban Database and Portal Tool
UEIB	Urban Energy Index for Buildings
UMI	Urban Modelling Interface
EUI	Energy Use Intensity
sDA	Spatial Daylight Autonomy
GCR	Greater Cairo Region
MHUUC	Egyptian Ministry of Housing, Utilities and Urban Communities
GOPP	Egyptian General Organisation of Physical Planning
HBRC	Egyptian Housing and Building National Research Centre
EGBC	Egyptian Green Building Council
HVAC	Heat, Ventilation, and Air Conditioning
GPRS	Green Pyramid Rating System
INDC	Intended Nationally Determined Contribution
PBL	Planetary Boundary Layer
UBL	Urban Boundary Layer
UCL	Urban Canopy Layer
RSL	Roughness Sub-Layer
ISL	Inertial Sub-Layer

UHI _{UCL}	canopy layer UHI
UHI _{UBL}	boundary layer UHI
SUHI	Surface UHI
SUHII	Surface UHI Intensity
LST	Land Surface Temperature
LULC	Land Use/Land Cover
SubUHI	Subsurface UHI
GWT	Ground Water Temperature
LAI	Leaf Area Index
LAD	Leaf Area Density
PCM	Phase Changing Materials
ASHRAE	American Society of Heating, Refrigerating, and Air conditioning Engineers
ET	Effective Temperature
DBT	Dry Bulb Temperature
CET	Corrected Effective Temperature
WBGT	Wet Bulb Globe Temperature
DI	Discomfort Index
ITS	Index of Thermal Stress
ET*	New Effective Temperature
SET*	New Standard Effective Temperature
PMV	Predicted Mean Vote
PPD	Predicted Percentage of Dissatisfied
MEMI	Munich Energy-balance Model for Individuals
PET	Physiologically Equivalent Temperature
UTCI	Universal Thermal Climate Index
MRT	Mean Radiant Temperature
COST	European Cooperation in Science and Technology
ISB	International Society of Biometeorology
WMO	World Meteorological Organization
ISO	International Organisation for Standardisation
SDK	Software Development Kit
CAD	Computer Aided Design
UWG	Urban Weather Generator
API	Application Programming Interface
CFD	Computational Fluid Dynamics
MENEX	Man-Environment Heat Exchange
EPW	EnergyPlus Weather
RMSE	Root Mean Squared Error
MPE	Mean Percentage Error

DoE	US Department of Energy
ERF	Effective Radiant Field
IWEC	International Weather for Energy Calculation
KPI	Key Performance Indicators
DEMs	Digital Elevation Models
BVD	Building Volume Density
FAI	Frontal Area Index
NZEB	Nearly Zero Energy Building
BEMs	Building Energy Models
UCMs	Urban Climate Models
WWR	Window-to-Wall Ratio
RSB	Residential Solar Block
SBG	Solar Block Generator
GAs	Genetic Algorithms
MOO	Multi-Objective Optimisation
EAs	Evolutionary Algorithms
MOEA	Multi-Objective Evolutionary Algorithms
SPEA	Strength-Pareto Evolutionary Algorithm
HypE	Hypervolume Estimation
Note	Other abbreviations are shown in their corresponding reference entry.

Nomenclature

Term	Description	Units
H	Height	m
W	Width	m
H/W	Height-to-Width ratio	-
SVF or f_{svv}	Sky View Factor	Decimal
FAR	Floor Area Ratio	-
BCR	Building Coverage Ratio	%
Q^*	Net all-wave radiation budget	W/m ²
K^*	Shortwave radiation flux	W/m ²
L^*	Longwave radiation flux	W/m ²
ΔT_{u-r}	Urban Heat Island intensity	°C
T_a	Air Temperature	°C
MRT	Mean Radiant Temperature	°C
V	Wind velocity	m/s
RH	Relative Humidity	%
UTCI	Universal Thermal Climate Index	°C
M	Metabolic heat production	met
Clo	Clothing insulation	clo
α_{sw}	shortwave absorption coefficient	Decimal
ε or α_{lw}	emissivity (longwave absorption coefficient)	Decimal
Q_{sk}	Heat loss from the skin	W/m ²
Q_{res}	Heat loss through respiration	W/m ²
A_D	Body surface area	m ²
h_c	Convective heat transfer coefficient	W/(m ² . K)
h_r	Radiative heat transfer coefficient	W/(m ² . K)
A_p	Projected area of the body	m ²
f_p	Projected area factor	Decimal
f_{eff}	Effective fraction of the body	Decimal
I_{Global}	Global horizontal radiation	W/m ²
I_{diff}	Diffused horizontal radiation	W/m ²
I_{Dir}	Direct normal radiation	W/m ²
I_{ref}	Reflected direct radiation	W/m ²
L_a	Sky longwave radiation	W/m ²
R_{floor}	Floor/ground reflectivity	Decimal
Note	Other terms are introduced as they are presented in the studies	

Dissemination

I. Peer-reviewed journal papers

Ibrahim, Y., Kershaw, T., Shepherd, P., & Elwy, I. (2021). A parametric optimisation study of urban geometry design to assess outdoor thermal comfort. *Sustainable Cities and Society*, 75 (103352), pp: 1-18. DOI: <https://doi.org/10.1016/j.scs.2021.103352>.

Ibrahim, Y., Kershaw, T., Shepherd, P., & Coley, D. (2021). On the optimisation of urban form design, energy consumption and outdoor thermal comfort using a parametric workflow in a hot arid zone. *Energies*, 14 (4026), 22. DOI: <https://doi.org/10.3390/en14134026>.

Ibrahim, Y., Kershaw, T., Shepherd, P., & ElKady, H. (2022). Multi-objective optimisation of urban courtyard blocks in hot arid zones. *Solar Energy*, 240 (July 2022), pp: 104-120. DOI: <https://doi.org/10.1016/j.solener.2022.05.024>.

II. Conference proceedings

Ibrahim, Y., Kershaw, T., & Shepherd, P. (2020). A Methodology For Modelling Microclimate: A Ladybug-tools and ENVI-met Verification Study. *Proceedings of the 35th PLEA Conference. Sustainable Architecture and Urban Design: Planning Post Carbon Cities*. A Coruña, Spain, 1–3 September.

Ibrahim, Y., Kershaw, T., & Shepherd, P. (2020). Improvement of the Ladybug-tools microclimate workflow: A verification study. *Proceedings of the Building Simulation and Optimization Virtual Conference 2020*. Loughborough, UK, 21-22 September.

III. Datasets

Ibrahim, Y. (2021). Dataset for "A parametric optimisation study of urban geometry design to assess outdoor thermal comfort. Bath: University of Bath Research Data Archive. Retrieved from: <https://researchdata.bath.ac.uk/1045>. DOI: <https://doi.org/10.15125/BATH-01045>.

Ibrahim, Y. (2021). Dataset for "On the optimisation of urban form design, energy consumption and outdoor thermal comfort using a parametric workflow in a hot arid zone". Retrieved from: <https://researchdata.bath.ac.uk/1021>. DOI: <https://doi.org/10.15125/BATH-01021>.

Ibrahim, Y., (2022). Dataset for “Multi-objective optimisation of urban courtyard blocks in hot arid zones”. Retrieved from: <https://researchdata.bath.ac.uk/id/eprint/1137>. DOI: <https://doi.org/10.15125/BATH-01137>.

1 Introduction

“Sustainable urban forms will only be achievable if they are underpinned by a policy background which commits to global sustainability goals, but leaves room for local formation and implementation of solutions.” (Williams et al., 2000)

1.1 Global concerns and the need for sustainable urban development

In a world inhabited by 7.7 billion people, 55% now live in cities and the number will spike to 70% by 2050. Showing the highest urbanisation rate, developing countries are predicted to accommodate 80% (Figure 1.1) of the global urban population (United Nations, 2018). The human influence on warming the climate system is “unequivocal” – the Intergovernmental Panel on Climate Change declared in their latest report (IPCC, 2021). The detrimental role urban areas carry on the ecological system, along with the environmental issues, has also major socio-economic implications, ushering further negative consequences on human health and well-being. Climate change has become a global priority rather than a fringe issue and, since the first United Nations Conference on the human environment in 1972, a spate of UN conferences and summits have taken place with ambitions for the preservation of ecosystems, biodiversity and natural resources. The rudiments of sustainability and Sustainable Development (SD) were established with the publication of *Our Common Future* (WCED, 1987), with direct implications for planning and urban design. The *Earth Summit*, held in Rio de Janeiro in 1992 - the then largest UN conference, witnessed the development of a programme of action, Local Agenda 21 (UNCED, 1992). The city came back to host the UN conference on SD in 2012, in which Member States agreed to develop a set of Sustainable Development Goals (SDGs) which delineate the post-2015 development agenda.

The deplorable fact that today's cities consume around 76% of global primary energy and produce 43% of the related CO₂ emissions (IEA, 2020) has had a vociferous echo on the global agenda, where the global efforts reached a pinnacle in the commitment of 184 countries to 17 SDGs (Figure 1.2), stipulated in the 2016 Paris Agreement, with ambitions to keep the global temperature rise throughout the century below 2° Celsius (CoP, 2015). With many countries lagging far behind the 2030 agenda, the 26th UN Conference of the Parties (CoP) in Glasgow kept alive the ambitious goals (UN, 2021).

The definition of sustainability and SD gained momentum in various disciplinary fields, especially in planning and urban design. Although the discussion on the nexus between urban form and sustainability started a few decades ago, the rationalisation of urban form, its sustainable initiatives and implications can be traced back to the early urban planning movements during the post-Industrial Revolution in the late 19th century. A cursory glimpse of the dominant urban planning paradigms reveals four chronologically overlapping, but contradictory voices. These paradigms had different approaches to the city-nature integration, and have influenced the physical planning aspects in several countries, with different interpretations of city compactness and density.

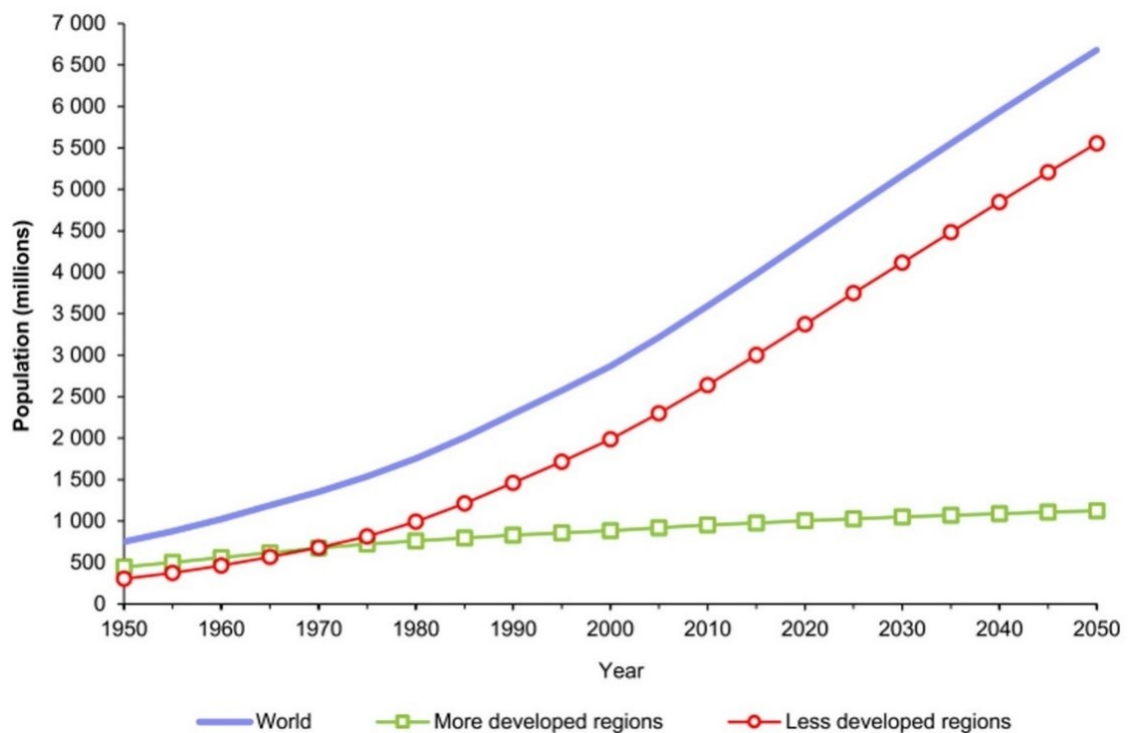


Figure 1.1: Estimated and projected urban populations from 1950 to 2050 (United Nations, 2018).



Figure 1.2: The 17 Sustainable Development Goals (SDGs).

Baron Haussmann, Daniel Burnham and others led the *Monumental City*, late 19th century, as a response to the then pervasive principles of *The City of Dreadful Night* – a concoction of crowded, murky and gloomy settlements (Hall, 1988). Theorists of this paradigm approached the penetration of relatively compact and moderately dense urban fabric with exuberant public parks, conceived as urban “lungs.” Burnham’s 1909 Chicago plan was a seminal implementation of the concepts of *City Beautiful*. The proposal, however, was criticised by social reformers for not addressing the needs of local commerce, nor the related amenities, yet rather leaving them to small businesses and private agencies (Hirt, 2007).

Ebenzer Howard sought to engineer a balance between the desirable aspects of urban fabric and nature. His ideas of polycentric self-contained towns, surrounded by green belts and connected by radial and circular roads (Figure 1.3) crystallised in his famous *Garden Cities of To-morrow* (Howard, 1902). Howard and his proponents, Lewis Mumford, Raymond Unwin, and others, put a strong emphasis on regionalism – where urban form is extremely dispersed and low in density allowing new towns on the periphery to mingle with the old city in a coherent regional system comprising a socially mixed population. Garden cities were criticised for lacking environmental determinism – the notion that social processes will follow physical planning changes, which Howard alleged his model would promote (Gillette Jr, 2011).

Influenced by the Garden City concepts, Clarence Perry proposed his salient *Neighbourhood Unit* to address social alienation and lack of civic participation. Perry's community centre comprised residential areas at a population density of around 150 ppl/ha surrounding local schools and public amenities within a 5-minute walking distance (Figure 1.3), with retails located on the fringes - a safe pedestrian environment as Perry touted his scheme (Perry, 1929). The Neighbourhood Unit was criticised for its increased automobile dependency, and functional and social segregation (Mehaffy *et al.*, 2015). Notwithstanding, Perry's scheme inspired Garden City planners, Henry Wright and Clarence Stein in their design for Sunnyside in 1924 and Radburn in 1929 (Brody, 2010).

The Neighbourhood Unit inspired many architects of the modernist movement, concerned with relatively compact and very high density urban forms. Modernist's philosophies, promoted by the Congrès International d'Architecture Moderne (CIAM), emphasised high-rise functional buildings, massive public green spaces, large block sizes or "superblocks" with internal pedestrian networks, and modern high-speed public transit. The *Plan Voisin* (Figure 1.4), by the *Modernist City* leader, Le Corbusier is an example, in which he suggested accommodating 76,000 people over 260 ha (Wheeler, 2004). In 1943, Le Corbusier documented the vision of the 4th CIAM meeting in Athens 10 years earlier in his publication of *The Athens Charter* (Corbusier & Eardley, 1973). Their principles were widely circulated in Europe and the US, albeit without considering the contextual needs of residents or natural ecosystems. In many cases, urban renewal plans resulted in the displacement of socially and economically weaker classes that the plan initially intended to support. Other criticism included the lack of human scale, rigid zoning, segregated land use, automobile dependency and waste of land (Silver, 2006).

Jane Jacobs, an American activist, had a scathing criticism over the previous planning movements in her salient book, *The Death and Life of Great American Cities* (Jacobs, 1961). Jacobs criticised the functional segregation of the Neighbourhood Unit and argued that Garden City concepts promoting the dispersal of human activity into large pieces of nature created the problems associated with urban sprawl - cities have become less crowded but poorer, the periphery more sprawling and richer. Her book, together with two other works, *The image of The City* (Lynch, 1960) and *The Concise Townscape* (Cullen, 1961), are considered the most influential against the post-World War II interpretation of modernist urban design concepts.

With the rise of the concept of sustainability, Jacob's colleagues Andrés Duany, Plater-Zyberk and Peter Calthorpe led several Neo-traditional planning paradigms, *Traditional Neighbourhood Development* (TND), *Transit-Oriented Development* (TOD), *New Urbanism*, and *Smart Growth* – the antipode of sprawl – to promote the sustainability of cities. Duany adopted a modified version of the neighbourhood unit in his TND approach (Figure 1.4), the neighbourhood, the district and the corridor, showing transformations in the traffic volume and enhancing the integration with the surrounding neighbourhoods (Figure 1.5) (Duany *et al.*, 2001). Calthorpe, on the other hand, focused on the walking distances, transit nodes, and the conservation of natural land emphasising TOD concepts (Rutheiser, 1997).

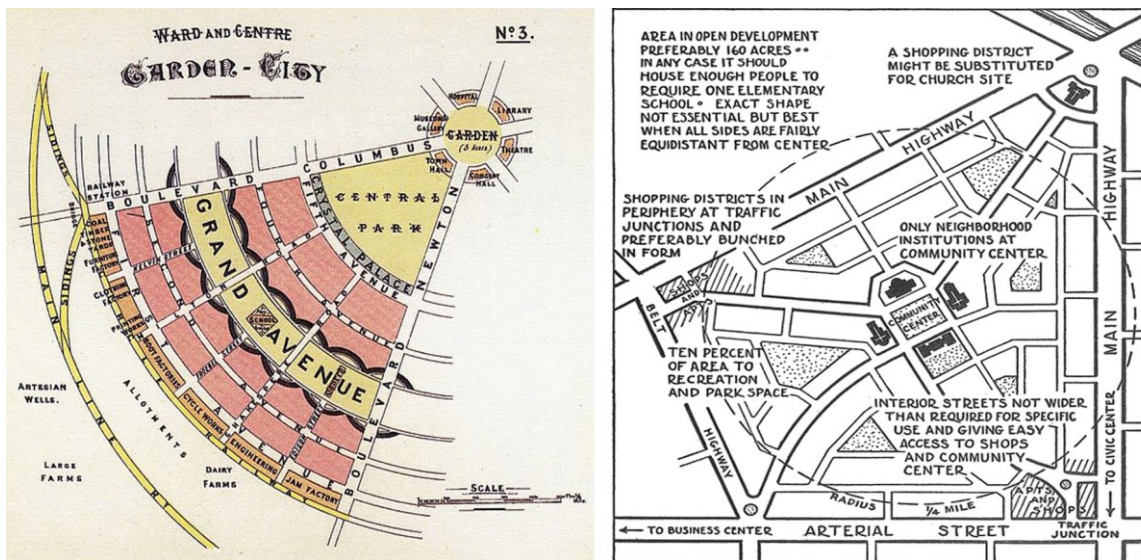


Figure 1.3: Howard's Garden City as a diagram (left), and Perry's Neighbourhood Unit (right).

Notable among these paradigms is the New Urbanism, which was institutionalised through annual conferences of the Congress for the New Urbanism (CNU) beginning in 1993 (Grant, 2009). Mixed use, diversity of housing types, housing-job proximity, minimised automobile dependence, human-scaled and attractive streetscape, interconnected and pedestrian-oriented streets, identifiable civic centres, adequate open spaces, compact and medium-high density urban forms and re-urbanisation of existing cities, are all the basic design principles of Neo-traditional planning approaches (MacLeod, 2013).

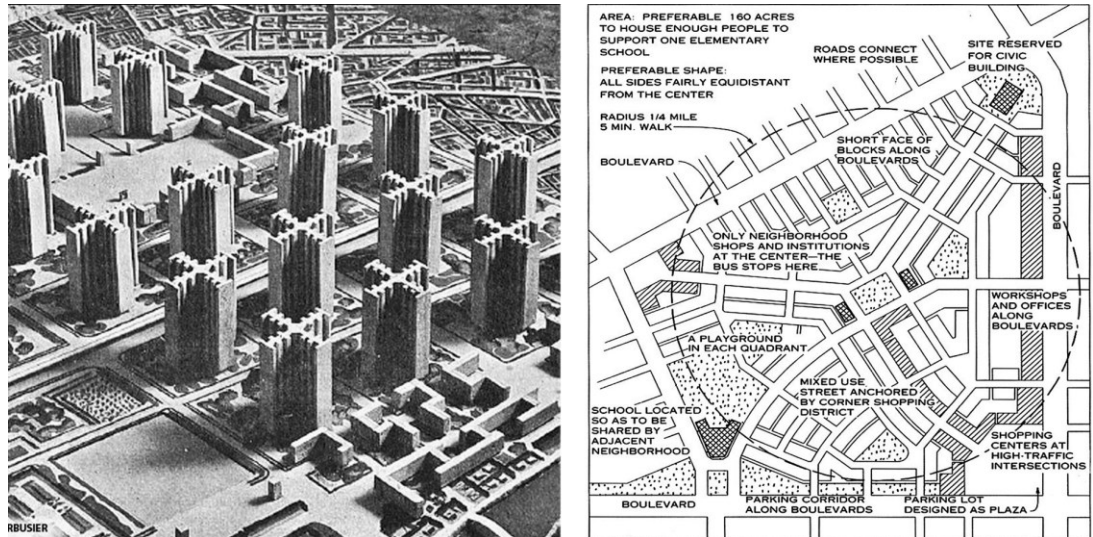


Figure 1.4: Plan Voisin by Le Corbusier in 1925 (left), and Duany-Plater-Zyberk's update of the neighbourhood unit (right).

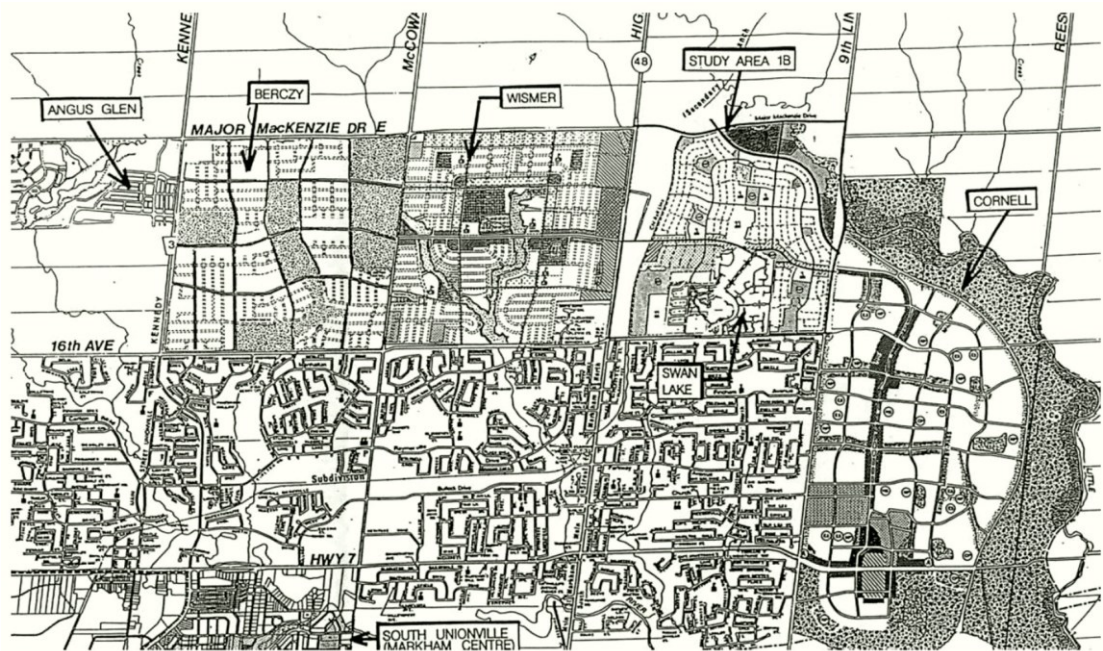


Figure 1.5: The Cornell New Urbanist community designed by Duany Plater-Zyberk (on the right) connecting to the 1970s and 1980s subdivisions. Adopted from (Wheeler, 2004).

In conjunction with the introduction of TND planning concepts, *The Compact City* was introduced as a hitherto flawless design approach to modern cities (Dantzig & Saaty, 1973). Compactness refers to urban contiguity and connectivity through the utilisation of previously developed land and the redevelopment of existing land (Jenks, 2000). The concept was widely investigated to address the physical dimensions of compact urban forms thought to promote sustainability, as well as the interconnections between them both quantitatively and qualitatively.

A series of publications by Jenks and others sought to address the questions of to what extent a compact urban form could achieve sustainability; what a sustainable urban form is; and how it can be achieved through empirical evidence from local surveys of dwellers of where the compact city concepts have been implemented. The first two books focused on the context of developed countries, concluding that there was no definitive sustainable form, but rather a variety of 'more sustainable' urban forms than typical patterns, and that despite their benefits with regard to public transport and saving of land, in some cases, misinterpretation of urban compaction - as a process - led to detrimental impacts on the environment, but also to a public backlash (Jenks *et al.*, 1996; Williams *et al.*, 2000). Jenks (2000) pointed out that there are limits beyond which urban intensification process will become unacceptable, and that the responses to intensification depend on a range of environmental and socio-economic factors. The third book focused on achieving higher densities in developing countries, concluding that, the intensification process should be driven by policies through the formal sector. Jenks ascribed the smaller ecological footprint of the developing countries to their low GNP, which, if increased, levels of consumption would increase unsustainably (Burgess & Jenks, 2000).

With the emergence of sustainability, Eco-Urbanism was introduced in the early 1980s to deal with challenges of climate change and resource constraints drawing upon the concepts of urban metabolism and sustainability. A key feature of Eco-urbanism is the incorporation of green technologies, for instance smart grid, solar technology (Figure 1.6), net-zero energy and carbon neutral buildings (Joss & Molella, 2013). In terms of density and morphology, eco-cities are conceived as amorphous cities (Jabareen, 2006), implying that incorporating smart technologies will be as efficient in the use of energy, resources and infrastructure as spatial design concepts of Howard and the compact city. Although Tianjin eco-city in China is the most prominent example of the movement (Low, 2013), French Éco-Quartiers, German eco-districts and British Eco-towns are all other examples of the implementation of the concept. In the US, Eco-urbanism evolved as an extension to Neo-traditional planning paradigms. A key distinguishing feature of Eco-urbanism from the other movements is promoting rating systems - LEED-ND in the US, BREEAM Communities in the UK, and CASBEE-UD in Japan are the most famous examples (Sharifi, 2016). Eco-urbanism has been criticised for over-reliance on economic sustainability at the expense of other dimensions which makes them

vulnerable to the market forces and marginalises the role of people. Caprotti (2014) explained how high-rise towers in Tianjin city separated by wide streets curtails the human scale, as did the modernism principles, describing eco-cities as isolated wealthy islands.



Figure 1.6: Siemens technology, Masdar City, UAE, designed with parametric optimisation of the façades for passive solar cooling and daylighting (AKDC, 2021).

Cheng (2009) discussed the importance of perceived density as a subjective quality, dependent on the interaction between individuals and the environment. Cheng pointed to previous studies highlighting the physical characteristics, e.g. building height, space between buildings, space enclosure and complexity, as well as the cognitive and socio-cultural factors predominant in people's perception of density, particularly in the context of high density developments. In the same context, Carmona *et al.* (2010) in their book *Public places – Urban spaces*, emphasised the concept of having better density rather than higher density. In their book, they concluded that a sustainable urban design strategy should consider to the inevitability of internal contradictions. For instance, to inappropriately emphasise one aspect of design (creating high density developments) to a probable detriment of other considerations (bio-diversity, social interactions, or energy demand).

Parallel to the dilemma of the acceptability of urban densification, several environmental qualities were debated as qualitative and quantitative measures of the sustainability of urban forms. For instance, Olgyay (1963) focused on the

bioclimatic design and the spatial regionalism, March and Martin (1972) on the daylighting and thermal performance of archetypal building forms, Knowles (1981) on the passive solar design, DeKay and Brown (1985) on the relationship between urban form, energy and on-site renewable resources, and Givoni (1998) on the climate-sensitive urban design (Emmanuel & Steemers, 2018). These measures, in line with the sustainable development goals, have paved the way, and continue to do, for many research studies on the environmental sustainability of urban form. That said, with the question of how sustainable an urban form could be is not yet fully addressed, the focus has now shifted from a single criterion to a set of environmental considerations which should be addressed in order to achieve a climate-sensitive built form.

1.2 Urban form: Analyses, approaches and recent advancements

Urban areas are accompanied by increased temperatures relative to the surrounding rural areas. The phenomenon known as Urban Heat Island (UHI) poses negative consequences on human health and well-being, and further exacerbates climate change induced heat waves (Oke, 1976). Recently, the debate on sustainable urban forms has extended to include urban resilience - the adaptability to environmental stress, with outdoor thermal comfort being of direct relevance and paramount importance in urban form studies. Despite the fact that there is no universal solution for climate-sensitive urban form design (Oke, 1988; Williams *et al.*, 2000), compact urban forms are still debated as the best solution for hot and arid climates. In this regard, early concepts of urban compactness can be traced back to the vernacular architecture of North Africa and the Middle East, characterised by narrow streets and courtyards.

Courtyard houses are ubiquitous, not only in the Arabic vernacular architecture, but also in the Ancient Egyptian settlements. However, courtyard houses were most recognised in Egypt during the Fatimid and Mamluk epoch during the 11th to 16th centuries (Figure 1.7). Courtyard houses and blocks have long been conceived as the surest way to design in the desert in hot-arid regions. Hassan Fathy, a prominent Egyptian architect, advocated the courtyard intervention in his work, *Architecture for the poor*, for several climatic benefits; it creates an outdoor sheltered space, works as a solar protector and collector, protects from wind, and facilitates natural cooling strategies (Fathy, 1973;1986). Fathy's innovative plan for New Gourna (Figure 1.8), the landmark of his legacy, comprised a group of

L-shaped courtyards, built with vernacular earthen building materials (mud bricks). The village was acknowledged for providing innovative solutions to environmental challenges as well as promoting local community engagement – in relevance to the current environmental and socio-economic sustainability of urban forms. The climatic benefits of courtyards were widely debated in a growing number of studies in various climates (Taleghani *et al.*, 2014b; Soflaei *et al.*, 2017), with ubiquitous interest in Seville, Spain (Rojas-Fernández *et al.*, 2017; Diz-Mellado *et al.*, 2021). The University of Seville has the highest number of affiliations in SCOPUS-indexed publications with the keyword “courtyard” – a direct response to the enormous courtyard houses built in the Andalusian capital during the 8th to 14th centuries.



Figure 1.7: Wikalat Al-Ghuri (Commercial caravanserai), originally built in 1504 (left), and Bayt Al-Suhaymi, originally built in 1648 (right), as they stand today after renovation (AKDC, 2021).

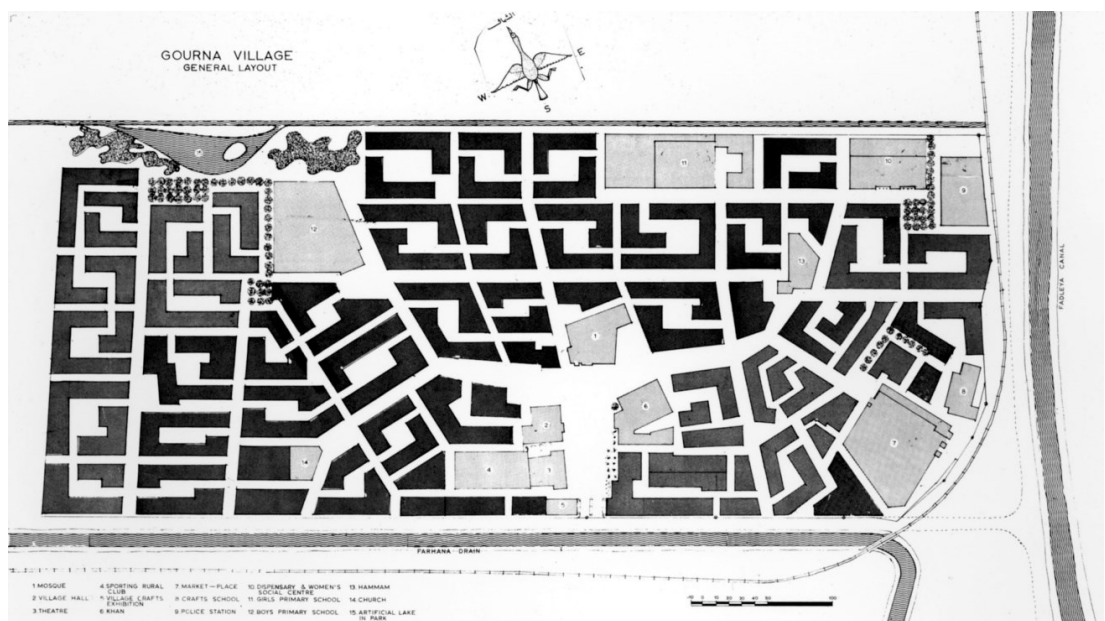


Figure 1.8: General layout of New Gournia Village, Luxor, Egypt (Fathy, 1973).

At the time New Urbanism concepts were being realised and implemented in developed countries, developing countries have been encouraging modernist theories to grow and expand. Driven by the rapid urbanisation and the demographic growth in these countries, functional zoning exemplified in Corbusier's towers in the park dominated the design schemes and obliterated the vernacular building traditions, regardless of their environmental benefits. Meanwhile, in Egypt for instance, neo-traditional planning has been confined to the private sector developments (section 1.3.1). Some of these developers touted their communities through accreditation with rating systems (e.g., LEED-ND) without paying attention to their contextual viability.

The study of Oke (1981) consolidated previous attempts to characterise the different built forms with their geometrical aspects, using the urban canyon dimensions. An urban canyon, which refers to a street section with buildings flanking on both sides, is defined with regards to its Height (H), Width (W), Length (L), and the H/W ratio - also called the aspect ratio, and in some cases, the W/L ratio.

Sky View Factor (SVF or ψ_{sky}) is another factor, and refers to ratio of the area of visible sky unobstructed by opaque surfaces to the area of the sky dome (Figure 1.9). On a wider scale, besides the Open Space Ratio (OSR), Surface-to-Volume ratio, and SVF (Figure 1.10), the Floor Area Ratio (FAR) and the Site or Building Coverage Ratio (BCR) are the most used in urban planning regulations and development budgeting (Cheng, 2009).

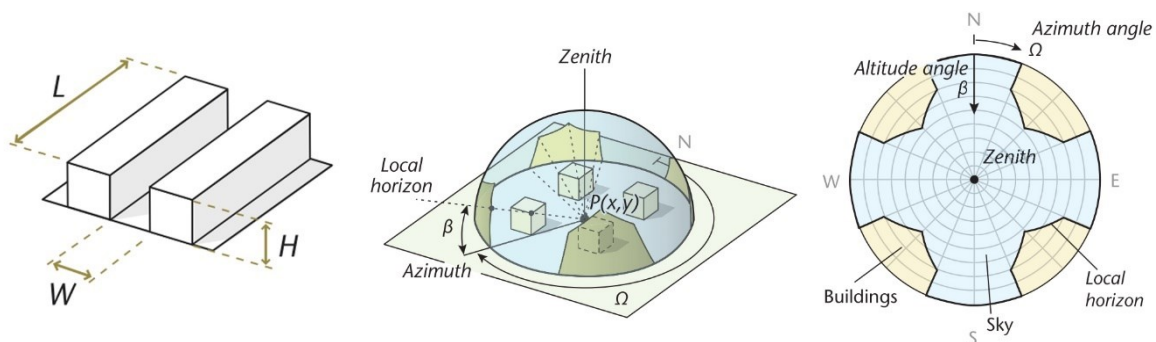


Figure 1.9: Urban canyon proportions (left), Sky view factor for a point P (middle), and a polar plot illustrating the angles in the (middle) projected onto a flat plane (right) (Oke *et al.*, 2017).

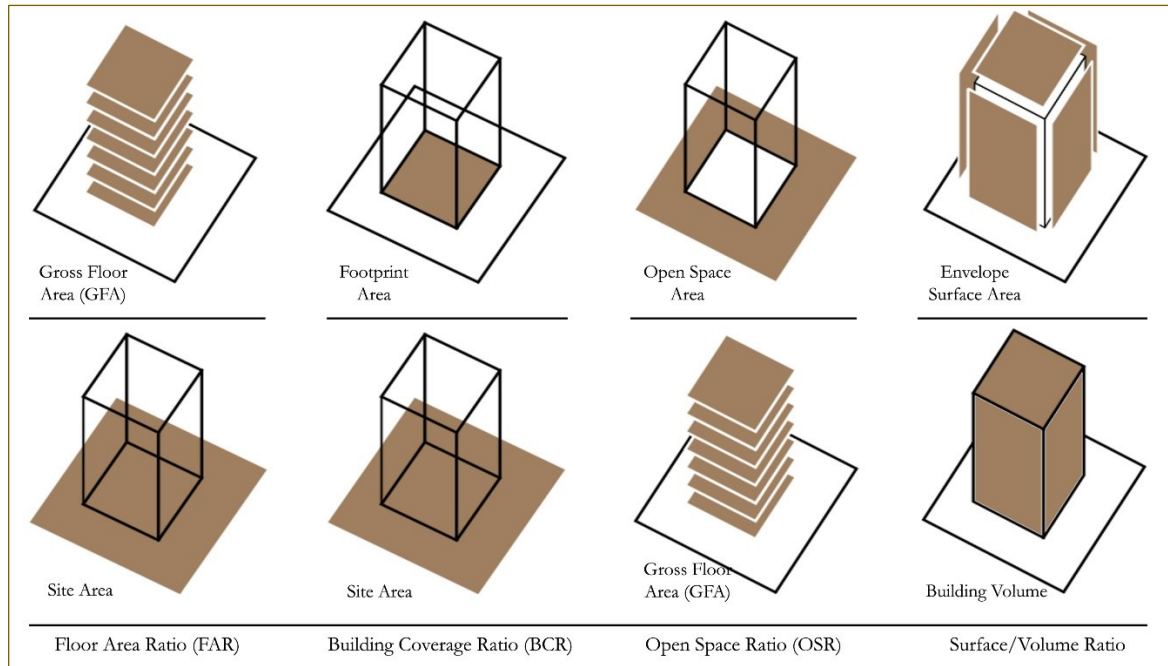
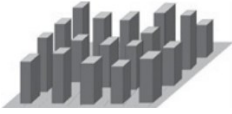

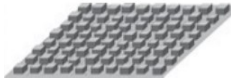



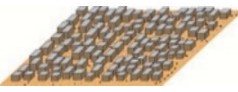





Figure 1.10: Most common urban-scale design parameters. Upper and lower rows represent the numerator and denominator in the calculation of each parameter, respectively. Adapted from (Zhang *et al.*, 2019).

Urban form is defined by three basic spatial elements; buildings along with surrounding open spaces; plots or lots; and streets. The analysis of physical form focuses on the street patterns, building typologies, and the urban syntax, as well as the interrelations between them. In urban planning, the term “typology” refers to the building shape, and has long been associated with urban fabric and streets in defining the morphology of a city. Despite the distinction between building typology and urban morphology (Conzen, 1960), it is often impractical to discuss one without the other (Cities, 2014).

Stewart and Oke (2012) presented the Local Climate Zone (LCZ) scheme to link urban morphology and urban climate conditions, based on the geometrical and land cover properties, supported by observational and numerical modelling data. The scheme comprised 17 LCZ’s, sorted as 10 built types (Table 1.1), and 7 land cover types (not shown). The geometrical parameters included SVF, H/W or interspaces, BCR, and the height of buildings and/or trees. Traverse measurements in Vancouver, Canada showed that differences in geometry and land cover entailed 5 K variation in air temperatures. The LCZ’s, as they described, can be “delineated on a city map or aerial photograph.”

Table 1.1: the 10 built-up Local Climate Zones (LCZ's) of Stewart and Oke (2012).

Compact high-rise	Compact midrise	Compact low-rise	Open high-rise	Open midrise
				
SVF (0.2-0.4), H/W (>2), BCR (40-60).	SVF (0.3-0.6), H/W (0.75-2), BCR (40-70).	SVF (0.2-0.6), H/W (0.75-1.5), BCR (40-70).	SVF (0.5-0.7), H/W (0.75-1.2), BCR (20-40).	SVF (0.5-0.8), H/W (0.3-0.75), BCR (20-40).
Open low-rise	Lightweight low-rise	Large low-rise	Sparsely built	Heavy industry
				
SVF (0.6-0.9), H/W (0.3-0.75), BCR (20-40).	SVF (0.2-0.5), H/W (1-2), BCR (60-90).	SVF (>0.7), H/W (0.1-0.3), BCR (30-50).	SVF (>0.8), H/W (0.1-0.25), BCR (10-20).	SVF (0.6-0.9), H/W (0.2-0.5), BCR (20-30).

The supra-scheme was adopted in several climate modelling studies, based on a top-down approach to support neighbourhood scale climate models with detailed 3D information on cities. The World Urban Database and Portal Tool (WUDAPT) is an example, which depends for its first level of data aggregation on the LCZ's (Mills *et al.*, 2015). Similar approaches using satellite images quickly followed; Xu *et al.* (2017) utilised advanced satellite and radar morphology extraction techniques to create an urban climate map for a case study in Hong Kong, and compare the satellite-derived radiant temperature map to that of the actual morphology (Figure 1.11).

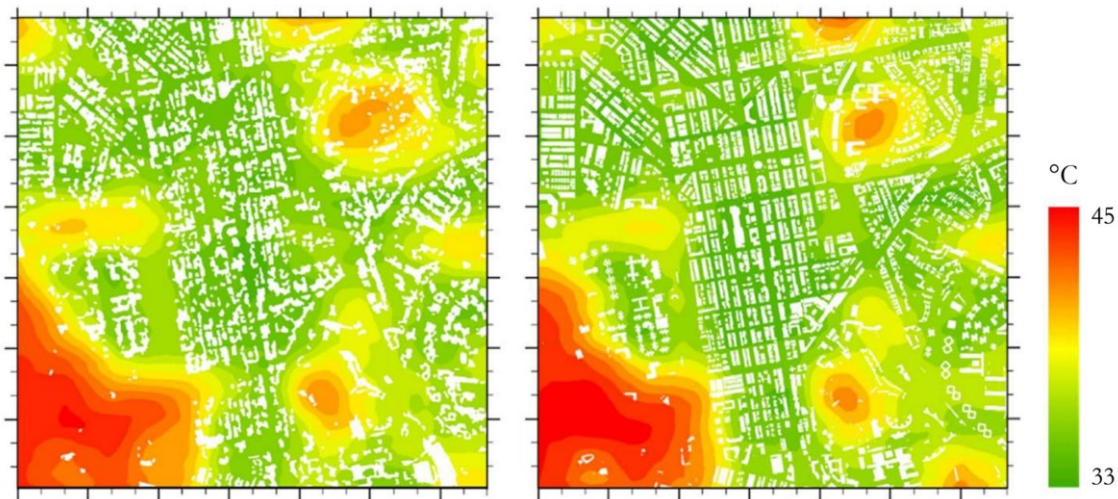


Figure 1.11: Radiant temperature thermal map based on satellite-derived morphology (left) and actual morphology (right), adapted from (Xu *et al.*, 2017).

A common approach in urban space modelling is to simplify the geometrical characteristics of built forms to some extent, without blurring their heterogeneity –

what Stewart and Oke (2012) emphasised in their scheme. Rodríguez-Álvarez (2016) proposed an Urban Energy Index for Buildings (UEIB) based on the simplification of urban morphologies to notional grids, to calculate annual lighting, heating and cooling loads. The model showed significant potentials for creating domestic heat maps on a city scale (Figure 1.12).

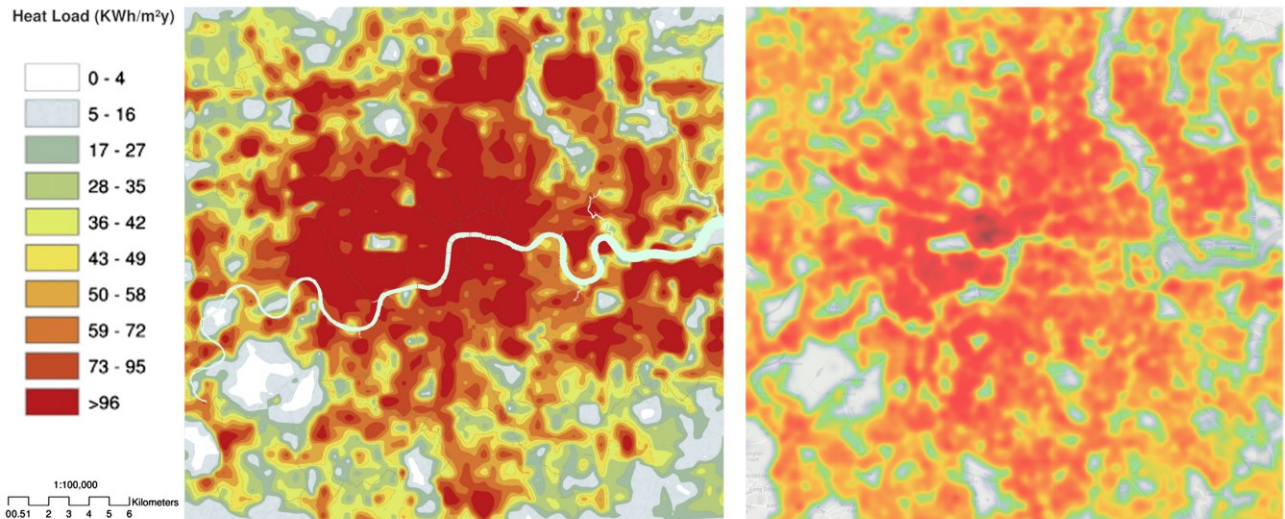


Figure 1.12: London's annual domestic heat density map as produced by the UEIB (left), and as retrieved from (MoL, 2022) (right).

On an urban block scale, bottom-up approaches are often adopted, due to the need for precise building information (e.g. building heights, materiality and glazing). Recently, this need has been widely recognised to be met by parametric design tools which offer a significant level of detail, but also allow for the integration of multiple performance criteria to be assessed. Grasshopper for Rhinoceros 3D is an example (see Chapter 3), whose popularity is rapidly increasing in both research and practice. Recent studies – corresponding to the three urban form elements mentioned above – have shown Grasshopper to be a versatile and reliable modelling environment.

Shi *et al.* (2021) used Grasshopper to explore hundreds of possible variations of hybrid block typologies, having the same FAR, BCR and pattern (Figure 1.13), by varying the number of buildings, and their locations (plot subdivision), to calculate energy demand and renewable energy potential. Vartholomaios (2017) investigated the parametric combinations of 4 building heights, 5 open space ratios, 3 orientations, 3 block lengths, and 3 side distances in Grasshopper, to calculate the cooling and heating loads of three building typologies (Figure 1.14).

Xu *et al.* (2019) studies the horizontal and vertical density of a grid layout by varying the height of individual buildings and the location of open spaces, to investigate the impact of density on thermal comfort in summer and winter (Figure 1.15).

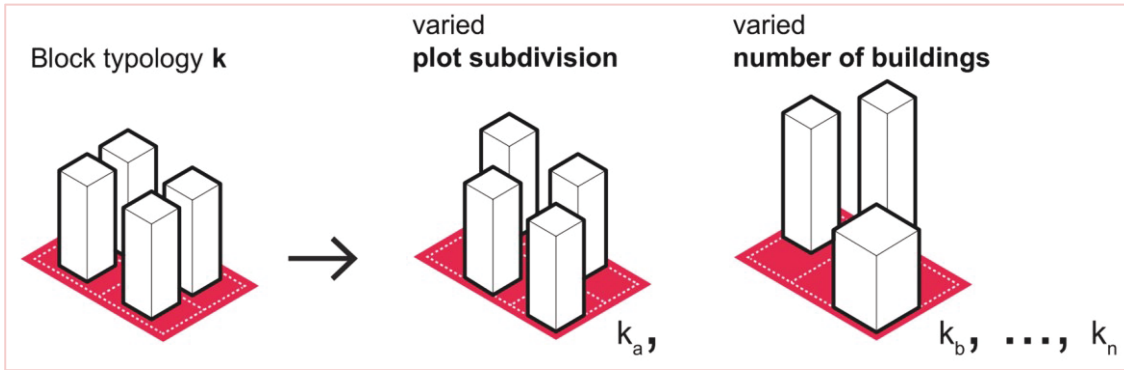


Figure 1.13: Evolution of a block typology (K) by varying plot subdivision and number of buildings (Shi *et al.*, 2021).

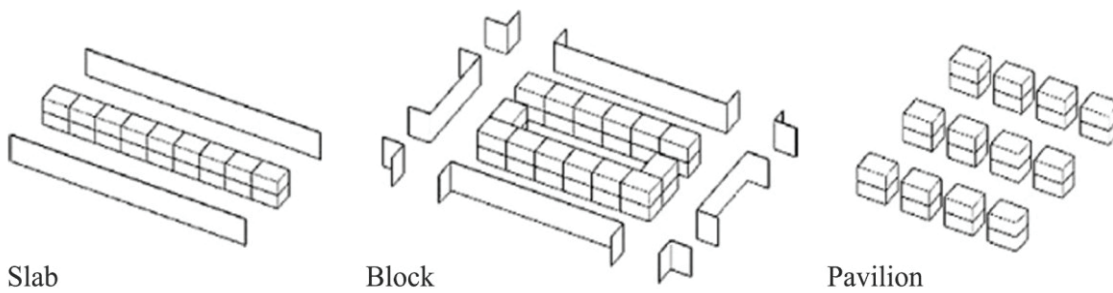


Figure 1.14: Three building typologies studied and optimised in (Vartholomaios, 2017).

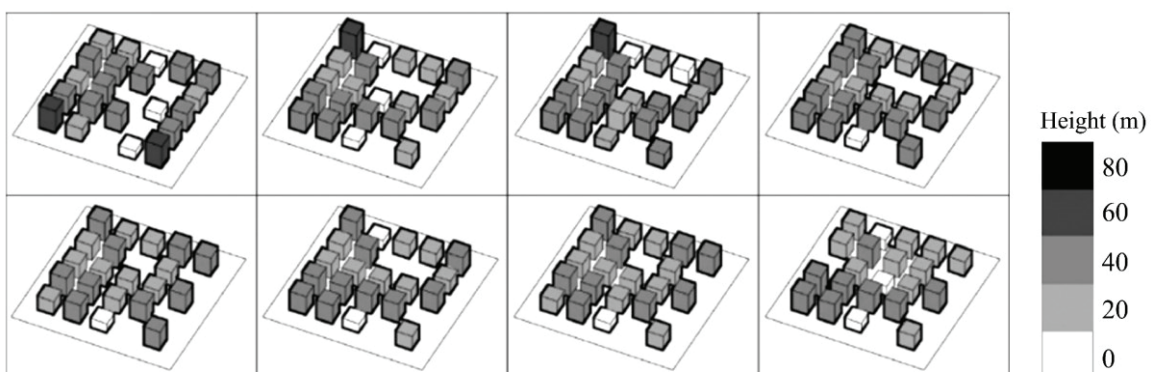


Figure 1.15: Thermal comfort-optimised building heights by (Xu *et al.*, 2019).

These studies highlight the great potential of parametric optimisation studies to be integrated in the design process – especially within the urban block scale – allowing for the consideration of several performance criteria. As this corresponds

to the multi-dimensional nature of the sustainable development goals, parametric design is now seen to be the mainspring for achieving these goals.

According to the UN Population Prospects (United Nations, 2019), Egypt, along with other eight countries, are anticipated to share more than half of the global population increase by 2050. Moreover, Egypt is predicted to share with other eleven countries almost 60% of the global increase in urban population up to 2050 (United Nations, 2018), showing the highest urbanisation rate in the Middle East and North Africa (MENA) region, whose countries are located in hot-arid climate zones. Cairo, Egypt's capital, is ranked sixth in urban agglomeration, and is expected to be the fifth by 2030 (United Nations, 2018). Standing on its commitment to the Paris Agreement, Egypt is looking forward to hosting the 27th UN CoP, in November this year, on behalf of Africa, aiming to close the commitment and action gap. Previously, Egypt hosted the Africa 2018 Forum, the 'Invest in Africa' 2019 Conference, and the Egypt-International Cooperation Forum in 2021. Also, Egypt has co-developed the Adaptation Action Coalition, in partnership with the UK, and the UN Development Program, to find solutions for the most challenging impacts of climate change (MoEE, 2021). From these standing points, and given the pioneering role Egypt plays in leading the agenda of green recovery in the region, Egypt is selected to be the research context of this thesis. Evidence from the IPCC (Niang *et al.*, 2014) has confirmed an overall warming in North Africa beyond the range of changes due to geographical variability. Therefore, the implications drawn from this research should be applicable to other hot-arid climate zones.

1.3 The Egyptian context | Urban and environmental insights

Egypt is located north-east of Africa, and extends between 22° - 31° 37' N and 24° 57' - 35° 45' E, over approximately one million km², overlooking the Mediterranean Sea in the north and the Red Sea in the east, and adjoining Libyan and Sudanese deserts from the western and southern sides, respectively. Egypt encompasses a diversity of climate conditions; extremely hot in the southwestern desert to very cold conditions in St. Catherine in Sinai. The general climate is classified as desert hot-arid climate "BWh" under the Köppen-Geiger classification (Figure 1.16). The diversity of climatic conditions can be distinguished into two seasons; hot dry summer spans over from May to October, and mild winter spans over from November to April.

Clay bricks were used until the Ayyubid and Mamluks epochs when light-coloured and highly reflective stone and limestone took over; external walls were 50 cm thick to provide thermal insulation. Wood was widely used in oriel windows with sophisticated shading systems, “Mashrabeya”, to decrease glare and maintain privacy (Figure 1.17), leaving red bricks only for domes and vaults (Mohamed & Ali, 2014).

The Ottoman empire reached an end, and so did the Islamic architecture in Egypt when Mohamed Ali Pasha – the founder of Modern Egypt, announced its independence in 1805. The viceroy of Egypt sought to modernise Egypt through several military, economic and cultural reforms that his dynasty kept alive after his death in 1848. Ismail Pasha -who received his education in Paris- entrusted the Europeanisation of Cairo to a French architect inspired by Baron Haussmann’s plans of Paris. Known today as Downtown Cairo, the new city fabric was planned on radial grids of wide streets with Baroque, Neo-classical and Renaissance architectural styles (Figure 1.17). By the turn of the 19th century, new lavish neighbourhoods resembling the garden cities of Howard were already built in Cairo, Garden City and Zamalek, followed by Heliopolis in the 1920s as the first satellite town. Buildings were still grandiose with average floor height of 4 m to facilitate air movement, however, the Islamic wooden ornaments were replaced by glass and metal ornaments with greater window-to-wall ratios (Elshahed, 2007).

Between 1937 and 1947, Cairo’s population doubled from 1.3 to 2.8 million inhabitants. In 1949, The Ministry of Housing, Utilities and Urban Communities (MHUUC) issued the first housing law, introducing the Municipality of Cairo as the official administration responsible for managing the city developments. Following the 1952 Revolution, which ended the monarchy and announced Egypt as a republic, the new government promoted subsidised public and social housing. Mixed land use and commercial zones were integrated into European Cairo, replacing pompous villas with high apartment blocks. Cairo became an attractive destination for rural residents, and new master plans were created, where the MHUUC had to issue a new law in 1964 to regulate the city’s expansion through new settlements in the east (Nasr City and 10th of Ramadan), and the west (6th October) (Sutton & Fahmi, 2001).

The war of 1967 was a turning point in the physical growth of Cairo; driven by the demographic growth, the informal sector promoted urban sprawl, especially on the west of the Nile (Giza and Mohandessin), with the absence of governmental

monitoring. Given the common knowledge, material availability and ease of application of reinforced concrete structural systems, villas and low-rise residential blocks were demolished and replaced by 12-story residential towers – ostensibly following the modernist approaches (Figure 1.17). During the 1970s, more than 80% of new constructions were illegal. In response, the MHUUC issued a series of laws delineating the provisions for construction (Law 106 of 1976), and new urban communities (Law 59 of 1979). In 1982, the GCR was defined on 32000 hectares, 67% of them for residential uses. New master plans were created (Figure 1.18) dividing Cairo into 16 sectors to transfer the population to new settlements, taking advantage of Cairo’s ring road (Fahmi & Sutton, 2008). In tandem, the government issued the first urban planning act (Act 3 of 1982) which only defined a BCR of 60% for residential uses, and entrusted the land use allocation, people’s density, and residential density to a concerted supervision from the local municipalities and the General Organisation of Physical Planning (GOPP).



Figure 1.17: 1540’s Amna bint Salim house (left), 1860’s Suleiman Pasha square, now Talaat Harb square (middle), and 1960’s Nasr City apartments (right), adapted from (Edeisy, 2020).

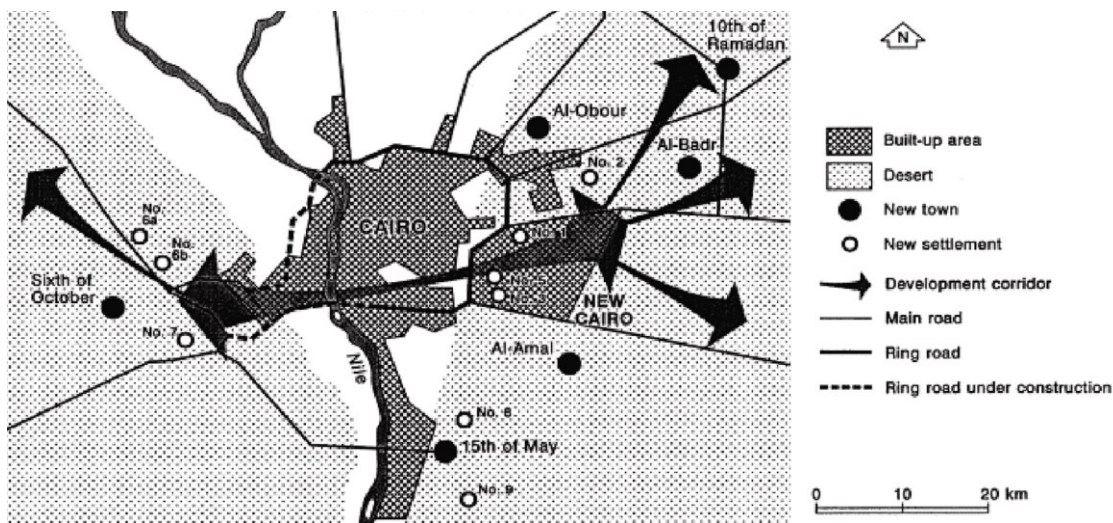


Figure 1.18: 1983 master plan of Cairo (Sutton & Fahmi, 2001).

1.3.2 *The gap between policy development and urban environmental challenges*

The failure of the 1956, 1970 and 1982 master plans was evident by the early 1990s; the new settlements failed to provide convenient housing solutions and accommodate the unprecedented population growth. The financial constraints on government expenditure escalated the dominance of the private sector with its concomitant market forces in lieu of the governmental legislations. Informal settlements, typically of apartment towers, became the dominant housing scheme, accommodating almost 70% of GCR's inhabitants (Edeisy, 2020). In 2008, the MHUUC issued a Unified Construction Act (no. 119) and its Executive Regulations – the hitherto endorsed construction act, indicating the abolishment of the previous laws 106 and 3 (MHUUC, 2008). As a direct response to the uncontrolled density patterns, the new regulations defined a number of spatial design thresholds; a minimum lot size of 120 m², maximum block length of 250 m, minimum street width of 10 m, maximum building height of 36 m, and maximum H/W of 1.5. The last decade, however, has not seen any different urban patterns, but rather a replication of the 1990's informal urbanisation. Neo-traditional planning is merely recognised in private and, in some cases, fenced communities. Currently, the government is considering a number of amendments to the regulations, having lower building heights is amongst them. Moreover, a redevelopment campaign of slums is being carried out to counteract what informal urbanisation has left behind. The fact that the government is striving to restrain the “illegal” high densities explains its tendency to promote lower densities, despite the potential benefits of higher densities in hot-arid climates, if deliberately designed and delivered. Meanwhile, with growing evidence of climate change impacts, the vulnerability of urban communities in developing countries to heat exposure has been highlighted. In 2015, Egypt witnessed a heat wave, during which 110 people died and 580 hospitalised with heat exhaustion (Bayomi *et al.*, 2021). This highlights a gap between the current regulations and the aspired climate-sensitive urban design in light of the global rising temperatures, and leaves the health and well-being of urban residents at risk.

Global rising temperatures have also had direct influences on indoor thermal comfort. The number of air conditioners in Egypt increased from 200,000 to 6 million units between 1999 and 2012, accounting for 20% of total electricity consumption (Edeisy & Cecere, 2018). The growing energy demand, encouraged

by energy subsidies, entailed an increase in the per capita primary energy use by 32% from 1990 to 2014 (EEAA, 2018). Between 2000 and 2020, Egypt's total final energy consumption has nearly doubled, with the residential sector responsible for 44% of it (IEA, 2021). In 2003, the UN Development Programme funded the Egyptian Government, represented by the Housing and Building National Research Centre (HBRC), to issue an energy efficiency code. The code for residential buildings (MHUUC, 2005) guarantees 20% energy savings through modifications to the building envelope, HVAC and domestic hot water systems, natural and artificial lighting, electric load divisions, and eventually verifying the annual consumption to a minimum threshold of improvement. Following an energy crisis in 2012, The Ministry of Electricity announced a 5-year programme aiming to eliminate subsidies by increasing the electricity tariff, but also to enforce the energy code, encourage the use of energy efficient appliances and promote the transition to renewable energy (EEAA, 2018). However, energy consumption per capita has grown by 9% between 2013 and 2020, highlighting the need for further adaptation measures, as well as for behavioural changes.

The Egyptian Green Building Council (EGBC) was established in 2009 to shift professional practices and raise public awareness towards sustainable and “green” design. In collaboration with the HBRC, the EGBC issued the Green Pyramid Rating System (GPRS), in line with other rating systems in the Middle East (e.g. Pearl rating for Estidama in UAE, and QSAS in Qatar). The GPRS was later updated to TARSHEED (Rationalisation in Arabic). However, there has not been any projects ever registered (EGBC, 2022). The rating system is not binding, and the lack of awareness by practitioners of the potential savings in energy (and others) in the long term, suppresses any intentions for the accreditation – in fact, developers avoid committing to sustainable practices due to their higher initial costs. The annual population growth rate in Egypt is anticipated to remain above 2% until 2040 (United Nations, 2019). In light of Egypt's Vision 2030 – Egypt's Intended Nationally Determined Contribution (INDC) to the SDGs in 2015 (MFA, 2015), the national efforts to control this growth seem daunting, and with environmental concerns on top, a challenging picture emerges considering the adaptation and mitigation measures specified within the INDC (“Identify climate change potential health risks” and “improve energy efficiency”). Given the extensive construction projects currently being carried out, the integration of quantitative and qualitative environmental considerations into the urban design process seems to be the only way of achieving the ambitious goals.

1.4 Motivation

With an ever increasing demographic growth, and the lack of urban planning laws which take account of the current environmental challenges, it becomes evident that amending the existing (or creating new) design regulations is imperative. This research is motivated by the need for design guidelines for new developments and redevelopments of existing urban communities, which balance urban density, and the thermal and energy performance of urban built forms. The research is also motivated by the potential of advanced methods and techniques to assess numerous design solutions and bring dichotomous environmental criteria into a single assessment workflow. In other words, the potential to improve one performance criterion (e.g., outdoor thermal comfort), without compromising others (e.g. energy demand), in correspondence to the urban design geometrical and morphological parameters – a capability which has always been sought after.

This multi-purpose capability fosters the exploration of new relationships between urban form and environmental performance, at different scales. In hot-arid climates, where pedestrians experience extreme hot weather conditions, and since outdoor air temperatures are in direct relevance to mortality rates, outdoor thermal comfort receives the greatest attention therein, especially at an urban canyon scale. With the above-mentioned capabilities, it becomes viable to redefine existing relationships at one scale (urban canyon), as such to investigate how they change with adding different design criteria at another scale (urban block). Furthermore, they allow for detailed sampling of the design parameters, and hence for better conceptualisation of the urban form.

1.5 Hypothesis, aims and objectives

The scope of this research is demarcated by a two-fold hypothesis. First, it is hypothesised that outdoor thermal comfort can be improved beyond what ensues from using the design thresholds of the Egyptian Construction Act, and that, in conjunction with the criteria of the Energy Efficiency Code, the thermal and energy performance of urban form, exemplified by generic typologies, can be further improved. Second, in light of the two codes, it is hypothesised that urban courtyard blocks are the best typology in hot-arid climates, and that their thermal and energy performance can be improved beyond what ensues from using the optimum ratios previously reported in the literature.

Therefore, this thesis aims to define the optimum design thresholds, in tandem with the density parameters of urban built forms, which improve outdoor thermal comfort without increasing energy consumption, in the hot-arid climate of Cairo, Egypt. This overall aim is pursued at different scales, through the optimisation of the geometrical (design), typological and morphological (density) parameters of built form. In doing so, the thesis scrutinises the relationship between urban canyon geometry, represented by the most important design parameters, and pedestrian thermal comfort, then analyses a contradicting nexus between urban geometry, and both thermal comfort and energy consumption, at an urban block scale. Finally, the thermal and energy performance of urban courtyard blocks are investigated with detailed sampling of their design parameters.

In light of the research gaps highlighted in section 1.3.2, the following research questions describe the objectives of this thesis, corresponding to the scale and scope of each part:

Chapter 4:

- *What are the urban canyon-scale optimum design parameters for improving outdoor thermal comfort?*

Chapter 5:

- *What are the optimum design parameters which yield the best thermal and energy performance for urban block typologies?*

Chapter 6:

- *To what extent could the urban-scale design parameters improve the thermal and energy performance of courtyard urban blocks?*

The fourth objective is to *present the optimised design thresholds as design guidelines* to inform urban planners, and policy makers on the design criteria, towards an environmental performance-based decision in the pre-design stage. Interpretations of the design criteria can help address the national goals based on quantitative scientific evidence, and on a broader scope, can pave the way for future quantitative studies on the sustainability of urban forms in Egypt, and also in other hot climate zones.

1.6 Thesis outline

This thesis is presented in alternative format; a literature review is first presented, followed by a description of the methodological approaches through the amalgamation of the work presented in two international conferences. The research conducted to address the thesis' objectives is then presented through peer-reviewed journal publications. Each of these journal papers includes a relevant literature review, methodology, analysis and discussion of the results. Since this thesis revolves around the design of urban form on different scales, overlaps might exist as appropriate. Moreover, the selection of the thresholds and the step size of the design parameters was refined from one chapter to the next, based on the results of the preceding one. Figure 1.19 shows the general structure on which the different constituents of this thesis are brought together to achieve its objectives. The following paragraphs summarise each of the following chapters.

Chapter 2 presents a literature review on urban climate, as well as on the thermal and radiative behaviour of the urban system. The Urban heat island, its formation, types and mitigation are then reviewed, followed by a discussion of human thermal comfort. Based on a comparison between the most relevant urban geometry modelling tools, the chapter concludes with the most appropriate tool and thermal comfort index to be used in this research.

Chapter 3 describes the methodological approaches adopted in this thesis, and further explains the simulation workflow. The chapter includes the improvements made to the simulation workflow and its verification against a valid software before and after the improvements.

Chapter 4 investigates the thermal comfort performance of urban canyons with symmetrical and asymmetrical configurations, and links their performance to canyon-scale design parameters. Validation of the simulation workflow against field measurements is presented, along with a detailed description of the equations governing the calculation of comfort indices. The results are discussed with reference to the design regulations of the Egyptian Construction Act, in order to highlight the potential improvements in thermal comfort achieved by using the optimised design thresholds. The chapter concludes with implications for urban design in the form of design guidelines.

Chapter 5 extends the scope to include urban scale design parameters of urban block typologies. As such it adds energy loads to the evaluation criteria as the second objective. An extensive literature review on the impact of urban geometry on urban heat island, thermal comfort and energy consumption is presented. The results highlight the best performing typology, along with its optimum design and density parameters, based on which, design guidelines are deduced.

Chapter 6 revisits the microclimatic and energy performance of urban courtyard blocks through a deliberate passive solar design of a courtyard block's individual buildings in a multi-objective optimisation study. Evolutionary algorithms are introduced to find the optimum solutions, which in turn are compared to the optimum schemes from the literature to highlight the improvements achieved in both objectives, as well as in solar exposure in winter. The chapter concludes with design guidelines inferred from the optimised solutions.

Chapter 7 summarises the studies, reflects on the results in light of the research questions, draws conclusions and recommendations with regards to the aims and objectives of this thesis, highlights the limitations of this study, and makes recommendations for future research.

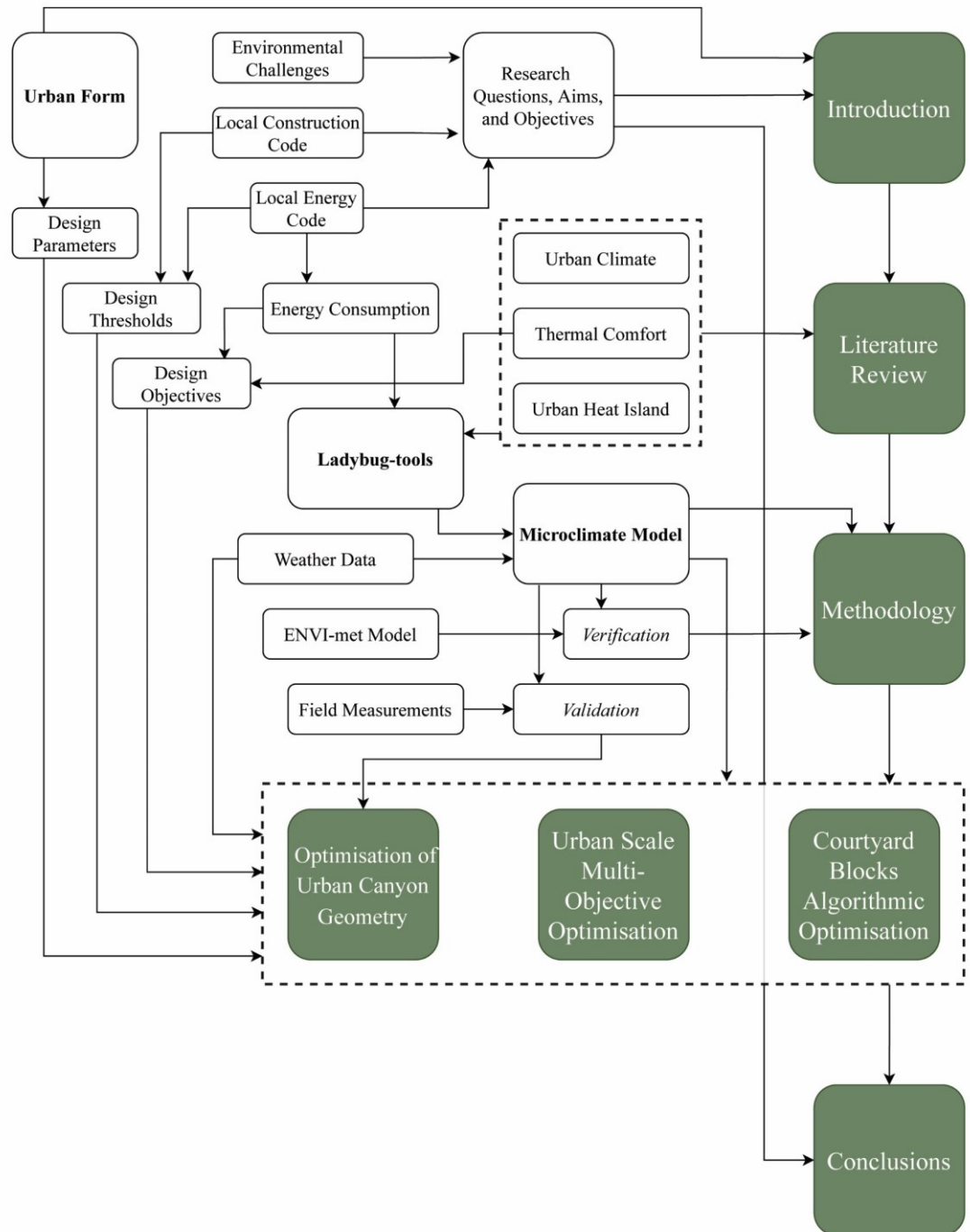


Figure 1.19: General structure of the thesis.

2 Literature review | Climate and the Built Environment

2.1 Preface

This chapter presents the basic knowledge on the built environment and its relationship with both urban climate and human thermal comfort. The chapter starts with a brief description of the urban climate scales, followed by the energy balance of an urban system. Urban Heat Island (UHI) as a city-induced phenomenon is reviewed along with its genesis, types and some aspects of its mitigation. Human thermal comfort, and the most common comfort indices are then discussed, followed by a brief discussion on the human energy balance, as well as the human adaptation in the outdoor environment. Finally, a review of some of the most relevant district-scale climate modelling tools is presented along with a comparison of their capabilities for modelling outdoor thermal comfort and energy demand. By the end of this chapter, the most appropriate thermal comfort index and simulation tool are specified according to the aims and the scope of this thesis.

2.2 Climate structures

The lowest level of the Earth's atmosphere, the troposphere, is the layer containing 75% of the Earth's atmospheric mass and water vapour. Intrinsically, this layer is split into two layers. The upper layer is the free troposphere, in which the rotational friction of the troposphere against the planet surface, and hence the thermal and aerodynamic influence is negligible. The lower is the planetary boundary layer (PBL) which is mainly influenced by the planet surface interactions underneath. PBL varies in depth on a diurnal and seasonal basis, and its height is mainly dependent on the mixing forces driven by the surface. As for the urban areas, increased surface roughness relative to their rural surroundings causes the PBL to be partitioned into an urban boundary layer (UBL) and urban canopy layer (UCL) (Oke *et al.*, 2017). The *boundary layer climates* by Oke (1987) is seen to have well elucidated the vertical and horizontal dissection of the UBL.

Vertically, the UBL, which seemingly takes the shape of a “dome” on top of the city, is formed by four main layers. The UCL which extends from the street level up to the mean height of the roughness elements, i.e. buildings and trees (z_h). The roughness sub-layer (RSL) and is principally formed due to the mechanical turbulence generated as air travels across (normal to) the canyons and produces vortices of different sizes. The height of this layer (z_r) is dependent on the built-up ratio, and ranges between 1.5-4 times the height of the UCL (z_h). RSL is overlain by the inertial sub-layer (ISL), within which the heat and vapour fluxes remain constant. The height of the ISL extends from the RSL to the surface layer, within which air flow is dominated by friction with Earth's surface following a logarithmic wind profile and based on its depth, the UBL is shaped. The different environmental conditions between the shaped UBL and the unhindered rural boundary layer (RBL) are blended in a mixing layer which forms on top of the surface layer and where the atmospheric properties are uniformly mixed by thermal turbulence (due to rising buoyancy-driven thermals), often capped by a temperature inversion (Kershaw, 2017; Oke *et al.*, 2017) (Figure 2.1).

The urban climate varies horizontally and so do the experiments conducted at each scale. In general, the urban climate can be classified into four scales; the microscale which includes the characteristics of buildings and vegetation (up to a kilometre) and is often associated with the UCL; the local-scale which encompasses a set of canyons, extends to several kilometres, and is associated with the ISL; the mesoscale which extends up to tens of kilometres of a city and is associated with

the mixing layer and the UBL; and the macroscale, defining regional climatic boundaries (thousands of kilometres). It can be inferred, therefore, that the UBL formation is a mesoscale phenomenon due to the urban surface roughness, while the UCL is microscale-induced, largely influenced by the wind flow regimes within the urban canyons in addition to other factors as shall be discussed (Fahmy, 2010; Oke *et al.*, 2017).

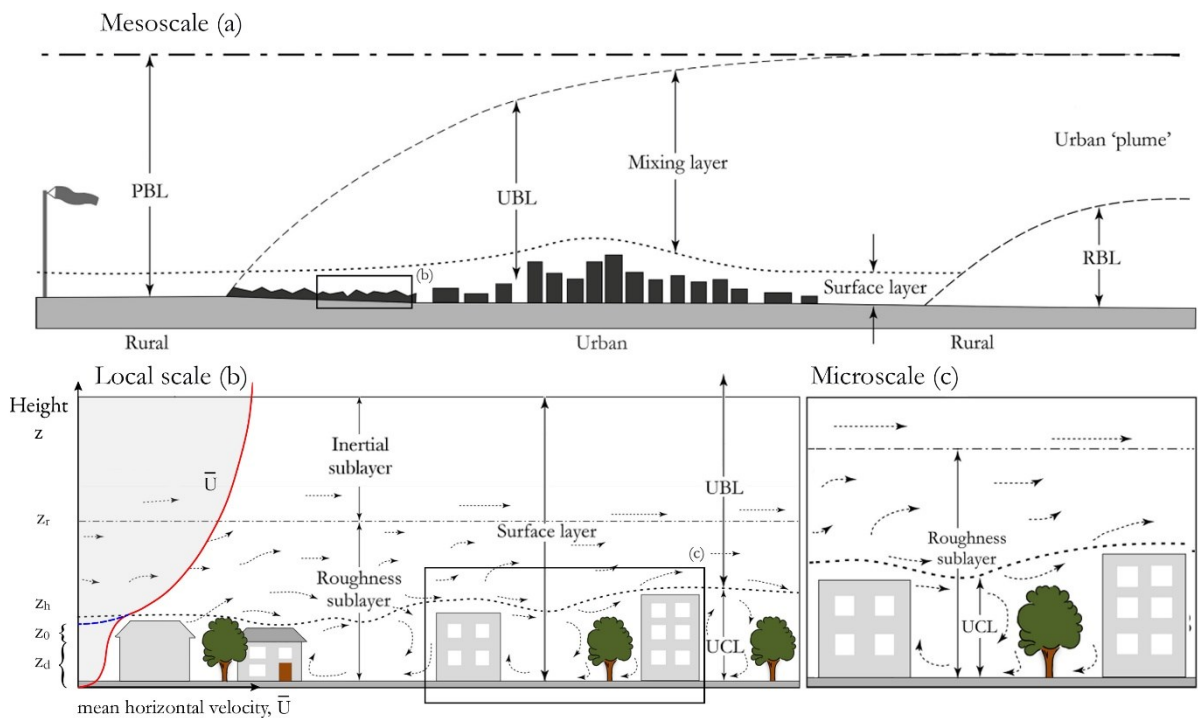


Figure 2.1: PBL vertical structure within (a) mesoscale, (b) local scale, and (c) microscale, with logarithmic urban wind profile superimposed on the left side. Adapted from (Kershaw, 2017).

2.3 Urban energy balance

Urban systems can be characterised by their urban form (land cover, fabric and geometric structure) and their urban function (land-use, industrial and transport processes). Both have an influence on the atmosphere, either physically or thermally. An urban system comprises a combination of facets (surfaces), each of which has different radiative, thermal, moisture and aerodynamic properties. These properties, along with other site-specific geometrical parameters, e.g. height to width ratio of an urban canyon, and environmental parameters, e.g. wind speed/direction and temperatures, create a unique microclimate for such a canyon. Pedestrian level urban climates thus are often described as a “collection of microclimates” (Oke *et al.*, 2017).

As urban surfaces receive solar radiation, the surface system undergoes a heat transfer cycle through which the energy is always conserved (Sundborg, 1951). Radiated surfaces will reflect part of the solar radiation yet absorb the greatest share of it. This absorbed energy in turn is dissipated by an assortment of energy exchange processes (Ali-Toudert, 2005; Fahmy, 2010);

- Radiated as long-wave radiation from the walls, roofs or ground and further transported to the air above by convection as sensible heat flux (Q_H);
- Evaporated as moisture from the ground and transported to the air by convection as latent heat flux (Q_E);
- Conducted to soil underneath (Q_G); or
- Stored within the surface as heat (ΔQ_s).
- Advected horizontally to the neighbouring spaces (ΔQ_A).

In their investigation for a north-south oriented street canyon, Nunez and Oke (1977) presented the rudiments of the energy balance of an urban canyon. The energy balance of an urban facet/surface is represented by the formula:

$$Q^* = Q_H + Q_E + \Delta Q_s \quad \text{Equation 2.1}$$

The net all-wave radiation budget Q^* defines the energy sources or sinks within the climate system, and is determined with regards to the net shortwave (K^*) and net longwave radiation (L^*) during the day, or only the longwave radiation during the night:

Daytime	Night-time
$Q^* = K^* + L^*$	$Q^* = L^*$

The heat transfer through conduction Q_G is often excluded due to its insignificant value over the day. The incoming shortwave ($K \downarrow$) and longwave ($L \downarrow$) radiation varies due to large scale atmospheric and Earth-to-sun geometric properties, while the outgoing shortwave ($K \uparrow$) and longwave ($L \uparrow$) are determined by surface-specific thermal properties, i.e. albedo or emissivity. Within a surface-atmosphere system, since radiation is only one form of energy, the surface system will be in surplus and the atmosphere in equal deficit during the day, and vice versa during night-time. The diurnal course of heat surplus dissipation is largely driven by convection of sensible and latent heat into the lower atmosphere (Figure 2.2-a).

During the night, where nocturnal stability suppresses convection, the surface becomes a net emitter and the heat drain is balanced by Q_G conducted from the warmer soil, and a minimal Q_H and Q_E from the atmosphere to surface (Figure 2.2-b) (Oke *et al.*, 2017). In the same context, orientation was reported as a key determinant of the canyon energy balance. That is shaded surfaces will have lower surface temperature than the air warmed by Q_H from the sunlit surfaces, and hence turbulent fluxes are generated towards the shaded surfaces leading to reduced canyon Q_H and a cross-sectional temperature gradient (Oke, 1987; Ali-Toudert, 2005).

Within an urban ecosystem, the energy balance of each facet is coupled with those of other facets, creating feedback and changes to the energy balance of the entire volume. In this context, Q_F is added to the energy balance equation as the anthropogenic heat produced by the air conditioning, cars and human metabolic heat, whereas the horizontal convective heat exchange (advection transport ΔQ_A) is accounted for when considering adjoining surfaces with dissimilar energy balances, and is dependent on the air flow velocity and the energy available exterior to a single canyon system (Figure 2.2-c). The energy balance equation of the entire volume becomes (Oke *et al.*, 2017):

$$Q^* + Q_F = Q_H + Q_E + \Delta Q_s + \Delta Q_A \quad \text{Equation 2.2}$$

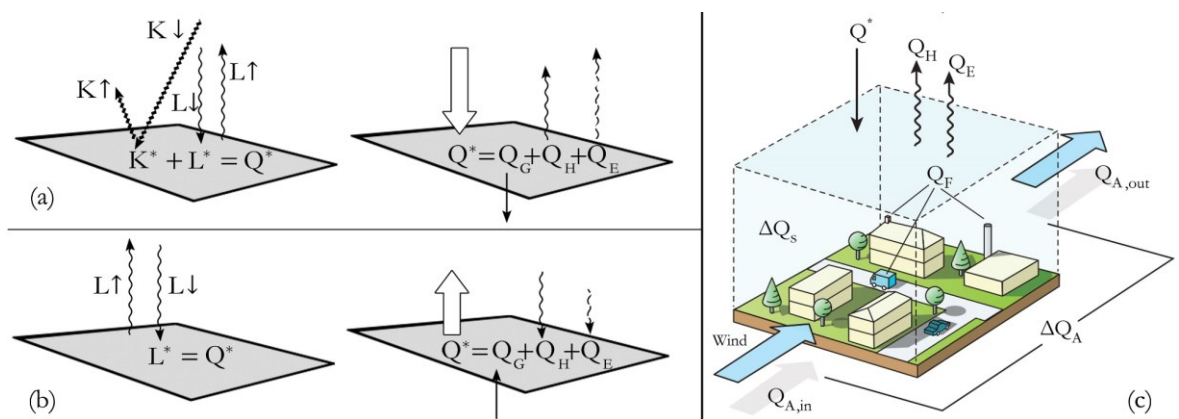


Figure 2.2: Surface energy balance during (a) daytime, and (b) night-time, adapted from (Oke, 1987), and (c) the energy balance of an urban system, adapted from (Oke *et al.*, 2017).

2.4 Urban heat island

The work of Luke Howard is hitherto believed to be the first published research under the rubric of urban heat island (UHI). Howard (1833) sought to study the air temperature variations between the city of London and the abutting suburban communities in Plaistow, Stratford and Tottenham, and found on average 1.5 °C higher temperatures in London. Several studies, accordingly have cascaded to study the phenomenon in North America (Bornstein, 1968), and Europe (Chandler, 1965). Howard's deductions have become the endorsed definition for the UHI intensity ΔT_{u-r} as the air temperature difference between the urban T_u and rural T_r areas:

$$\Delta T_{u-r} = T_u - T_r \quad \text{Equation 2.3}$$

The first prognostic model to predict the UHI intensity via empirical equations is discernibly represented in the study of Oke (1973), who postulated the proportional correlation between ΔT_{u-r} and the population size of a city. Oke (1976) empirically quantified the UHI based on the advection from rural to urban areas as a function of the fetch – the radius of a hypothetically circular city. In that study, he differentiated between the boundary layer UHI which is dependent on the synoptic conditions and the canopy layer UHI which is rather dependent on the geometrical structure and materiality of an urban area.

Kolokotroni and Giridharan (2008) reported a maximum nocturnal UHI intensity in London of 8.6 °C, under clear sky conditions. These findings, when compared to Howard's 1.1 °C and Chandler's 4 °C, indicate that increasing urbanisation, with greater anthropogenic heat exacerbate the effect. Given the uncertainty in the UHI intensity measurements and the empirical estimations, urban climate research since the 1980s scrutinised the physical aspects and the development of viable climatic models.

2.4.1 Heat island energetics

Urban developments are accompanied by the replacement of permeable surfaces with impervious construction materials, reduced vegetation, increased pollution, and relatively narrower canyon ratios. On the notion of canopy layer UHI, Oke (1995) articulated the negative impacts urban areas pose to the microclimate. This includes increased sky long-wave radiation absorption owing to the air pollution, and increased sensible heat storage due to the greater thermal

admittance of building constructions. In addition, evaporative cooling is hampered by impervious paving, while anthropogenic heat from buildings and traffic is evident. Canyon geometry is another important constituent in amplifying short-wave radiation absorption due to recurrent reflections, and attenuating net long-wave radiation loss as well as suppressing the turbulent heat transfer by convection (Oke, 1995; Toparlak *et al.*, 2015) (Figure 2.3).

During the daytime, land surfaces and their near-surface quasi-stable atmospheric layer are heated by the solar radiation. Air mass instability conveys the air parcels (thermals) upward and induces the UBL to increase in depth up to 1.5-2 km in accordance with the growth of the mixed layer underneath. Buoyancy-driven turbulence due to the mass convergence and the surface sensible heat flux Q_H constitute a nearly-stable mixed layer with constant temperature and having thermals aloft as a capping inversion layer. The distinction between the urban and their background rural conditions is well pronounced by the height and depth of that inversion layer.

During the night, land surfaces are cooled by the release of absorbed heat and a downward flux from the shallow layer of stable air. Rural areas exhibit geometrical and surface properties with which heat disposal is expedited and thermals generation is damped, and hence maintain a ground-based inversion layer. On the other hand, urban surfaces continue to emit heat for several hours after sunset, and retain a surface mixed layer with neutral lapse rate and more thermals converging at the top of the UCL, and consequently, constitutes the canopy layer UHI (UHI_{UCL}). In other words, UHI_{UCL} is a nocturnal phenomenon ascribed to the urban-rural cooling differences (Oke, 1982;1995).

After sunrise, rural areas start to warm again with a sharp temperature profile, while cities are warmed relatively slower. However, the greater upward Q_H from the city, combined with increased buoyancy-driven turbulence is sufficient for convective plumes to undercut the base of UBL capping inversion and turn it warmer and thicker than it is in rural parts. Reduced urban evapotranspiration accounts for an extra warming. The difference between the urban and rural capping inversion warming and thickening indicates the boundary layer UHI (UHI_{UBL}), which is less intense than UHI_{UCL} and undergoes insignificant temporal changes.

The influence of UHI_{UCL} extends to the overlying atmosphere. Therefore, UBL is prone to a bi-fold heat convergence effect from both above (capping inversion) and below (UHI_{UCL}), besides the increased aerosols absorption and the anthropogenic heat sources (Figure 2.3).

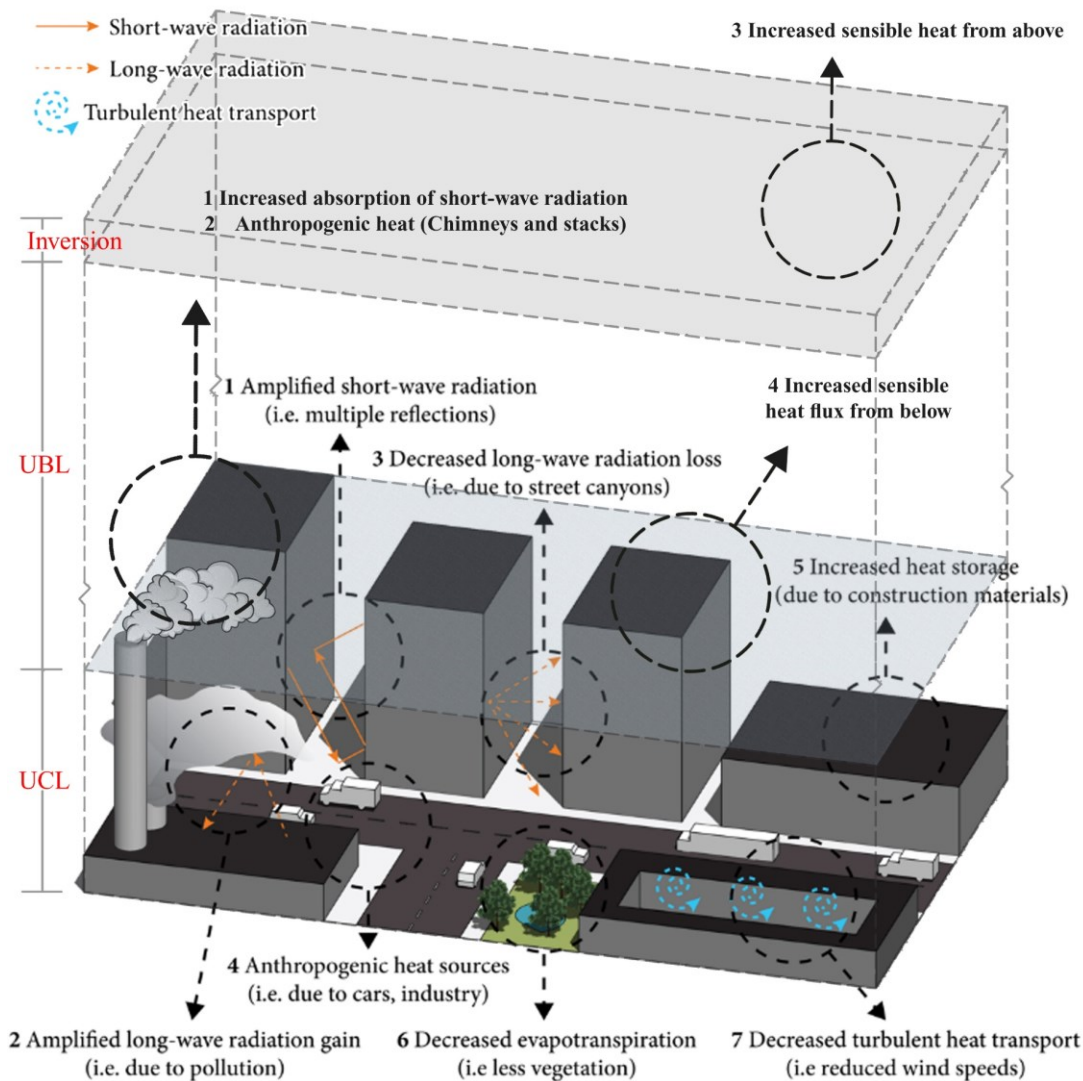


Figure 2.3: Urban heat island causes, adapted from Toparlar *et al.* (2015).

In summary, UHI_{UCL} mechanism is attributed to the “ground inversion,” characterised by the immediate site characteristics (geometry and materials), while UHI_{UBL} is a result of “turbulence inversion,” driven by the advective accumulation of warm air with that occluded from above, and the internal radiative effects. While the study of UHI_{UBL} is interrelated with the synoptic conditions, quality of airflow and pollution dispersion, UHI_{UCL} occurs on the microclimate scale, which is more prominent when human activities and thermal comfort are included (Oke, 1987;1995; Kershaw, 2017).

2.4.2 Heat island types

Although UHI is often denoted by the surface-atmosphere energy exchanges, it also has direct implications on the surface-ground energy balance. Three distinct types of heat islands can be distinguished; atmospheric; surface; and subsurface (Oke, 1995). The former two are, to large extent, governed by the radiative and convective heat exchange, while the latter is dominated by heat conduction. The three types are often discussed separately since their spatial and temporal variation and intensities vary considerably.

2.4.2.1 Atmospheric heat islands

As aforementioned, UHI_{UCL} is of relevance to the human health and comfort, energy consumption, flora and fauna, and moisture availability, and thus receives more attention. That is, most of the studies concerned with the atmospheric UHI are, one way or another, referring to that of the canopy layer. UHI intensity (UHII) has been reported and agreed by many to be as evident in the warmer half of the year, and during the night as it is more influenced by the wind speed and cloud conditions. However, numerous studies investigated UHII under different seasonal variations, while many have scrutinised other factors, for instance, local topography, canyon geometry, and advection from large water bodies (Oke, 1982; Arnfield, 2003; Yow, 2007). Others have examined the UHI impact on water resources (Baker *et al.*, 2004), energy consumption (Akbari & Konopacki, 2005), comfort and health (Zaitchik *et al.*, 2006), precipitation and humidity (Changnon, 2003) and land-sea circulations.

Standing for the observations, higher altitude measurements (UBL) are made by means of stationary towers, or instrumentations on weather balloons, aircrafts, helicopters and drones. On the other hand, lower altitude measurements (UCL) can be monitored by weather stations with fixed-sensors, longitudinal mobile traverses, or a network of fixed-point stations. Mobile traverses and multiple point networks are more effective than single point stations, as they transcend the barrier of site-specific characteristics. Nonetheless, mobile traverses are limited by the distance travelled and the rugged areas, whereas networks are constrained by the infrastructure cost. By and large, caution should be taken when considering the site selection, instrument exposure, and potential anthropogenic pollution (Oke, 2006; Yow, 2007).

2.4.2.2 Surface heat islands

Urban modulation of surface energy balance occurs due to reduced evaporative and convective cooling, and increase heat storage within the canopy layer, and is responsible for the urban-rural gradient of surface energy exchange (Morris *et al.*, 2017; Chakraborty & Lee, 2019). Surface UHI (SUHI) is typically delineated in terms of their intensity (SUHII), represented by the land surface temperature (LST) difference between urban and rural areas, which in turn is correlated to several geospatial aspects. On the annual cycles, SUHII was reported to be similar to that within the canopy, albeit possesses different diurnal and seasonal patterns (Chakraborty & Lee, 2019). In that context, urban centres in Washington were reported to exhibit 10 °C higher surface temperatures than suburban communities (Thanh Hoan *et al.*, 2018). The LST can be obtained by stationary or mobile measurements, however, the uneven distribution of weather stations curtails their potential to represent the heterogeneity of LST spatial variation. Furthermore, temperatures recorded at the rural stations are influenced by the advection from urban centres, thus the definition of urban-rural boundary and the consideration of scale in SUHI quantification are imperative, where the UHI footprint may exceed that of the city (Chakraborty & Lee, 2019).

Instead, LST are widely retrieved from satellite remote sensing, with some uncertainties notwithstanding, due to the scarcity of chronological cloud-free images, and the absence of urban surfaces' emissivity data. Temporally aggregated data was proposed as a compromise for the former. Moreover, LST derived from remote sensing remains questionable due the uncertainty of the correlation between land surface properties and the LST. By utilising a Geographical Weighted Regression (GWR) method, Zhao *et al.* (2018) concluded that LST is strongly correlated to the land use/land cover (LULC) distribution and, to some extent, to the surface elevation. Lai *et al.* (2018) utilised a quality control-informed MODIS LST to depict the SUHII variations between seven megacities in China, and found annual mean SUHII differences of more than 5 K, most evident during the daytime and within the extreme seasons. Moreover, vegetation was found to play a key role in the seasonal variations of SUHI and could attain -0.94 K lower LST from rural surroundings (Chakraborty & Lee, 2019).

2.4.2.3 Subsurface heat islands

Subsurface UHI (SubUHI) typically occurs at three levels; very deep (>100m); deep (10-100m); and shallow (0-10m), and is influenced by the temporal variations of surface temperature over a century, a decade and a year, respectively. The phenomenon was recorded and well documented in several countries, are among them Japan, USA, Canada, Germany and the UK (Zhu *et al.*, 2015). Temperature anomalies are driven not only by the conductive heat flux from buildings, underground basements and subway tunnels, but also sewage networks, uninsulated heating pipes, anthropogenic geothermal processes, and increased ground water temperatures (GWT) (Bidarmaghz *et al.*, 2020). The former effect typically occurs within the urban hot spots where higher ground surface temperatures due to altering land covers, human activities and the atmospheric concentrations, exacerbate the effect. Menberg *et al.* (2013) reported the monthly ground conductive (Q_G) heat flux under urban areas ranges from -10 to 20 W/m² depending on the soil conductivity. Ground temperature increase due to subway networks in London was reported to range between 4-7 °C.

Meanwhile, the process of heat loss to the ground water reservoirs was found to be similar to that of building facades to the surrounding air, nonetheless, the relationship is reciprocal. In other words, GWT were reported to reach 5 K higher, and to affect the chemical and biological properties of water and hence affect the quality, filtration and purification of water, while, on the other hand, higher GWT exhibits advantages for microbiological remediation and benefits the geothermal potential, depending on the depth of water table and the temperature. The shallower the water table and the higher the GWT, the lower the heat flux becomes. Moreover, SubUHI intensity within deep layers gives insights about the surface UHI. While ground surface temperatures could be inferred from deep borehole temperature deviations, water table depths can imply the distribution of subsurface temperature gradients. Furthermore, the applicability of assessing SubUHI using satellite remote sensing at certain depths is proportional to the availability of annual data cycles and thus the deeper the layer of interest is located, the older the datasets required (Zhan *et al.*, 2014).

2.4.3 UHI Mitigation

2.4.3.1 Urban geometry

Urban geometry can play a significant role in mitigating the UHI through modification to the net radiation balance, as well as the convective heat exchange. As opposing terms, the key processes are obstructing solar radiation (shading), and reflecting shortwave and longwave radiation (trapping), where the net result of which process becomes dominant, depends on the availability of incoming radiation and the timing of the nocturnal UHI formation, and determines the canopy layer temperatures. An urban canyon with a high aspect ratio (H/W) experiences a “shading effect” on both its buildings and the street surface. This effect can reduce daytime temperatures to a limit where they can be lower than surrounding urban and even rural areas. The trapping effect, however, contributes to the longwave radiation increase at night, thereby to the nocturnal UHI (Oke, 1981;1988; Steemers *et al.*, 1998). Theeuwes *et al.* (2014) found that the shading effect extends to the start of the night, while that of the trapping typically occurs later in the night. Compact urban forms with low SVF and high H/W are characterised by reduced solar exposure and lower wind speeds, thus having greater thermal comfort during the day, but lower cooling rates during the night (Holmer, 1992; Bourbia & Boucheriba, 2010). Daytime cooling, however, was found to exceed night-time warming in hot-arid (Johansson, 2006) and hot-humid (Johansson & Emmanuel, 2006) climates. Moreover, Giannopoulou *et al.* (2010) found that higher wind speeds reduce cooling rates if the ambient air temperatures are high, due to substantial convective heating in the canyon. Also, a parametric study by Andreou (2013) showed a difference in thermal stress of 10 °C between shaded and unshaded areas, while the differences between 1 m/s and 3.5 m/s wind speeds were 6 °C in direct solar radiation conditions, and only 1 °C in shaded conditions.

In tropical regions, both shading and ventilation are equally important. Although courtyard blocks have a great potential to shade the urban environment, in tropical regions, they should be connected to the street, with permanent openings in the walls to promote ventilation (Giridharan & Emmanuel, 2018). Rajagopalan *et al.* (2014) found that varying building heights with scattered towers in the windward side of the street yielded the best ventilation – a conclusion also confirmed by Sharmin *et al.* (2017).

In the same context, Emmanuel (1993) proposed the “shadow umbrella” which depends on the positioning of shorter buildings on the north-east directions, and taller buildings on the south-west directions to shade the outdoor spaces and the shorter buildings, and placing water ponds in the centre to cool the air on the main (southwestern) ventilation path. Moreover, tall buildings scattered within the urban texture increase the aerodynamic roughness, thus increase mechanical turbulence and vertical transport, necessary for the dispersion of pollutants associated with compact cities (Ratti *et al.*, 2006).

A study by Charalampopoulos *et al.* (2013) in Athens, Greece, found a significant correlation between higher SVF and the frequency of heat stress. A parametric study by Hu *et al.* (2016) used the SVF as an indicator to manipulate building forms to mitigate the UHI, concluding that increasing density (lowering SVF) in the centre, and keeping lower densities on the peripheries corresponded to the best scenarios of different FAR's. Sharmin *et al.* (2017) and Qaid *et al.* (2018), on the other hand, found that SVF alone cannot explain the irregularities of dense urban forms, and hence cannot indicate the thermal performance of urban canyons.

Orientation is another key aspect of determining the solar exposure duration, the area of radiated surfaces, thus the amount of heat gains/losses. This implies a direct influence on both thermal stress in outdoor spaces, and cooling/heating loads in buildings, being this influence dependent on the season, latitude, and background conditions. The relationship between orientation, H/W and the thermal and energy performance has not been systematically investigated in different climates. In hot-arid regions, North-South (NS) canyons provide the greatest shade during the day, and hence maintain better thermal comfort conditions (Bourbia & Awbi, 2004). The effect of orientation is more pronounced in deep canyons ($H/W = 2$), but the effect diminishes in very deep canyons ($H/W > 3$) (Ali-Toudert & Mayer, 2006). Krüger *et al.* (2010) found that variations in cooling loads corresponding to H/W changes are more significant in NS canyons, and that cooling loads are 40% less in deep East-West (EW) canyons. The same study recommended using lower H/W ratios for East-West (EW) orientations in winter.

Similar implications have been drawn in temperate climates (Elnahas, 2003; Ali-Toudert & Mayer, 2007b; Taleghani *et al.*, 2013; Allegrini *et al.*, 2016). In Mediterranean climates, southern side of EW deep canyons provides lower thermal stress in summer mid-day, while intermediate orientations (NE-SW and NW-SE)

offer better conditions in winter (Chatzidimitriou & Yannas, 2017; Nouri *et al.*, 2017). Vartholomaios (2017) showed that lower H/W ratios are better for NS oriented perimeter blocks, but not NS slabs, and that EW elongated perimeter blocks yielded the best annual energy consumption. In hot-humid regions, where ventilation is most needed, NE-SW asymmetrical canyons with higher buildings facing NW were recommended for lower daytime air temperatures and night-time UHI (Qaid & Ossen, 2015). Also, a study in Campinas, Brazil recommended EW and NE-SW orientations for shallow and deep canyons, respectively (Abreu-Harbich *et al.*, 2014).

On an urban scale, the density parameters, FAR, BCR and building heights (see section 1.3), have been used to explain the spatial and seasonal differences of UHI and energy consumption. For a constant FAR, increasing BCR (decreasing building heights, but increasing H/W ratio) decreases the area of exposed vertical surfaces, and hence reduces solar gains and heat loss through building envelope. Urban morphology can lead to a difference in heating energy demand of a factor of six, a result found by Rode *et al.* (2014), when they reiterated the abovementioned relationship, and advocated high-rise apartments and high-density urban block typologies. Salvati *et al.* (2017), on the other hand, showed that urban textures with BCR greater than 40% conduce an UHI intensity which compensates for reduced solar gains in winter, thereby consume lower annual energy than rural areas. In another study, they found that winter UHI increased in horizontally dense areas, whereas summer UHI was higher in vertically dense areas (Salvati *et al.*, 2019). Wei *et al.* (2016) demonstrated that mid-day maximum ambient air temperatures increased with increasing BCR up to a turning point (25%), then constantly decreased due to shading; the opposite was true for maximum radiant temperatures at a turning point of 55%, after which a constant increase was evident due to trapping. The same study concluded that higher BCR yields lower daily average air and radiant temperatures. Contrarily, increasing FAR was found to reduce annual energy consumption for heating and cooling down to a certain level, depending on BCR, then increases it. The transition appeared to occur abruptly, and correspond to significant changes in energy loads for lower BCR's, as opposed to a smooth transition and insignificant changes for higher BCR's (Quan *et al.*, 2014).

2.4.3.2 Vegetation and pavements

Abundant studies investigated the role of vegetation and pavements to mitigate the UHI within the UCL. Vegetation possesses a great potential to alleviate higher temperatures, besides other benefits, such as pollution reduction and energy savings in addition to their aesthetic values. In essence, vegetation features three prominent characteristics which regulate the microclimate, namely evapotranspiration, shading, and wind blockage. Rijal *et al.* (2010) found that large-scale green areas can reduce surface and air temperatures by up to 20 °C and 4 °C, respectively. Abundant studies have asserted that canyon green-to-built-up ratio is a key determinant of the vegetation efficacy, as are the trees' geometrical aspects and orientation (Dimoudi & Nikolopoulou, 2003). As reported by Akbari (2009), urban trees, when properly located, have the potential to reduce cooling energy loads on summer days by almost 10-50%. Shashua-Bar and Hoffman (2000) studied the evaporative cooling of trees in eleven sites and found that, on average, 80% of the cooling effect is attributed to shading. Pollution reduction has also been investigated by Tong *et al.* (2016), in terms of the aerosol concentrations. The evaporative cooling is governed by the evapotranspiration process, principally due to the soil-tree-air vapour circulation, where the process is dependent on the specific humidity and the stomatal resistance of leaves.

Within a tree "realm", water evaporates into the air, increasing latent heat in preference to sensible heat flux thereby attenuating the surrounding air temperatures (Figure 2.4). Moreover, the relatively lower density of water vapour creates vertical transport of heat and air. This effect can remove pollutants and heat from a street canyon and in some cases disrupt the atmospheric boundary layer effects above the city (Kershaw, 2017).

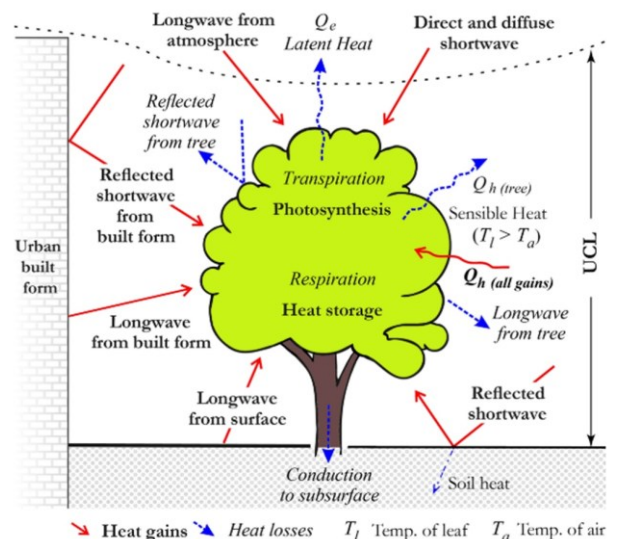


Figure 2.4: Heat exchange between a tree and urban form (Kershaw, 2017).

The tree canopy parameters, leaf area index (LAI) and leaf area density (LAD) govern the shading efficiency (Fahmy, 2010; Shahidan, 2015). The study by Shahidan (2015) has advocated the use of clustered urban trees with higher LAD, i.e. *Ficus benjamina*, to maximise both shading and evapotranspiration.

Typical cities possess nearly 20-40% of their urban fabric as pavements. Residential areas, on average have 35% of tarmac and concrete which retain higher surface temperatures, thereby increasing UHI (Akbari *et al.*, 1999). Cool pavements are acknowledged for their relatively higher solar reflectivity and thermal emissivity as well as their potential to foster water evaporation (USEPA, 2020). The energy balance of pavements is governed by their reflectivity, emissivity, thermal absorptivity and conductivity, as well as surface roughness. Of these properties, surface reflectivity and long-wave emissivity were found to be the dominant factors within the surface energy balance (Shi & Zhang, 2011). Reflective pavements are considered vital for mitigating the UHI, particularly in highly exposed sites (Santamouris, 2013). Besides their capability of reducing both the surface and ambient air temperatures, they have the potential to curtail CO₂ emissions, reduce murk, and increase illumination. Also, they can retain their features for up to three decades and thus offset their higher initial costs (Akbari *et al.*, 2012).

Reflectivity is represented by the surface albedo, which is defined as “the ratio between the reflected energy and the incident energy over a unit area” and is dependent on the colour. Kyriakodis and Santamouris (2017) concluded that cooled asphalt and concrete registered, respectively, 7.5 and 6.1 °C lower surface temperatures. Air temperature reductions, however, are not as potent as are the surface temperatures’. Santamouris *et al.* (2012) found 1.9 and 7 °C reduction in air and surface temperature, respectively.

Thermochromic pigments is another technique, where mixed pavements change their albedo relative to the surface temperatures. Hu and Yu (2013) reported a temperature reduction of an asphalt mixture by almost 6 °C in hot and 3 °C in cold periods. Moreover, Phase Changing Materials (PCM) when embedded within concrete slabs, were found to reduce temperatures by 3-8 °C during extreme conditions (Karlessi *et al.*, 2009; Qin, 2015). Fahmy *et al.* (2018) found that the combined effect of using green roofs, tree lines, and high reflectivity pavements, in Cairo, Egypt, can reduce air and radiant temperatures by up to 2.5 and 1.85 °C, respectively.

2.5 Thermal comfort

Thermal comfort is defined as “the condition of mind which expresses satisfaction with the thermal environment.” (ASHRAE, 2017b). Thermal sensation in the outdoor environment is transient and is often described by the subjective expression of sensation on a scale from hot to cold conditions. Early endeavours to portray a comfort zone date back to the 1920s with the development of the Effective Temperature (ET) by Houghton and Yagloglou (1923), later found by the same authors to overestimate the effect of humidity. The work by Vernon and Warner (1932) was the first to add the effect of radiation, substituting dry bulb temperature in their Corrected Effective Temperature (CET). Several indices with linear equation approach have followed, for instance the Wet Bulb Globe Temperature (WBGT), Givoni’s Index of Thermal Stress (ITS), among others. None of these indices, however, consider the effect of metabolic rate and clothing. Gagge (1936) was the first to propose a generalized energy balance model, which is still used in today’s human thermoregulation studies (Auliciems & Szokolay, 2007). In 1971, Gagge presented a new Effective Temperature (ET*), followed by the new Standard Effective Temperature (SET*) based on his two-node model – a thermal model which uses separate energy balance equations for the core and the skin (Gagge *et al.*, 1972).

Concomitantly, Fanger (1970) postulated that human thermal comfort is a response to the combination of six basic parameters; air temperature, radiant temperature, relative humidity, air velocity, metabolism and clothing insulation (Auliciems & Szokolay, 2007), and presented the Predicted Mean Vote (PMV) and the Predicted Percentage of Dissatisfied (PPD). Fanger’s model was empirically derived from sensation votes of ~1500 subjects in a climate chamber based on a one-node model. Gagge *et al.* (1986) argued that PMV underestimates the effects of humidity and is only suitable for steady-state thermal environments close to neutrality. They proposed a new PMV* which is identical to the PMV, albeit substituting SET* for the operative temperature (t_o) in Fanger’s equation. Similar to Gagge’s model, the Munich Energy-balance Model for Individuals (MEMI) is a two-node model applied in the Physiologically Equivalent Temperature (PET) (Matzarakis & Amelung, 2008). In a standardised indoor environment, the human energy budget is balanced, with different climatic parameters than those within outdoor conditions. Having the same core and skin temperatures in the outdoor conditions, PET equals the air temperature at which the energy budget is balanced

in a standardised environment for a standardised person (see Höpfe, 1999; Matzarakis *et al.*, 1999).

2.5.1 Human energy balance

The internal temperature of the human body should be maintained at around 37 °C, whilst that of the skin varies between 31 and 34 °C, and hence there is a heat balance between the body and its environment. Typically, the human body produces heat from metabolic processes, with an average of 100 W, but also can reach up to over 700 W in heavy work. The heat generation within the body surpasses the amount of heat transferred into it, and this surplus must be balanced by an assortment of heat dissipation processes or else the body temperature will rise. This implies maintaining a dynamic balance rather than being in a steady state condition. Although there are many forms to describe the heat balance equation, the underlying concept involves the same three types of processes; heat generation, heat transfer, and heat storage. The term (M - W) describes the difference between the metabolic heat production (M) and the amount exerted in mechanical work (W). The difference is always positive and thus in some formulae is only represented by (M). Heat transfer normally occurs due to convection (C), radiation (R), evaporation (E), or conduction (K), with the latter being always negligible (Figure 2.5). The amount of heat storage indicates whether the body temperature will rise (net heat gain), fall (net heat loss), or remain constant (S = 0). The conceptual equation for balanced conditions is (Parsons, 2006; Szokolay, 2008):

$$M - W - E - R - C - K = 0 \quad \text{Equation 2.4}$$

ASHRAE (2017b), provides the heat balance equation in terms of heat production within the body, heat loss from the skin, and heat loss from respiration as follows:

$$M - W = Q_{sk} + Q_{res} = (C + R + E_{sk}) + (C_{res} + E_{res}) \quad \text{Equation 2.5}$$

Where Q_{sk} is the heat loss from the skin through convection, radiation and evaporation (or diffusion) (E_{sk}), while Q_{res} is the heat loss from respiration through convection (C_{res}) and evaporation (E_{res}). All terms are in W/m² of the total body surface area (A_D), which is estimated from the formula by DuBois (1916) to standardise over people with different sizes as follows:

$$A_D = 0.202 \times \text{Weight}^{0.425} \times \text{Height}^{0.725} \quad \text{Equation 2.6}$$

For simplification, a value of 1.8 m² is often used, representative of a 70 kg and 1.73 m individual. Organisms of the same shape yet different size have different heat transfer coefficients, though this difference is often considered systematic and unimportant (Parsons, 2006). Metabolic rate is a function of activity level, and is measured by *met*, which corresponds to 58.2 W/m², with an average metabolic rate of 100 W/m² during light work. Clothing is the thermal insulation, first proposed by Gagge *et al.* (1941), and is measured by *clo* which equals a thermal resistance of 0.155 m².K/W over the whole body surface, and corresponds to a 3-piece business suit, with cotton underwear (Szokolay, 2008). The sensible heat loss (C + R) can be estimated with reference to the operative temperature (t_o), skin temperature (t_{sk}), intrinsic clothing resistance (R_{cl}) and clothing factor¹ (f_{cl}) and the combined heat transfer coefficient (h) as follows (ASHRAE, 2017b):

$$C + R = \frac{(t_{sk} - t_o)}{\left(R_{cl} + \frac{1}{f_{cl} \times h}\right)} \quad \text{Equation 2.7}$$

Both the operative temperature and the combined heat transfer coefficient are calculated in terms of the convective and radiative heat transfer coefficients. Nishi and Gagge (1970) gave the expression for the convective heat transfer coefficient (h_c) for a person walking at speed (V) as:

$$h_c = 8.6 \times V^{0.53} \quad \text{Equation 2.8}$$

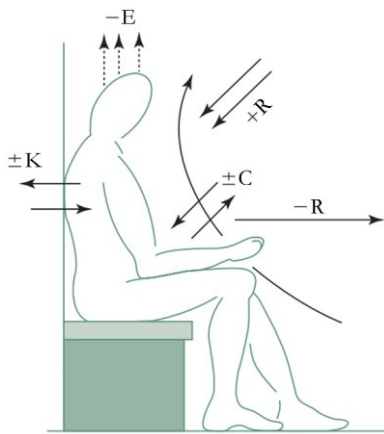
The radiative heat transfer coefficient (h_r) can be estimated in terms of the effective fraction of the body exposed to radiation (f_{eff}), temperature of the clothed body (t_{cl}), and the mean radiant temperature (MRT) as follows (ASHRAE, 2017b):

$$h_r = 4\varepsilon\sigma \times f_{eff} \left[273.2 + \frac{t_{cl} + MRT}{2}\right]^3 \quad \text{Equation 2.9}$$

ε is the emissivity of the human body, which equals the absorption coefficient for long-wave radiation (standard = 0.95), and σ is the Stephan Boltzmann constant (5.667×10^{-8} W/m²K⁴). The effective fraction (f_{eff}) is a function of the Dubois ratio described above and the effective radiation area (A_r). The latter is a function of the projected area - the cross-sectional area of the body normal to the solar rays (A_p), and the projected area factor (f_p) - the ratio between (A_p) and the effective area (A_{eff}). The projected area (A_p) can be estimated as (Underwood & Ward, 1966):

¹ Clothing factor is the ratio between the clothed body surface and the nude body surface area, and it differs based on the clothing ensembles worn in different regions. Details in (ASHRAE, 2017b).

$$A_p = 0.043 \sin\theta_s + 2.997 \cos\theta_s \sqrt{(0.02133 \cos^2\phi + 0.0091 \sin^2\phi)} \quad \text{Equation 2.10}$$



Where θ_s and ϕ are the solar altitude and azimuth angles, respectively (Figure 2.6). Fanger (1970) empirically derived the values for f_p for both male and female objects. f_p ranged between 0.15 and 0.33 for a seated person, and 0.08 and 0.35 for a standing person. Evaporative heat loss from the skin (E_{sk}) is estimated with regards to the water vapour pressure in the air and at the skin, the evaporative resistance of clothing, evaporative heat transfer coefficient and

Figure 2.5: Heat exchanges of the skin wittedness. human body (Szokolay, 2008).

Heat loss from respiration, both convective and evaporative, is estimated with regards to the metabolic heat production, ambient air temperature and its water vapour pressure (details in Parsons, 2006).

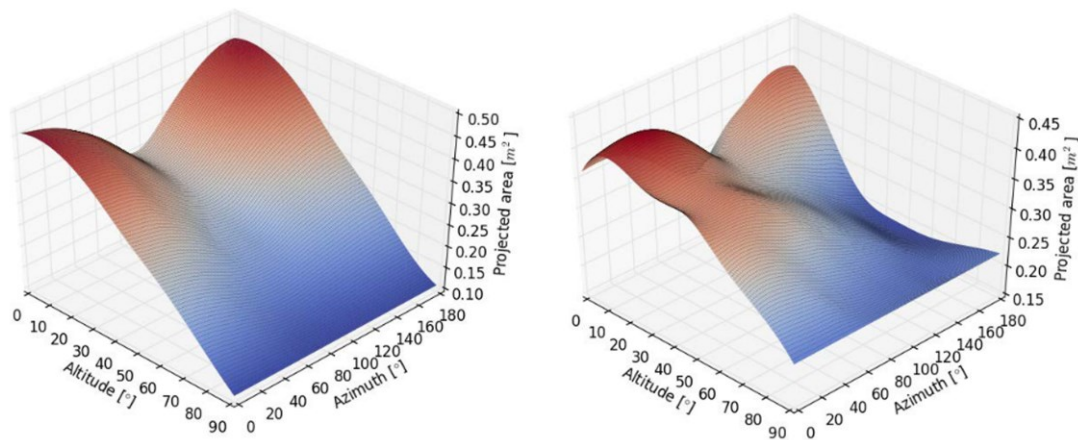


Figure 2.6: Projected area exposed (A_p) as a function of solar altitude and azimuth for standing (left) and seated (right) postures. Azimuth zero is facing the sun (Arens *et al.*, 2015).

2.5.2 Outdoor thermal comfort

Human comfort in the outdoor environment is transient due to the variations in temperatures, air flow and solar radiation intensities over time, making subjective responses to outdoor environments disparate from those to indoor spaces. Human tolerance of temperature outdoors is extended to a diversity of thermal conditions (Nikolopoulou *et al.*, 2001).

Nikolopoulou and Steemers (2003) found that microclimatic parameters contributes only 50% of the variations between subjective and objective evaluation, the rest is due to psychological adaptation. Early adaptive models to evaluate indoor thermal environments were proposed by Humphreys (1975) and Auliciems (1981). The study of de-Dear and Brager (1998) formed the basis of adaptive models sponsored by ASHRAE-55 and ISO 7730. Notwithstanding, adaptive models have not yet been developed for outdoor comfort. Nikolopoulou and Steemers (2003) have categorised the human body adaptation to the thermal environment as; physiological, physical and psychological adaptation.

The term physiological refers to the mechanism of physiologically acclimatising to the stimulus. Physical adaptation indicates both interactive adaptation, e.g. to open a window or a parasol, and/or reactive adaptation, to change position and posture or activity level for instance. Psychological adaptation is not proportional to the magnitude of the stimulus, but rather as a cognitive process is dependent on such psychological factors as one's short-term *experience* and its associated *expectations*, *naturalness* of the incident stimuli, along with people's *control* over their choices, i.e. to stay in sunny or shaded spaces. Other factors include the *time of exposure* and *environmental stimulation* - people's perception of fresh air, the sun and wind as invigorating stimulation for their senses.

In that sense, neutral sensation may differ drastically from one climatic region to another (Coccolo *et al.*, 2016). Moreover, individual characteristics such as social, cultural, and idiosyncratic hallmarks have a similar impact on subjective sensation as does the space design. In other words, the subjective thermal perception for different people will vary, even when exposed to the same physical conditions (Pearlmutter *et al.*, 2014).

For outdoor spaces, MRT is almost the most significant variable governing the human thermal comfort and energy balance. MRT is defined as the “the uniform temperature of an imaginary enclosure in which radiant heat transfer from the human body is equal to those in the actual non-uniform enclosure” (BSI, 2001).

MRT accounts for all short-wave, i.e. direct, diffused and reflected solar radiation as well as longwave radiation from the atmosphere and urban surfaces to which a human body is exposed (Figure 2.7). Moreover, within dense urban environments, where increased longwave fluxes from urban surfaces are evident as are the climate interdependencies, MRT becomes imperative for analysing pedestrians' thermal comfort.

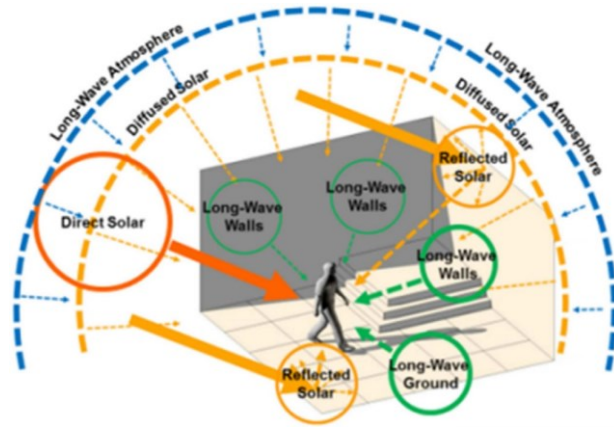


Figure 2.7: Components of MRT in an urban environment (Huang *et al.*, 2014).

MRT can be measured empirically using the globe thermometer, two-sphere radiometer, constant air temperature sensor, surrounding surfaces temperatures, or the plane radiant temperature (BSI, 2001), or modelled computationally (Lindberg *et al.*, 2016; Bruse, 2020) which is less time consuming. The majority of computational models for estimating MRT consider only the radiative heat transfer between the human body and the surrounding environment, since they account for almost two thirds of the net heat exchange (Folk Jr, 1974; Huang *et al.*, 2014). MRT can be estimated using the globe thermometer method using the following formula (Thorsson *et al.*, 2007):

$$\text{MRT} = \sqrt[4]{(T_g + 273)^4 + \frac{1.1 \times 10^8 \times v^{0.6}}{\epsilon_g \times D^{0.4}} \times (T_g - T_a) - 273} \quad \text{Equation 2.11}$$

Where T_g is the globe temperature, T_a is the ambient temperature, v is the air speed, ϵ_g and D are the globe emissivity and diameter, respectively.

Typically, human thermoregulatory models are classified into passive and active systems. Passive systems consider the heat exchange between the body and the environment, while active systems consider the human body's thermoregulatory processes necessary for thermal balance, e.g. responses to vasodilation, vasoconstriction, sweating and shivering (Binarti *et al.*, 2020). Fiala *et al.* (2001) built a multi-node model, upon the limitations of dual-node models as not considering the transient conditions of skin blood flow, in which he applied both active and passive systems (Figure 2.8).

The model includes local heat gains and losses from the body by forced and free convection, solar radiation, long-wave radiation, moisture evaporation from the skin and clothing. The passive system is divided into 15 spherical elements; each element comprises 7 different tissue materials, where the skin is accounted for as two separate inner and outer layers. Blood circulation and heat exchange are calculated using a finite element method. The active system calculates the thermoregulatory responses based on the regression analysis of the physiological response of subjects under discomfort (Fiala *et al.*, 2012; Binarti *et al.*, 2020). The model was extensively validated with measured data showing good agreement for thermoregulatory responses, mean and local skin and body core temperatures.

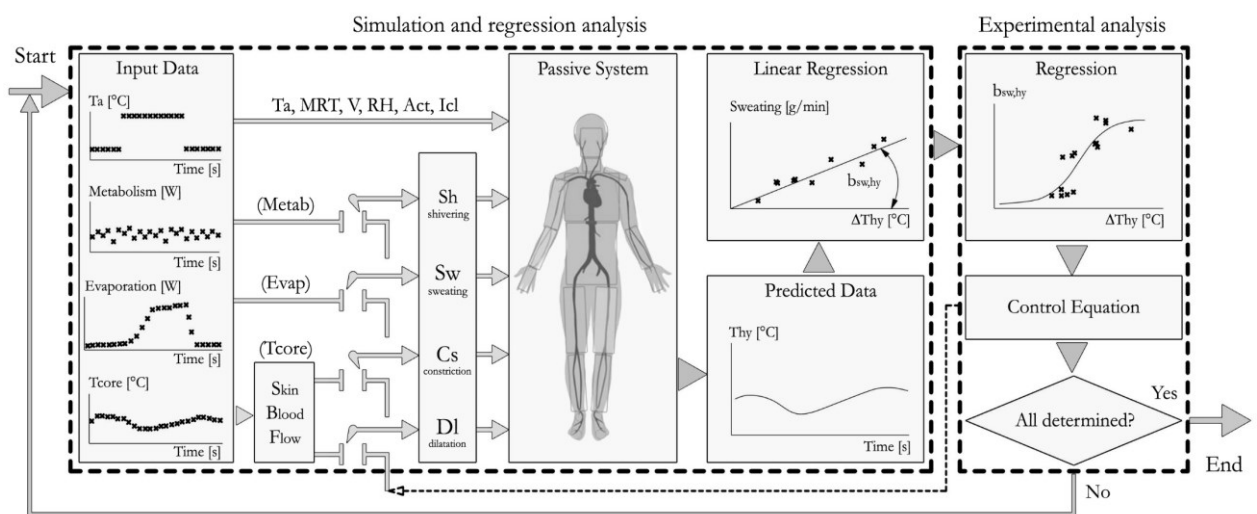


Figure 2.8: The thermo-physiological model, adapted from (Fiala *et al.*, 2001)

The Universal Thermal Climate Index (UTCI) was developed based on Fiala's model as well as an advanced clothing model which accounts for the adaptation and distribution of clothing (Havenith *et al.*, 2012). UTCI indicates the air temperature in a reference environment which elicits a similar physiological response to that of the actual environment (Bröde *et al.*, 2012). Reference conditions included a person walking at a speed of 4 km/h and metabolic heat production of 135 W/m²; wind speed is 0.5 m/s at 10 m above ground level; radiant temperature is equal to the air temperature; relative humidity is at 50%, capped at a vapour pressure of 20 hPa for air temperature > 29 °C. UTCI was endorsed by the European Cooperation in Science and Technology (COST), the International Society of Biometeorology (ISB), and the World Meteorological Organization (WMO) as the most suitable thermal comfort index for outdoor conditions (Coccolo *et al.*, 2016).

Furthermore, UTCI has been applied in all Köppen-Geiger climate regions and has been validated against monitored data and other thermal indices. Further, UTCI presents a detailed representation of thermal sensation for the neutral as well as the extreme cold and hot conditions (Blazejczyk *et al.*, 2012). As a function of air temperature (T_a), radiation (MRT), wind speed (V), and humidity represented as vapour pressure (P_a), the general equation for UTCI is in Equation 2.12, while the heat exchange is described in the heat balance equation in Equation 2.13 as follows (Jendritzky *et al.*, 2012):

$$\text{UTCI}(T_a, \text{MRT}, V, P_a) = T_a + \text{Offset}(T_a, \text{MRT}, V, P_a) \quad \text{Equation 2.12}$$

$$M - W - [Q_H(T_a, V) + Q^*(\text{MRT})] - [Q_L(P_a, V) + Q_{\text{SW}}(P_a, V)] - Q_{\text{Re}}(T_a, P_a) \pm S = 0 \quad \text{Equation 2.13}$$

Where Q^* is the radiation budget, Q_H is the turbulent flux of sensible heat, Q_L and Q_{SW} are turbulent fluxes of latent heat due to water vapour diffusion through the skin and due to sweat evaporation, respectively. Q_{Re} is the combined sensible and latent heat flux through respiration.

Over the last century, 165 thermal comfort indices have been developed (De Freitas & Grigorieva, 2017), however, the most commonly used indices are the PMV (Fanger, 1970; ISO, 2005), PET (Höppe, 1999), and the UTCI (Bröde *et al.*, 2012). These indices provide the full range of thermal sensation, up to ten categories, in hot and cold conditions. Jendritzky (1990) transformed Fanger's PMV into a Perceived Temperature (PT) for outdoor conditions, through the introduction of ΔPMV , which parametrises the radiant fluxes (Klima-Michel model), based on Gagge's two-node model used in PMV*. Although both PT and UTCI consider the adaptation of clothing, UTCI additionally accounts for reductions of clothing insulation (I_{cl}) due to wind and the movement of the person. Hence, in case of higher wind speeds, I_{cl} can strongly differ in the actual and the reference environment (Staiger *et al.*, 2012). Table 2.1 shows the main characteristics as well as the thermal scale of the three indices.

Table 2.1: Main characteristics and thermal scale of selected thermal comfort indices

Criteria	PT (°C) (Jendritzky, 1990)	PET (°C) (Höppe, 1999)	UTCI (°C) (Bröde <i>et al.</i> , 2012)	
Approach	Empirical	Rational	Rational	
Heat transfer	Static – Steady state	Static – Steady state	Dynamic – Steady state and transient	
Clothing	One node	One node	Multi-node static	
Physical variables	T_a, VP_a, MRT, V	T_a, RH, MRT, V	T_a, RH, MRT, V	
Personal variables	$M = 135 \text{ W/m}^2$; $1.75 > I_{cl} > 0.5$	Standardised activity (80 W; 0.9 clo)	$M = 135 \text{ W/m}^2$, walking speed 1.1 m/s and I_{cl}	
Intended for	Indoors and outdoors	Indoors and outdoors	Outdoors	
Climate	All	All	All	
Advantages	Simple to use; real skin temperature in warm/humid conditions.	Calculates all thermoregulatory processes; predicts real skin and body core temperatures	Calculates all thermoregulatory processes; Very sensitive to temporal changes of MRT and V.	
Limitations	Average sweat rate are dependent only on activity; shivering not considered in cold.	Influence of humidity and clothing variations is weak	Influence of specific clothing behaviour on thermal response is limited.	
Thermal Scale	Sweltering		> 46	
	Very hot	> 38	> 41	46 to 38
	Hot	32 to 38	41 to 35	38 to 32
	Warm	26 to 32	35 to 29	32 to 26
	Slightly warm	20 to 26	29 to 23	26 to 20
	Comfortable	0 to 20	23 to 18	20 to 9
	Slightly Cool	-13 to 0	18 to 13	9 to 0
	Cool	-26 to -13	13 to 8	0 to -13
	Cold	-39 to -26	8 to 4	-13 to -27
	Very cold	< -39	< 4	-27 to -40
Extremely cold			< -40	

2.6 Urban climate modelling

The discussions on urban geometry, UHI and thermal comfort are inextricably linked, where design choices alter the thermodynamic phenomena and hence change the human thermal comfort. Given the dynamic nature of the urban environment, it is always difficult to quantify the variables affecting urban microclimates. Urban climate modelling is an approach, which has flourished in the last two decades, aiming to quantify the impact of the built environment on the microclimate and pedestrians' health and well-being. Several tools have been developed with various approaches, pros and cons, and the designer has to decide which tool would fit into their “digital ecosystem” (Mauree *et al.*, 2019).

Among the models developed within the field of urban climatology, the 3D numerical model ENVI-met is one of the most convenient for assessing thermal comfort, particularly within urban canyons (Emmanuel *et al.*, 2007b; Bruse, 2020). The model accounts for all the heat exchange processes between the urban surfaces, vegetation and the airflow field, in high temporal and spatial resolutions, as well as calculating all the parameters governing outdoor thermal comfort. ENVI-met has been validated against field measurements (Huttner, 2012), and has already been widely used in UHI studies (Tsilini *et al.*, 2015). Drawbacks of the model, nonetheless, include overestimation of global radiation (Jänicke *et al.*, 2015), unless measured data is forced to the simulation inputs. In addition, the increased time requirements of modelling geometries within ENVI-met, unless linked with Grasshopper for Rhinoceros 3D which allows modelling geometries parametrically and exporting to ENVI-met, albeit, with slight differences due to the grid cells variations. The main disadvantage of the model is its excessive simulation time, which approximates real time, in other words, 24 hours to simulate a day of the year.

RayMan is capable of calculating radiation flux density in the form of MRT and common bioclimatic thermal indices, e.g. PET and PMV, by means of basic meteorological input parameters, i.e. air temperature, relative humidity, vapour pressure, and wind speed (Matzarakis *et al.*, 2010). Within the model, view factors are accounted for by using a fish-eye photograph. Disadvantages of the model lie in discretising all the long-wave radiation exchanges into that of the ground surfaces, as well as the inability to handle minimal solar altitudes. The inability to calculate MRT at one point for a given time is another disadvantage, as is being incapable of taking short-wave reflected radiation into account (Naboni *et al.*, 2017).

Along with the meteorological inputs, the SOLWEIG model utilises a GIS-based digital surface model (DSM) to estimate the MRT based on the plane radiant temperature from the short and long-wave radiation received from six directions. Shortcomings of the model arise from assuming fixed values for different variables. For instance, view factors are assumed to be constant for cardinal directions, as are they for upper and lower surfaces. Furthermore, according to the Lindberg *et al.* (2016) version, the model assigns a single emissivity and albedo for both buildings and vegetation with fixed transmissivity for the latter. Other shortcomings are, in addition to neglecting wind flow and building wall material variations, that

temperatures of shaded surfaces follow a pre-set linear equation for two hours, after which surface and air temperatures are set to be equal (Lindberg *et al.*, 2008).

CityComfort+ is another development for estimating MRT in denser urban areas. The model calculates short-wave radiation by virtue of the software RADIANCE, while the longwave radiation from the atmosphere is based on the Angstrom formula. A weighted mean between the radiant temperature of the sky and the surrounding urban surfaces represents the longwave radiation from the latter (Huang *et al.*, 2014). It's worth mentioning that the algorithm applied within CityComfort+ attributes the surface temperatures to the ambient air temperature by assuming that heat exchanges within urban canyons could be neglected when accounting for boundary layer radiant exchanges. Besides that, the model sorts the urban surfaces into four groups, within each, isothermal conditions apply for each surface. Validation results of Huang *et al.* (2014) with on-site measurements have shown that neither did the model represent analogous MRT variations within each time-step, nor was it suitable for canopy layer simulations.

CitySim Pro is capable of predicting the energy fluxes on different urban scales taking into account the evaporation and transpiration energy loss from the ground and vegetation respectively. For doing so, the model needs inputs of detailed human body aspects in terms of the shape, posture, shortwave absorption coefficient and longwave emissivity, as well as the emissivity of surrounding surfaces (Robinson *et al.*, 2009). Further, the model has been validated against Building Energy Simulation Test as well as EnergyPlus. CitySim Pro was found to be suitable for complex urban environments, with some limitations in importing and exporting 3D geometries (Guo *et al.*, 2019). Autodesk CFD, on the other hand, uses a finite element method to estimate MRT, taking into account the conductive, convective and radiative turbulence between urban elements. The software package encompasses radiative and thermal models, however, they have not been validated within outdoor studies. Drawbacks of the model stem from the simplification of body aspects, and neglecting angle factors between the surfaces as well as the vegetation transpiration (Naboni *et al.*, 2017).

More recently, Rakha *et al.* (2017) proposed a workflow for estimating the MRT based on the surface temperatures calculated by heat diffusion equations. The model incorporates DAYSIM for solar irradiation quantification, DIVA for Rhino to account for the shortwave radiation component, and RADIANCE for view factors calculation via ray-tracing and thus the estimation of longwave surface radiation.

Urban surfaces are meshed by virtue of DAYSIM with analysis nodes at each surface to register the surface temperature into a database, and MRT is calculated accordingly. Rakha, however, included scarce details about the workflow. Notably, neither the sky radiation, heat transfer through the ground nor the heat loss by evapotranspiration are considered in the model.

Ladybug-tools are open source environmental plugins for Grasshopper, built upon validated simulation engines. They integrate outdoor comfort into the design process and thus can be an essential tool to bring awareness to architects and urban planners. The tools indicate the outdoor environmental conditions, as well the pedestrians' thermal sensation, through several indices, for instance PMV, PET and the UTCI. They have been applied to compute climatic conditions that range from urban canyons to city scale. Table 2.2 compares the different tools in terms of their capabilities to model the urban microclimate, outdoor thermal comfort and energy demand and supply.

Table 2.2: Capabilities of tools for evaluating the microclimate, outdoor comfort and energy demand.

Tool	MRT	OTC	EU	PV	ITR	YR	UR
ENVI-met	✓	✓					✓
Rayman	✓	✓					
SOLWEIG	✓	✓*				✓	✓
CityComfort+	✓						
CitySim Pro	✓		✓	✓		✓	✓
Rakha et al.	✓		✓		✓	✓	✓
Ladybug-tools	✓	✓	✓	✓	✓	✓	✓

(MRT) Radiant Exchanges (OTC) Outdoor Thermal Comfort (EU) Energy Use, (PV) Renewable production, (ITR) Iterative simulations, (YR) Yearly simulations, and (UR) Urban-scale simulation. * Only for certain points of interest.

2.7 Epilogue

This chapter presented the interactions between the built environment and urban climate. This included the urban climate scales corresponding to the urban form, the urban energy balance and the UHI phenomenon. A discussion on the human adaptation outdoors was preceded by understanding the origins of human thermal comfort within indoor environments and the most prominent comfort indices. The most relevant microclimate and local-climate simulation tools were compared in terms of their capabilities. The discussion on the role of urban geometry to mitigate UHI revealed an intertwined relationship that requires further investigations, especially in hot-arid climates. Quantitative studies on the relationship between the urban canyon geometry and outdoor thermal comfort are further reviewed as part of chapter 4, while those concerned with urban blocks or districts and their influence on UHI, outdoor comfort and energy demand are further reviewed in chapter 5.

In line with the aims of this thesis, the local-scale climate is selected which deals with the thermal interactions between a set of urban canyons or blocks. Also, the UTCI is selected for this work, as it reflects the detailed human thermoregulatory responses within the outdoor environments. The Ladybug-tools are selected for this work as it ticks all the boxes necessary for achieving the objectives of this thesis, the most important of which are integrating all the simulations in a single platform, and mapping thermal comfort in UTCI. The next chapter further elaborates the simulation tools used in the thesis as well as the methodological approaches adopted.

3 Methodology

3.1 Preface

This chapter describes the methodological approaches adopted throughout this thesis, the methods used and their verification, and concludes with a brief description of the validation against field measurements. According to the aims of this thesis, this study is concerned with the optimisation of urban form design parameters, generating as many geometrical configurations as could possibly be created in urban communities, to gauge their environmental performance with regards to different performance criteria. This myriad of design permutations is hardly found in reality, and even a small number of them are unwieldy to monitor using comprehensive field measurements. Parametric modelling and simulation of hypothetical urban forms are advantaged in this regard, and are therefore, adopted in this study.

3.2 Experimental Approach

Unlike standard methodologies which outline all the methodological steps, assumptions, and analysis protocols before presenting the main work, the methodology of this thesis evolved as the research progressed. This arose from the fact that the scale of each stage, as well as the results of the preceding one dictated the change in the design thresholds of the design parameters, as well as the analysis method in that stage. This research was conducted in three consecutive stages, corresponding to the research objectives defined in section 1.5. As for the performance criteria, outdoor thermal comfort was represented by the average UTCI recorded during daytime hours at all the grid points analysed. Energy consumption was represented by the aggregate cooling, lighting and electrical equipment loads for the period investigated. This work used the total energy loads rather than being normalised by floor area, since the latter ambiguate the absolute impact of urban geometry on energy loads. For example, a building form might have higher energy loads than another with lower floor area; by increasing the former's floor area, normalised energy loads might be relatively reduced, though will ambiguate the reasons for this effect, i.e., whether due to shading or increasing floor space. Total energy loads, thus help to draw straightforward relationships between the design parameters and their absolute effect on the consumption, which are more interpretable by urban planners and designers.

Maximum and minimum design thresholds were set in accordance with the Executive Regulations (MHUUC, 2008), with some exceptions made regarding the minimum street width and the maximum H/W ratio. Thermal properties of construction materials, window-to-wall ratios, HVAC and occupation schedules were set based on the common building traditions, and lifestyle of Egyptian residents, following Mahdy and Nikolopoulou (2014), and according to the Egyptian Residential Energy Code (MHUUC, 2005). Typically, energy consumption studies are conducted for a typical period (week, month, annum, etc.), whereas, in some cases, thermal comfort studies are conducted on a single day to represent a worst-case condition, a heat wave for instance. Stand-alone urban canyons, or buildings of the same type (length and height) in asymmetrical canyons, with opposing directions (east or west facing) could show identical energy loads, unless they are surrounded by a dynamic urban context (Fletcher *et al.*, 2013). Allegrini *et al.* (2016) studied the radiation exchange of four rows of buildings with different orientations (EW and NS), showing identical cooling loads of the intermediate two,

also highlighting the above issue. From these standing points, and since the first stage deals with a worst-case situation on an extreme hot day, energy consumption was not included in the first stage. The climatic context of Cairo was represented by an International Weather for Energy Calculations (IWEC) file, which was compared to different types of weather files, namely, the Egyptian Typical Meteorological Year (ETMY) file, and the updated Typical Meteorological Year (TMYx) file, as well as to real measurements to ensure the validity of the weather data.

In the first stage, a hypothetical urban canyon was simulated in three consecutive phases, changing the street width, building heights and orientation. The heights of the buildings changed simultaneously in the first phase, creating 1716 symmetrical urban canyons, and independently in the second and third phases, creating 3840 and 2160 asymmetrical canyons, respectively. This ensured a comprehensive study of urban canyon geometry and its impact on thermal comfort, with more emphasis given to the effect of building heights, and the H/W ratio of each flanking side, in the second and third phases, respectively. Results of this stage, on the one hand, defined the optimum design thresholds for improving thermal comfort, and on the other, refined the design parameters used in the next stage; for instance, excluding street widths wider than 24 m, and building heights lower than 9 m.

In the second stage, a hypothetical urban block representing three typologies derived from real built forms in Cairo, was modelled and simulated within an identical surrounding context. The parametric combination of design parameters, i.e., street widths in both NS and EW directions, building heights and orientation, entailed the simulation of 3430 geometrical cases in a single run. Buildings were vertically split into floors, corresponding to the step size of building height increments, and associated with a number of thermal zones for energy calculations. Simulation were conducted in the hottest month of July, where a combined fitness was used to account for both UTCI and energy loads simultaneously. The results defined the optimum design and density thresholds for improving thermal comfort and energy consumption, then specified the best performing typology, which was selected for further investigation in the next stage, based on the combined fitness. Also, based on the energy analysis, electrical and equipment loads have shown insignificant changes throughout the different iterations, hence they were excluded from the next stage.

In the third stage, three courtyard blocks comprising 8, 10 and 12 buildings were simulated, with changing street widths, orientation, and having their building heights changing separately. With such a parametric combination, the number of possible permutations exceeded 7 million cases, where evolutionary algorithms were used by means of the Grasshopper plugin, Octopus (next section). The results defined the optimum street widths and orientations of each courtyard type, as well as the optimum height in each direction thereof. Also, the best performing cases in each type were specified, then compared to a reference case to gauge the potential of thermal comfort and cooling loads improvement in summer, and solar exposure and heating loads in winter.

In an iterative process, the data associated with the dynamic parameters (e.g. building heights, street widths, FAR, BCR, and orientation) flowed within a parametric design environment (next section), whose plugins triggered validated simulation engines dedicated to output the different performance metrics. Following a comparative analytical approach, the thermal and energy performance of the various geometrical configurations were quantitatively compared in each stage, to optimise the performance criteria. The data were then post-processed, analysed and visualised. (Figure 3.1).

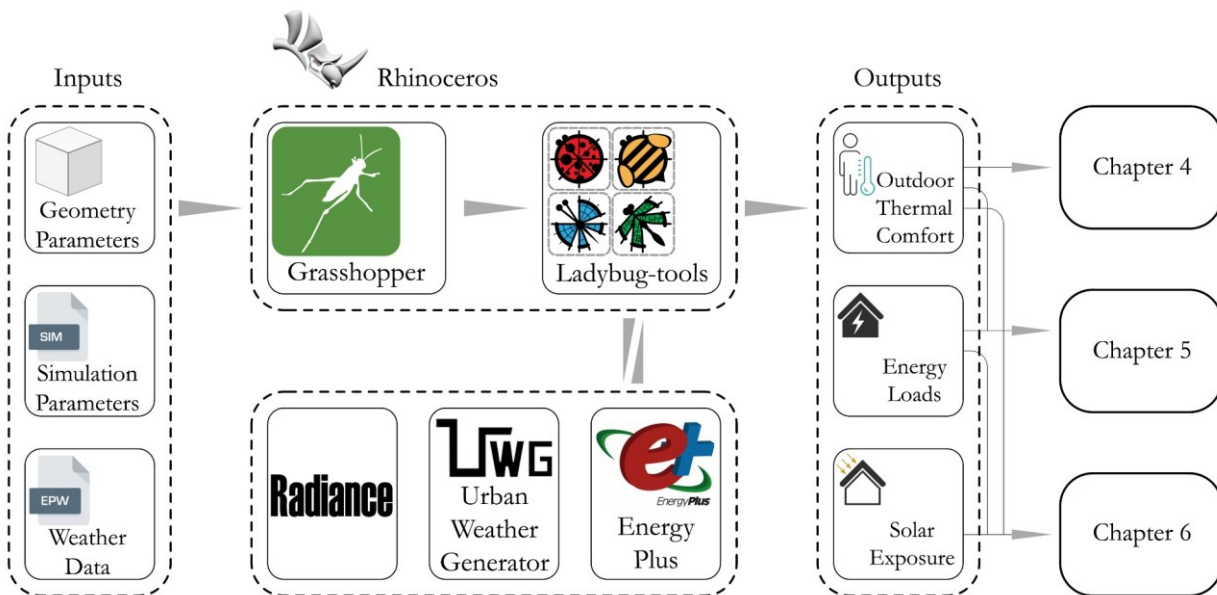


Figure 3.1: General methodological approach used throughout the thesis.

3.3 Grasshopper

Grasshopper was developed by David Rutten in 2007 at Robert McNeel & Associates (Rutten, 2021). It allows users to drag and place components onto a canvas via a user-friendly graphical scripting interface that comes as an integrated feature inside Rhinoceros 3D (Rhino) (McNeel, 2021). This way, it allows architects, designers and many others to develop their own algorithmic designs without the need to script. Grasshopper's popularity amongst students and professionals is increasing with the ever-growing family of plugins, for instance but not limited to, Kangaroo - which embeds physical behaviour within the model, Ladybug-tools - for environmental design and analyses, and Karamba - for structural analyses. In a flow chart working procedure, the data associated with the geometrical design parameters seamlessly stream from one component to the other(s), with real-time feedback on the Rhino viewports. Recent developments included two-way data streaming (looping) plugins, such as Hoopsnake, allowing for iterative analyses of regenerative urban design. Notably, the Rhino Common Software Development Kit (SDK), integrates common scripting platforms, e.g. Python, and C# into Grasshopper, giving the designers opportunities to develop their own components or rather modify existing ones. Furthermore, Grasshopper allows evolutionary optimisation via its single-objective (Galapagos) and multi-objective (Octopus) plugins. This thesis capitalises on the environmental design plugins, Ladybug-tools to investigate the impact of urban geometry on different performance criteria.

3.4 Methods | Ladybug-tools

Ladybug-tools are a group of Grasshopper plugins which support environmental design and education, connecting Computer Aided Design (CAD) interfaces to validated simulation engines, for instance RADIANCE, EnergyPlus, Urban Weather Generator (UWG) and OpenFOAM. Ladybug-tools are open-source plugins written in Python which unite the underlying open-source simulation engines. The plugins allow chaining the inputs and outputs of its simulation engines, and hence geometry manipulation and visualisation take place within one interface. As a set of modular components, the plugins offer a great flexibility within different design stages. By harnessing the capabilities of Rhino, they offer a variety of 3D graphics and data visualisations. Ladybug-tools, as written in Python, work as an Application Programming Interface (API) which can be run on any operating system or connected to any geometry engine (Roudsari & Mackey, 2022).

Mostapha Roudsari documented the first version of Ladybug in 2013, comprising 28 components for weather data visualisation, and solar radiation analyses (Roudsari *et al.*, 2013). Soon after, Honeybee was released in 2014 to connect Grasshopper to daylighting and energy simulation engines. Chris Mackey, in his thesis (Mackey, 2015) added thermal comfort models to Ladybug, followed by several developments of components for detailed comfort mapping. In 2017, Mostapha and Theodore released the Butterfly plugin to connect Grasshopper with CFD simulation engines. Following in 2018, the team released the Dragonfly plugin which links Grasshopper to urban climate models such as the UWG. Recent developments include the Ladybug-tools Pollination as a commercial web-based simulation interface allowing for cross-disciplinary collaboration (Roudsari & Mackey, 2022). Ladybug-tools are undergoing constant development by an open community of experts, researchers and engineers who contributed in several libraries and plugins (Roudsari *et al.*, 2022). At the time this thesis is being written, there are two branch lines of the Ladybug-tools; Ladybug version 0.0.69 and Honeybee version 0.0.66 together are the legacy plugins; and Ladybug Tools version 1.4 which are under development - the developers' approach to minimise simulation time and link them to cloud computation. The work presented in this thesis are conducted using the legacy plugins, which are briefly described below.

Ladybug is a plugin which allows the designer to not only leverage the full spectrum of environmental data and visualise them along with the corresponding geometries, but also iterate building forms based on simultaneous graphical representation for this data. As for radiation, Ladybug delineates the solar incidence following the GenCumulativeSky (Robinson & Stone, 2004) approach by calculating the amount of radiation impinging the sky vault as discretised into sky patches. In a similar vein, *Honeybee* utilises the environmental data and connects Grasshopper to a series of validated stand-alone pieces of software, e.g. RADIANCE for daylighting simulation, EnergyPlus for energy modelling, and THERM/Window for building envelope heat flow monitoring (Roudsari *et al.*, 2013). *Butterfly* exports geometries from Grasshopper into the rigorously-validated CFD engine, OpenFOAM, in order to run indoor and outdoor airflow simulations. Moreover, the *Dragonfly* plugin allows for modelling macro and micro-scale climate phenomena such as UHI by virtue of the Urban Weather Generator (UWG) (Bueno *et al.*, 2013), as such it allows for the comparison of hourly surface temperatures against datasets of Landsat thermal satellite images within the Grasshopper environment (Roudsari & Mackey, 2022).

As being part of the parametric platform of Grasshopper, it is viable to integrate them with the built-in evolutionary single and multi-objective optimisation engines (Galapagos and Octopus). Likewise, Ladybug-tools could potentially be linked to generative urban models, e.g. L-System and Cellular Automata by means of *Rabbit* for Grasshopper (Fathy *et al.*, 2015).

3.5 Model verification

This section explains the simulation workflow used throughout this thesis following the work by Mackey *et al.* (2017). This includes the verification of the model's performance against the validated microclimate simulation software, ENVI-met v.4.4.3, where it is hypothesised that Ladybug-tools are as accurate and time-efficient for modelling the microclimate. In this study, buildings are modelled without fenestrations, since glazing representation is not available in ENVI-met. The hottest day was selected to represent a worst-case condition, and extracted using Ladybug.

A sensitivity analysis was conducted by the candidate to test the effect of running CFD simulations on the results. This included simulating the wind flow, using a steady-state solver from OpenFOAM, from eight directions following Mackey *et al.* (2017), dividing the simulated wind velocities by the inlet velocity, scaled down to the pedestrian height using a logarithmic wind profile, to obtain a spatial matrix of wind factors at each grid point. This spatial matrix was then multiplied by hourly wind speeds from the weather file, whose direction corresponds to the nearest one of eight directions, to obtain a temporal matrix of wind speeds at each grid point. The temporal matrix was used in the UTCI calculation. The results has shown a marginal effect of wind speed on the UTCI, in agreement with the work of Natanian *et al.* (2020) in a Mediterranean hot climate. Given the computational cost required for the analyses, it was decided to exclude the CFD analysis from the study. This section is based on the paper "A methodology for modelling microclimates: A Ladybug-tools and ENVI-met verification study" published in the 2020 conference "35th PLEA Sustainable Architecture and Urban Design: *Planning Post Carbon Cities*", in A Coruña, Spain. The candidate has predominantly contributed to the publication. Details of authorship of this paper are given in Table 3.1.

Table 3.1: Declaration of authorship.

This declaration concerns the paper entitled:

A methodology for modelling microclimates: A Ladybug-tools and ENVI-met verification study.

Publication status (tick one)

Draft manuscript Submitted In review Accepted Published

Publication details (reference):

Ibrahim, Y., Kershaw, T., & Shepherd, P. (2020). A Methodology For Modelling Microclimate: A Ladybug-tools and ENVI-met Verification Study. In *35th PLEA Conference. Sustainable Architecture and Urban Design: Planning Post Carbon Cities*, A Coruña, Spain, 1–3 September.

Copyright status (tick the appropriate statement):

- I hold the copyright for this material
- Copyright is retained by the publisher, but I have been given permission to replicate the material here

Candidate's contribution to the paper (%):

The candidate has predominantly contributed to:

- Formulation of ideas (90%): **Y. Ibrahim** developed the idea, in consultation with T. Kershaw.
- Design of methodology (80%): **Y. Ibrahim** developed the methodology, in consultation with T. Kershaw.
- Data analysis (100%): **Y. Ibrahim** conducted the data analysis.
- Presentation of data in paper format (90%): **Y. Ibrahim** wrote the paper and submitted it to the conference. The co-authors provided feedback for improvements.

Statement from Candidate:

This paper reports on original research I conducted during the period of my Higher Degree by Research candidature.

Signed:

Date: September 2022

3.5.1 Abstract

Over the last decade, outdoor thermal comfort has become of considerable significance to urban designers and planners. In that concern, parametric design models were acknowledged for supporting the design process with iterative performance-based solutions and for being relatively less time and resource consuming. However, validation studies for such parametric models on the outdoor urban scale are lacking. Meanwhile, studies concerned with geometry optimisation are computationally expensive due to the time required per each simulation. This paper consequently investigates the accuracy and time efficiency of using the workflow comprising the environmental analysis Ladybug-tools, the plugins of Grasshopper3D for modelling the outdoor microclimate. The study verifies the model's results against the microclimate CFD simulation tool, ENVI-met. The two models are compared in terms of two environmental metrics, the mean radiant temperature and the universal thermal climate index. In this paper, three hypothetical layouts representing basic urban geometry patterns, namely linear, dotted, and courtyard, are simulated in both models. Results show an acceptable range of consistency between Ladybug-tools and ENVI-met, particularly during the hours 8 am to 5 pm. Timewise, Ladybug-tools show their capabilities of not only modelling the microclimate but also their suitability for optimisation studies characterised by a vast number of design solutions.

3.5.2 Introduction

Over the past few years, outdoor thermal comfort has gained increased attention between urban climatologists and developers who have sought to precisely imitate the built environment. In this sense, researchers have been trying to either distinguish the most accurate models or develop an ad-hoc methodology. Some have coupled different models for a concerted performance, while others have validated the computational models to field observations or verified against already validated engines. A case in point is the study of Naboni *et al.* (2017) who compared five models, namely ENVI-met, RayMan, CitySim Pro, Ladybug-Tools and Autodesk CFD. Their study, however, showed a significant incongruity between the models, particularly during the summer. This incongruity could be ascribed to the materiality of building constructions and the meteorological inputs for each model.

Furthermore, Jänicke *et al.* (2015) compared ENVI-met, RayMan and SOLWEIG to field measurements of a green façade for the estimation of heat stress.

Their results for calculating the Mean Radiant Temperature (MRT) have shown a mean deviation up to 7 K from the observations. (Perini *et al.*, 2017) interpolated the output wind speeds, and plants vapour flux from ENVI-met into TRNSYS in a coupled methodology for estimating the Universal Thermal Climate Index (UTCI). Finally, Elwy *et al.* (2018) validated the Ladybug workflow against ENVI-met and field measurements. Results have shown an acceptable range of agreement in terms of Physiological Equivalent Temperature (PET) comparisons, however without a clear elaboration for the temperatures' variations. Meanwhile, the study of the effect of urban morphology on the microclimate entails a huge computational power and extensive simulation time, particularly when using CFD simulations, and hence most of the studies concerned with geometry optimisation are limited to a few number of canyon configurations (Allegrini *et al.*, 2015; Jamei & Rajagopalan, 2019). Consequently, this paper aims at presenting the Ladybug-tools as accurate and time-efficient for modelling the microclimate as compared to the CFD simulation model, ENVI-met v.4.4.3.

3.5.3 Methodology

Before the version 4.4.0, ENVI-met did not allow for forcing the solar radiation inputs and instead used its embedded terrestrial coordinates to obtain solar radiation values all across the globe (Huttner, 2012). From version 4.4.0 onwards, ENVI-met has enabled the users to full force the meteorological parameters, allowing users to make direct comparisons with other simulation engines. It is worth noting that ENVI-met accounts for the vegetation interaction with the microclimate elaborately, as opposed to Ladybug-Tools which gives an estimation of the evapotranspiration based on the green coverage ratio along with the plant's albedo and uses the UWG for doing so. Accordingly, in order to avoid these ambiguities, the three hypothetical simple layouts representing the commonly used urban geometry arrangements in Cairo, viz. linear, dotted, and courtyard (Figure 3.2), are modelled solely in the form of buildings and a ground surface.

3.5.3.1 Methods

Mackey *et al.* (2017) introduced the hybrid workflow for estimating the MRT, and mapping the microclimate in a graphical representation. The workflow is based on utilising the plugins of Grasshopper, presumed to simulate each of the thermal comfort determinants individually, and further combine them collectively for comfort calculation. Geometries are firstly created on the Grasshopper canvas to

serve as a feeder for different plugins. An elevation model along with average building heights, ground and green coverage ratios, façade to wall ratio as well as thermal properties of constructions are fed into the -UWG- Dragonfly components to morph the .epw file to reflect the urban conditions. MRT is estimated by the three fundamental components; direct solar radiation; atmospheric long-wave radiation; and surface long-wave radiation. The latter is estimated through the EnergyPlus simulation, which is part and parcel of the Ladybug-Tools. The output of this step is outdoor surface temperatures which are further weighted by their view factors using the ray-tracing engine in Rhino. Butterfly could potentially integrate OpenFOAM simulations within the workflow for modelling the urban wind patterns. The sky long-wave radiation and the direct short-wave radiation are accounted for by following the equations specified within the MENEX model and the SolarCal model, respectively. Eventually, by virtue of a generic component, the model provides a full range of thermal comfort indices, e.g. PMV, PET, and UTCI with a graphical representation.

On the other hand, among the models developed within the field of urban climatology, the 3D numerical model ENVI-met is one of the most convenient models for assessing thermal comfort. The model accounts for all the heat exchange processes between the urban surfaces, vegetation and the airflow field in high temporal and spatial resolutions, as well as calculating all the meteorological parameters governing outdoor thermal comfort, e.g. MRT (Ali-Toudert, 2005). ENVI-met has been validated against field measurements (Huttner, 2012) and has already been widely used in UHI studies (O'Malley *et al.*, 2015). Drawbacks of the model, nonetheless, include overestimation of global radiation (Jänicke *et al.*, 2015), unless measured data is forced to the simulation inputs. Also, ENVI-met requires increased time for modelling geometries from raster-based images, unless linked with Grasshopper which allows for exporting geometries to ENVI-met, albeit, with slight differences due to grid cells variations. The main disadvantage of the model is its excessive simulation time required which approximates real-time; in other words, 24 hours to simulate a day of the year.

3.5.3.2 Modelling and parameterisation

Layouts were modelled so far as is reasonably practicable and time-efficient within each model. Geometries are modelled in ENVI-met on a raster basis while for Ladybug-Tools are modelled parametrically in Grasshopper.

Figure 3.2 and Figure 3.3 show the geometry configurations and a 3D presentation for each layout, where these configurations were estimated from real case studies in Cairo. The coloured circles denote to the points of interest, which shall be further analysed and discussed. Since the study is concerned with the assessment of outdoor conditions, buildings were modelled with no fenestrations.

3.5.3.2.1 ENVI-met

Buildings were modelled on a 2 m grid horizontally and $h_{max} \times 4$ m grid vertically with ten nesting grids from all directions, assuming a flat terrain and the absence of anthropogenic sources. Default building construction materials were used from the ENVI-met database. Building indoor temperature is set to 20° C, where ground temperatures are set to 25 and 22.5° C at 2 m and 4 m depths respectively.

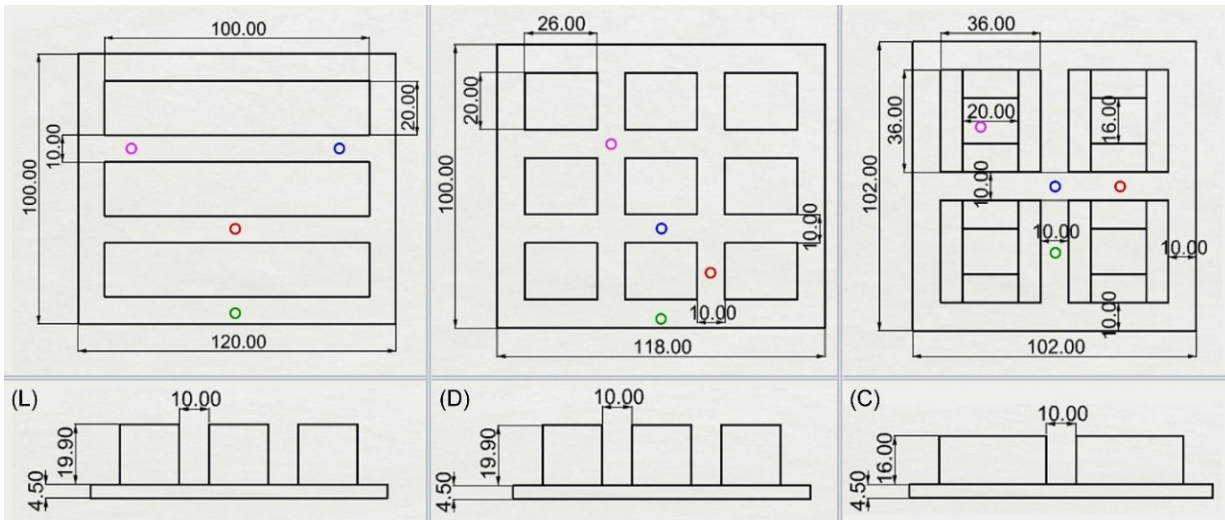


Figure 3.2: Geometry configurations for the three layouts; (L) Linear; (D) Dotted; and (C) Courtyard (dimensions in meters). Coloured circles denote to (Green) Receptor R1, (Red) R2, (Blue) R3, and (Purple) R4.

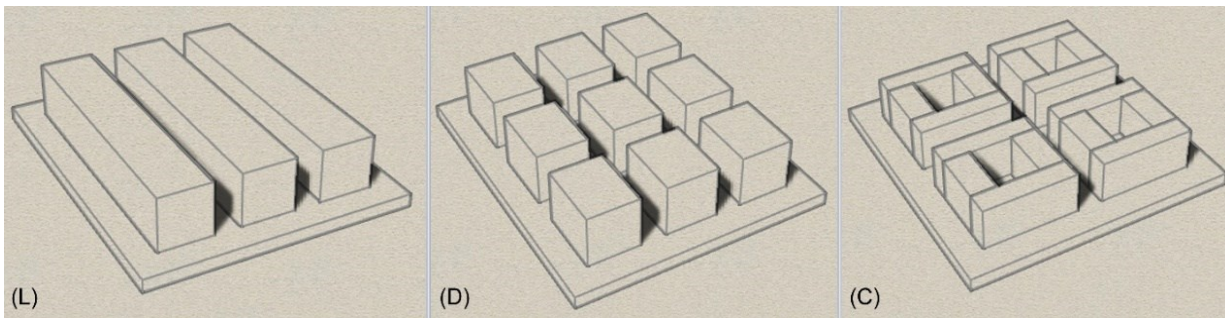


Figure 3.3: 3D presentation for the three layouts (Exported from Rhino viewport).

Table 3.2: Construction materials input for both models.

Construction Properties	Unit	Roofs		Walls		Ground		Reference
		[R1] Tiles	Roofing	[B2] Wall	Brick	[KK] road	Brick	
Thickness	m	0.3		0.45		4.5		* obtained
Solar Absorption	Decimal	0.50		0.60		0.7**		from
Solar Reflection / albedo	Decimal	0.50**		0.40**		0.3		(Engineering-
Thermal Absorptance	Decimal	0.90		0.90		0.93*		ToolBox,
Density	kg/m ³	1900		1500		1900 [#]		2001);
Specific Heat Capacity	J/kg·K	800		650		1053**		** derived; or
Vol. Heat Capacity	MJ/m ³ ·K	1.52**		0.98**		2.00		[#] assumed
Thermal Conductivity	W/m·K	0.84		0.44		1.00		
Material Roughness	-	Medium		Medium		Medium		
		Rough [#]		Rough [#]		Rough [#]		

3.5.3.2.2 *Ladybug-Tools*

Layouts were modelled in Grasshopper to match those grid points as in ENVI-met. Unless defined within ENVI-met database, materials' properties were either obtained online (Engineering-ToolBox, 2001), derived or assumed with reference to the relevant properties (Table 3.2). Buildings are defined as Honeybee zones with building program set to “not conditioned” Midrise Apartments, where the ground is defined as a virtual EnergyPlus ground, assuming no wind or sun exposure and no internal loads. Following (Mackey et al., 2017), EnergyPlus simulation is set to “Full Exterior with Reflections” at a time step of 15 minutes.

3.5.3.2.3 *Boundary Conditions*

As a representation of the hot-arid climate in Cairo, Egypt, a EnergyPlus Weather (.epw) file for both models was available at (DoE, 2020). As mentioned earlier, ENVI-met allows for the full forcing of meteorological conditions, where the lateral boundary conditions and the cloud cover are disabled and rather being inferred from the .epw file. While EnergyPlus intrinsically extracts the global horizontal, direct normal, and diffused horizontal radiation values necessary for surface temperature calculation from the .epw file, ENVI-met parses the file to get a unique direct maximum radiation which is necessary for ENVI-met to perform the simulations.

3.5.3.2.4 *Comfort calculations*

Simulations were carried out for a total of 15 hours, on June 7th from 5 am to 8 pm representing the .epw extreme hot day in the weather file. Results are demonstrated on the next section in terms of the MRT as one of the main

constituents of the human energy balance, and the UTCI as a representation for the outdoor thermal comfort. Results values were measured at 1.2 m above ground level as to present a pedestrian thermal sensation point of view. It is worth noting here that, CFD simulations via Butterfly are not performed in this study since it has notoriously increased the time of simulation and curtailed the continuity of the workflow with no substantial effects to the UTCI values. Thus, this study, instead, calculates the canyon wind speeds based on the power law using a specific Honeybee component.

3.5.4 Results

In this section, the Ladybug-tools model is referred to as LB, while ENVI-met as EM, and Linear, Dotted and Courtyard as L, D, and C respectively. Figure 3.4 shows the temporal variations of MRT at each of the points of interest, as well as the average values over each layout. The general trend of the curves at all patterns seem to be congruent except where the beam radiation abruptly changes due to being obstructed by buildings (L-R2, L-R3, D-R2, C-R1, and C-R4). Temperature differences of these cases occurred at 2-4 pm with a maximum difference of 32.5° C in L-R2, while the other maximum differences are registered at 5 am as not exceeding 13.5° C. Also, apart from the outliers, LB appeared to have higher MRT values during the early hours (5-8 am) by almost 12° C, then rises in tandem with EM, and holds in proximity during the peak hours, and then falls yet with the same higher values during (6-8 pm) by almost 10° C. Moreover, a thorough analysis of the receptors has shown that those laid in similar canyon positions fluctuated in the same manner. For instance, located outside the canyon, LB-D-R1 and L-R1 keep a pace higher than those of EM by almost 8° C, except at 4 pm drops by nearly 14° C. Receptors in N-S canyons (LB-D-R2 and C-R1) maintain minor variations during the shaded hours, yet leap to match the EM peak values during sunlit hours, and register a variation of 17° C at 2 pm. Additionally, E-W receptors (LB-L-R2, L-R3, C-R2 and D-R3) plummet at 3 pm recording the highest difference of 32.5° C due to the solar obstruction.

Further, canyon intersections (D-R4 and C-R3) and the west side L-R4 possess higher consistency with EM. However, the longer block length in the courtyard design curtails the solar radiation exposure of C-R3 and hence drops at 4 pm by 17.05° C. Finally, although C-R4 maintains a high congruity during (8 am-1 pm), it plummets at 2 pm to record a 20° C difference. More intriguing, the general trend of average MRT over the three layouts is quasi-similar. Apart from the early (5-8 am)

and late (6-8 pm) hours where differences approach 12° C, LB stays close to EM with variations not exceeding 6° C. Influenced by the MRT values, UTCI values have followed the same trend, however with no drastic variations (Figure 3.5). Maximum differences are manifest during the early and late hours, not exceeding 6.43° C. That is, with 5.8° C maximum variation for the average UTCI over the three layouts, LB shows a great conformity with EM during the simulation period and hence exhibits a significant potential to speculate the impact of different urban configurations on the microclimate. Error calculations are presented in Table 3.3 showing the Root Mean Squared Error (RMSE), Mean Percentage Error (MPE) and Coefficient of Determination (R^2). In terms of UTCI, LB results have shown a substantial level of agreement with EM ($R^2 = 0.97$). Figure 3.6 depicts the comfort maps for each layout and shows the resemblance of each pertaining pattern. As aforesaid, differences are evident during the early and late hours. The maps, thus show the Ladybug-Tools model to be capable of presenting the microclimate and hence is practical for mutating multiple design solutions due to the improved time efficiency.

Table 3.3: Error calculations for MRT and UTCI.

	Linear		Dotted		Courtyard	
	MRT	UTCI	MRT	UTCI	MRT	UTCI
RMSE	5.65	2.42	5.41	2.43	5.44	2.45
MPE	18.97	7.43	18.76	7.30	18.70	7.53
R^2	0.94	0.97	0.96	0.97	0.95	0.96

3.5.5 Discussion and Conclusion

As shown in the results, the variations between the two models can be ascribed to different causes. The surface heat balance within both ENVI-met (EM) and EnergyPlus (EP) is calculated based on empirical equations with slight differences for estimating each component. However, the deduced amount of heat emitted and stored are not accounted for in EP. The heat conduction equation in EM is calculated by a simplified three-node method based on the exterior and interior surfaces' temperatures with reference to the previous single timestep, while in EP is calculated with reference to a series of temperatures and heat fluxes' history of the previous timesteps. In terms of the outside surface temperature, EM calculation of the absorbed short-wave radiation is set to be 50% of the incoming solar radiation, while on the other hand EP uses the *Clear Sky Solar Model* (as the default in this study) which was reported to overestimate the solar radiation available to the building (DoE, 2019).

Moreover, EP intrinsically accounts for the radiative heat flux from the internal lighting (short-wave) and the zone surfaces (long-wave) in addition to the convective heat flux from the zone air. This could potentially affect the inside surface heat balance and result in a reduced conduction heat flux from the outside surface, thus keeping the outside surface temperature higher.

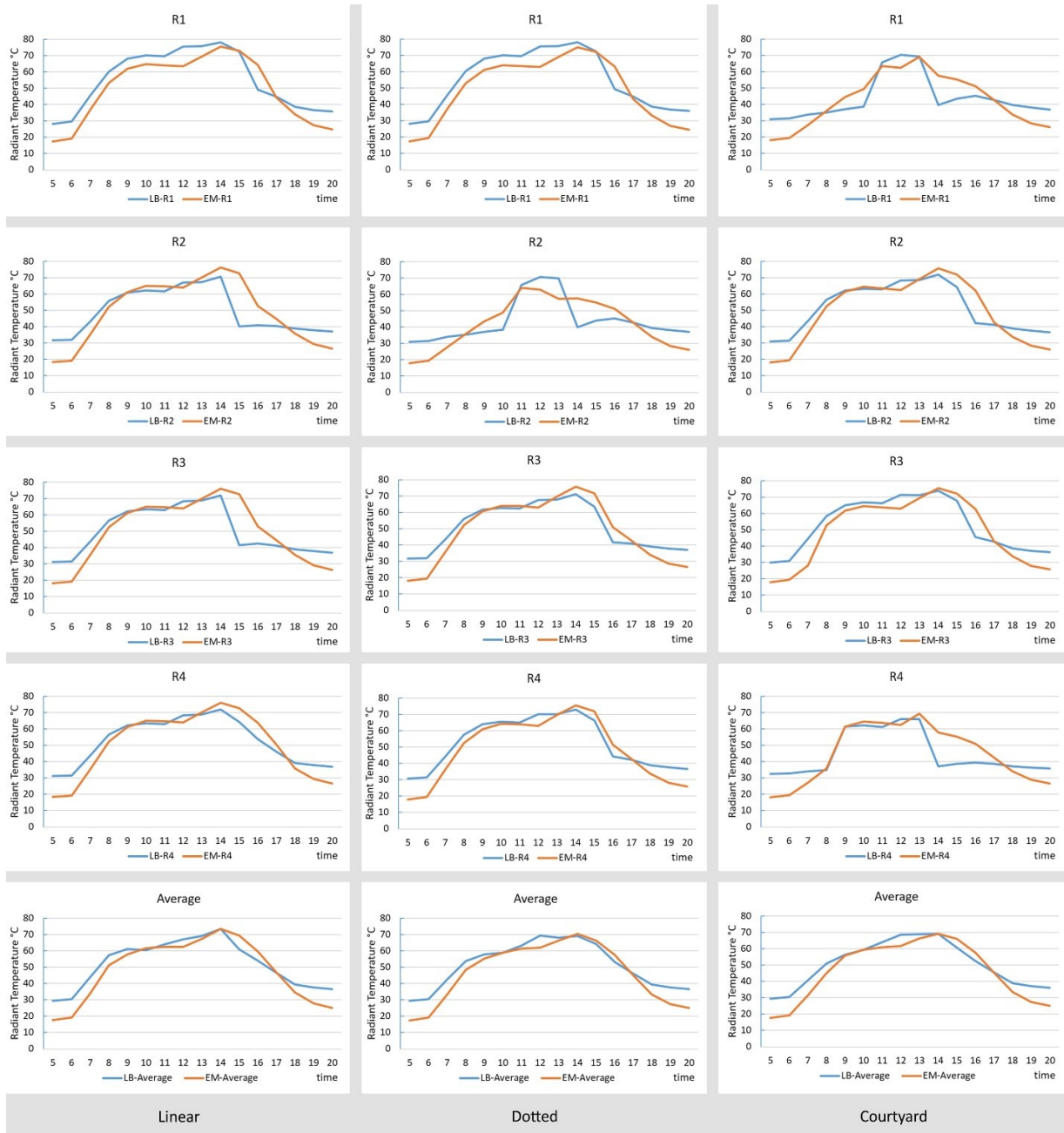


Figure 3.4: MRT comparison within the three layouts. Receptors R1-4 in a single layout are not meant to be comparable to their counterparts in other layouts across the figure.

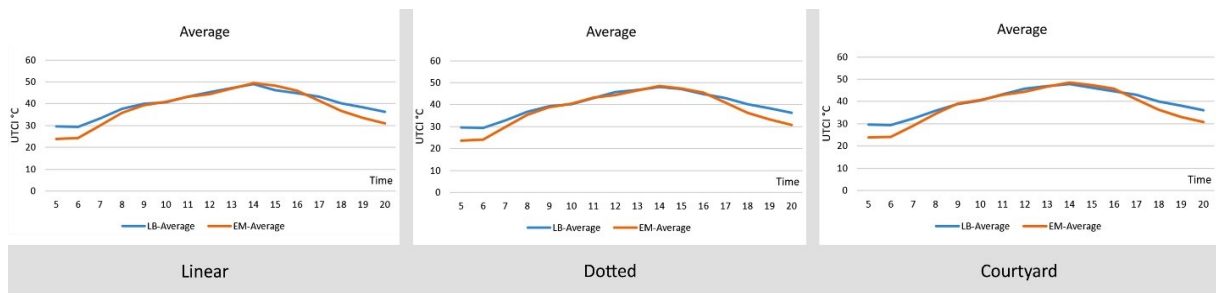


Figure 3.5: Average UTCI comparison within the three layouts.

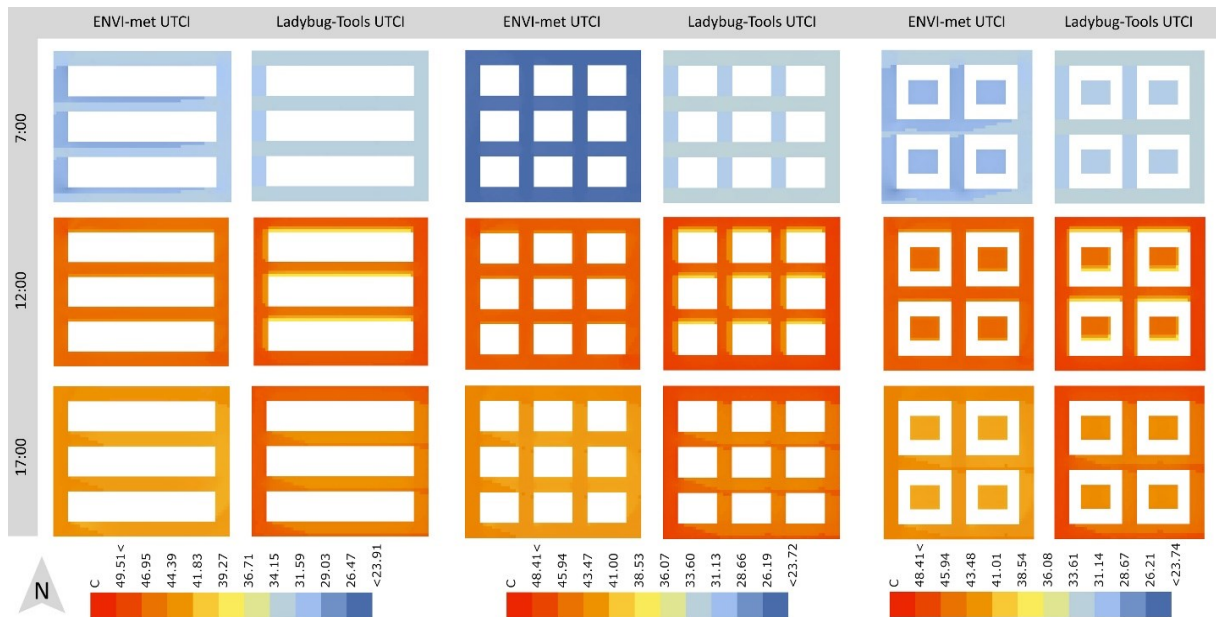


Figure 3.6: UTCI thermal maps for each layout at 7 am, 12 pm and 5 pm.

Although the amount of absorbed long-wave radiation in EM is almost similar to that of Ladybug-tools (LB) using the ray-tracing with almost 10° vector angles, EM takes into account the geometrical characteristics of the hemisphere, i.e. each vector is weighted by a factor of the angle of incidence to the surface (which tends to be more accurate). Furthermore, absorbed long-wave radiation from surrounding walls and the ground in EM are averaged over the model area. Consequently, irradiated surfaces' temperatures are indirectly lowered by the cooler surfaces in other shaded parts and vice versa. The effect is diminished during the peak hours where the solar radiation is fairly distributed over the model area. The aforesaid provides some explanation for the increased MRT of LB during the early hours of the day, which is evident in all cases. The scrutiny of the Python source code has revealed that, when the solar beam is blocked, LB confines the global horizontal radiation to the diffused component.

The reflected radiation is defined within the SolarCal model as a function of global radiation, which is limited to the diffused radiation in case of obstructing the solar beam. This explains the sudden rise and fall in LB D-R2, L-R1 and C-R4 as well as the plummets of L-R2, L-R3, as opposed to the EM point MRT which receives an additional amount of reflected short-wave radiation from the ground and the walls, since the reflected radiation in EM is a function of the direct normal radiation times the inverse view factors. With the notion that the solar altitude reaches its maximum at midday, and the reflected short-wave and emitted long-wave radiation from the irradiated walls are minimised, point MRT receives a relatively less net all-wave radiation. This is clear in the case of EM at noon, while LB appears to show this trend earlier at 11 am and instead registers higher MRT at 12 pm. The latter might be attributed to the additional Δ MRT within the LB model.

As aforementioned, the MRT calculation within the LB model is based on the three components equally, i.e. the MENEX sky temperature, the solar adjusted MRT and the long-wave radiation from the surfaces. EM, on the other hand, partitions the incoming long-wave radiation into two equal portions, where the long-wave radiation from the ground represents one of them, while the sky and surfaces share the other portion, uncontestedly, underestimating the latter two (Huttner, 2012). This is another attribution for the lower MRT EM possesses during the early and late hours. It is also worth noting that EP uses the TARP and DoE-2 algorithms for estimating the convection heat transfer coefficients for indoor and outdoor surfaces respectively in terms of the surface roughness and the difference between the surface and the immediate air temperatures as opposed to EM which depends in its calculation on merely the wind speed. This might have possibly resulted in slight differences in the outside surface temperatures and thus more MRT variations.

Furthermore, the UTCI variations are shown to follow a similar trend for all the receptors as well as the average UTCI, however with attenuated differences. This is clearly due to the combination of the MRT values with the meteorological variables; wind speed; relative humidity; and air temperature. For a better representation for the UTCI maps as in Figure 3.6, a Grasshopper plugin, Gismo, was used to allow for the extraction of ENVI-met UTCI values and presenting them in the Rhino scene with the same legend. It is worth mentioning, however, that the “microclimate map” component in LB depicts the UTCI values as a time interval, e.g. 6-7 am, rather than at a single hour as in EM (at 7 am).

Therefore, slight differences exist from those values plotted in Figure 3.5. Despite the UTCI variations, the times required for the simulations in each model are considerably disparate. For each layout, the elapsed time differed from ~ 30 hours for EM to ~ 5 minutes for LB. It should also be noted that EM simulations run on a single-core processor as opposed to the LB simulations which were parallelised. Notwithstanding, a parallel core simulation in EM is anticipated to run in ~ 8 hours, which is still much longer than LB. In that sense, LB allows for assessing multiple design iterations with high spatial and temporal resolutions in a significantly shorter time. Hence it is suitable for optimisation studies yielding an immense number of design solutions, which would be infeasible using EM.

3.5.6 Future work

As discussed, the accuracy of the Ladybug-Tools model is mostly a function of the radiation components determined through a set of Python functions describing the MENEX and SolarCal models. While the latter was initially designed for the indoor environments, future work includes intervening with the source code so as for a more accurate representation for the outdoor conditions and less MRT deviations.

3.5.7 Postscript

This paper presented the basic foundation of understanding the model's performance in the hot arid climate of Cairo. The results have shown a good level of agreement between the validated model, ENVI-met, and the Ladybug-tools model. Further quantitative analysis was performed to ensure the adequacy of the Ladybug-tools model, according to the criteria defined in Guideline 14 of ASHRAE (2014). This was done using two indicators, namely the Mean Bias Error (MBE) for the overall mean error, and the Coefficient of Variation of the Root Mean Squared Error (CVRMSE) for the goodness of fit at timestep level, according to the following two formulae, respectively:

$$\text{MBE (\%)} = \frac{100}{T_{o,av}} \times \frac{\sum(T_o - T_s)}{n} \quad \text{Equation 3.1}$$

$$\text{CV(RMSE) (\%)} = \frac{100}{T_{o,av}} \times \sqrt{\frac{\sum(T_o - T_s)^2}{n}} \quad \text{Equation 3.2}$$

Where $T_{o,av}$ is the average of the observed data (ENVI-met in this study), T_s is the simulated data for n observations, and T_o is the observed data for n observations.

ASHRAE considers a model is calibrated when MBE is within $\pm 10\%$, and when CV(RMSE) is within $\pm 30\%$. Table 3.4 shows that the overall mean agreement in the three layouts fall within ± 10 for MRT, and within ± 6 for UTCI, while the CV(RMSE) values are within ± 12 for MRT, and ± 7 for UTCI, indicating a high level of fit.

Table 3.4: Goodness of fit according to Guideline 14 (ASHRAE, 2014).

	Linear		Dotted		Courtyard	
	MRT	UTCI	MRT	UTCI	MRT	UTCI
CV(RMSE) (%)	11.72	6.29	11.59	6.39	11.73	6.45
MBE (%)	-7.91	-4.75	-9.59	-5.24	-9.01	-5.00

The discussion in this paper highlighted some of the shortcomings of the model that lead to the deviation from the validated model, ENVI-met. On top of these shortcomings was designing the original model to account for outdoor thermal comfort by following equations and/or models originally designed for indoor environments. Although the results of the verification have shown a good agreement with ENVI-met under sunlit conditions, significant variations existed when solar radiation was obstructed. This is why it was necessary to intervene with the Python source code to adapt some of the functions with the outdoor thermal environment. The next section describes these modifications and then verifies the new model's performance against ENVI-met with reference to the original model.

3.6 Model improvement

This section briefly describes the modifications to the Python source code, in terms of ground reflectivity, radiative heat transfer coefficient, projected area factor and reflected radiation, made to improve the accuracy of the model. The modified model's accuracy is verified against ENVI-met V.4.4.4. A hypothetical simple urban geometry was simulated within each model. The analyses of the thermal performance are presented for two different locations, representing hot arid and temperate climates, namely Cairo, Egypt, and London, UK, for extreme summer and winter conditions. The work presented in this section was published in the 2020 conference "Building Simulation and Optimisation" in Loughborough University, UK (Ibrahim *et al.*, 2020a).

3.6.1 Model modifications

Examination of the Python code at each step of the MRT calculation has revealed a number of inaccuracies. First, the clothing absorptivity which might be

input by the user within the “Comfort Recipe” component, to replace the α_{sw} is fixed to 0.7, no matter the input value. This was modified to allow user input to change the absorptivity. The floor reflectivity of the outdoor surfaces was fixed within the “View Factor Calculator” component as a default value of 0.2. A new piece of code was developed to allow the user to change the reflectivity. In this work, floor reflectivity was changed to 0.3 as an average between the walls and ground albedo. Second, the radiative heat transfer coefficient, h_r was assigned the same value for both indoor and outdoor calculations as 6.012. This was changed conditionally to be 4.7 for indoor calculations as recommended by the ASHRAE handbook of fundamentals (ASHRAE, 2017b), and 6.0 for outdoor calculations in line with the JavaScript code within the ASHRAE 55-2017, Normative Appendix “C” (ASHRAE, 2017a). Thirdly, since the standing position is more common for outdoor microclimate simulations, the effective fraction of the body, f_{eff} and the projected area factor, f_p were set to represent a standing person ($f_{eff} = 0.725$ and f_p was derived from the “SplineStand” function in the Ladybug legacy component) instead of a sedentary position. Fourthly, the MRT values were only multiplied by their inverted sky view factor (surface view factor) during the sunlit hours. This was modified to include the night-time hours. Moreover, based on Arens *et al.* (2015), the SolarCal model postulates that the reductions in diffuse radiation due to protruding surfaces are compensated by the reflected radiation and vice versa. As mentioned in the previous section, the reflected radiation was defined in terms of the global horizontal radiation, and hence, it is assumed that I_{Global} is confined to I_{diff} in case of solar beam obstruction. The assumption is fairly accurate within internal environments where the amount of radiation received is limited to that coming from the window aperture. However, within the external environment, an organism will receive an additional amount of direct normal radiation, reflected by the urban surfaces. Consequently, the reflected radiation (I_{ref}) was redefined in terms of I_{Dir} following (ASHRAE, 2017a) as:

$$I_{ref} = 0.5 \cdot f_{eff} \cdot (1 - f_{svv}) \cdot I_{dir} \cdot R_{floor} \quad \text{Equation 3.3}$$

The reflectance of diffused radiation was not considered. Finally, Solar Time was used within the Ladybug legacy component in order for the solar altitude (defining sunlit hours) to match those within the epw file.

3.6.2 Simulation setup

A hypothetical geometry layout was modelled in both ENVI-met and Ladybug-tools on a grid size of 2 m assuming no vegetation nor building fenestrations (Figure 3.7). Construction materials, ground temperatures, indoor temperature, internal gains and equipment loads were set similar to those in section 3.5.3.2. The weather files for both cities were obtained from DoE (2020), and then was used as the boundary conditions for each model (using the full-forcing option in case of ENVI-met). Simulations were run for a 24-hour period on the extreme hot and cold days within the .epw files; 7th June and 17th January in Cairo; and 19th August and 14th February in London. It is worth mentioning that ENVI-met simulations were run using a student license which does not allow parallel core computing.

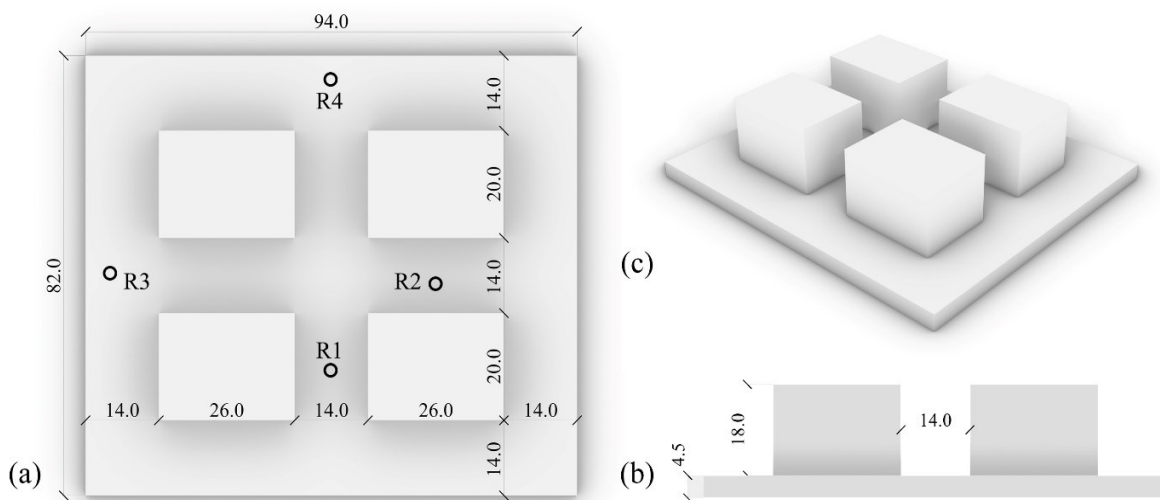


Figure 3.7: Model geometry and receptors of interest (a) top view (b) side view, and (c) 3D view (Dimensions in metres).

3.6.3 Results

3.6.3.1 Summer MRT

As for Cairo, the modifications appear to be effective within north-south (N-S) canyons as in R1, in other words where the solar radiation is blocked most of the day except for around the noon hours (11 am-1 pm) in addition to the points outside the canyon (R3 and R4). As shown in Figure 3.8, within R1, the new model resembles ENVI-met (EM) values particularly during the hours 8-10 am and 2-4 pm due to the amount of reflected radiation it receives. Having EM as the benchmark, MRT difference, (Δ MRT) between the new (LB-N) and the original model (LB-O)

has reached its maximum at 2 pm as 14.8° C. At 12 pm, EM and LB-N decline due to the high solar altitude and hence reduced long-wave radiation are received from surfaces, however the declination is steeper in LB-N most probably owing to the low projected area factor (f_p) of the human body whereas in EM the human body is represented by a cylindrical shape. Moreover, modifications to the long-wave radiation received during the night hours are not as clear as they are in the points outside the canyon as in R3, where the points have less surface view factor. Having the notion that EM averages the long-wave radiation from all the surfaces within a layout so as to reduce the calculation time, and the notion that EM was reported to underestimate the MRT during the night hours (Huttner, 2012; Forouzandeh, 2018), it could be claimed that LB-N might possibly be more accurate if compared to field measurements. Δ MRT in R3 is highest at 12 pm of 11.4° C where the LB-O receives large amount of global horizontal radiation (I_{Global}) associated with the solar altitude of the succeeding hour and its corresponding higher projected area factor.

In London, where the highest solar altitude in August is $\sim 51^\circ$, east-west (E-W) canyons as in R2 remain shaded for most of the day. This is clear where EM and LB-N maintain higher MRT values during the hours 9 am-5 pm with maximum Δ MRT at 3 pm of 13.2° C. Night-time differences are slightly larger than Cairo since the sky downward long-wave radiation in EM is calculated based on the air temperature (which is lower in London), and the atmospheric water vapor, whereas in LB-N is simplified and calculated in terms of the terrestrial sky long-wave radiation (almost similar to Cairo). Another potential reason is the heat storage within the surfaces which is accounted for in EM as opposed to LB (EnergyPlus) which takes no account of the heat storage in its surface energy balance when using the *Conduction Transfer Function* algorithm, as used in this work (DoE, 2019). Similar to Cairo, weighting the surfaces' long-wave radiation by their view factors is more potent within the points outside the canyon. Maximum Δ MRT at R4 is noticed at 2 pm as 9.24° C. On the other hand, LB-N has overestimated the MRT during 9 am-12 pm, however maintained less deviation at 1 pm-3 pm. This could be ascribed to the relatively higher f_p of a standing person compared to a seated one due to self-shading in case of the latter during the hours (9 am-11 pm). Also, while the highest solar altitude is incident at 1 pm, LB-O shows a leap due to not considering the solar time.



Figure 3.8: MRT results at different receptors for the four scenarios.

3.6.3.2 Winter MRT

In Cairo, the modifications appear to be almost uniform throughout the whole layout. The effect is clearly perceptible during the sunlit hours due to the differences between the global and direct radiation, which range between (42-342 W/m²) and (6-92 W/m²) for I_{Global} and I_{dir} respectively. Hence, the reflected radiation is diminished regardless the other factors, f_p and f_{eff} . It is worth mentioning that the MRT is calculated for the day-time and night-time separately in LB. That explains the LB-O falls at sunrise (7 am) and leaps at sunset (6 pm) which are clearer in R4, and which are dampened in LB-N. The greatest ΔMRT was registered during the hours 6 pm-12 am as on average 2.4° C and 6.1° C in R2 and R4 respectively.

Maximum differences during sunlit hours were registered at 1 pm as 1.5° C for R2 and at 11 am as 4.4° C for R4. Peculiarly, in London, although the day of simulation is overcast, direct normal radiation values are higher than those of the global and the diffused radiation which range between (222-337 W/m²) and (32-239 W/m²) for I_{dir} and both I_{Global} and I_{diff} respectively. Having the notion that the highest solar altitude on Feb 14th is $\sim 25^\circ$, both R1 and R3 remain shaded from the sunrise until 11 am. This explains the higher MRT values the LB-N possesses during these hours while being calculated with reference to the higher I_{dir} values as opposed to the LB-O whose values are estimated with regards to the lower I_{diff} values. Apart from these outliers, LB-N maintains a reasonable trend compared to that of EM. It's worth noting that the inside surface temperatures, as calculated by EnergyPlus, have an average of 6° C, a share of which is conducted to the outside face, keeping the outside surface temperatures at an average of 2° C. A slight increase ensue owing to the ambient air temperature. This clarifies the relatively higher deviations during the night hours where EM surfaces absorb rather than emit the heat to the outdoor spaces, keeping the MRT values at an average of -6.5° C.

3.6.3.3 Average MRT

Figure 3.9 shows the MRT distribution for the average values over the whole layout. LB-N appears to show better performance in all scenarios, with greater improvements in winter both in Cairo and London. It can be noticed that, within Cairo 7th June, redefining the reflected radiation with reference to the direct normal radiation (daytime hours) have shown the greatest improvement, whereas within

the other scenarios weighting the surfaces' long-wave radiation by their view factors (night-time hours) was the most effective. Maximum Δ MRT was registered at 12 pm in Cairo 7th June as 6.7° C while 5.6° C, 5.8° C and 1.8° C were registered during the hours 6 pm-12 am for London 19th August, Cairo 17th January and London 14th February respectively. Both models' correlations with EM along with RMSE are showed in Table 3.5.

Table 3.5: RMSE and R² for the ladybug original and new models compared to ENVI-met.

	RMSE		R ²	
	LB-N	LB-O	LB-N	LB-O
7 th June	3.9	7.9	0.974	0.966
19 th August	6.9	9.1	0.973	0.952
17 th January	6.1	10.1	0.972	0.851
14 th February	7.1	8.2	0.872	0.816

3.6.3.4 Average UTCI

Influenced by the radiant temperature results, the UTCI values are seen to be improved relative to the respective newly estimated MRT. Figure 3.10 is an example of the average UTCI values over the layout in Cairo on 7th June. The modifications are clearer during the night hours with a maximum UTCI difference at 4 am of 2.1° C. During the daytime, although the LB-N shows lower values than both LB-O and EM, the general trend resembles that of EM. RMSE was lowered from 4.44 to 3.45 with a stronger correlation, R² of 0.982 as compared to 0.969 for LB-O.

In conclusion, the following insights can be drawn. Variations in the models' surface energy balance calculation played a key role in the model's deviation. The three-node model used in ENVI-met accounts for the heat storage as opposed to the two-node model used in the *Conduction Transfer Function* by EnergyPlus. Using other conduction transfer algorithms, for instance, the *Heat And Moisture Transfer* algorithm would have been more accurate since it considers the heat storage within a construction material.

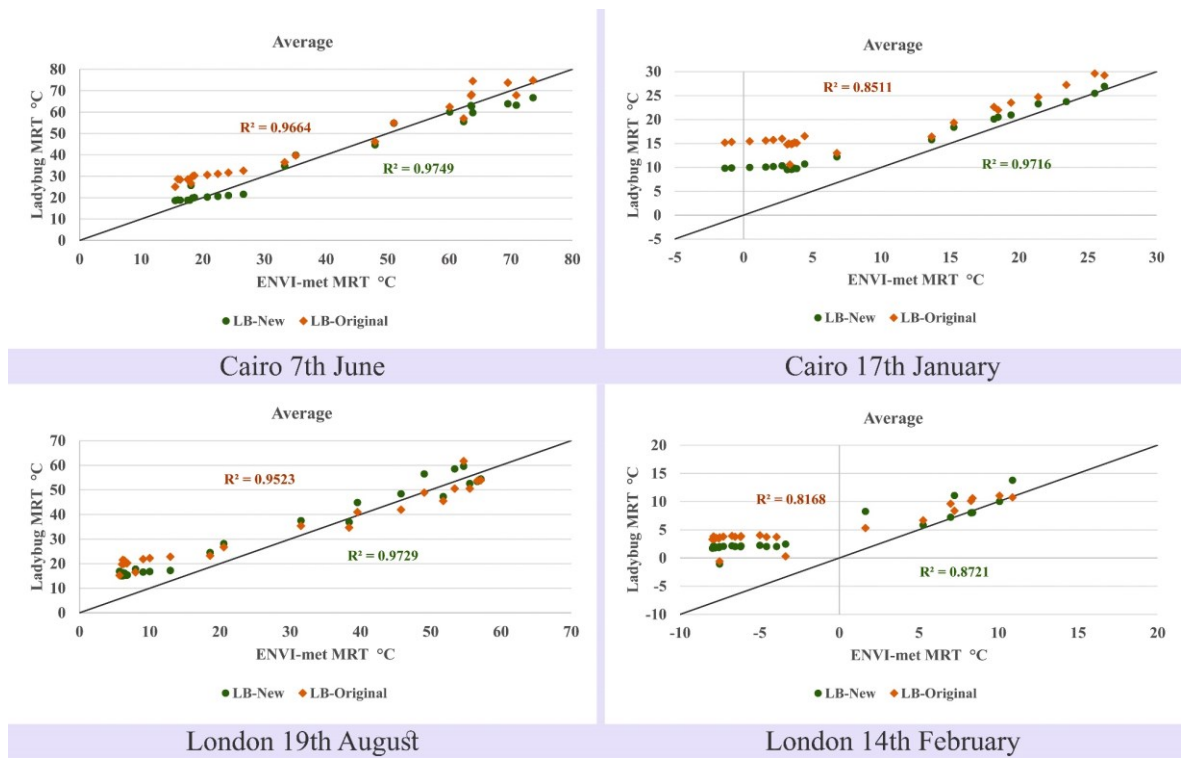


Figure 3.9: Scatter plots for the average MRT values over the whole layout within the four scenarios.

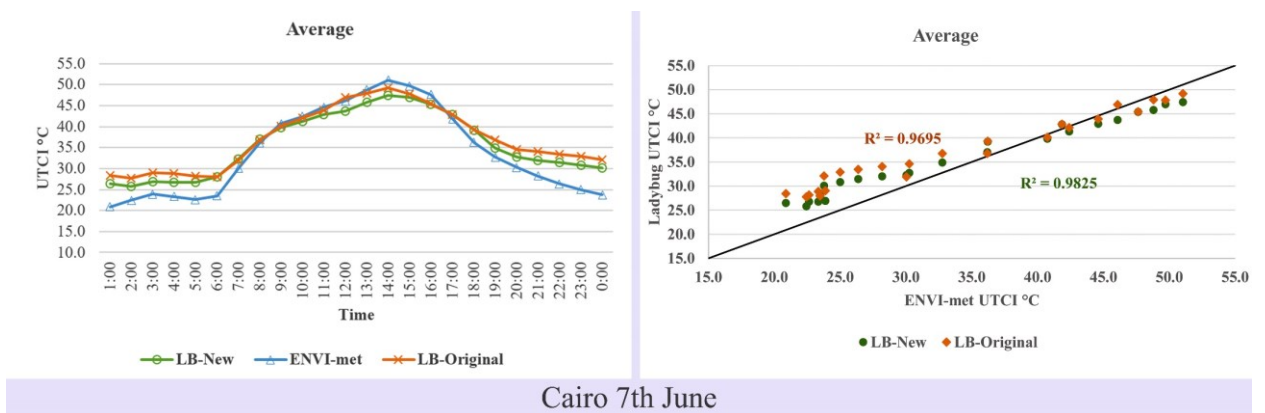


Figure 3.10: Average UTCI for Cairo on 7th June.

3.6.4 Postscript

Further quantitative analysis was performed to ensure the adequacy of the new Ladybug-tools model in summer, in Cairo, according to the criteria defined in Guideline 14 of ASHRAE (2014). This was done using the two indicators, the MBE for the overall mean error, and the CV(RMSE) for the goodness of fit at timestep level. Table 3.6 shows that both MBE and CV(RMSE) were reduced in the new Ladybug-tools model for both MRT and UTCI, as compared to the original model.

Table 3.6: Goodness of fit, in Cairo 7th June scenario, according to Guideline 14 (ASHRAE, 2014).

	CV(RMSE) (%)		MBE (%)	
	LB-N	LB-O	LB-N	LB-O
MRT	10.29	20.65	1.54	-16.18
UTCI	10.13	13.01	-4.77	-8.56

Despite the new model's deviations, the modifications made to the source code have been proven effective in improving the model's performance in outdoor conditions. Based on these variations, it was necessary to validate the improved Ladybug-tools model against field measurements.

3.7 Model validation

Field measurements were conducted in 2018 collaboratively between the candidate and a researcher from Egypt-Japan University of Science and Technology in Egypt. Measurements data were used to validate the original Ladybug-tools model (Elwy et al., 2018). The cited paper concluded with an acceptable range of deviation. The candidate acquired the data and used it to validate the model after applying the above mentioned modifications along with other improvements to the parameterisation of the model with regards to the sky resolution and building materials. The validation showed an improved performance of the new model with respect to both MRT and UTCI with $R^2 = 0.90$ and 0.91 , respectively. Although the preceding validation included running CFD analysis in OpenFOAM using the Butterfly plugin, the improved model has proved to be more accurate using wind speeds from the weather file. Maximum deviation of the UTCI reached 3.5°C , even though it cannot be utterly attributed to the model, since the meteorological parameters measured (air temperature, relative humidity, and wind speed) have also shown some discrepancies with those in the weather file. Details of the validation, calculation techniques and methods are further illustrated in the next chapter.

3.8 References

- Ali-Toudert, F. (2005). Dependence of Outdoor Thermal Comfort on Street Design in Hot and Dry Climate. (PhD). Institutes der Universität Freiburg, Freiburg, Germany. (15)
- Allegrini, J., Dorer, V., & Carmeliet, J. (2015). Influence of morphologies on the microclimate in urban neighbourhoods. *Journal of Wind Engineering and Industrial Aerodynamics*, 144, 108-117. doi: <https://doi.org/10.1016/j.jweia.2015.03.024>.
- Arens, E., Hoyt, T., Zhou, X., Huang, L., Zhang, H., & Schiavon, S. (2015). Modeling the comfort effects of short-wave solar radiation indoors. *Building and Environment*, 88, 3-9. doi: <http://dx.doi.org/10.1016/j.buildenv.2014.09.004>.
- ASHRAE. (2017a). ANSI/ASHRAE Standard 55-2017: Thermal environmental conditions for human occupancy. In (pp. 22-29). Atlanta, GA: American Society of Heating, Refrigerating and Air-Conditioning Engineers, .
- ASHRAE. (2017b). ASHRAE HandBook of Fundamentals (SI Edition). In. Atlanta: American Society of Heating, refrigerating, and Air-Conditioning Engineers Inc.
- Bueno, B., Norford, L., Hidalgo, J., & Pigeon, G. (2013). The urban weather generator. *Journal of Building Performance Simulation*, 6(4), 269-281. doi: <https://doi.org/10.1080/19401493.2012.718797>.
- DoE. (2019). Engineering reference: EnergyPlus version 9.2.0. In (pp. 58-167).
- DoE. (2020). Weather Data. Retrieved from <https://energyplus.net/weather>
- Elwy, I., Ibrahim, Y., Fahmy, M., & Mahdy, M. (2018). Outdoor microclimatic validation for hybrid simulation workflow in hot arid climates against ENVI-met and field measurements. *Energy Procedia*, 153, 29-34. doi: <https://doi.org/10.1016/j.egypro.2018.10.009>.
- Engineering-ToolBox. (2001). Engineering ToolBox. Retrieved from <https://www.engineeringtoolbox.com/>
- Fathy, F., Mansour, Y., Sabry, H., Abdelmohsen, S., & Wagdy, A. (2015). Cellular Automata for Efficient Daylighting Performance: Optimized Façade Treatment. In *Proceedings of the 14th Conference of the International Building Performance Simulation Association (IBPSA)*.
- Forouzandeh, A. (2018). Numerical modeling validation for the microclimate thermal condition of semi-closed courtyard spaces between buildings. *Sustainable Cities and Society*, 36, 327-345. doi: <https://doi.org/10.1016/j.scs.2017.07.025>.
- Huttner, S. (2012). Further development and application of the 3D microclimate simulation ENVI-met. (PhD). Mainz University, Germany,
- Ibrahim, Y., Kershaw, T., & Shepherd, P. (2020). Improvement of the Ladybug-tools microclimate workflow: A verification study. In *Building Simulation and Optimization 2020*, Loughborough University, Loughborough, UK.
- Jamei, E., & Rajagopalan, P. (2019). Effect of street design on pedestrian thermal comfort. *Architectural Science Review*, 62(2), 92-111. doi: <https://doi.org/10.1080/00038628.2018.1537236>.
- Jänicke, B., Meier, F., Hoelscher, M.-T., & Scherer, D. (2015). Evaluating the effects of façade greening on human bioclimate in a complex urban environment. *Advances in Meteorology*, 2015. doi: <https://doi.org/10.1155/2015/747259>.
- Mackey, C. (2015). Pan climatic humans: shaping thermal habits in an unconditioned society. (PhD). Massachusetts Institute of Technology,

- Mackey, C., Galanos, T., Norford, L., Roudsari, M. S., & Architects, P. (2017). Wind, sun, surface temperature, and heat island: critical variables for high-resolution outdoor thermal comfort. In *Proceedings of the 15th International conference of Building Performance Simulation Association*. San Francisco, USA.
- McNeel, R. (2021). Rhino3D. Retrieved from <https://www.rhino3d.com/>
- Naboni, E., Meloni, M., Coccolo, S., Kaempf, J., & Scartezzini, J.-L. (2017). An overview of simulation tools for predicting the mean radiant temperature in an outdoor space. *Energy Procedia*, 122, 1111-1116. doi: <https://doi.org/10.1016/j.egypro.2017.07.471>.
- O'Malley, C., Piroozfar, P., Farr, E. R., & Pomponi, F. (2015). Urban Heat Island (UHI) mitigating strategies: A case-based comparative analysis. *Sustainable Cities and Society*, 19(2), 222-235. doi: <https://doi.org/10.1016/j.scs.2015.05.009>.
- Perini, K., Chokhachian, A., Dong, S., & Auer, T. (2017). Modeling and simulating urban outdoor comfort: Coupling ENVI-Met and TRNSYS by grasshopper. *Energy and Buildings*, 152, 373-384. doi: <https://doi.org/10.1016/j.enbuild.2017.07.061>.
- Robinson, D., & Stone, A. (2004, 19 - 22 September 2004). Irradiation modelling made simple: the cumulative sky approach and its applications. In *21st PLEA Conference*, Eindhoven, The Netherlands.
- Roudsari, M., Mackey, C., & Armour, T. (2022). Ladybug-Tools forum. Retrieved from <https://discourse.ladybug.tools/>
- Roudsari, M. S., & Mackey, C. (2022). Ladybug-tools. Retrieved from <https://www.ladybug.tools/>
- Roudsari, M. S., Pak, M., & Smith, A. (2013). Ladybug: a parametric environmental plugin for grasshopper to help designers create an environmentally-conscious design. In *Proceedings of the 13th international IBPSA conference*, Lyon, France, 25-30 August.
- Rutten, D. (2021). Grasshopper3D. Retrieved from <https://www.grasshopper3d.com/>

3.9 Epilogue

This chapter presented the methodological approaches adopted in this thesis, the Ladybug-tools model and its improvement, and the verification against ENVI-met as well as the validation against field measurements. The improved model appeared to be consistently appropriate in the context of this thesis. This is due to its capability to capture the spatial and temporal patterns of the solar exposure and produce the performance metric most relevant to the aims of this thesis, the UTCI. Moreover, in the context of analysing hypothetical urban forms to inform the pre-design process, the reduced simulation time compensates the deviations recorded and thus qualifies the Ladybug-tools model to be top of the list of the microclimate models when it comes to optimisation studies, where simulating hundreds of geometry configurations becomes viable. A main advantage of using this model is its dependence on previously validated simulation engines such as the UWG and EnergyPlus. The latter provides the energy loads conceived as the second performance criteria in chapters 5 and 6. Also, RADIANCE is used in solar exposure analysis in chapter 6.

Based on the results and discussion of the two papers presented, and based on the validation of the model, the model was shown to offer good accuracy by using the wind speeds from the weather file. Thus, it was decided to exclude the CFD analyses from the workflow in order to facilitate the continuity of the optimisation analyses throughout the thesis. The next chapter commences the work on the optimisation of urban geometry design parameters and their impact on the UTCI by analysing the performance of several urban canyon configurations.

4 Thermal Comfort Optimisation of Urban Canyon Geometries

4.1 Preface

The discussion on the importance of urban canyon geometry and its impact on the radiation access, shading and trapping, wind patterns and thermal comfort started decades ago (Nunez & Oke, 1977), and continues still. Urban canyons, as described by Oke (1981), are the basic geometric unit of urban spaces, constituting almost two-thirds of urban areas, and thus the configuration of their characteristic features have a key role to play in changing the energy balance and pedestrians' thermal comfort.

This chapter addresses the first research question “*What are the canyon-scale optimum design parameters for improving outdoor thermal comfort?*”, as the first stage of investigating the relationship between the built geometry and the microclimate. Although there have been studies in the literature aimed at establishing such a relationship, the parametric nature of the simulation workflow presented in the previous chapter and used throughout this thesis allows for better sampling, and thus more precise investigation of the design parameters than previous studies, particularly those in the hot arid climate of Egypt (Shalaby & Shafey, 2018), thereby providing a deeper understanding of these relationships.

Outdoor thermal comfort is represented by the average UTCI of different locations within the urban canyon during the daytime hours of the hottest day, referred to in the paper as average diurnal UTCI. The selection of the design parameters is consistent with those typified in the literature (Oke, 1981); these are street width (W), also referred to as the distance between buildings, building heights (H), and orientation. Further relationships are drawn with regards to common geometrical attributes of urban canyons; the height-to-width (H/W) – the aspect ratio, and the sky view factor (SVF).

The study of the canyon geometry is exemplified in this chapter by the microclimatic performance of urban canyons with symmetrical and asymmetrical heights of their flanking buildings – two arrays of 5 residential units, 24 m × 20 m each, with a total length of 100 m. In the literature, the geometrical configurations of asymmetrical urban canyons are often represented by standardised attributes to indicate their environmental performance, for instance, the average H/W or the average SVF. In this study, however, detailed insights are drawn regarding the heights of each flanking side and the ratio of its height to the street width, rather than the average of the two sides (flanks). The analysis was conducted in three phases, where the sampling of the design parameters in one phase depended on the results of its preceding phase. For instance, although an urban canyon orientated 0° was expected to yield identical results to that orientated 180° , orientation 180° was included in the first phase to ensure that the model is deterministic, however, it was excluded in the second the third phases. Also, street widths wider than 18 m were found to yield higher UTCI, with no significant changes, thus were excluded in the succeeding phases. Likewise, the minimum building height and step size of increment were adjusted based on the nature and magnitude of the difference in UTCI in the preceding phase.

This chapter is based on the paper “A parametric optimisation study of urban geometry design to assess outdoor thermal comfort” published in the journal *Sustainable Cities and Society* in 2021, in collaboration with a researcher from Egypt-Japan University of Science and Technology in Egypt. The collaboration included conducting the field measurements in Cairo necessary to validate the simulation workflow. The contents of this chapter are identical to the original manuscript, however, minor changes were added as footnotes where clarification is needed. The candidate has predominantly contributed to the publication. Details of authorship of this paper are given in Table 3.1.

Table 4.1: Declaration of authorship.

This declaration concerns the article entitled:
A parametric optimisation study of urban geometry design to assess outdoor thermal comfort.
Publication status (tick one)
Draft manuscript <input type="checkbox"/> Submitted <input type="checkbox"/> In review <input type="checkbox"/> Accepted <input type="checkbox"/> Published <input checked="" type="checkbox"/>
Publication details (reference):
Ibrahim, Y. , Kershaw, T., Shepherd, P., & Elwy, I. (2021). A parametric optimisation study of urban geometry design to assess outdoor thermal comfort. <i>Sustainable Cities and Society</i> , 75 (103352), pp: 1-18. DOI: https://doi.org/10.1016/j.scs.2021.103352 .
Copyright status (tick the appropriate statement):
<ul style="list-style-type: none"> • I hold the copyright for this material <input type="checkbox"/> • Copyright is retained by the publisher, but I have been given permission to replicate the material here <input checked="" type="checkbox"/>
Candidate's contribution to the paper (%):
The candidate has predominantly contributed to: <ul style="list-style-type: none"> • Formulation of ideas (80%): Y. Ibrahim developed the ideas, in consultation with T. Kershaw. • Design of methodology (80%): Y. Ibrahim developed the methodology, in consultation with T. Kershaw. • Data analysis (100%): Y. Ibrahim conducted the data analysis. • Presentation of data in journal format (80%): Y. Ibrahim wrote the paper. T. Kershaw submitted the paper. T. Kershaw and P. Shepherd provided feedback for improvements, and for addressing reviewers' comments. • Validation (50%): Y. Ibrahim conducted the field measurements with I. Elwy.
Statement from Candidate:
This paper reports on original research I conducted during the period of my Higher Degree by Research candidature.
Signed:
Date: September 2022

4.2 Abstract

Over the last two decades, urban geometry has been shown to be a key determinant of the microclimatic conditions in urban areas. This study uses the Ladybug-tools, the plugins of Grasshopper3D to optimise building heights, street widths and orientation to maximise outdoor thermal comfort, represented by the diurnal average Universal Thermal Climate Index (UTCI). In the hot-arid climate of Cairo, Egypt, the optimised parameters of symmetrical and asymmetrical urban canyons are compared with the Egyptian Construction Act's design regulations. The results show a strong negative correlation between the height-to-width (H/W) ratios and the output UTCI, with $R^2 = 0.71$, and much stronger ($R^2 = 0.91$) if east-west orientations are excluded from the results, exceeding correlations previously reported for Cairo. Maximum UTCI reductions due to changing H/W and orientation approach ~ 6 °C. Considerable variation is shown in the strength of the correlation between UTCI and the asymmetrical H/W ratio of each flank, with $R^2 = 0.81$ for Southeast side compared to $R^2 = 0.4$ for Northwest side. Design recommendations are given urban planners based on using the optimised parameters that at least achieve a UTCI reduction benchmark that exceeds those resulting from using the regulations' thresholds.

4.3 Introduction

Urban areas are expected to accommodate almost 70% of the global population by 2050 (United Nations, 2018). With such global urbanisation rates, increasing attention has been paid to the negative environmental impacts of urban areas, and many discussions on the resilience and liveability of current and future urban developments have expanded to include other environmental qualities such as urban health and well-being. The impact of the urban microclimate on public health has already been documented (Kovats & Hajat, 2008), and over the past three decades, the attention given to outdoor thermal comfort as one of the key performance indicators for urban environmental assessment has grown (Jamei *et al.*, 2016). For outdoor urban environments, thermal comfort is temporal and is dependent on the inter-connectivity of the physiological and micro-climatological conditions (Coccolo *et al.*, 2016), where pedestrians are exposed to large fluctuations in air temperatures, wind velocities and solar irradiation over time. Moreover, the thermal stress-induced sensation can drive pedestrians into adaptation practices, i.e. increasing dependency on automobiles and use of indoor

space, which in turn increases their associated energy consumption and greenhouse gas emissions (Fletcher *et al.*, 2013). Given knowledge of human thermoregulation and the recent development of computational models (Naboni *et al.*, 2019a), comfort metrics have become easier to understand and more viable to quantify. Indeed, the integration of these metrics in climate-responsive design policies and guidelines has become an inevitable practice (Ruefenacht *et al.*, 2020), although this is not fully realised across the globe.

Densification of the built environment leads to the replacement of permeable surfaces with impervious construction materials, reduced vegetation, increased pollution, and relatively narrower canyon ratios. Dubbed the urban heat island (UHI), Oke (1995) articulated the negative impacts that urban areas pose to the microclimate. This includes increased long-wave radiation absorption as a result of air pollution and the sensible heat storage due to the higher thermal admittance of building constructions. Evaporative cooling is also limited by impervious paving and reduced percolation, while anthropogenic heat is released into the local environment from buildings and traffic. Canyon geometry is another crucial factor, with recurrent reflections trapping short-wave radiation at street level, leading to greater absorption and attenuating net long-wave radiation loss, as well as inhibiting turbulent heat transfer by convection (Oke, 1995; Toparlar *et al.*, 2015). In this context, urban form plays a crucial role in shaping the microclimatic conditions to which pedestrians are exposed, and hence the perceived thermal comfort. Studies that have investigated canyon geometry in temperate and humid climates are abundant (Qaid & Ossen, 2015; Sharmin *et al.*, 2017), as opposed to those conducted in hot and dry areas, though the latter accommodates about one-third of the world's population (Pearlmutter *et al.*, 2007). Given the interdependencies of the energy budgets of urban elements, in-situ measurements are typically laborious compared to computational simulations. In this regard, there has been significant interest among bio-climatologists to develop computational models capable of estimating human thermal comfort in response to their ever-changing surrounding thermal environment (Naboni *et al.*, 2017). Additionally, the tendency to engage parametric design tools within urban environmental simulations has increased remarkably, where the exploration of a myriad of design solutions is feasible (Wagdy *et al.*, 2017).

4.3.1 Urban geometry

The planetary boundary layer, the lowest layer of the Earth's atmosphere, is partitioned into an urban canopy layer (UCL) which extends from the street level up to the mean height of the roughness elements, i.e. buildings and trees, and the urban boundary layer (UBL) which can extend to up to 2 km above the city (Ampatzidis & Kershaw, 2020). Besides the thermal mixing and level of moisture and pollutant content of the atmosphere, the height, spacing and configuration of the urban roughness elements dictate the air flow characteristics, and hence shape the structure and the depth of the UBL (Oke *et al.*, 2017). At a city scale, neighbourhoods with similar land use and land cover can generate different local microclimates due to several factors, among which are urban morphology, construction materials, provision of vegetation and human activity (Stewart & Oke, 2012). Urban forms comprise of several urban canyons with varying geometric parameters such as canyon orientation, street width (W), building heights (H), canyon aspect ratio (H/W), and sky view factors (Ali-Toudert & Mayer, 2006). These different configurations, together with other surface-specific parameters, e.g. albedo and emissivity (Andreou, 2013), and environmental parameters, e.g. air temperatures, humidity, wind speed and solar irradiation, are sufficient to modulate the radiant exchanges and wind flow patterns within the canyon, resulting in distinct microclimatic conditions for an urban canyon (Grimmond *et al.*, 2010).

The local climate of given urban form could be implied from the microclimatic performance of these canyons (Fahmy, 2010; Lin *et al.*, 2017). Hot-dry areas are accompanied by substantial heat stress, due to the increased magnitude of short-wave solar radiation and increased long-wave radiation emitted from urban surfaces, and hence should not accommodate dispersed urban forms typical of hot-humid areas (Ratti *et al.*, 2003). However, the suitability of a given urban layout for a specific climate remains a function of the geometrical proportions, which might if changed significantly, entail a radical change in performance (Golany, 1996).

The influence of canyon aspect ratio on the microclimate is disparate, with its induced thermal performance being highly dependent on the climatic region. A higher H/W ratio (lower sky view factor) reduces the amount of solar radiation received and absorbed by the urban surfaces, entailing lower daytime temperatures, albeit with slightly higher nocturnal temperatures (Johansson, 2006), partially due to trapping the long-wave radiation within the street canyon (known as the canyon effect). As a result, abundant studies have acknowledged that higher

H/W ratios can be beneficial in dry climates (Ahmed, 1994; Bourbia & Boucheriba, 2010), while others have argued their benefits due to lower wind penetration and reduced cooling rates (Niachou *et al.*, 2008; Giannopoulou *et al.*, 2010). In terms of their shading effect, studies conducted in various climatic regions have attested that improved thermal comfort levels can be achieved by the shading generated by increased building heights (Ali-Toudert & Mayer, 2007a; Perini & Magliocco, 2014).

On the other hand, studies investigating canyon orientation in different climates have shown significant variability. Street orientation, unless notably wide, defines the diurnal course of the canyon's solar exposure. However, seasonal variations play as important a role as the orientation. Thus, an "optimum" orientation is ostensibly unattainable, and a "preferred" one should be a trade-off between hot and cold seasons. Nonetheless, East-West (E-W) canyons have been reported to maintain the worst daily thermal conditions, particularly during summer, owing to increased solar exposure (Watkins *et al.*, 2007). In this sense, North-South (N-S), NE-SW, and NW-SE oriented canyons have been advocated by many studies to be appropriate within arid, semi-arid, and Mediterranean climates (Jamei & Rajagopalan, 2019), while others have claimed the suitability of E-W canyons for temperate and Mediterranean climates only if galleries and overhanging facades are used (Ali-Toudert, 2005).

Furthermore, a canyon's airflow is influenced by its geometry (H/W ratio and the orientation) and is governed by the mean wind at the average roof level. In simple terms, the lower the H/W ratio, the less undisturbed airflow there is above the canopy layer. H/W ratios of ~ 0.05 are characterised by an isolated roughness flow. This is disturbed by the canyon's flow as the H/W increases up to 0.7 and is turned into a wake interference flow with deflection-reinforced eddies generated within the canyon. A skimming flow occurs as the H/W increases above 0.7, where the canyon is characterised by circulatory vortices (Oke, 1988). The speed of a single vortex in a skimming flow regime is a function of air flow above the roof level, thermal stratification inside the canyon, and the advective motions from the buildings' corners (Ali-Toudert, 2005). In case of light winds, thermal variations due to the warming of canyon facets can shift the flow from one regime to another (Sini *et al.*, 1996) and a second contra-rotating vortex may be generated (He *et al.*, 2019). Moreover, canyons with an orientation parallel to the wind direction will experience a "channelling effect", whereas those perpendicular to the wind flow will experience transverse flows at the downwind side of the street.

An air flow with an oblique angle will result in corkscrew-like eddies along the length of the canyon (Oke, 1988). At a neighbourhood scale, as cities are densified from scattered to compact areas, wind speed and the ventilation potential decrease (He *et al.*, 2019). The heterogeneity of building heights, however, plays an important role in enhancing the ventilation potential, where higher buildings downwash the ambient flow to the street level (Golany, 1996; He *et al.*, 2019).

4.3.2 *Thermal Comfort*

Human thermal comfort is usually defined as “the condition of mind which expresses satisfaction with the thermal environment”. It is mainly influenced by such bio-meteorological factors as air temperature, radiant temperature, velocity of air, humidity, clothing and metabolic rate production (ASHRAE, 2017a). Fanger (1970) derived the first expression to indicate both heat and cold stress, the Predicted Mean Vote (PMV), and its corresponding Predicted Percentage of Dissatisfied (PPD) on account of indoor comfort quantification. However, such indices are not as efficient to model the human interaction with their ever-changing outdoor microclimate as they are for the thermoregulatory equilibrium state within an indoor environment. This has led to the development of indices specifically for outdoor comfort evaluation (Potchter *et al.*, 2018). The preceding half-century has seen the development of diverse comfort models in search of a holistic index, capable not only of gauging thermal sensation within warm and cold climates, but also specifying to what extent people perceive the thermal stress to which they are exposed. Examples are abundant, albeit the most commonly used indices are the Physiologically Equivalent Temperature (PET) (Höppe, 1999) and the Universal Thermal Climate Index (UTCI) (Bröde *et al.*, 2012). These indices provide the full range of thermal sensation, up to ten categories, in hot and cold conditions and provide the equivalent temperature for sensation (Potchter *et al.*, 2018). UTCI was developed to indicate the air temperature in a reference environment which elicits a similar physiological response to that of the actual environment. UTCI has been developed based on the multi-node Fiala thermoregulatory model (Fiala *et al.*, 2012) which accounts for the dynamic thermal body responses, as well as the advanced clothing model by (Havenith *et al.*, 2012) to account for the adaptation and distribution of clothing. The accuracy of the model stems from the calculation of body thermal and nervous responses in twelve body segments, while at the same time taking into account the inner and outer body heat transfer (Coccolo *et al.*, 2016).

UTCI has been applied across all Köppen Geiger climate regions and has been validated against monitored data and other thermal indices, e.g. PET and PMV. Furthermore, UTCI presents a detailed representation of thermal sensation for the neutral as well as the extreme cold and hot conditions (Figure 4.1) (Blazejczyk *et al.*, 2012). Unlike PMV which sorts thermal stress into categories, UTCI provides the equivalent temperature for sensation in degrees Celsius, which makes it more perceptible by urban designers and planners.

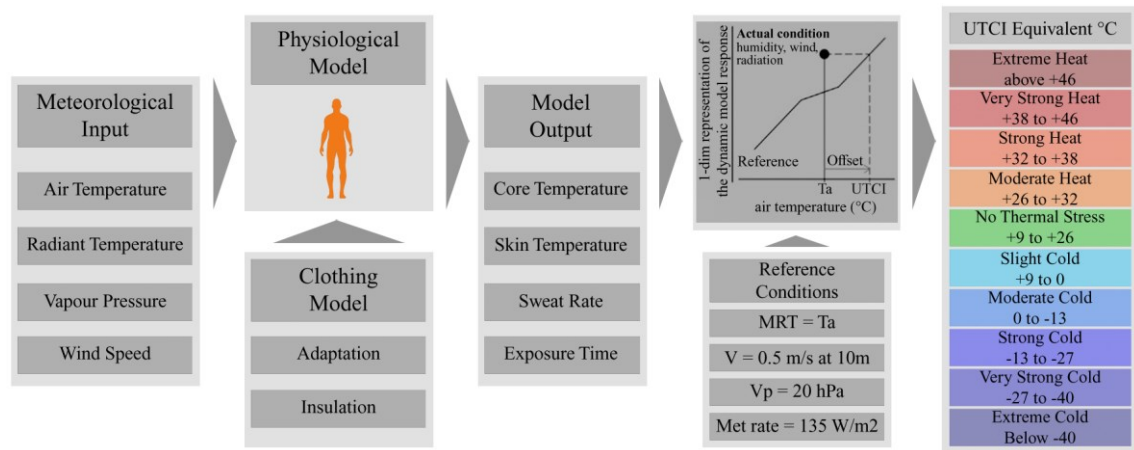


Figure 4.1: Concept of the UTCI equivalent temperature, adapted from (Bröde *et al.*, 2012)

4.3.3 Research problem and objectives

Egypt, as a developing country, is striving to contain overpopulation, and provide adequate and affordable housing, whilst also constricting urban sprawl. In 2015, the government set out a long-term action plan for the physical expansion of existing cities, and the planning for new urban communities. However, the endeavours to integrate environmental performance assessment into practice in Egypt are still voluntary. Moreover, the Executive Regulations for the Egyptian Unified Construction Act (MHUUC, 2008) specifies merely spatial, rather than climate-responsive urban form design norms and criteria, particularly with respect to the canyon-scale design. This gap between the study of outdoor thermal comfort and the design practice inhibits the improvement of cities' microclimates, thereby deteriorating health and well-being. A number of studies have investigated the impact of canyon geometry design on the microclimate in Egypt. Labib and Beltran (2015) studied the outdoor thermal comfort (represented by PET) of a single urban canyon in Cairo, Egypt, using ENVI-met. The urban canyon however had a fixed street width of 9m, and the simulations ran over only 4 orientations and only 4 height-to-width (H/W) ratios (4 building heights).

In their conclusions, the authors pointed out that, timewise, examining a large number of canyon configurations using ENVI-met is cumbersome, and they recommended using a parametric modelling platform that could be efficient to produce a larger number of street configurations. Similarly, Shalaby and Shafey (2018) investigated the microclimate of a simple hypothetical urban layout in Cairo, using ENVI-met. However, the study examined a limited number of canyon configurations, having a street width fixed to 12m and 5 H/W ratios with building heights ranging between 12m and 60m, for different orientations. In their investigation of four urban communities in Cairo, (Galal et al., 2020) claimed that PET at the street level is strongly dependent on the H/W ratio, rather than the mere height or width thereof. However, having a closer look at the H/W ratios examined at this study, only 3 out of 68 streets had a H/W greater than 2. Moreover, none of these studies have considered the performance of asymmetrical urban canyons and if they perform any differently from symmetrical ones.

This paper utilises the parametric design capabilities of modern software packages to be the first to investigate thousands of canyon geometry configurations. The parameters being examined in this study are the street widths, building heights (symmetrical and asymmetrical with respect to the street axis), H/W ratios and orientation. In this research, our objective is to simulate a wider variety of widths, heights, H/W ratios and orientations to find the optimal urban canyon parameters to improve outdoor thermal comfort and compare these thresholds to those of the Egyptian Construction Act, and then provide recommendations and guidelines that should be adopted in the Executive Regulations.

The study is performed in the hot arid climate of Cairo, Egypt, where Cairo accounts for almost 32% of the current new residential projects, and along with Alexandria, around 88% of the residential apartments with air conditioning (Mahdy, 2014; CAPMAS, 2019). In this research, the Ladybug-tools (Roudsari & Mackey, 2022), the plugins for Grasshopper 3D, are used to calculate the UTCI as a metric for outdoor thermal comfort within the street canyon. Also, taking the same approach of the above-mentioned studies, simulations are conducted over a single day that represents severe climatic conditions, which occur during June and July in Egypt.

4.4 Methodology

The Executive Regulations for the Egyptian Construction Act (MHUUC, 2008) specifies some canyon parameter thresholds for urban communities, such as a minimum street width of 10m, maximum building heights of 36m and a maximum H/W ratio of 1.5. Currently, the Egyptian government is considering the applicability of a few amendments to the regulations, with even lower thresholds. Since the aim of this study is to examine a wider variety of H/W's to find the optimum thresholds, the design parameters thresholds were set according to the Executive Regulations (MHUUC, 2008), with the exception that street widths were set to a lower bound of 6m (Table 4.2). A hypothetical urban canyon geometry was created and simulated in three consecutive and correlated phases, with building constructions obtained from Engineering-ToolBox (2001).

The first phase includes the simulation of a sole urban canyon, having the building heights on both sides of the canyon (Array A and Array B in Table 4.2) changing simultaneously to investigate the thermal comfort in symmetric urban canyons, followed by a regression analysis to scrutinise the relationship between the design parameters and the output UTCI. In the first phase, Orientation 180° is anticipated to be identical to orientation 0°. However, it was included to verify the model's performance. The thermal performance (UTCI) of the canyon is assessed at a single point on the central axis of the canyon at a height of 1.1m to represent pedestrian level thermal comfort, and the outputs of this phase are presented as the average diurnal UTCI recorded from 5 am (sunrise) to 7 pm (sunset). Based on the first phase's results, the thresholds and steps of the parameters are refined in both phases 2 and 3 to those eliciting relatively lower UTCI values (Table 4.2).

In the second phase, the canyon is simulated within an urban context of an existing newly constructed urban community to provide a more realistic estimation of the urban heat island effect. Heights of the flanking building arrays A & B are varied independently to address the potential of asymmetrical urban canyons for better thermal comfort. The second phase's results are presented as the average value of all points on a 2m grid inside the canyon, rather than a single point. This gives a better overall view of the thermal performance of the canyon and as such avoids any anomalies -if any- of a single point output. The results of this phase are also shown as the average diurnal UTCI recorded from 5 pm to 9 pm (2 hours after sunset) to investigate the impact of solar radiation exposure/blockage on thermal comfort at certain hours.

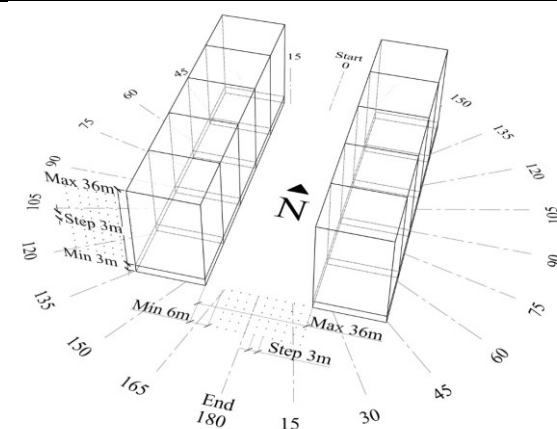
This helps to accentuate the effect of each flank's height on the UTCI and thus supports the design strategies to increase the sky view factor to mitigate the UHI effect; this also helps to interpret the results of the third phase. As per the second phase, in the third phase, building heights are simulated independently, however with fewer steps (Table 4.2). Results of this phase are averaged across the canyon and presented as the average UTCI registered from 5 am to 7 pm to provide an overall analysis during the daytime. This way, the third phase links the analysis approach of both the first and second phases but with more attention given to each flank's H/W rather than their mere heights. Johansson (2006) investigated the thermal performance of 12 urban canyons in the hot-arid climate of Fez, Morocco, and reported that the relative cooling by day due to shading exceeded the warming by night. For this reason and to better understand the urban geometry response to the solar exposure without being misinterpreted by averaging, nocturnal temperatures were not included in this study.

4.4.1 *Simulation workflow*

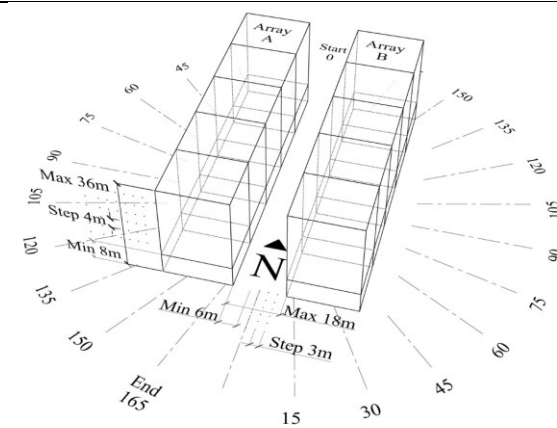
The ladybug-tools model is selected for this study for several reasons; it is considerably less time consuming to perform calculations than ENVI-met, allowing for the simulation of thousands of canyon configurations, it produces a variety of thermal indices, among them is the UTCI which is the focus of this study, and the ability to parametrically model canyon geometries and to visualise the results within the Grasshopper environment. The ladybug-tools microclimate model is a combination of Grasshopper plugins (Roudsari & Mackey, 2022) used to estimate the outdoor thermal comfort with a graphical representation. The model is based on linking Grasshopper to already validated software engines dedicated to calculating the thermal comfort determinants individually. For instance, Honeybee links Grasshopper to EnergyPlus (Crawley *et al.*, 2001) which calculates the surface temperatures. Dragonfly utilises the Urban Weather Generator (UWG) (Bueno *et al.*, 2013) to calculate the urban air temperature and relative humidity. The algorithm combines a variety of input parameters, such as the average building heights and the surface roughness, to morph the 'rural' weather file into a new 'urban' file containing modified hourly urban air temperatures and relative humidity.

Table 4.2: Thresholds and steps of the parameters simulated in all phases.

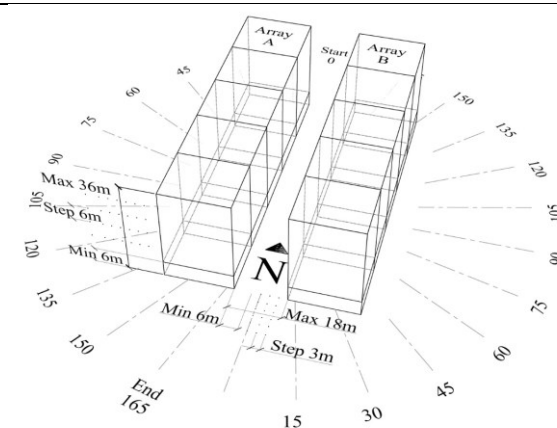
Phase 1 (a total of 1716 cases)			
	Min	Max	Step
Building Heights	3m	36m	3m
Street Width	6m	36m	3m
Orientation	0°	180°	15°



Phase 2 (a total of 3840 cases)			
	Min	Max	Step
Building Heights A	8m	36m	4m
Building Heights B	8m	36m	4m
Street Width	6m	18m	3m
Orientation	0°	165°	15°



Phase 3 (a total of 2160 cases)			
	Min	Max	Step
Building Heights A	6m	36m	6m
Building Heights B	6m	36m	6m
Street Width	6m	18m	3m
Orientation	0°	165°	15°



Ladybug components are used to visualise the environmental data and the output results. The Butterfly plug-in could potentially integrate OpenFOAM software for CFD air flow analyses, but this would involve prohibitively high computation time. Therefore, wind speeds in this study are retrieved from the weather file, where the weather station 10m-high wind speeds are translated into 2m-high wind speeds and vice versa, where necessary, using a Ladybug component based on the wind profile power law.

The mean radiant temperature (MRT) is calculated as the agglomeration of the three components; the long-wave radiation from the surfaces; the amount of the sky long-wave radiation absorbed by the human body; and the additional amount of absorbed solar short-wave radiation. The long-wave radiation from surfaces is estimated by using the following formula:

$$\text{MRT}_{\text{Surface}} = \left[\frac{\sum_{i=1}^N (T_s^4 \cdot F_s + T_e^4 \cdot F_{ns})}{\sum_{i=1}^N F_s} \right]^{1/4} \quad \text{Equation 4.1}$$

Where T_s is the outside surface temperature calculated by EnergyPlus. T_e is the ambient temperature² of one surface and is assumed to be equal to the ambient air temperature as shaped by the surrounding surfaces. F_s is the view factor between the point of interest and a specific surface and F_{ns} is the non-surface view factor, i.e. view factor to surfaces other than that specific surface. Angle factors are calculated by tracing back the number of spherical vectors impinging one surface and dividing that number by the total number of vectors emanating from each point. The absorbed sky long-wave radiation is calculated by following the formula specified within the MENEX model (Blazejczyk, 2005) as follows:

$$\text{MRT}_{\text{sky}} = f_{\text{svv}} \cdot \left(\frac{L_a}{\alpha_{\text{lw}} \cdot \sigma} \right)^{1/4} - 273.15 \quad \text{Equation 4.2}$$

Where f_{svv} is the sky view from a certain point unobstructed by opaque surfaces. L_a is the terrestrial sky long-wave radiation, and is obtained from the weather file. α_{lw} is the emissivity of the human body for long-wave radiation (default value of 0.95), and σ is the Stephan Boltzmann constant ($5.667 \cdot 10^{-8} \text{ W/m}^2\text{K}^4$). As for the short-wave solar radiation, the model accounts for the absorbed portion by means of the effective radiant field (ERF) specified within the SolarCal model (Arens *et al.*, 2015) and the normative appendix (C) of (ASHRAE, 2017a) in terms of the three components; the direct; diffused; and reflected solar radiation, where the latter is defined with reference to the global horizontal radiation as follows:

$$\text{ERF}_{\text{solar}} = \frac{\alpha_{\text{sw}}}{\alpha_{\text{lw}}} \cdot [(0.5 \cdot f_{\text{eff}} \cdot f_{\text{svv}}) (I_{\text{Global}} \cdot R_{\text{floor}} + I_{\text{diff}}) + (f_p \cdot f_{\text{eff}} \cdot I_{\text{Dir}})] \quad \text{Equation 4.3}$$

Where α_{sw} is the absorption coefficient for the short-wave radiation (default value of 0.7), f_{eff} is the fraction of the body exposed to radiation (0.696 and 0.725 for a seated and a standing person respectively). I_{Global} , I_{diff} , I_{Dir} are the global, diffused and direct normal radiation respectively. R_{floor} is the floor/ground

² Ambient temperature refers to the near surface temperature.

reflectivity and f_p is the projected area factor and is derived with reference to the solar altitude and azimuth as in (Fanger, 1970) and (ASHRAE, 2017a). The amount of additional MRT due to solar radiation is eventually calculated in terms of ERF, f_{eff} , and the radiative heat transfer coefficient (h_r) as follows:

$$\text{MRT}_{\text{sol}} = \frac{\text{ERF}_{\text{solar}}}{f_{\text{eff}} \cdot h_r} \quad \text{Equation 4.4}$$

Figure 4.2 shows the data streaming between the different plugins, components and simulation engines as used in this study.

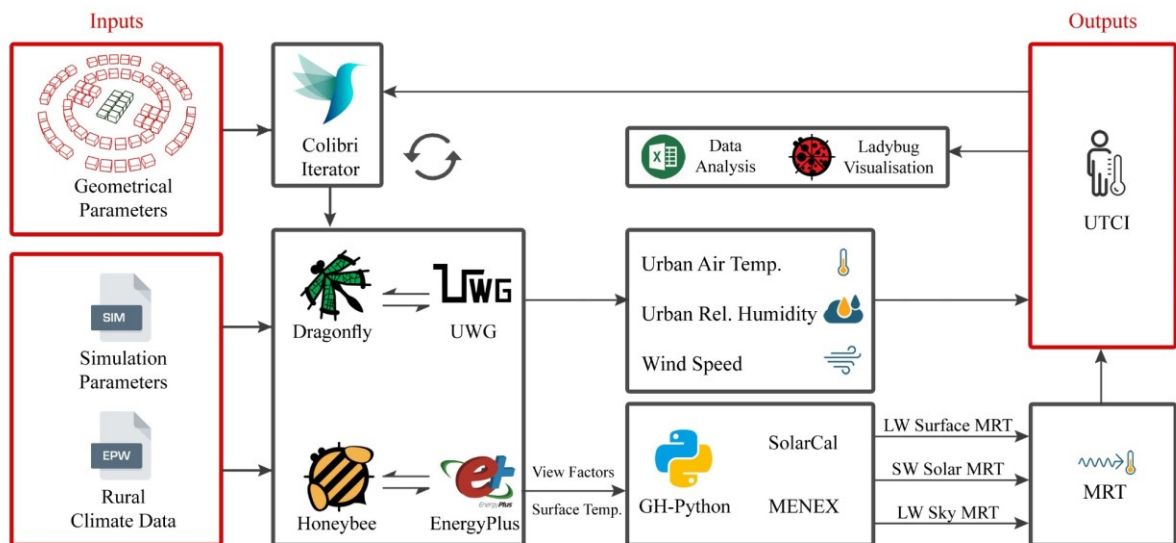


Figure 4.2: Schematic diagram showing the data streaming between Ladybug-tools plugins and the simulation engines in the workflow used in this study.

4.4.2 Validation of the workflow

As mentioned in previous sections, the workflow depends on validated software engines to determine the MRT and the thermal comfort components. EnergyPlus was validated with the ASHRAE 1052RP test and verified with a series of building energy simulation programs (BESTEST) as endorsed in ASHRAE Standard 140-2001 as a Standard Method of Test (Witte *et al.*). The UWG was validated with field measurements in different climates (Bueno *et al.*, 2013; Bueno *et al.*, 2014). It is then how the workflow applies the MRT equations and combines the different UTCI components that needs to be validated. A recent study by Evola *et al.* (2020) included the validation of the Ladybug-tools workflow with experimental measurements in a Mediterranean climate context, namely Catania, Italy, in terms of the MRT.

Results of that study has shown good agreement with measurements with a coefficient of determination $R^2 = 0.92$. Moreover, in studies by the authors, the workflow has been verified against the CFD modelling package, ENVI-met, in Cairo, Egypt (Ibrahim *et al.*, 2020b), and London, UK (Ibrahim *et al.*, 2020a). Figure 4.3 shows the results for the average MRT and UTCI of all grid points in the case of Cairo, having a congruent performance in terms of the MRT and UTCI ($R^2 = 0.94$ and 0.96 respectively).

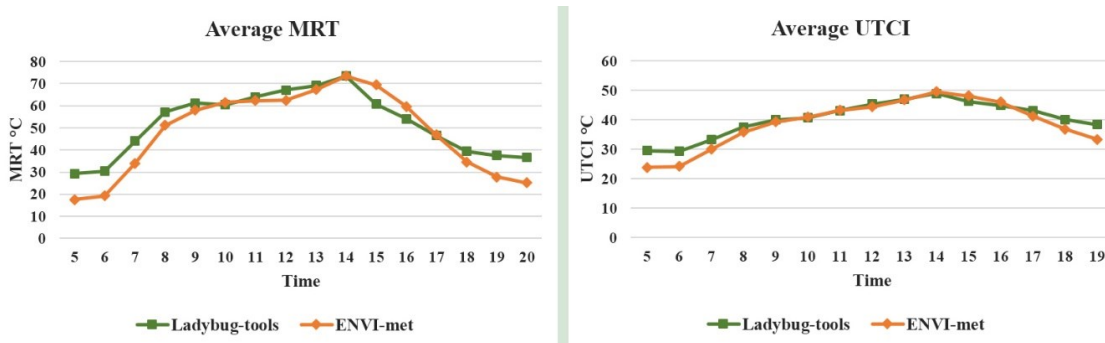


Figure 4.3: Results for the average of all grid points as simulated by both Ladybug-tools and ENVI-met.

In this study, an urban canyon, located in a university campus in Cairo, was selected to validate the workflow against field measurements (Figure 4.4-a). The canyon comprises office buildings with a total length of around 50m and asymmetrical H/W of 0.9:1:1.3 and is orientated 42° North-eastwards³. The canyon was modelled in Rhino along with the surrounding context of area around 170×110m as shown in Figure 4.4-b.

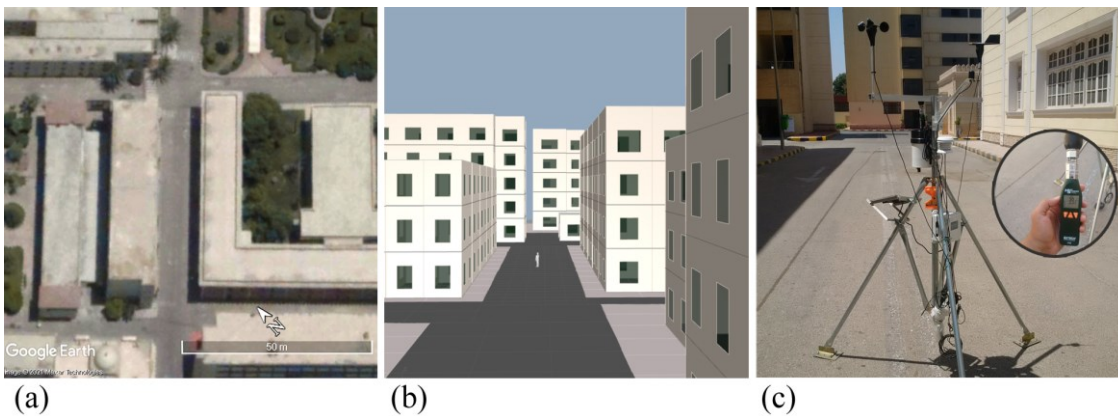


Figure 4.4: Site of measurements as shown (a) in Google Earth, (b) in the Rhino scene, and (c) during measurements.

³ Relative to a unit street width, a H/W of 1.3 of the north-eastern side, and 0.9 of the south-western side.

Construction materials along with their physical and thermal properties were defined in Grasshopper as similar to the real case as possible. An Onset HOBO-U30 (Onset, 2021) weather station and Extech HT30 Heat Stress WBGT Meter (Extech, 2021) were placed at the centre of the street to measure the meteorological parameters needed for validation as shown in Figure 4.4-c. Table 4.3 lists the parameters measured in the campaign, the sensors used and their corresponding range and accuracy.

Table 4.3: The parameters measured by the sensors and their corresponding range and accuracy.

Parameter	Sensor	Range	Accuracy
Air temperature	S-THB-M002	-40 to 75 °C	±0.21 °C (at 0-50 °C)
Relative humidity	S-THB-M002	0 to 100%	±2.5% (at 10-90%)
Wind speed	S-WSB-M003	0 to 76 m/s	±1.1 m/s OR 4% of reading
Black globe temperature	HT30	0 to 80 °C	±3 °C (Outdoors)

Measurements were recorded on the 6th August, 2018 every hour from 7 am to 7 pm. Measured air temperature (T_a), relative humidity (Rh) and wind speed (v) were compared to their counterparts in an International Weather for Energy Calculation (IWEC) weather file (DoE, 2020), which is used for the simulations in the validation and the rest of this study to check the reliability of the weather file. The mean radiant temperature (MRT) was calculated on site in terms of the black globe temperature (T_g) and the air temperature (T_a) following the formula (BSI, 2001):

$$MRT = \sqrt[4]{(T_g+273)^4 + \frac{1.1 * 10^8 * v^{0.6}}{\epsilon_g * D^{0.4}} * (T_g - T_a) - 273} \quad \text{Equation 4.5}$$

Where ($\epsilon_g = 0.95$) and ($D = 0.04$ m) are the globe emissivity and diameter, respectively. A Honeybee component was used to convert the 10m-high wind speeds from the IWEC file into 2m-high wind speeds and vice versa, required for MRT and UTCI calculations. The latter was calculated by a Ladybug component which takes T_a , Rh, v and MRT and produces the UTCI. Figure 4.5 plots the relationship between the measured parameters and their counterparts in the IWEC file. The IWEC parameters appear to be strongly correlated to the measured values with the wind speed having the lowest correlation. This can be explained by the low resolution of the wind speed sensor (0.25 m/s) which resulted in reading (zero m/s) in almost half of the recordings. Even so, the general trends of the three parameters are congruent with the measurements.

The relationship between the measured and simulated MRT is shown in the top row of Figure 4.6, where the simulation workflow appears to be sufficiently reflecting the MRT temporal variations. Based on a sensitivity analysis, the discrepancy in MRT at 10 am can be attributed to the difference between the simulation model and the real site in three main parameters; global horizontal radiation; thermal admittance of the ground surface; and the spatial resolution of the simulation model. Apart from that, the general trend is in agreement with the measurements with maximum difference of 8.01 °C. This is in line with previous studies concerning the outdoor thermal comfort and using the same workflow, for instance, 6.1 °C in Evola et al. (2020) and ~7 °C in Naboni *et al.* (2019c).

It can clearly be seen that although the parameters, T_a , Rh, and v have some discrepancies with the measured values (Figure 4.5), the UTCI follows trend of the MRT throughout the day (Figure 4.6), showing a good agreement with the field measurements UTCI, with a maximum difference of ~3.5 °C. The results shown above indicate that the Ladybug-tools workflow can simulate the thermal performance of geometry configurations with a considerable reliability, but also with a comparable accuracy to valid microclimate models such as ENVI-met with dramatically decreased simulation times and hence, it can be used in this study. The results also indicate that the IWEC weather file is appropriate for the simulation of hypothetical case studies.

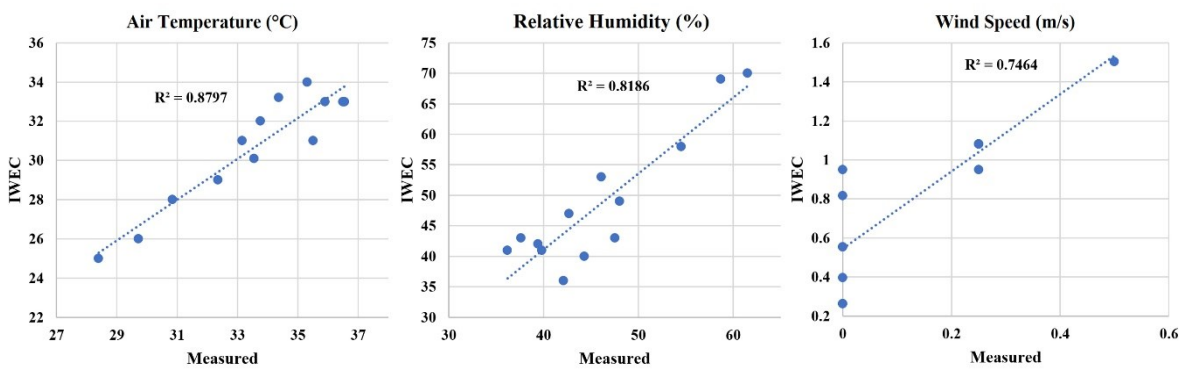


Figure 4.5: Scattered plots showing the relationship between the measured parameters and the IWEC parameters.

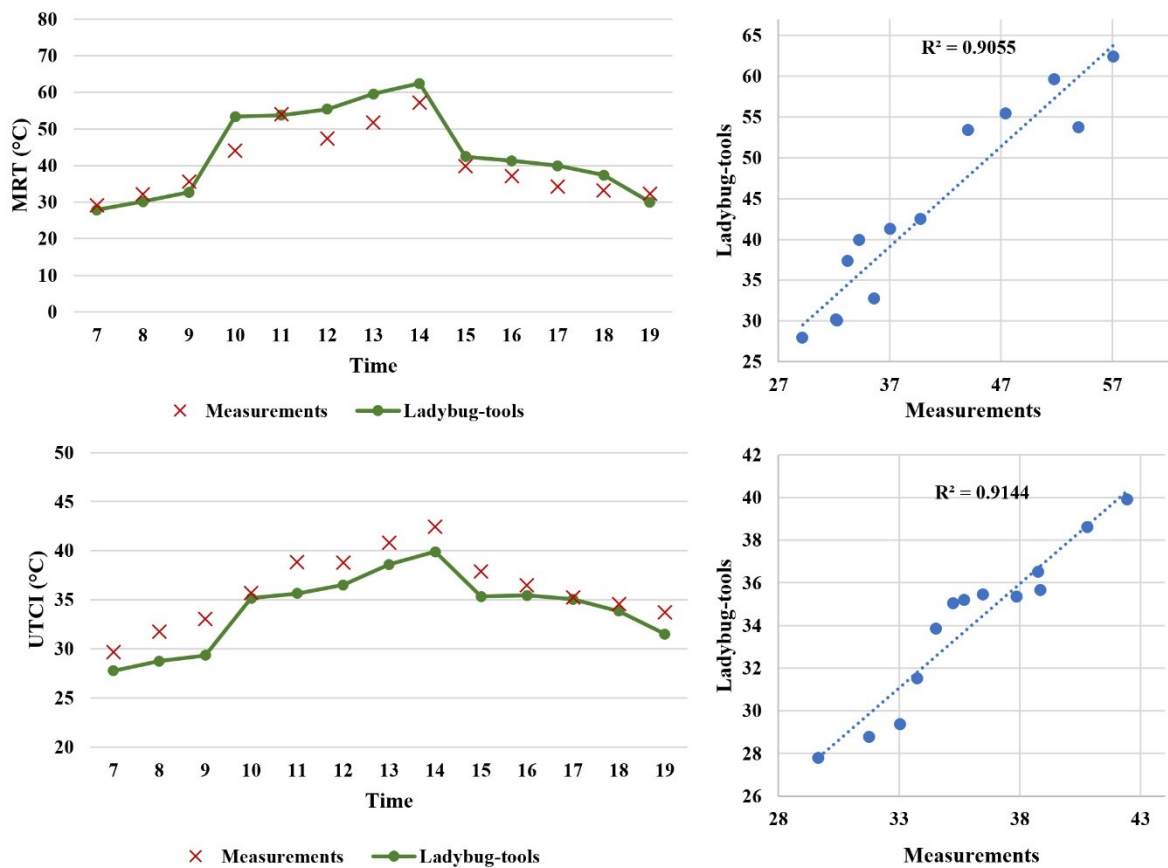


Figure 4.6: Relationships between measured and simulated MRT (top row) and UTCI (bottom row).

Additionally, the results reported in this validation are not including CFD wind simulation. This was recommended based on a preliminary sensitivity analysis by the authors. Natanian et al. (2020) performed a sensitivity analysis on the solar and wind parameters included in the calculation of UTCI using the same workflow in a hot desert climate, similar to our study. Their results showed that MRT had the strongest impact on UTCI, and that using the wind data from the weather file (rather than a detailed CFD analysis) had a minimal effect on the output UTCI.

Also in a hot-arid climate, Krüger et al. (2010) concluded that wind exposure is not as significant as mutual shading for improving the heat transfer by convection and reducing cooling loads. Accordingly, based on our preliminary study and the inferences from the literature, and given the exhaustive computation time needed for the CFD analyses, wind speeds in this study are extracted directly from the IWEC file, in favour of performing a total of 7716 permutations.

4.4.3 Hypothetical study modelling

The hypothetical urban canyon, comprised of two arrays of 5 residential units, 24m × 20m each, was modelled parametrically in Grasshopper (100m total canyon length). The ground in the ladybug-tools model was defined as a thermal zone in EnergyPlus in order to account for ground temperature changes. The ground zone was further divided into 5 zones during the first phase and 20 zones during the second and third phases, to capture the dynamic variation of the shading without increasing the computation time. Building materials typical of the residential sector in Egypt were defined as the construction materials for the model, with all material roughness set to “rough”.

Table 4.4 lists the thermal and physical properties used in this study. Upon the second and third phases, an existing newly constructed urban area in Cairo is modelled with average building heights of 18m are assumed. Note that the UWG module within the Dragonfly plugin uses the average building heights, building footprints, density and material thermal properties to calculate the UHI effect. Since the context neighbourhood is not orientated with the urban canyon, the morphology and the spacing between neighbouring buildings will not affect the results of the UWG. Figure 4.7-a depicts the canyon as modelled in phase 1, while Figure 4.7-b and Figure 4.7-c show the canyon as modelled within the context neighbourhood and used in both phases 2 and 3.

Table 4.4: Physical and thermal properties of construction materials (Engineering-ToolBox, 2001).

Material Properties	Roofs Roofing tiles	Walls Wall bricks	Ground Asphalt
Solar Absorption (-)	0.50	0.60	0.88
Solar Reflection / albedo (-)	0.50	0.40	0.10
Thermal Absorptance (-)	0.90	0.90	0.93
Density (kg/m ³)	1900	1500	2100
Specific Heat Capacity (J/kg·K)	800	650	920
Thermal Conductivity (W/m·K)	0.84	0.44	1.40

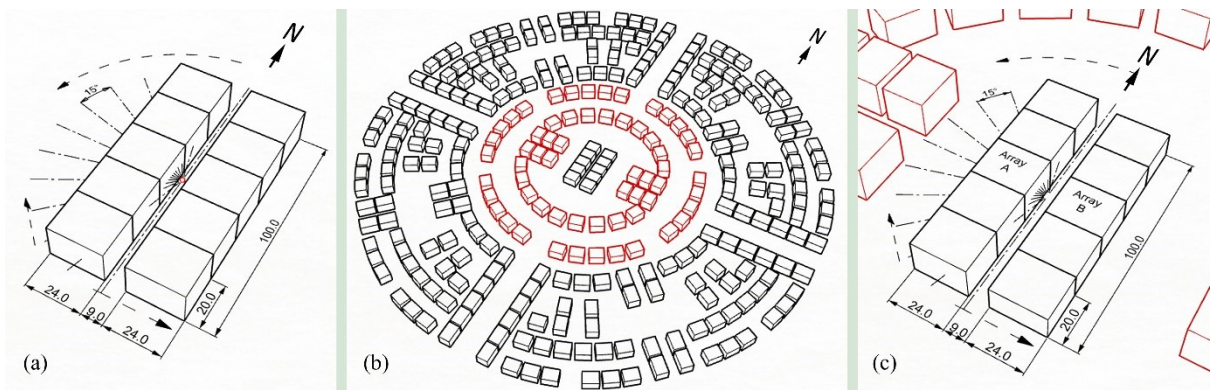


Figure 4.7: 3D view of the urban canyon simulated in (a) phase 1, and (b) and (c) in both phases 2 and 3. Neighbouring buildings in red colour are included in the view factor calculations.

4.4.4 Simulation setup

For the Dragonfly Urban Weather Generator inputs, a building programme was set to “mid-rise apartments”. For the parameterisation of EnergyPlus simulation via Honeybee, each building was divided into a number of thermal zones equal to the building’s floors, i.e. one thermal zone per floor, to capture the variations in surface temperatures relative to the dynamic shading pattern. Building zones were set to “not conditioned”, with equipment and lighting loads set to zero. In the same context, the timestep was set to 10 mins with reporting every hour, and using the solar distribution module “Full exterior with reflections”. The points of measurements were distributed along the canyon on a 2m grid, e.g. a 100m long street of width 6m entails a total of $50 \times 3 = 150$ points. Results were recorded at a height of 1.1m to represent the centre of gravity of a human body, thus taking a thermal sensation point of view. For phase 2 and 3, the nearest neighbouring buildings (shown in red colour in Figure 4.7-b) are included for view factor calculations, yet not for shadowing. The TT-Toolbox (Tomasetti, 2020) Colibri component was used to iterate a total of 1716, 3840 and 2160 cases respectively for the first, second and third phases.

4.4.5 Climate context

Egypt encompasses a range of diverse climatic conditions; however, it is generally categorised as a hot-desert climate according to the Köppen Geiger classification. The climate is characterised by a hot-arid summer and a temperate winter with low precipitation levels. The highest mean temperatures are typically in July while the coldest temperatures are in January.

An International Weather for Energy Calculation (IWEC) file for Cairo was obtained from the U.S. DoE (2020) and used in this study. Simulations, however, were conducted on June 7th as the hottest day to represent the worst-case scenario. Figure 4.8 shows the meteorological data of June 7th that were input into the simulation. It's clear that the radiation values are not typically symmetrical around noon. Consequently, the performance of canyons providing similar shading patterns across the day will slightly vary based on the radiation values that they receive and/or block, as discussed below.

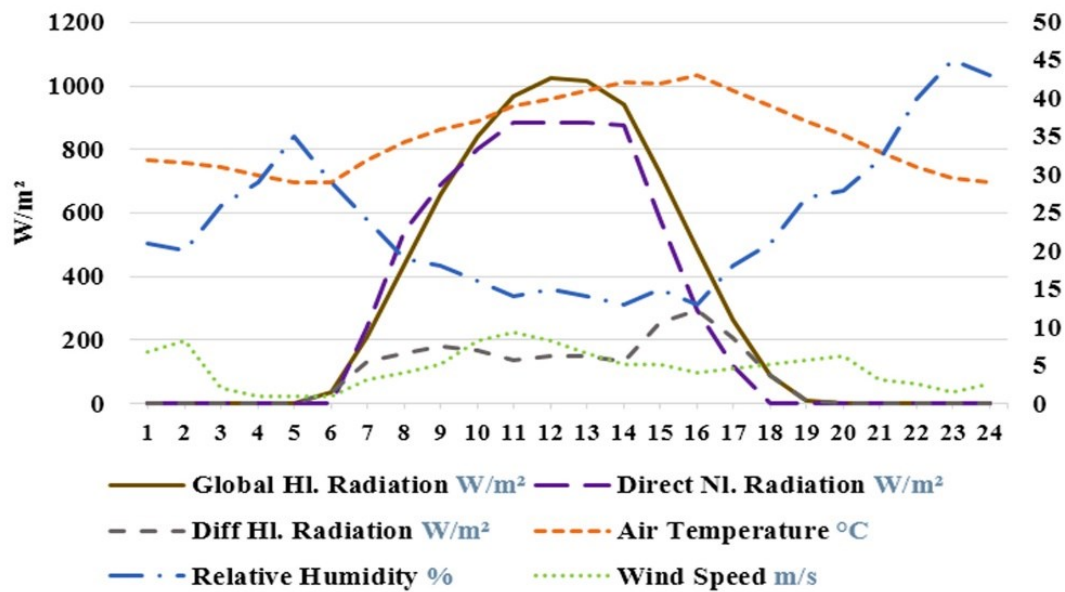


Figure 4.8: Meteorological data in Cairo, on June 7th, as retrieved from the IWEC file and input to the model.

4.5 Results and discussion

For symmetrical canyons in phase 1, besides showing the optimum H/W ratios within each orientation, a focus is given to allocating specific heights and widths that produce these optimum ratios, where different height and widths may produce the same H/W. In phase 2, asymmetrical canyons are analysed with more emphasis on the heights of each array of buildings (flank). In phase 3, the heights of each flank within different widths are analysed with more attention to each flank's H/W. This set of analyses gives a comprehensive interpretation of the relationship between design parameters and the output thermal comfort.

4.5.1 Phase 1

Results of the first phase were interpolated using 2D Non-Uniform Rational Based Spline (NURBS) surfaces, and then transformed into coloured meshes, with each face delineating a resultant UTCI value of using a certain street width and building height as shown in Figure 4.9 Results of orientation 180° were excluded since they showed identical performance to those of orientation zero, as expected. In general, it can be noted that higher H/W ratios within all orientations lead to the lowest UTCI. However, N-S, NW-SE (15-45°) and NE-SW (135-165°) orientations tend to produce a wider variety of lower UTCI H/W ratios than those orientations close to E-W (60-120°). Given that the solar altitude reaches ~82° at noon, E-W canyons remain exposed almost the entire day and thus maintain the highest UTCI values.

The more E-W orientated the canyons are, the less impact the street widths have on the UTCI. This is attributed to the longer exposure time not only for the canyon ground but also for the building surfaces, hence, the taller the buildings within these canyons, the more long-wave radiation a receptor point receives. Also, NE-SW canyons (120, 135 and 150°) having H/W ratios between 1 and 1.5 (Figure 4.9) tend to be a preferred orientation relative to their NW-SE counterparts (60, 45 and 30°). Despite both NE-SW and NW-SE spending almost the same time sun-exposed or shaded, NE-SW canyons provide shading during the morning hours, obstructing radiation values relatively higher than those in the late afternoon. As canyon ground starts to heat up around 9 am, NW-SE canyons, on the other hand, provide shading during the late afternoon hours where surfaces are already heated, and the shading effect is lessened. Also, canyons within orientation 90° showed slightly better performance than those within orientation 75 and 105° with streets wider than 12m, as the former casts more shading during the noon hours (12-1 pm) characterised by the highest solar radiation intensities. Results of this phase are in agreement with previous studies in hot arid climates (Ali-Toudert *et al.*, 2005; Ali-Toudert & Mayer, 2006; Johansson, 2006; Bourbia & Boucheriba, 2010; Shalaby & Shafey, 2018; Galal *et al.*, 2020) which advocated the use of NS-oriented deeper canyons for better thermal conditions. The lowest UTCI values of less than 39 °C were recorded for canyon heights of ≥18m within 6m streets and heights of ≥27m within 9m streets (H/W ranging between 3 and 6) within all orientations other than E-W canyons (75, 90 and 105°). The latter registered lower UTCI, of less than 40 °C, with building heights of 27m or more on a 6m street with H/W between 4.5 and 6.

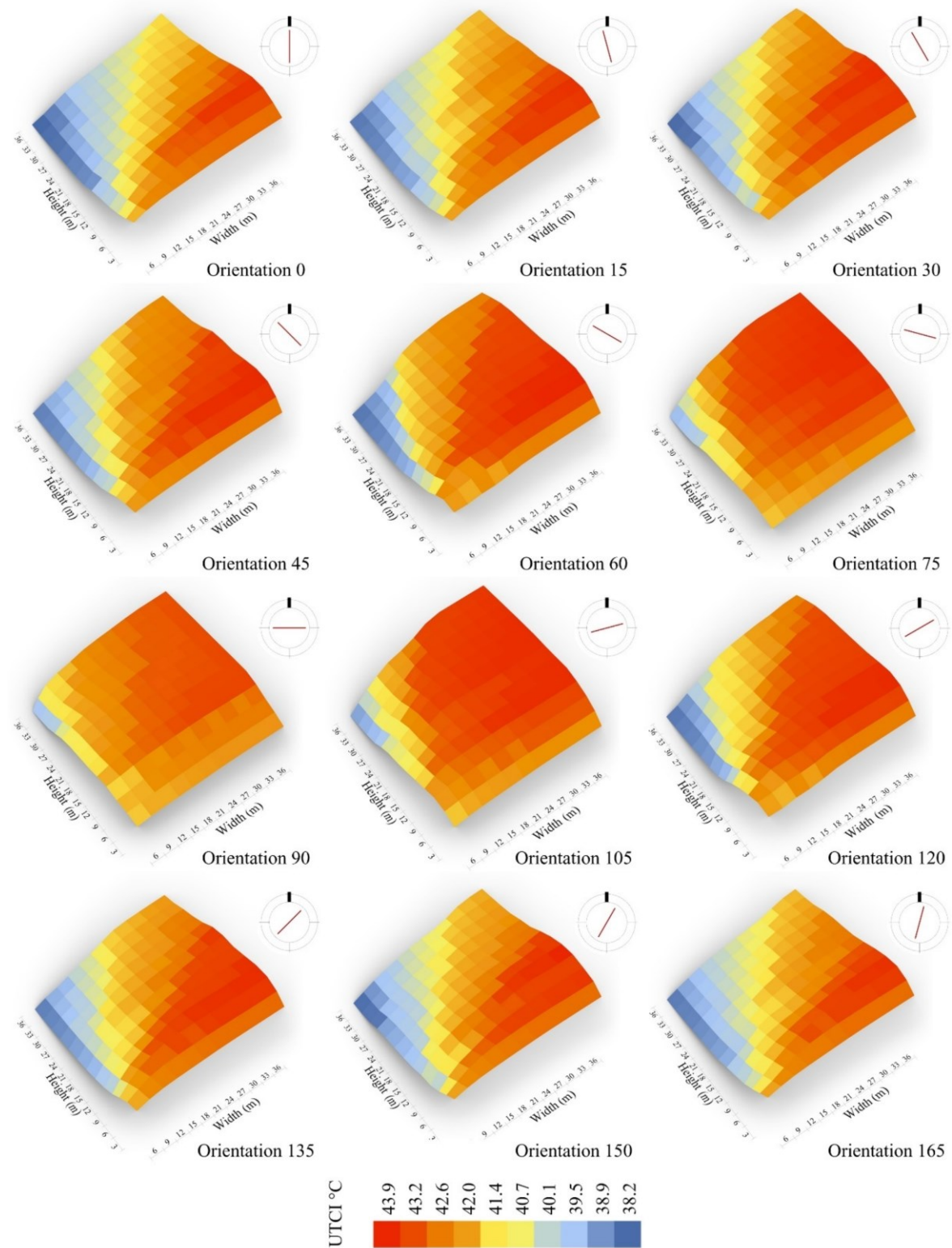


Figure 4.9: Coloured meshes showing the height-to-width based UTCI for different orientations in degrees relative to North, recorded in the middle of the canyon on June 7th, from 5 am to 7 pm.

Heights	36	6.00	4.00	3.00	2.40	2.00	1.71	1.50	1.33	1.20	1.09	1.00
	33	5.50	3.67	2.75	2.20	1.83	1.57	1.38	1.22	1.10	1.00	0.92
	30	5.00	3.33	2.50	2.00	1.67	1.43	1.25	1.11	1.00	0.91	0.83
	27	4.50	3.00	2.25	1.80	1.50	1.29	1.13	1.00	0.90	0.82	0.75
	24	4.00	2.67	2.00	1.60	1.33	1.14	1.00	0.89	0.80	0.73	0.67
	21	3.50	2.33	1.75	1.40	1.17	1.00	0.88	0.78	0.70	0.64	0.58
	18	3.00	2.00	1.50	1.20	1.00	0.86	0.75	0.67	0.60	0.55	0.50
	15	2.50	1.67	1.25	1.00	0.83	0.71	0.63	0.56	0.50	0.45	0.42
	12	2.00	1.33	1.00	0.80	0.67	0.57	0.50	0.44	0.40	0.36	0.33
	9	1.50	1.00	0.75	0.60	0.50	0.43	0.38	0.33	0.30	0.27	0.25
	6	1.00	0.67	0.50	0.40	0.33	0.29	0.25	0.22	0.20	0.18	0.17
3	0.50	0.33	0.25	0.20	0.17	0.14	0.13	0.11	0.10	0.09	0.08	
		6	9	12	15	18	21	24	27	30	33	36
		Widths										

Figure 4.10: H/W matrix as a product of all building heights and street widths in phase 1. Colours indicate the UTCI performance, in accordance with Figure 4.9.

Canyons close to N-S orientation (0 , 15 and 165°) start to register their highest UTCI values, $\geq 43^\circ\text{C}$, as building heights decrease to $\leq 15\text{m}$ within 18m and wider streets so long as they have H/W ratios between 0.16 and 0.45 , respective to their parameters. Whereas NW-SE (30 and 45°) and NE-SW (135 and 150°) canyons register their highest UTCI, $\geq 43^\circ\text{C}$, as building heights decrease to $\leq 21\text{m}$, street widths increase to $\geq 15\text{m}$, so long as they have H/W ratios between 0.16 and 0.66 , respective to their parameters (Figure 4.10). Within orientations (60° and 120°), the ratios move to $\leq 30\text{m}$ height and $\geq 12\text{m}$ width with H/W between 1.6 and 0.9 , respective to their parameters. On the other hand, E-W canyons register UTCI higher than 43°C as building heights increase above 6m (except for 9m in 90°) within 12m streets and wider so long as they have H/W ratios between 0.16 and 1.67 , respective to their parameters (Figure 4.10). Table 4.5 lists the lower and higher bounds for the geometry parameters, within which minimum and maximum UTCI values were registered.

Table 4.5: Upper and lower bounds for geometry parameters to produce minima and maxima UTCI.

Parameter	Minima UTCI (<39 °C)*					Maxima UTCI (>43 °C)						
	Heights (m)		Widths (m)		H/W	Heights (m)		Widths (m)		H/W		
Bounds	Min	Max	Min	Max	Min	Max	Min	Max	Min	Max	Min	Max
0, 15, 165°	18	36	6	9	3	6	6	15	18	36	0.16	0.45
30, 45, 135, 150°	27	36	6	9	3.6	6	6	21	15	36	0.16	0.66
60, 120°	24	36	6	9	4	6	6	30	12	36	0.16	0.9
75, 90, 105°	27	36	6	6	4.5	6	6	36	12	36	0.16	1.67

* <40 °C in case of 75, 90 and 105°

Having a closer look at Figure 4.9 and Figure 4.10, it should be noted that canyons with different heights (H) and widths (W) albeit with the same H/W may produce different UTCI values, in contrast to the findings previously reported by (Galal *et al.*, 2020). For instance, an urban canyon with H6 and W12 (H/W = 0.5) produces lower UTCI than a canyon with H9 and W18 by 0.8 °C and 1.2 °C in orientations 0 and 60°, respectively, and lower than a canyon with H12 and W24 by 1.1 °C in orientation 90°. A regression analysis for a sample size of 1716 cases was conducted to distinguish the effect of urban form variables in symmetric urban canyons as in this phase. A 2nd order polynomial trendline was used as it has shown the best fit with the sample data.

Of the different variables investigated, H/W and sky view factor had the most significant correlations with UTCI with $R^2 = 0.71$ and 0.73 , respectively (Figure 4.11), compared to 0.48 and 0.44 , reported by (Galal *et al.*, 2020). When orientations 60 to 120° were excluded from the authors’ analysis, a stronger correlation was found for the H/W with $R^2 = 0.91$, compared to 0.56 , also reported by (Galal *et al.*, 2020). Furthermore, the authors also found a moderate correlation between UTCI and street widths with $R^2 = 0.49$.

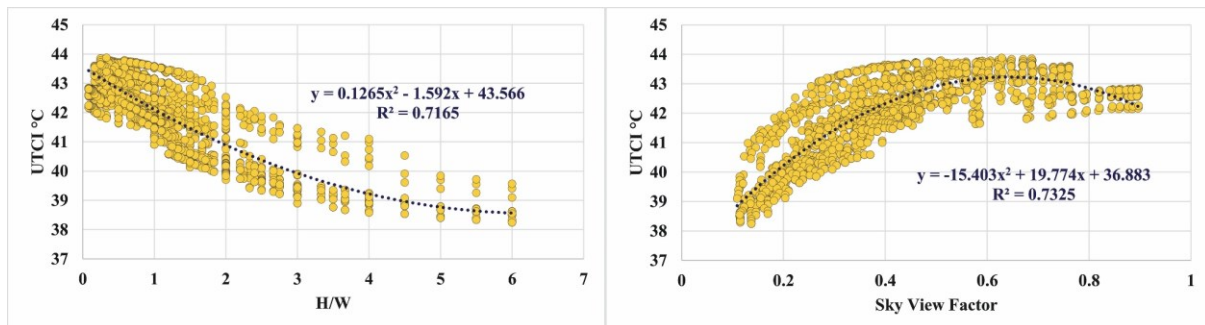


Figure 4.11: scattered plots for the correlation between UTCI and H/W (left) and sky view factor (right).

This indicates that having a wider variety of canyon parameters in our study allows a more precise estimation of the relationship between urban form and thermal comfort, and identifies new relationships not previously reported, highlighting the significance of this study.

4.5.2 Phase 2

Results of phase 2 show that the lowest UTCI values are a product of the narrowest streets and the highest buildings and vice versa. Consequently, results are shown in Figure 4.12 as clustered columns, each of which presents the variation of heights of array B with respect to each height of array A within a street width of 6m. Error bars represent the worst cases, within a street width of 18m, which generally produces the highest UTCI values, except for orientations 75, 90 and 105° within 8m-high array A. It is worth noting that although the results of this phase are only presented for 5 pm to 9 pm, EnergyPlus calculation of surface temperatures ran over the whole day. Consequently, surface temperature deviations during the morning and early afternoon hours should be taken into consideration. On a 6m wide street, a general trend can be seen within all orientations; UTCI values decrease with increasing the heights of array A. The effect is clearly seen within orientations where array A faces the southwest direction (45, 60 and 75°). In a similar vein, the effect of increasing the heights of array B is more prominent beyond orientation 90°. It is worth mentioning that although the turbulent heat fluxes are not considered in the model, the natural convective heat transfer coefficient in EnergyPlus is based on the surface temperature variance with the air temperature, in addition to the wind speed, which is consistent over the whole layout. Given the disparate surface temperatures from one building height to another, heat transfer by convection becomes proportional to the mean difference between the surface and air temperature. In other words, the higher the surface temperature, the higher the natural convective heat transfer coefficient. Consequently, as buildings move from lower heights (exposed with high surface temperature) towards higher building heights (shaded with lower surface temperature), the natural convective heat transfer coefficient diminishes, and so does the heat transfer by convection. Thus, differences between higher buildings (28-36m) tend to be minimal as opposed to those between lower buildings (8-24m). In the next four sections, building heights are referred to by joining the array character “A or B” with its corresponding height in meters. For instance, “A-16 and B-32” indicate 16m-high array A and 32m-high array B.

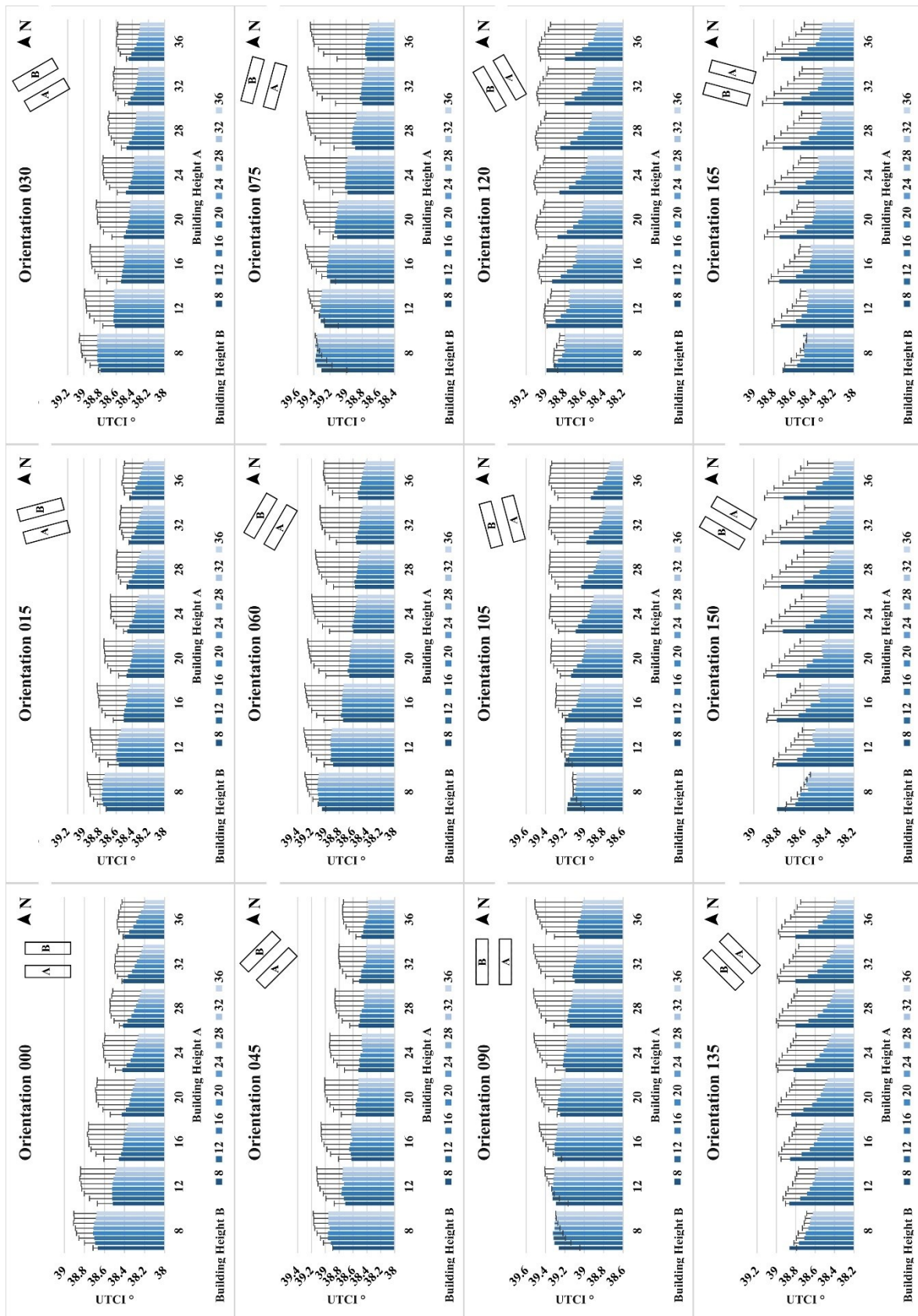


Figure 4.12: Clustered columns showing the relationship between building heights of array A and array B. The (thick) blue columns represent a 6m wide street, while the (ticked) error bars represent an 18m wide street.

4.5.2.1 Orientations 0-30°

Within these orientations, the effect of array B on reducing UTCI starts to be clear with increasing array A (20m onwards) for narrow streets. Increasing array B (except for heights B-32 and B-36) in tandem with array A-8 and A-12 increased the UTCI through increased long-wave radiation more than they decrease it by shading. For the same reason, increasing array B on wide streets (18m) resulted in increasing UTCI within arrays A-8 up to A-20, while the effect is attenuated within arrays A-24 up to A-36 due to the combined shading of arrays A and B. Table 4.6 shows the minimum and maximum UTCI values relative to their canyons on 6m and 18m streets for the three orientations.

Table 4.6: Minimum and maximum UTCI for orientations 0-30°.

	Max UTCI °C		Max Canyon		Min UTCI °C		Min Canyon		Attenuation °C (Max-Min)	
	6m	18m	6m	18m	6m	18m	6m	18m	6m	18m
0°	38.71	38.89	A8/B20	A8/B24	38.19	38.41	A36/B36	A36/B8	0.52	0.50
15°	38.78	38.96	A8/B16	A8/B36	38.26	38.43	A36/B36	A36/B8	0.52	0.53
30°	38.84	39.06	A8/B28	A8/B32	38.30	38.47	A36/B36	A36/B8	0.53	0.58

4.5.2.2 Orientations 45-75°

The behaviour of these orientations is dominated by array A blocking solar radiation in the late afternoon and evening. This can be seen through the reductions in UTCI being registered with increasing heights of array A within narrow streets. Increasing the heights of array B appears to increase the UTCI within arrays A-8 to A-16, have a minimal effect within arrays A-20 and A-24, and then decrease the UTCI within arrays A-28 to A-36, especially B-24 and higher. Conversely, on wider streets (18m), lower heights of array B led to a reduction of the UTCI within all heights of array A. Similar to orientations 0-30°, this is attributed to the long-wave radiation received from array B and the lack of shading from array A. However, angle factors between the points of measurements and the surfaces play an important role in shaping the UTCI, particularly in orientation 75°. This is clear in canyon A-8/B-8 where the points have a lower view factor to the surfaces, regardless their temperatures, and hence register a lower UTCI than those of A-36, provided that array B has a minimal shading effect over the whole day. Table 4.7 shows the minimum and maximum UTCI values relative to their canyons on 6m and 18m streets for the three orientations.

Table 4.7: Minimum and maximum UTCI for orientations 45-75°.

	Max UTCI °C		Max Canyon		Min UTCI °C		Min Canyon		Attenuation °C (Max-Min)	
	6m	18m	6m	18m	6m	18m	6m	18m	6m	18m
45°	38.96	39.18	A8/B16	A8/B36	38.38	38.56	A36/B32	A36/B8	0.58	0.61
60°	39.11	39.31	A8/B24	A12/B36	38.43	38.80	A36/B36	A36/B36	0.69	0.51
75°	39.38	39.52	A8/B28	A20/B36	38.71	38.99	A36/B36	A8/B8	0.67	0.53

4.5.2.3 Orientations 90-120°

For orientation 90°, the UTCI is driven by mutual shading between array A and B. Within narrow streets, increasing heights of array A starts to have an impact on the UTCI at A-24 onwards. This is also the case for array B. This is due to the shading cast by array A during the early afternoon hours (12 pm – 3 pm) and that casted by array B during the late afternoon (4 pm – 7 pm). As streets get wider, the points of measurement receive a negligible amount of shading compared to the long-wave radiation they receive from the building surfaces, thereby increasing the UTCI. As canyons move north-eastward (Orientations 105-120°), array B starts to cast shadow during the late afternoon and alleviates the UTCI regardless the height of array A. Even within wider streets (18m), where increasing heights of array A increase the UTCI, array B alleviates the UTCI as it increases beyond 24m. Table 4.8 shows the minimum and maximum UTCI values respective to their canyons on 6m and 18m streets for the three orientations.

Table 4.8: Minimum and maximum UTCI for orientations 90-120°.

	Max UTCI °C		Max Canyon		Min UTCI °C		Min Canyon		Attenuation °C (Max-Min)	
	6m	18m	6m	18m	6m	18m	6m	18m	6m	18m
90°	39.34	39.52	A12/B20	A32/B36	39.02	39.05	A36/B36	A8/B8	0.32	0.48
105°	39.20	39.37	A12/B8	A32/B20	38.74	39.00	A36/B36	A8/B8	0.47	0.37
120°	38.99	39.12	A8/B28	A24/B16	38.46	38.85	A36/B36	A8/B36	0.53	0.27

4.5.2.4 Orientations 135-165°

It is clear that the effect of increasing heights of array B is predominant due to keeping canyons of all widths shaded. Given the lower solar altitude from 5 pm to 7 pm (~22°), the shading effect extends to wider streets. Array A appears to have a minimum effect on the UTCI due to the shading it provides during the early and noon hours. However, the wider the street, the larger the difference between the long-wave radiation it delivers, and the shading benefits it provides. This is similar to the effect of array B within orientations 45-90°. The impact of array B is more

pronounced when it is shaded by array A before 3 pm, especially within orientations 150 and 165° in 6m Table 4.9 shows the minimum and maximum UTCI values relative to their canyons on 6m and 18m streets for the three orientations.

Table 4.9: Minimum and maximum UTCI for orientations 135-165°.

	Max UTCI °C		Max Canyon		Min UTCI °C		Min Canyon		Attenuation °C (Max-Min)	
	6m	18m	6m	18m	6m	18m	6m	18m	6m	18m
135°	38.87	39.01	A12/B8	A20/B12	38.38	38.69	A36/B36	A8/B36	0.48	0.32
150°	38.82	38.92	A16/B8	A24/B8	38.35	38.55	A32/B36	A8/B36	0.46	0.38
165°	38.74	38.91	A16/B8	A32/B8	38.30	38.47	A32/B32	A8/B36	0.44	0.44

4.5.3 Phase 3

Results of this phase are presented as the average UTCI for each 6 heights of one flank against a single height of the other flank, e.g. the average of 6 UTCI values as a product of 6 heights of A (A-6 up to A-36) against B-12. This demonstrates the effect of a single height of one flank regardless the other heights of the other flank. The averages of flank A (single B) are shown in green columns in Figure 4.13 for 5 street widths, while the averages of flank B (single A) are shown as dash-lined columns. In N-S canyons (0, 15, 165, 30 and 150°), the effect of increasing the height of one flank within an orientation (15° for instance) is contrary to the effect of increasing the same flank within its supplementary orientation (165°). In NW-SE (45, 60 and 75°) and NE-SW (135, 120 and 105°) canyons, the effect is almost similar, though the magnitude slightly differs depending on the hours of the day being exposed/blocked as discussed in phase 2. As streets get wider, UTCI increases for all heights of flank B. On the other hand, for A-6, a street width of 15m (W15) entails lower UTCI than W12 in orientations 30, 45, 135, 150 and 90° and so does W9 than W6 in orientations 60, 75, 105 and 120°. This is due to the reduced amount of longwave radiation received as streets get wider and the surface view factors decrease accordingly.

Moreover, results of this phase demonstrate how the magnitude of UTCI is dependent on the heights of flanks A and B and the different widths in N-S, NE-SW and NW-SE canyons more than it is in E-W canyons. As such, within E-W canyons, the effect of heights is negligible compared to that of changing the width. Apart from orientations 0, 15 and 75°, heights A-30 and A-36 lead to the minimal UTCI in street widths W6 and W9. This was clear when we investigated the correlation of Heights-A/W and Heights-B/W independently across the different orientations (Figure 4.14-a and Figure 4.14-b), and then within each orientation (Figure 4.14-d).

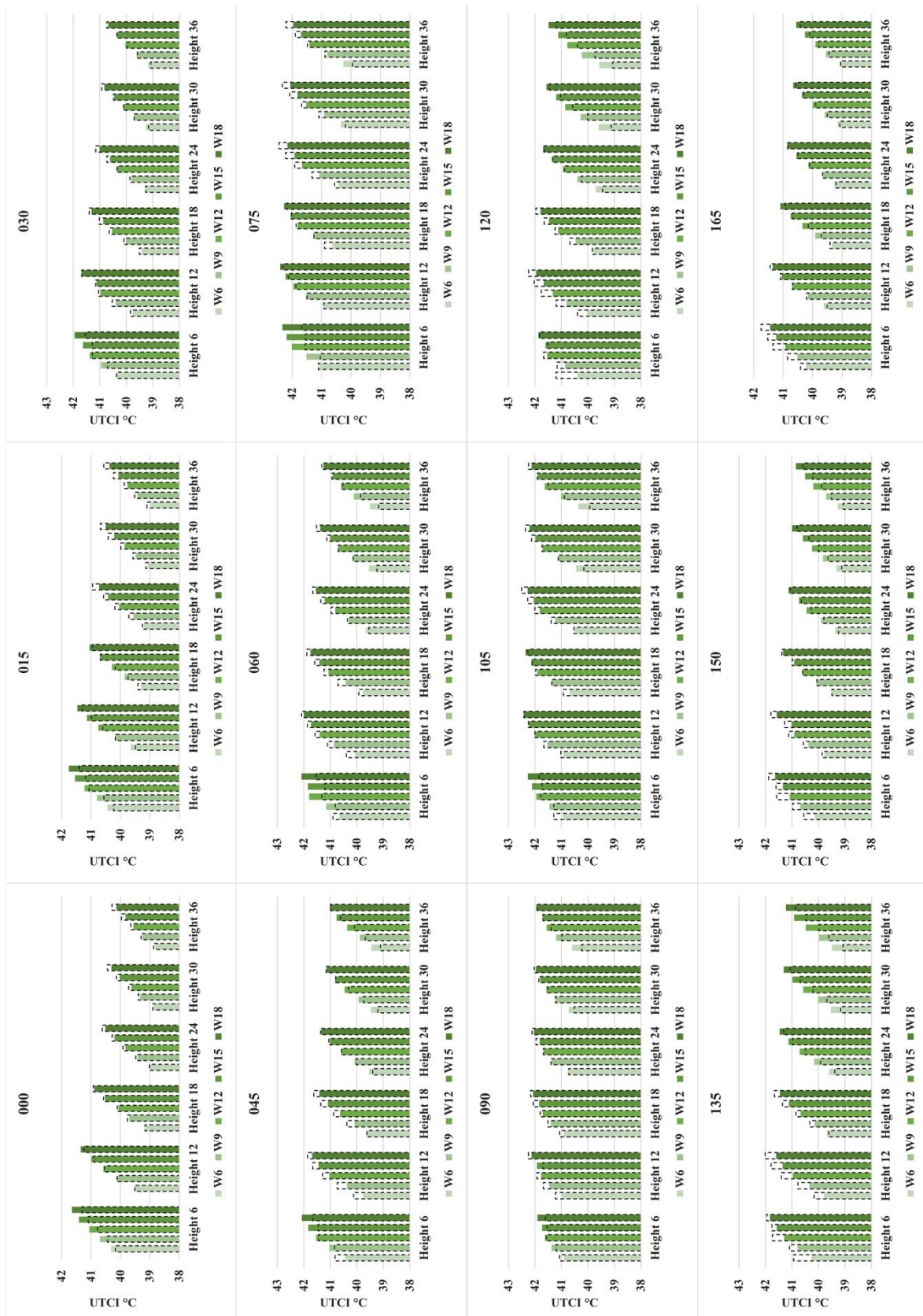


Figure 4.13: Clustered columns showing the average UTCI for 6 heights of flank A against one height of flank B in (green) and the average for 6 heights of B against a single height of A in (dash lines), within 5 street widths.

It was found that Height-A/W has a relatively higher correlation with UTCI than Height-B/W ($R^2 = 0.44$ compared to 0.38). Figure 4.14-d demonstrates that within orientations 120 to 165°, heights of A had a strong correlation with UTCI compared to a moderate correlation of heights B. Also, in orientations 75 and 90°, flank A had relatively higher correlation than flank B. This is due to being flank A responsible for blocking the solar radiation during most of the sunlit hours. Hence, improved thermal comfort can be achieved by increasing the heights of the southern flank (A in this case) and maintaining lower heights of the northern one (B).

This is different from what has been reported in the study of (Shalaby & Shafey, 2018), which recommended using $H/W = 1$ in E-W canyons, the difference being that they did not include asymmetrical urban canyons in their study. Furthermore, Figure 4.14-c and Figure 4.14-d manifest the importance of using each flank's H/W rather than using an average H/W in asymmetrical urban canyon studies, even if the latter maintains a good correlation with the output thermal comfort.

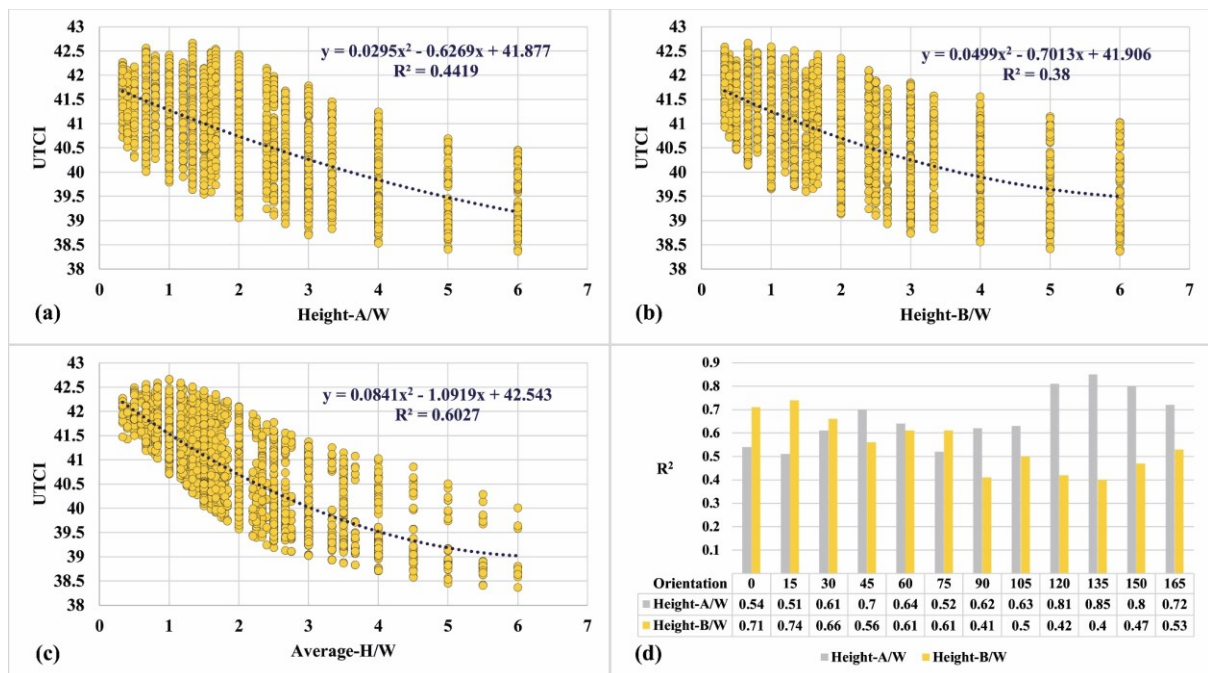


Figure 4.14: Scattered plots showing the correlation between UTCI and (a) height-A/W, (b) height-B/W, (c) average-H/W. (d) coefficient of determination for height-A/W and height-B/W in different orientations

Note that the asymmetrical nature of the other meteorological variables around midday may have overestimated or underestimated the output UTCI. However, urban shading remains the most dominating factor in determining the relationship between each flank and the output thermal comfort (also see Emmanuel *et al.*, 2007a). Again, having both canyon flanks modelled independently has allowed the examination of the nuances of their relationship with the outdoor thermal comfort, highlighting another contribution of this study.

4.6 Implications for urban design

As mentioned earlier, the Egyptian Construction Act (MHUUC, 2008) specifies urban form thresholds for urban communities; a minimum street width of 10m, maximum building heights of 36m, a maximum H/W of 1.5 and even lower thresholds for new conurbations. Since the results of this study fall within the same UTCI category, we set the benchmark for UTCI reduction as the difference between the highest UTCI recorded and the lowest UTCI resulting from using a H/W of 1.5. Consequently, a reduction in UTCI of 3.7 °C and 2.6 °C were set as the benchmarks for phase 1 and 3, respectively. Table 4.10 lists the minimum H/W thresholds to meet these reduction benchmarks in both symmetrical and asymmetrical configurations. Note that since the study was conducted on the hottest day, the thresholds are still appropriate for less severe conditions. Based on these findings, higher H/W's and narrower streets should be allowed within the regulations. Street widths 6 to 9m should be orientated E-W wherever possible to serve as local and sub-local roads, or pedestrian alleys. Wider streets should be orientated N-S wherever possible to serve as collectors, whereas intermediate orientations could serve as both. It can be deduced that higher and medium H/W ratios lead to relatively low and moderate heat stresses in NS, NE-SW and NW-SE canyons. Within these canyons, wider streets with varying building heights can still yield lower heat stresses relative to the other orientations. This is useful for leveraging the solar radiation in winter and allowing air movement for better convective cooling in summer (Qaid & Ossen, 2015).

Table 4.10: Minimum H/W thresholds for achieving the UTCI reduction benchmarks.

	Orientation											
	0	15	30	45	60	75	90	105	120	135	150	165
Symmetrical H/W	1.67	2	2	2.25	2.5	4.5	5	4.5	2.5	2	1.5	2
Asymmetrical H-A/W	0.67	1	2	2	2.67	5	6	5	2.67	2	2	1.3
Asymmetrical H-B/W	1	1.3	1	1	1	3	5	3	1	1	1	1

Based on the results of the first and third phases, a “UTCI rose” is presented to help draw implications for urban designers, planners and decision-makers as a guideline for a lower heat stress urban environment during the early design stages. Figure 4.15 depicts the results of both phases, summarised in three bars within each orientation. The left-hand bars represent the resultant UTCI due to increasing or decreasing both canyon flanks’ H/W ratios. The middle and the right-hand stacked bars represent the resultant UTCI from increasing or decreasing the canyon flanks A and B respectively, within different street widths. In these stacked bars, the UTCI results are averaged for each 6 heights of one flank with respect to every single height of the other flank. The effect of increasing either building arrays in NS canyons is almost equivalent. In NE-SW canyons, the resultant UTCI is more dependent on the southern array (B in the rose) than it is on the northern array (A). Increasing the heights of the southern array (B) decreases the UTCI relatively more than array A does, although the lower heights of array B lead to higher UTCI than their counterparts in array A. The difference is attenuated as canyons are directed NS, however with slightly higher UTCI values in the lower heights of array B, owing to the higher solar radiation values in the morning and noon compared to the afternoon and evening. The opposite conditions are evident in NW-SE canyons. Canyons close to E-W, on the other hand, maintain relatively higher heat stresses across the majority of their H/W ratios, apart from the highest ones (narrowest streets). Within these canyons, increasing the heights of the northern array is only beneficial as long as they are shaded by the southern array. This is clear in wider streets (15 and 18m), where building heights 12 to 18m of the southern array lead to higher UTCI than that of height 8m. In the latter case, canyon shading can be achieved by artificial shading devices, galleries (Ali-Toudert & Mayer, 2007a) or tree lines (Fahmy *et al.*, 2018). As the southern array increases above 18m, the UTCI starts to decrease again, and it further decreases as streets get narrower. It also can be suggested that, of the heights being tested in phase 3, an 18 to 24m-height of the southern array in E-W canyons works as a trade-off between solar penetration in winter and thermal loads induced within different street widths. The methodology presented in this paper can be replicated and used to test other performance criteria, e.g. energy loads, by means of its core simulation engine, EnergyPlus (Ibrahim *et al.*, 2021a). The user-friendly nature of Grasshopper allows architects, designers and others without proficiency in programming to use this methodology.

Undoubtedly, the use of open-source plugins in Grasshopper has increased its popularity in research, but also spurred the integration of Grasshopper and its environmental plugins into educational curriculums, and it is fast becoming an indispensable tool in practice. The UTCI results reported in this study are in degrees Celsius, which describe how pedestrians “feel” within a street canyon, and hence, designers can use these results as they are, without the need for further interpretation. The Egyptian government’s current initiative to amend the design regulations is not yet fully implemented. Such amendments can be extended to include climate informed design guidelines such as those reported in this study. Moreover, this paper’s methodology can be applied to district and small urban scale studies (Ibrahim *et al.*, 2021a), giving the opportunity to include performance driven insights into the design guidelines at different scales, thereby promoting the creation of resilient and sustainable built environments which ensure pedestrians’ health and well-being.

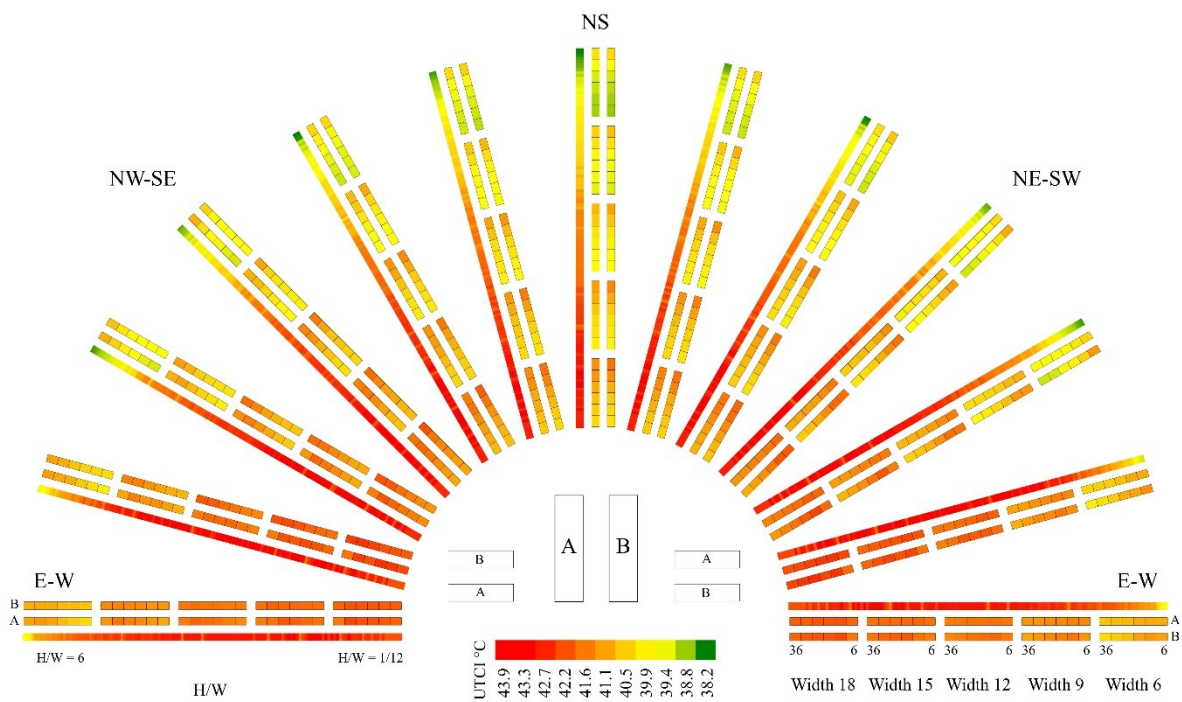


Figure 4.15: UTCI rose. For each orientation, left-hand bars represent 132 H/W ratios and their resultant UTCI. Within the 5 street widths, middle stacked bars represent 6 heights of flank A along with their resultant UTCI as averaged over each respective 6 heights of flank B. Right-hand bars represent 6 heights of flank B along with their resultant UTCI as averaged over each respective 6 heights of flank A.

4.7 Study limitations

The simulation workflow presented in this study is based on an aggregated bottom-up approach by chaining the inputs and outputs of validated software engines, i.e., EnergyPlus and UWG, within the Grasshopper environment. This approach is appropriate in parametric studies aiming to support urban planners and designers in the planning stage, where the use of standardised design parameters facilitates the simulation of a higher number of case studies, whose results are most needed in this stage. The applicability of the workflow is, however, confronted by the necessity to balance the computational cost of including detailed bottom-up approaches, e.g. running CFD analyses, and the reliability of the model's performance. In this study, we chose not to include wind analyses in favour of running a remarkably increased number of geometric permutations, since the workflow has shown considerable reliability using wind speeds from the IWEC file. Other approaches available in Grasshopper include wind analyses using Butterfly (Mackey *et al.*, 2017) or Eddy3D (Natanian *et al.*, 2020) which produce wind factors, the ratio between the simulated wind speeds and the inlet wind speed generated from a number of directions. These approaches, however, are not as accurate as if the turbulent heat exchanges are considered within the model, which is a feature in the OpenFOAM software, but is not yet integrated (currently under development) in either of the two plug-ins.

Furthermore, compared with field measurements, it was shown that the ladybug-tools model underestimates the UTCI by some 3.5 °C. As mentioned in section 4.4.2, the main deviation stems from the differences between the simulation model and the real case in three main parameters. Firstly, in sunlit hours, the radiation model mainly depends on the global horizontal radiation, retrieved from the weather file, which might suggest inaccuracies if not identical to reality. Secondly, the definition of the ground surface as the upper surface of an EnergyPlus thermal zone, assuming all other surfaces are adiabatic. Currently, there is no evidence from the literature about the convective nor the long-wave radiative heat transfer with this ground zone (Evola *et al.*, 2020). Finally, the spatial resolution of the simulation model which may suggest inaccuracies regarding the sun obstruction angles. Notwithstanding, these differences are consistent over the hypothetical cases, and hence can be accepted for the purpose of running a comparative analysis in this pre-design stage. Further improvements to the model need to be made in detailed analyses.

For most geometry configurations, this study has recommended using high aspect ratios for improved thermal comfort conditions. These configurations, nonetheless, might not seem applicable in practice in Egypt, although they are extensively found in other countries with similar climates, for instance Morocco (Johansson, 2006) (Figure 4.16-left) and Algeria (Bourbia & Boucheriba, 2010). The fact that Egypt has suffered from urban sprawl since 1950 with around 50% of the existing building stock not complying with the building regulations (Edeisy & Cecere, 2018) has spurred the government to instigate a redevelopment campaign for slums. Figure 4.16-right shows a sprawled area in Cairo, included in the government redevelopment action plan, where the rightmost part of the image is a neighbourhood, newly constructed in compliance with the Construction Act. That is to say, the limitation of applying these configurations in Egypt is subject to the interventions by stakeholders and decision makers in the design policies and regulations.



Figure 4.16: Satellite images of a neighbourhood in Fez, Morocco (Left), and Ezbet El-Haggana, Cairo, Egypt (right). The rightmost part of the image is a public sector newly constructed neighbourhood.

4.8 Conclusion

This study investigated the effect of H/W ratio and orientation of urban canyons on the outdoor thermal comfort represented by the UTCI. The Ladybug-tools microclimate model has shown its capability to capture the dynamic patterns of solar radiation and the resultant outdoor thermal comfort. In a hot arid climate, it was shown that modification of H/W and orientation can reduce the UTCI by almost 6°C . Higher H/W ratios are favourable in N-S, NE-SW and NW-SE canyons

and have the potential to reduce the heat stress in the urban canyon, whereas the more canyons are orientated E-W, the less effect H/W ratios have on the microclimate. Moreover, asymmetrical urban canyons are a feasible option, so long as taller buildings cast shadows on the canyon ground and shorter buildings, allowing for openness to the sky for convective cooling. The obtained UTCI thermal stress could be reduced significantly if the calculations were made on a typical day rather than an extreme one, not to mention the uncertainties of the weather file (Chinazzo *et al.*, 2015).

Given the shorter time required for computer simulations, which exceeds a thousand runs per day, this study could be applied in various climatic contexts. In Egypt, where the summer solar shading is prioritised over the winter solar heat gain, the study focused on the compromise between different H/W's and orientations in summer. In other climatic zones, seasonal variations should be considered. The study provides climate-based insights for urban planners aiming at creating healthy and sustainable built environments.

Data Availability Statement

Data available in a publicly accessible repository. The data presented in this study are openly available in University of Bath Research Data Archive at [<https://doi.org/10.15125/BATH-01045>] (Ibrahim, 2021a).

4.9 References

- Ahmed, K. (1994). A comparative analysis of the outdoor thermal environment of the urban vernacular and the contemporary development: case studies in Dhaka. In *Proceedings of the 11 th PLEA International Conference*, Dead Sea.
- Ali-Toudert, F. (2005). Dependence of Outdoor Thermal Comfort on Street Design in Hot and Dry Climate. (PhD). Institutes der Universität Freiburg, Freiburg, Germany. (15)
- Ali-Toudert, F., Djenane, M., Bensalem, R., & Mayer, H. (2005). Outdoor thermal comfort in the old desert city of Beni-Isguen, Algeria. *Climate Research*, 28(3), 243-256. doi: <http://doi.org/10.3354/cr028243>.
- Ali-Toudert, F., & Mayer, H. (2006). Numerical study on the effects of aspect ratio and orientation of an urban street canyon on outdoor thermal comfort in hot and dry climate. *Building and Environment*, 41(2), 94-108. doi: <http://doi.org/10.1016/j.buildenv.2005.01.013>.
- Ali-Toudert, F., & Mayer, H. (2007). Effects of asymmetry, galleries, overhanging facades and vegetation on thermal comfort in urban street canyons. *Solar Energy*, 81(6), 742-754. doi: <https://doi.org/10.1016/j.solener.2006.10.007>.

- Ampatzidis, P., & Kershaw, T. (2020). A review of the impact of blue space on the urban microclimate. *Science of the total environment*, 730, 1-18. doi: <https://doi.org/10.1016/j.scitotenv.2020.139068>.
- Andreou, E. (2013). Thermal comfort in outdoor spaces and urban canyon microclimate. *Renewable energy*, 55, 182-188. doi: <http://dx.doi.org/10.1016/j.renene.2012.12.040>.
- Arens, E., Hoyt, T., Zhou, X., Huang, L., Zhang, H., & Schiavon, S. (2015). Modeling the comfort effects of short-wave solar radiation indoors. *Building and Environment*, 88, 3-9. doi: <http://dx.doi.org/10.1016/j.buildenv.2014.09.004>.
- ASHRAE. (2017). ANSI/ASHRAE Standard 55-2017: Thermal environmental conditions for human occupancy. In (pp. 22-29). Atlanta, GA: American Society of Heating, Refrigerating and Air-Conditioning Engineers, .
- Blazejczyk, K. (2005). MENEX_2005. The Updated Version of Man-Environment Heat Exchange Model.
- Blazejczyk, K., Epstein, Y., Jendritzky, G., Staiger, H., & Tinz, B. (2012). Comparison of UTCI to selected thermal indices. *International journal of biometeorology*, 56(3), 515-535. doi: <https://doi.org/10.1007/s00484-011-0453-2>.
- Bourbia, F., & Boucheriba, F. (2010). Impact of street design on urban microclimate for semi arid climate (Constantine). *Renewable energy*, 35(2), 343-347. doi: <https://doi.org/10.1016/j.renene.2009.07.017>.
- Bröde, P., Fiala, D., Blazejczyk, K., Holmér, I., Jendritzky, G., Kampmann, B., Tinz, B., & Havenith, G. (2012). Deriving the operational procedure for the Universal Thermal Climate Index (UTCI). *International journal of biometeorology*, 56(3), 481-494. doi: <https://doi.org/10.1007/s00484-011-0454-1>.
- BSI, British Standards Institution. (2001). Ergonomics of the thermal environment—Instruments for measuring physical quantities (BS EN ISO 7726:2001). In (pp. 51).
- Bueno, B., Norford, L., Hidalgo, J., & Pigeon, G. (2013). The urban weather generator. *Journal of Building Performance Simulation*, 6(4), 269-281. doi: <https://doi.org/10.1080/19401493.2012.718797>.
- Bueno, B., Roth, M., Norford, L., & Li, R. (2014). Computationally efficient prediction of canopy level urban air temperature at the neighbourhood scale. *Urban Climate*, 9, 35-53. doi: <http://dx.doi.org/10.1016/j.uclim.2014.05.005>.
- CAPMAS. (2019). Bulletin of Housing in Egypt. (71-21123-2019). Cairo, Egypt: Central Agency for Public Mobilization & Statistics Retrieved from https://www.capmas.gov.eg/Pages/Publications.aspx?page_id=5104&Year=23415
- Chinazzo, G., Rastogi, P., & Andersen, M. (2015). Assessing robustness regarding weather uncertainties for energy-efficiency-driven building refurbishments. *Energy Procedia*, 78, 931-936. doi: [10.1016/j.egypro.2015.11.021](https://doi.org/10.1016/j.egypro.2015.11.021).
- Coccolo, S., Kämpf, J., Scartezzini, J.-L., & Pearlmutter, D. (2016). Outdoor human comfort and thermal stress: A comprehensive review on models and standards. *Urban Climate*, 18, 33-57. doi: <http://dx.doi.org/10.1016/j.uclim.2016.08.004>.
- Crawley, D. B., Lawrie, L. K., Winkelmann, F. C., Buhl, W. F., Huang, Y. J., Pedersen, C. O., Strand, R. K., Liesen, R. J., Fisher, D. E., & Witte, M. J. (2001). EnergyPlus: creating a new-generation building energy simulation program. *Energy and Buildings*, 33(4), 319-331. doi: [https://doi.org/10.1016/S0378-7788\(00\)00114-6](https://doi.org/10.1016/S0378-7788(00)00114-6).
- DoE. (2020). Weather Data. Retrieved from <https://energyplus.net/weather>

- Edeisy, M., & Cecere, C. (2018). Energy Efficiency for Egyptian Housing: Code Compliance and Enforcement. *International Journal of the Constructed Environment*, 9(3), 1-19. doi: <http://doi.org/10.18848/2154-8587/CGP/v09i03/1-15>.
- Emmanuel, R., Rosenlund, H., & Johansson, E. (2007). Urban shading—a design option for the tropics? A study in Colombo, Sri Lanka. *International Journal of Climatology: A Journal of the Royal Meteorological Society*, 27(14), 1995-2004. doi: 10.1002/joc.1609.
- Engineering-ToolBox. (2001). Engineering ToolBox. Retrieved from <https://www.engineeringtoolbox.com/>
- Evola, G., Costanzo, V., Magri, C., Margani, G., Marletta, L., & Naboni, E. (2020). A novel comprehensive workflow for modelling outdoor thermal comfort and energy demand in urban canyons: results and critical issues. *Energy and Buildings*, 216(109946), 1-19. doi: <https://doi.org/10.1016/j.enbuild.2020.109946>.
- Extech. (2021). Extech HT30: Heat Stress WBGT (Wet Bulb Globe Temperature) Meter. Retrieved from <http://www.extech.com/ht30/>
- Fahmy, M. (2010). Interactive urban form design of local climate scale in hot semi-arid zone. (PhD). The University of Sheffield,
- Fahmy, M., Ibrahim, Y., Hanafi, E., & Barakat, M. (2018). Would LEED-UHI greenery and high albedo strategies mitigate climate change at neighborhood scale in Cairo, Egypt? *Building Simulation*, 11(6), 1273-1288. doi: <https://doi.org/10.1007/s12273-018-0463-7>.
- Fanger, P. O. (1970). Thermal comfort; Analysis and applications in environmental engineering. New York: McGraw-Hill, first published in 1970, Danish Technical Press, Copenhagen.
- Fiala, D., Havenith, G., Bröde, P., Kampmann, B., & Jendritzky, G. (2012). UTCI-Fiala multi-node model of human heat transfer and temperature regulation. *International journal of biometeorology*, 56(3), 429-441. doi: <https://doi.org/10.1007/s00484-011-0424-7>.
- Fletcher, J. A., Kershaw, T., & Mills, G. (2013). Urban form and function as building performance parameters. *Building and Environment*, 62, 112-123. doi: <https://doi.org/10.1016/j.buildenv.2013.01.021>.
- Galal, O. M., Sailor, D. J., & Mahmoud, H. (2020). The impact of urban form on outdoor thermal comfort in hot arid environments during daylight hours, case study: New Aswan. *Building and Environment*, 184(107222), 1-15. doi: <https://doi.org/10.1016/j.buildenv.2020.107222>.
- Giannopoulou, K., Santamouris, M., Livada, I., Georgakis, C., & Caouris, Y. (2010). The impact of canyon geometry on intra urban and urban: suburban night temperature differences under warm weather conditions. *Pure and applied geophysics*, 167(11), 1433-1449. doi: <https://doi.org/10.1007/s00024-010-0099-8>.
- Golany, G. S. (1996). Urban design morphology and thermal performance. *Atmospheric Environment*, 30(3), 455-465. doi: [https://doi.org/10.1016/1352-2310\(95\)00266-9](https://doi.org/10.1016/1352-2310(95)00266-9).
- Grimmond, C., Roth, M., Oke, T. R., Au, Y., Best, M., Betts, R., Carmichael, G., Cleugh, H., Dabberdt, W., & Emmanuel, R. (2010). Climate and more sustainable cities: climate information for improved planning and management of cities (producers/capabilities perspective). *Procedia Environmental Sciences*, 1, 247-274. doi: <https://doi.org/10.1016/j.proenv.2010.09.016>.
- Havenith, G., Fiala, D., Błazejczyk, K., Richards, M., Bröde, P., Holmér, I., Rintamaki, H., Benschabat, Y., & Jendritzky, G. (2012). The UTCI-clothing model. *International journal of biometeorology*, 56(3), 461-470. doi: <https://doi.org/10.1007/s00484-011-0451-4>.

- He, B.-J., Ding, L., & Prasad, D. (2019). Enhancing urban ventilation performance through the development of precinct ventilation zones: A case study based on the Greater Sydney, Australia. *Sustainable Cities and Society*, 47(101472), 14. doi: <https://doi.org/10.1016/j.scs.2019.101472>.
- Höppe, P. (1999). The physiological equivalent temperature—a universal index for the biometeorological assessment of the thermal environment. *International journal of biometeorology*, 43(2), 71-75. doi: <https://doi.org/10.1007/s004840050118>.
- Ibrahim, Y. (2021). Dataset for "A parametric optimisation study of urban geometry design to assess outdoor thermal comfort". Retrieved from: <https://researchdata.bath.ac.uk/1045>
- Ibrahim, Y., Kershaw, T., & Shepherd, P. (2020a). Improvement of the Ladybug-tools microclimate workflow: A verification study. In *Building Simulation and Optimization 2020*, Loughborough University, Loughborough, UK.
- Ibrahim, Y., Kershaw, T., & Shepherd, P. (2020b). A methodology For Modelling Microclimate: A Ladybug-tools and ENVI-met Verification Study. In *35th PLEA Conference. Sustainable Architecture and Urban Design: Planning Post Carbon Cities*, A Coruña, Spain, 1–3 September.
- Ibrahim, Y., Kershaw, T., Shepherd, P., & Coley, D. (2021). On the Optimisation of Urban form Design, Energy Consumption and Outdoor Thermal Comfort Using a Parametric Workflow in a Hot Arid Zone. *Energies*, 14(4026), 22. doi: <https://doi.org/10.3390/en14134026>.
- Jamei, E., & Rajagopalan, P. (2019). Effect of street design on pedestrian thermal comfort. *Architectural Science Review*, 62(2), 92-111. doi: <https://doi.org/10.1080/00038628.2018.1537236>.
- Jamei, E., Rajagopalan, P., Seyedmahmoudian, M., & Jamei, Y. (2016). Review on the impact of urban geometry and pedestrian level greening on outdoor thermal comfort. *Renewable and Sustainable Energy Reviews*, 54, 1002-1017. doi: <http://dx.doi.org/10.1016/j.rser.2015.10.104>.
- Johansson, E. (2006). Influence of urban geometry on outdoor thermal comfort in a hot dry climate: A study in Fez, Morocco. *Building and Environment*, 41(10), 1326-1338. doi: <https://doi.org/10.1016/j.buildenv.2005.05.022>.
- Kovats, R. S., & Hajat, S. (2008). Heat stress and public health: a critical review. *Annu. Rev. Public Health*, 29, 41-55. doi: <https://doi.org/10.1146/annurev.publhealth.29.020907.090843>.
- Krüger, E., Pearlmutter, D., & Rasia, F. (2010). Evaluating the impact of canyon geometry and orientation on cooling loads in a high-mass building in a hot dry environment. *Applied Energy*, 87(6), 2068-2078.
- Labib, R., & Beltran, L. (2015). Optimized Street Design to Balance Outdoor Thermal Comfort And Indoor Daylighting Performance Within Large Scale Urban Settings in Hot Arid Climates.
- Lin, P., Gou, Z., Lau, S. S.-Y., & Qin, H. (2017). The impact of urban design descriptors on outdoor thermal environment: A literature review. *Energies*, 10(12), 2151. doi: [doi:10.3390/en10122151](https://doi.org/10.3390/en10122151).
- Mackey, C., Galanos, T., Norford, L., Roudsari, M. S., & Architects, P. (2017). Wind, sun, surface temperature, and heat island: critical variables for high-resolution outdoor thermal comfort. In *Proceedings of the 15th International conference of Building Performance Simulation Association. San Francisco, USA*.
- Mahdy, M. M. (2014). Applying architecture simulation tools to assess building sustainable design: Adapting the Egyptian residential energy code for climate change. (PhD). University of Kent, Retrieved from <https://books.google.co.uk/books?id=2mDjvgEACAAJ>

- MHUUC, Ministry of Housing Utilities & Urban Communities. (2008). The Executive Regulations for the Egyptian Unified Construction Act. In (pp. 163). Cairo, Egypt: General Organisation for Physical Planning.
- Naboni, E., Meloni, M., Coccolo, S., Kaempf, J., & Scartezzini, J.-L. (2017). An overview of simulation tools for predicting the mean radiant temperature in an outdoor space. *Energy Procedia*, 122, 1111-1116. doi: <https://doi.org/10.1016/j.egypro.2017.07.471>.
- Naboni, E., Meloni, M., Mackey, C., & Kaempf, J. (2019a). The simulation of mean radiant temperature in outdoor conditions: A review of software tools capabilities. In *Proceedings of the 16th IBPSA Conference*, Rome, Italy, Sept. 2-4, 2019.
- Naboni, E., Ofria, L., & Danzo, E. (2019b). A Parametric Workflow to Conceive Facades as Indoor and Outdoor Climate Givers. In *SimAUD 2019*, April 07-09: Atlanta, Georgia.
- Natanian, J., Kastner, P., Dogan, T., & Auer, T. (2020). From energy performative to livable Mediterranean cities: An annual outdoor thermal comfort and energy balance cross-climatic typological study. *Energy and Buildings*, 224(110283). doi: <https://doi.org/10.1016/j.enbuild.2020.110283>.
- Niachou, K., Hassid, S., Santamouris, M., & Livada, I. (2008). Experimental performance investigation of natural, mechanical and hybrid ventilation in urban environment. *Building and Environment*, 43(8), 1373-1382. doi: <https://doi.org/10.1016/j.buildenv.2007.01.046>.
- Nunez, M., & Oke, T. R. (1977). The Energy Balance of an Urban Canyon. *Journal of Applied Meteorology*, 16(1), 11-19.
- Oke, T., Mills, G., Christen, A., & Voogt, J. (2017). *Urban Climates*. Cambridge Cambridge University Press.
- Oke, T. R. (1981). Canyon geometry and the nocturnal heat island: comparison of scale model and field observations. *Journal of Climatology*, 1(3), 237-254.
- Oke, T. R. (1988). Street Design and Urban Canopy Layer Climate. *Energy and Buildings*, 11(3), 103-113. doi: [https://doi.org/10.1016/0378-7788\(88\)90026-6](https://doi.org/10.1016/0378-7788(88)90026-6).
- Oke, T. R. (1995). The heat island of the urban boundary layer: characteristics, causes and effects. In *Wind climate in cities* (pp. 81-107). Berlin/Heidelberg, Germany: Springer.
- Onset. (2021). HOBO U30 Data Loggers. Retrieved from <http://www.onsetcomp.com/products/data-loggers/U30-data-loggers>
- Pearlmutter, D., Berliner, P., & Shaviv, E. (2007). Urban climatology in arid regions: current research in the Negev desert. *International Journal of Climatology*, 27(14), 1875-1885. doi: <https://doi.org/10.1002/joc.1523>.
- Perini, K., & Magliocco, A. (2014). Effects of vegetation, urban density, building height, and atmospheric conditions on local temperatures and thermal comfort. *Urban Forestry & Urban Greening*, 13(3), 495-506. doi: <http://dx.doi.org/10.1016/j.ufug.2014.03.003>.
- Potchter, O., Cohen, P., Lin, T.-P., & Matzarakis, A. (2018). Outdoor human thermal perception in various climates: A comprehensive review of approaches, methods and quantification. *Science of the total environment*, 631, 390-406. doi: <https://doi.org/10.1016/j.scitotenv.2018.02.276>.
- Qaid, A., & Ossen, D. R. (2015). Effect of asymmetrical street aspect ratios on microclimates in hot, humid regions. *International journal of biometeorology*, 59(6), 657-677. doi: <https://doi.org/10.1007/s00484-014-0878-5>.

- Ratti, C., Raydan, D., & Steemers, K. (2003). Building form and environmental performance: archetypes, analysis and an arid climate. *Energy and Buildings*, 35(1), 49-59. doi: [https://doi.org/10.1016/S0378-7788\(02\)00079-8](https://doi.org/10.1016/S0378-7788(02)00079-8).
- Roudsari, M. S., & Mackey, C. (2022). Ladybug-tools. Retrieved from <https://www.ladybug.tools/>
- Ruefenacht, L., Sukma, A., Acero, J. A., & Nevat, I. (2020). Climate-responsive design guidelines: Urban design guidelines to improve outdoor thermal comfort in the southern shore area of singapore.
- Shalaby, A. S., & Shafey, A. M. (2018). Optimizing the Thermal Performance of Street Canyons in New Cairo, Egypt, Using ENVI-met. 5(4), 5639-5654.
- Sharmin, T., Steemers, K., & Matzarakis, A. (2017). Microclimatic modelling in assessing the impact of urban geometry on urban thermal environment. *Sustainable Cities and Society*, 34, 293-308. doi: <http://dx.doi.org/10.1016/j.scs.2017.07.006>.
- Sini, J.-F., Anquetin, S., & Mestayer, P. G. (1996). Pollutant dispersion and thermal effects in urban street canyons. *Atmospheric Environment*, 30(15), 2659-2677. doi: [https://doi.org/10.1016/1352-2310\(95\)00321-5](https://doi.org/10.1016/1352-2310(95)00321-5).
- Stewart, I. D., & Oke, T. R. (2012). Local climate zones for urban temperature studies. *Bulletin of the American Meteorological Society*, 93(12), 1879-1900. doi: <https://doi.org/10.1175/BAMS-D-11-00019.1>.
- Tomasetti, T. (2020). Core Studio. Retrieved from <http://core.thorntontomasetti.com/>
- Toparlar, Y., Blocken, B., Vos, P. v., Van Heijst, G., Janssen, W., van Hooff, T., Montazeri, H., & Timmermans, H. (2015). CFD simulation and validation of urban microclimate: A case study for Bergpolder Zuid, Rotterdam. *Building and Environment*, 83, 79-90. doi: <http://dx.doi.org/10.1016/j.buildenv.2014.08.004>.
- United Nations, Department of Economic and Social Affairs Population Division. (2018). World Urbanization Prospects: The 2018 Revision. New York: United Nations
- Wagdy, A., Sherif, A., Sabry, H., Arafa, R., & Mashaly, I. (2017). Daylighting simulation for the configuration of external sun-breakers on south oriented windows of hospital patient rooms under a clear desert sky. *Solar Energy*, 149, 164-175. doi: <http://dx.doi.org/10.1016/j.solener.2017.04.009>.
- Watkins, R., Palmer, J., & Kolokotroni, M. (2007). Increased temperature and intensification of the urban heat island: implications for human comfort and urban design. *Built Environment*, 33(1), 85-96. doi: <https://doi.org/10.2148/benv.33.1.85>.
- Witte, M. J., Henninger, R. H., Glazer, J., & Crawley, D. B. Testing and validation of a new building energy simulation program. In *7th IBSPA Conference*.

4.10 Addendum

In this study, the Ladybug-tools model was validated against field measurements, which were conducted using calibrated sensors, whose accuracy comply with the recommended accuracy, defined within the Measurement and Instruments guidelines of ASHRAE handbook of fundamentals (ASHRAE, 2017b). Typical Meteorological Year (TMY) weather files represent the long-term averages rather than actual/extreme weather conditions of a given location, and are widely used in building performance simulations. In this study, the weather data from the TMY file were compared to those obtained by measurements, to check the reliability of the weather file. In other words, to ensure that the deviations from the actual weather conditions are within an acceptable range, and thus ensure the reliability of the reported thermal sensation. Although high temperatures in Cairo occur most frequently in July, the highest are recorded on 7th June (Figure 4.17), and hence it was selected to represent the worst-case scenario in this study.

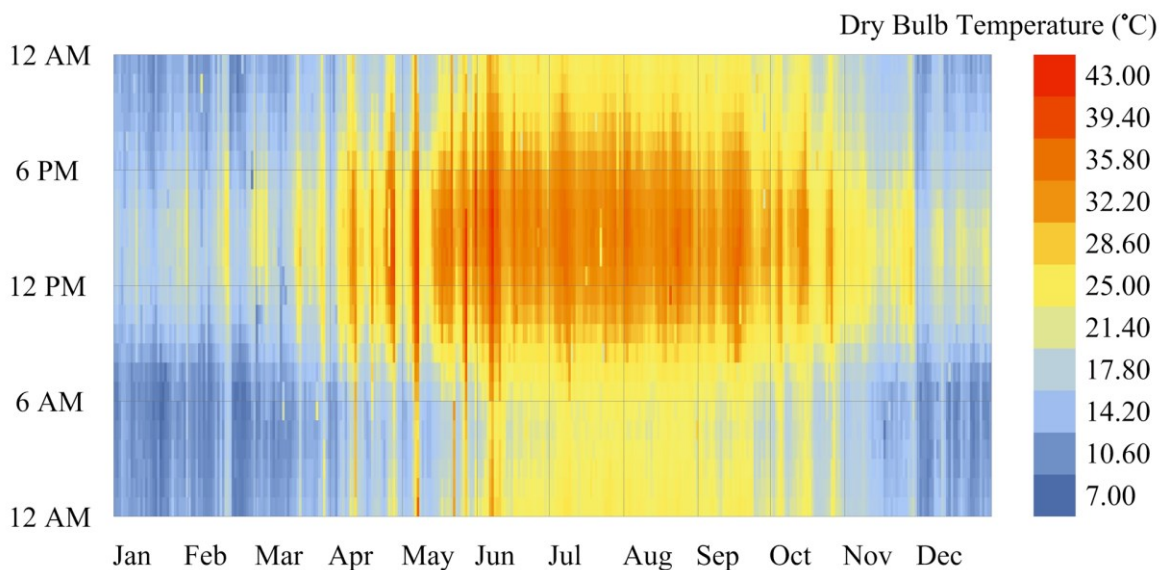


Figure 4.17: Cairo's hourly dry bulb temperatures as extracted from the IWEC file and represented using Ladybug.

Results of the validation have shown that maximum differences of MRT and UTCI did not exceed ± 10 °C (Figure 4.18), where the Mean Bias Error (MBE) was -7.61 % and 5.55 % for MRT and UTCI, respectively. Also, the Coefficient of Variation of the Root Mean Squared Error (CVRMSE) was calculated for the goodness of fit at timestep level. This was 12.55 % and 6.26 % for MRT and UTCI, respectively, which meets the criteria defined in Guideline 14 of ASHRAE (2014) for the calibration of simulation models.

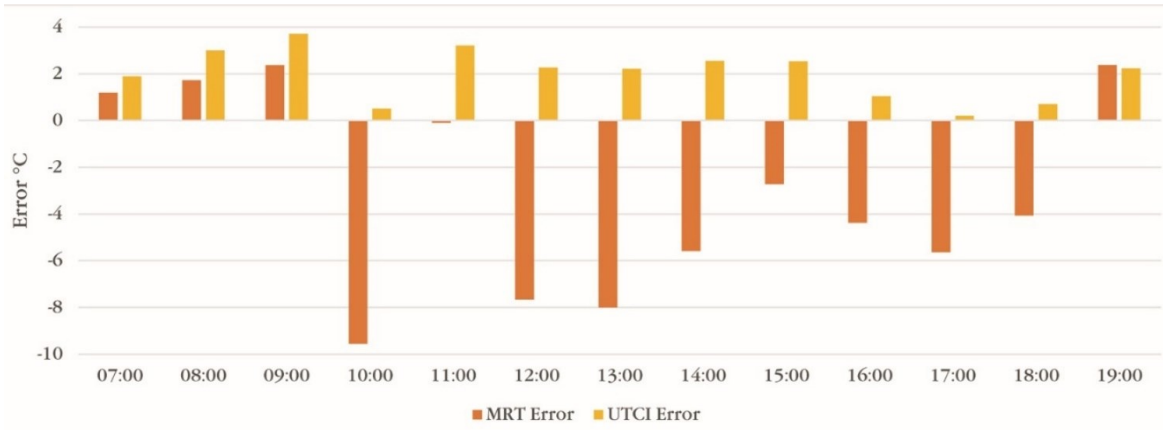


Figure 4.18: MRT and UTCI absolute error between the Ladybug-tools model and field measurements.

4.11 Epilogue

This study presented a deeper understanding of the impact of canyon-scale design parameters with respect to outdoor thermal comfort than those reported in previous studies in hot-arid climates (Ali-Toudert, 2005). The discussion in this study showed that an optimal H/W ratio is capable of reducing the UTCI by almost 6 °C and 4 °C in NS and EW orientations, respectively. The UTCI performance of very deep urban canyons (H/W = 6) changed by up to 2° C due to orientation only. The results highlighted new correlations of the UTCI with SVF, and the H/W's of both symmetrical and asymmetrical urban canyons. Not only this, but also the results provided a thorough analysis of the relationship between the canyons' flanks, their individual heights and interspaces in different orientations. The results of the validation against field measurements in this study, along with the verification against ENVI-met in the previous chapter, together constitute a robust assessment of the reliability of the simulation workflow to be used in this climate context.

The implications of this study with regards to the aims of this thesis introduced a set of optimum design parameters, the use of which has been quantitatively shown to yield lower UTCI than using the design thresholds of the Egyptian Construction Act by up to 2.3° C. This necessitates a rethinking of the efficacy of the current design regulations in the light of a rapidly growing urban population in Greater Cairo, associated with UHI exacerbation as well as thermal comfort deterioration. In this context, the design guidelines and the UTCI rose presented in the discussion help shifting the focus of policy making from density-based spatial configurations into those informed by the environmental performance.

Based on the conclusions of this study, the next chapter expands the scope of this chapter to include the urban scale design parameters and their impact on both outdoor thermal comfort and energy consumption in the hottest month rather than just a single day. This is done through the study of the performance of generic urban typologies - comprising a group of urban canyons - with material properties and occupancy schedules inferred from common practices in Egypt. This should provide a better understanding of the heat stress in this climate context and add a new perspective of designing energy efficient urban communities.

5 Urban Scale Multi-Objective Optimisation

5.1 Preface

The previous chapter discussed the impact of the urban canyon geometry on outdoor thermal comfort. At the urban scale, this has direct implications on the energy performance of urban forms. In conjunction with the discussion on the typological approach as a discipline of how cities should grow, with respect to social and cultural aspects (Oliveira, 2016), March and Martin (1972), in their book *Urban Space and Structure*, investigated the environmental aspects of urban built forms, particularly, the impact of density and surface coverage on daylighting. In doing so, they presented six elementary building forms from the point of view of land utilisation (Figure 5.1). Gupta (1984), in his analysis of solar exposure of urban forms in hot climates, argued about the applicability of March and Martin's archetypes in reality, and further presented a modified version of their forms (Figure 5.1). The new archetypes have been adopted in a myriad of studies on the nexus between urban form and environmental performance.

The majority of studies on the smaller urban scale (a group of urban blocks) can be categorised into three groups; using generic building forms such as those in Figure 5.1 within a grid of similar surrounding contexts; using real urban forms as the target and the surrounding geometries; or using a hybrid of the previous two

with simplified geometries, albeit representing vernacular urban forms and building regulations. Of the third category, Fahmy (2010) studied the thermal performance of two precincts in Cairo by comparing the real built forms to design suggestions synthesised by residential clusters (courtyards) whose proportions were inferred from the literature. His results showed that the latter provide more comfortable conditions. Mahmoud *et al.* (2021) concluded that North-South slabs performed better than staggered blocks (pavilions) and courtyards in New Aswan, Egypt. The works of Attia *et al.* (2012) and Mahdy (2014), on the other hand, considered the improvement of energy consumption in the residential sector in Cairo and Alexandria through modification of the building envelope (thermal insulation), window-to-wall ratios and occupancy schedules. There is a dearth of studies in Egypt which consider both outdoor thermal comfort and energy consumption at the local urban scale.

This chapter covers this gap by addressing the second research question “*what are the optimum design parameters which yield the best thermal and energy performance of urban typologies?*” For a two-fold question, the study addresses the best performance out of three typologies derived from real built forms in Cairo (Figure 5.2 and Figure 5.3), altering their morphological parameters to maximise outdoor thermal comfort in terms of UTCI and minimise energy consumption in the hottest month of July. Energy consumption is accounted for as the monthly aggregate cooling, lighting and electric equipment loads per building per unit area of a single floor (441 m²), hypothetically comprising four residential apartments, but modelled as a single thermal zone, i.e., total energy loads per thermal zone per building. Although this is not a common metric for presenting the energy loads, the implications of this metric on the different analyses presented throughout the paper hold constant. Moreover, a comprehensive performance metric is presented though combining both outdoor thermal comfort and energy loads, referred to as the combined fitness. The application of the abovementioned energy metric in the calculation of the combined fitness does not change the implications drawn about the optimum typology, nor the optimum design parameters. In this work, 4, 6 and 8 buildings are used in scattered (pavilion), linear (slab) and courtyards, respectively. The morphological parameters in this work are distances between buildings in both directions, building heights, orientation to describe the configuration of urban forms, along with the commonly used Floor Area Ratio (FAR) and Building Coverage Ratio (BCR) to represent their density.

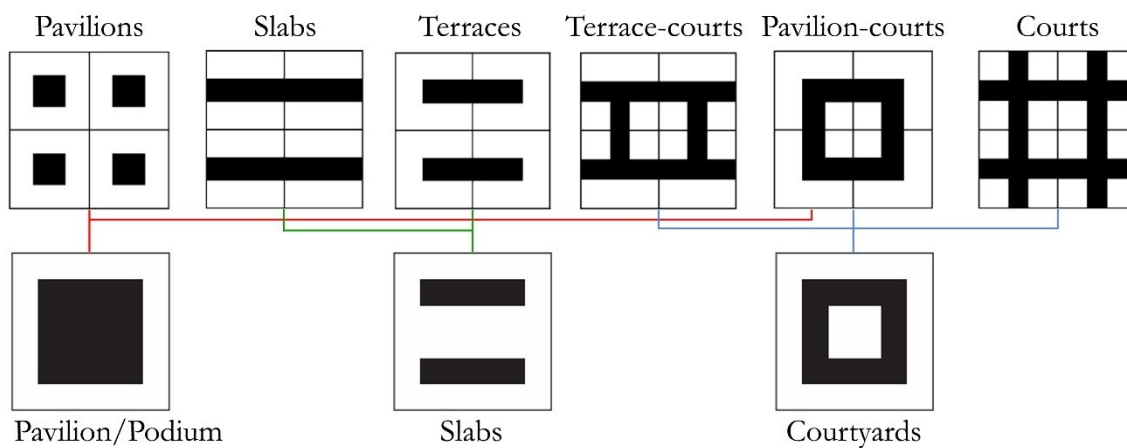


Figure 5.1: Generic urban forms (top), and their adapted version (bottom)

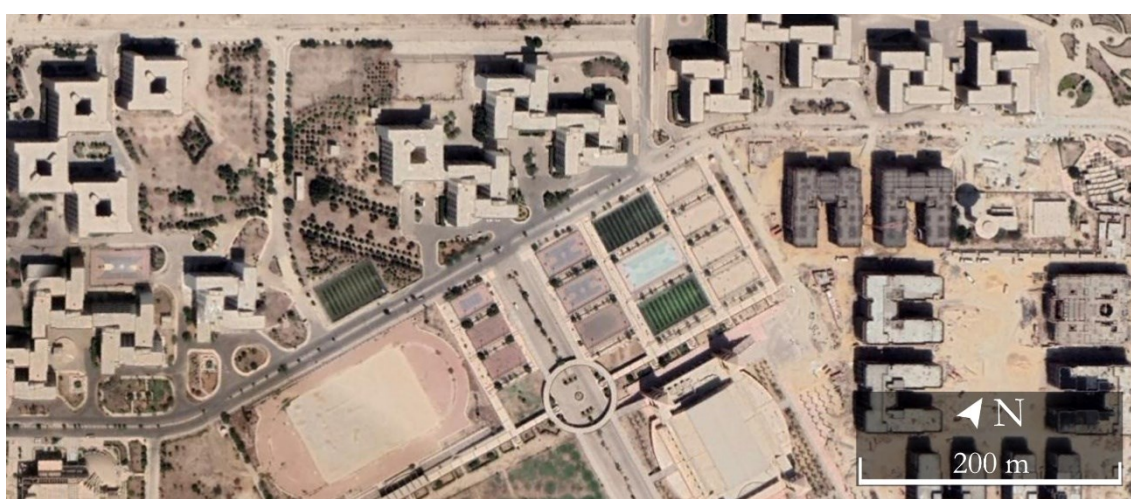


Figure 5.2: Courtyard typology in Helwan University dorms (Google Earth).

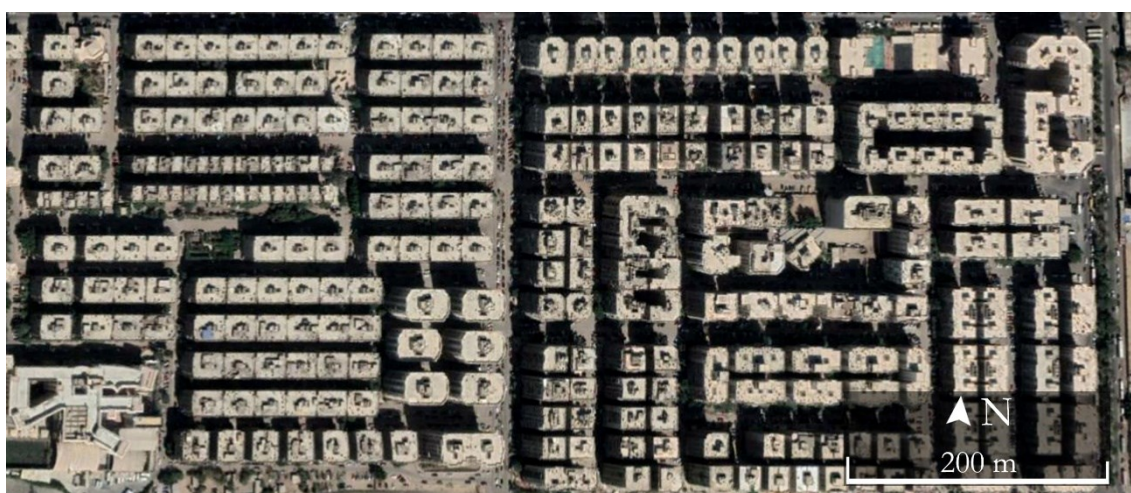


Figure 5.3: Linear (left) and scattered (right) typologies in Alwafa' Wal Amal precinct, Cairo (Google Earth).

This chapter is based on the paper “On the Optimisation of Urban form Design, Energy Consumption and Outdoor Thermal Comfort Using a Parametric Workflow in a Hot Arid Zone” published in the journal *Energies* in 2021 as an invited paper to the special issue “Resilience and Climate Adaptability of Buildings and Urban Areas.” The candidate has predominantly contributed to the publication. Details of authorship of this paper are given in Table 5.1.

Table 5.1: Declaration of Authorship.

This declaration concerns the article entitled:	
On the Optimisation of Urban form Design, Energy Consumption and Outdoor Thermal Comfort Using a Parametric Workflow in a Hot Arid Zone.	
Publication status (tick one):	
Draft manuscript <input type="checkbox"/> Submitted <input type="checkbox"/> In review <input type="checkbox"/> Accepted <input type="checkbox"/> Published <input checked="" type="checkbox"/>	
Publication details (reference):	
Ibrahim, Y. , Kershaw, T., Shepherd, P., & Coley, D. (2021). On the Optimisation of Urban form Design, Energy Consumption and Outdoor Thermal Comfort Using a Parametric Workflow in a Hot Arid Zone. <i>Energies</i> , 14 (4026), 22. DOI: https://doi.org/10.3390/en14134026 .	
Copyright status (tick the appropriate statement):	
<ul style="list-style-type: none"> • I hold the copyright for this material <input checked="" type="checkbox"/> • Copyright is retained by the publisher, but I have been given permission to replicate the material here <input type="checkbox"/> 	
Candidate's contribution to the paper (%):	
The candidate has predominantly contributed to :	
<ul style="list-style-type: none"> • Formulation of ideas (70%): Y. Ibrahim developed the ideas, in consultation with the co-authors. • Design of methodology (90%): Y. Ibrahim developed the methodology, in consultation with T. Kershaw. • Data analysis (100%): Y. Ibrahim conducted the data analysis. • Presentation of data in journal format (80%): Y. Ibrahim wrote and submitted the paper. T. Kershaw and P. Shepherd provided feedback for improvements and for addressing the reviewers' comments. 	
Statement from Candidate:	
This paper reports on original research I conducted during the period of my Higher Degree by Research candidature.	
Signed:	Date: September 2022

5.2 Abstract

The recent reports from the Intergovernmental Panel on Climate Change (IPCC) urge for the reconceptualization of our design of the urban built environments. However, current efforts to integrate urban environmental assessment into practice in Egypt are proving insufficient. This paper utilises the Ladybug tools simulation plugins to investigate the impact of changing the morphological characteristics of three-block typologies (scattered, linear and courtyard) and their associated parameters to understand their multidimensional relationship with environmental conditions, outdoor thermal comfort and energy use intensity. This study based in Cairo, Egypt, considers 3430 hypothetical geometrical configurations comprising of a variety of design parameters and indicators. The results show a strong correlation between the design parameters and the combined performance of thermal comfort and energy consumption ($R^2 = 0.84$), with urban density having the strongest impact on both thermal comfort and energy use ($R^2 = 0.7$ and 0.95 , respectively). The design parameters exhibited a consistent impact on the different typologies, albeit with varying magnitude. Compact and medium-density urban forms are shown to elicit the best overall performance, especially for ordinal orientations (e.g., $\sim 45^\circ$) across all typologies. Compact high-density scattered forms are favoured when considering thermal comfort, while courtyards outperform other typologies when considering energy efficiency and overall performance.

5.3 Introduction

The global population is expected to grow to 9.7 billion by 2050, with $\sim 70\%$ of those people living in urban areas (United Nations, 2018). With cities currently consuming $\sim 76\%$ of global primary energy and producing 43% of the related CO_2 emissions (Seto *et al.*, 2014), it is clear that urban scale studies are a crucial part of the discussion about the future of built environments. Moreover, the building sector alone accounts for approximately 30% of the global final energy consumed, 70% of which are shared by the residential sector (IEA, 2020). Urbanisation, as a process, not only transforms the spatial and socio-economic distribution of rural and urban populations, but also alters the energy budget of the built environment. Densification of the built environment is often typified by narrower urban canyons with impervious construction materials, reduced vegetation, and increased pollution, leading to increased sensible heat storage, shifting longwave heat

emission, entrapment of shortwave radiation within the street level, as well as hindering the potential for evaporative and convective cooling, creating an Urban Heat Island (UHI) (Oke, 1995).

The study of the built environment is inextricably linked with the energy exchanges between the pedestrians and their surrounding urban elements. Outdoor thermal comfort is recognised as one of the key performance indicators (KPI)s for urban environmental assessment and further can be a determinant of travel choices pedestrians make and activities they undertake. However, there are relatively few studies dealing with outdoor comfort compared to those dealing with indoor spaces. This is mainly due to the huge spatial and temporal fluctuations of microclimatic conditions surrounding pedestrians, e.g., air temperature, wind speed, humidity and solar radiation, as well as the interconnectivity between these conditions and how pedestrians react physically and physiologically to achieve psychological satisfaction (Nikolopoulou & Steemers, 2003; Jamei *et al.*, 2016). Given the interdependent relationship between the size, density, morphological and typological characteristics of a city and both the urban microclimate and energy consumption, the built environment has a key role to play in addressing global environmental issues, rather than just being part of the dilemma (Cities, 2014; Naboni *et al.*, 2019b).

5.3.1 Background

The relationship between the local climate and the urban form design is reciprocal, such that the design response of architects and urban designers is often informed by the local climatic conditions, and in return, urban elements pose an impact on the local as well as the micro-scale climate (Golany, 1996). One of the pioneering studies trying to understand this relationship was the work of March and Martin (1972) who suggested six simplified urban patterns in the form of archetypal building forms to investigate how density and surface coverage affect daylighting. Studies using these archetypes have recently proliferated to investigate different environmental qualities. Gupta (1987) studied the thermal performance of three archetypes in a hot-arid climate with respect to their discomfort index as a function of solar exposure. In the same context, Ratti *et al.* (2003), by virtue of image processing of Digital Elevation Models (DEMs), analysed shadow density and daylight distribution along with sky view factors as indicators for the thermal performance of March and Martin's archetypes.

Both studies have acknowledged the courtyard design as appropriate for hot-arid climates. Within those studies, the rationale behind employing generic urban forms was to seamlessly standardise a set of morphological parameters and link them to environmental conditions. Following the same approach, Oke proposed a simplified classification of urban climate zones based on the built form configuration, terrain roughness, aspect ratio and ground imperviousness (Oke, 2006), which was further developed into 17 Local Climate Zones (LCZs) that delineate regions of uniform built types, land cover, material and human activity that extend horizontally from several hundreds of meters up to several kilometers (Stewart & Oke, 2012). “The internal homogeneity portrayed by each LCZ is unlikely to be found in the real world. The 17 patterns should nevertheless be familiar to users in most cities, and should be adaptable to the local character of most sites” Oke articulated (Stewart & Oke, 2012).

In a series of studies by Salvati and others (Salvati *et al.*, 2017; Salvati *et al.*, 2019), they examined the UHI intensity, heating and cooling demand along with the diurnal cycles of air temperature in five normalised urban textures in Rome and Barcelona. They concluded that, in a Mediterranean climate, compact (horizontally dense) urban textures with Site Coverage Ratio (SCR) greater than 0.5 entail lower annual energy consumption than in rural areas, although they exhibit relatively higher UHI intensities in winter. Tereci *et al.* (2013), pointed out that courtyard forms are disadvantaged in the oceanic climate of Stuttgart, where they showed higher heating demand that reached up to 20% at their highest density. Taleghani *et al.* (2013) on the other hand, compared the pavilion, linear and courtyard forms in the temperate climate of Rotterdam, with regards to their annual heating and lighting energy demand, and using the running mean temperature as an indication for thermal comfort. Their results showed the courtyard saving up to 22% of heating energy and, besides the linear forms, with less discomfort hours at both low and high densities. Part of this disparity can be explained by the way Taleghani *et al.* compared their results on each apartment’s total energy rather than the whole building’s consumption as in Tereci *et al.* (2013). The main reason, nonetheless, remains the different climatic contexts, built form configurations and their corresponding design objectives as Oke (1988) explained.

The definition of design parameters is largely associated with the scale, objectives and study approach. On the urban canyon scale, building heights (H), street width (W) and the aspect ratio (H/W) along with Sky View Factor (SVF) have

long been agreed upon among researchers to represent the urban geometry (Ali-Toudert, 2005; Johansson, 2006). Orientation is another key aspect that affects the canyon performance but also the seasonal variations of energy loads (Futcher *et al.*, 2013) and comfort levels (Elnahas, 2003). On the block or urban scale, the parameters extend to include, but are not limited to, Floor Area Ratio (FAR), Surface to Volume ratio (S/V), building coverage ratio (BCR) and Open Space Ratio (OSR) (Rode *et al.*, 2014).

Martins *et al.* (2016) used CitySim to investigate the impact of eight morphological parameters on solar radiation availability to a generic scattered layout in Maceió, Brazil, to conclude that albedo, H/W and distance between buildings together account for 80% of the impact over west facades and roofs. A recent study proposed a new satellite-based method for extracting six morphological parameters, namely, BCR, H, SVF, as well as Building Volume Density (BVD), Frontal Area Index (FAI) and roughness length (Xu *et al.*, 2017). Meanwhile, urban scale studies are always confronted by conflicting objectives, even using simulation tools. Despite the advancements in computational capabilities, the integration of multiple tools to bring different environmental considerations together is computationally expensive and time-consuming. For this reason, urban geometry studies in the last 2 decades, by and large, can be categorised into; (1) studies investigating the impact of urban geometry on energy consumption, passive solar radiation and daylight availability and; (2) studies concerned with urban geometry, UHI and microclimate.

5.3.1.1 Urban Geometry and Energy Consumption

The study of Ratti *et al.* (2005) sought to link the gap between solar gain modelling and energy demand. They used the Light and Thermal (LT) method to estimate building energy demand in three case studies in London, Toulouse and Berlin. Their results showed that the passive (reflected/diffuse light only) to non-passive area is a stronger indicator of energy consumption than S/V. Additionally, around 10% and 55% difference in energy usage is due to morphology variations and glazing optimisation, respectively. Okeil (2010) introduced the residential solar block—a hypothetical building form—that outperforms linear and conventional block typologies by maximising winter but minimising summer solar radiation as a strategy for minimising heating and cooling demands, respectively.

Space cooling demands for stand-alone buildings were compared to that of buildings within a street canyon configuration in Allegrini *et al.* (2016) and Vallati *et al.* (2016). Both studies have shown that the latter requires less cooling demand than stand-alone buildings. With the increased tendency of using parametric studies, the concept of regenerative urban design became evident in energy usage studies, which included either Martin's archetypes or hybrids thereof. Vartholomaios (2017) utilised the Ladybug tools (Roudsari *et al.*, 2013) to calculate the annual energy loads for three typologies with a total of 540 possible configurations, in a Mediterranean climate of Thessaloniki, Greece. Their results proposed an elongated perimeter block over E-W axis with minimum distances as the best configuration. Javanroodi *et al.* (2018) simulated 1600 cases of different built densities, building forms and urban patterns of the neighbouring buildings to test the cooling loads and ventilation potential of a target building in a hot-arid climate in Tehran. Recorded from April to September, their results showed that maximum density, U-shaped and Courtyard-shaped forms presented the lowest cooling loads and the highest ventilation potential, respectively, among the different patterns.

While some authors argue about the higher cooling demand of the courtyard typology (Quan *et al.*, 2014; Natanian *et al.*, 2019c), other authors took the concept of "nearly zero-energy buildings" (NZEB) (Recast, 2010) to the broader level of urban scale, to claim that courtyards are the most eligible forms for achieving 100% load match (Load match stands for the ratio between energy demand and energy supply by on-site PV generation.), compared to other typologies (Natanian *et al.*, 2019a; Zhang *et al.*, 2019). Furthermore, a multi-objective optimisation algorithm was used to evaluate the cooling and heating demands as well as PV potential for 12 generic typologies in the humid subtropical climate of Shanghai by Wortmann and Natanian (2020). Their analysis showed that L-shaped courtyard represented 33% of the optimum cases followed by high FAR linear and open courtyard typologies.

5.3.1.2 Urban Geometry and the Microclimate

The energy budget of an urban canyon was first investigated in the pioneering study of Nunez and Oke (1977), followed by studies on the vertical gradients of air (Nakamura & Oke, 1988) and surface temperatures (Santamouris *et al.*, 1999). The relationship between the canyon's aspect ratio (H/W), SVF and UHI was established by Oke (Oke, 1981), and confirmed by many others.

Higher H/W with lower SVF provides more shading to the canyon facets and the ground (Matzarakis *et al.*, 2007), and hence offers lower daytime air and ground temperatures (Shashua-Bar & Hoffman, 2004; Bourbia & Boucheriba, 2010), albeit with lower radiative losses (Holmer, 1992) and cooling rates during the night (Giannopoulou *et al.*, 2010). Johansson (2006), on the other hand, found that the relative cooling of the canyon's daytime air temperature exceeded the night-time warming in a hot-dry climate of Fez (Johansson, 2006), and in another study in a hot humid climate of Colombo (Johansson & Emmanuel, 2006).

Additionally, orientation has a key role in defining a canyon's thermal performance. For instance, studies in hot-arid climates advocated the use of deep canyons with NS orientations (Ali-Toudert *et al.*, 2005; Bourbia & Awbi, 2004), while EW orientations were recommended in temperate (Elnahas, 2003) and tropical wet-dry climates (Sharmin *et al.*, 2017). Qaid and Ossen (2015) found that NE-SW canyons with higher building heights on the NW side performed better in the hot-humid climate of Putrajaya, Malaysia, when they investigated six asymmetrical canyons in terms of their daytime air temperature and night-time UHI. Notwithstanding, the role of orientation is also dependent on the H/W. In their study of 18 urban canyons in a Mediterranean climate in Thessaloniki, Greece, Chatzidimitriou and Yannas (2017) recommended using very deep canyons ($H/W \sim 3.3$) in all orientations except NE-SW canyons where medium ratios ($H/W \sim 1.7$) were shown to be favourable in both summer and winter. A few studies have sought to understand the relationship between a city's morphology and the local climate. Taleghani *et al.* (2015) compared three typologies within two orientations and claimed that courtyard and NS slab typologies are best for lower air temperatures, Mean Radiant Temperature (MRT) and Physiological Equivalent Temperature (PET) in a temperate climate. Allegrini *et al.* (2015), although in a similar climate, criticised the two typologies with regards to their lower convective cooling. Moreover, some authors have sought to link the thermal performance of urban blocks to their morphological parameters. Jin *et al.* (2018) compared eight parameters of 27 locations in Singapore, characterised by tropical rainforest climate. Their regression analysis showed correlations of daytime air temperatures with an SVF and green plot ratio of 0.59 and 0.47, respectively. Further, a study of five quarters comprising 50 urban blocks in New Aswan, Egypt has revealed that 56% of blocks' PET depend on FAR and space enclosure (Galal *et al.*, 2020).

More recently, in a Mediterranean climate, a parametric study of four FARs, three widths and four window-to-wall ratios was conducted by Natanian and Auer (Natanian & Auer, 2020), to estimate the thermal comfort, daylighting as well as the load match of four different typologies (192 total cases). Courtyard typology was shown to outperform other typologies in thermal comfort, and so did they in average load match, given lower FAR are used (Natanian & Auer, 2020).

It is clear from this review of previous studies that results and trends in performance are disparate and constitutively driven by various conflicting design objectives, regional and climatic contexts, as well as the geometrical characteristics investigated. Additionally, the fact that the computational capabilities are rapidly increasing spurs the research on the multi-aspect environmental qualities of the built environment, specially in areas susceptible to severe climatic conditions, specially, where performance-informed decisions are most needed, such as in Egypt. The recent transformation in many Arabic countries, including Egypt, from the concept of a traditional neighbourhood unit into luxurious but socially segregated private communities has increased the number of factors (land value, privacy, etc) competing with environmental considerations. This explains why low-rise apartment buildings and villas are ubiquitous in preference of the courtyard residential complexes, despite the agreement on the improved performance of the courtyard typology in hot-arid regions.

5.3.1.3 Advancements in Urban Modelling Tools

Building and urban performance simulation has become an essential approach for modelling and evaluating the built environment. Given the recent growth of computational capabilities, several models have been developed. Building Energy Models (BEMs), such as EnergyPlus (Crawley *et al.*, 2001), TRNSYS (Thermal Energy System Specialists, 2021) and CitySim (Robinson *et al.*, 2009) are often criticised for not using the real microclimatic conditions of the outdoor environment within urban areas and rather using typical meteorological data files representative of open and rural areas. District-scale Urban Climate Models (UCMs) such as the Urban Weather Generator (UWG) (Bueno *et al.*, 2013) and ENVI-met (Bruse, 2020) have widely been acknowledged to successfully reflect the outdoor conditions and as such been coupled with BEMs in a growing body of research (Rodler *et al.*, 2021). Examples are abundant, for instance, ENVI-met with TRNSYS (Perini *et al.*, 2017), UWG with EnergyPlus (Salvati *et al.*, 2017), and METEONORM

with CitySim (Allegrini *et al.*, 2016). A recent example of chaining models was using the World Urban Database and Access Portal Tools (WUDAPT) to generate LCZs based on Stewart and Oke's classification (Stewart & Oke, 2012) as inputs to the district scale Weather Research and Forecasting (WRF) model which in turn generates the boundary conditions needed in the microclimate simulations using ENVI-met (McRae *et al.*, 2020). The tendency to couple UCM and BEM, however, is often confronted by the need to balance the computational cost of detailed bottom-up approaches and the reliability of simplified top-down approaches, as well as having different inputs needed. Moreover, most of these workflows are rarely used in parametric analyses or urban scale optimisations due to the considerable computational overhead (Natanian *et al.*, 2019a). The necessity to couple—or chain—various tools and automatically exchange data between them qualifies Grasshopper (Rutten, 2021) to be a panacea for urban design rigidity and foreshadows a paradigm shift in environmental performance-based design exploration.

Grasshopper, the visual platform for scripting, is an integrated feature of Rhinoceros 3D (Rhino), which allows architects, designers and others with no significant knowledge about programming to develop their own generative algorithmic designs in a user-friendly graphical interface. Developed in 2007 by David Rutten, at McNeel & Associates (McNeel, 2021), Grasshopper allows users to seamlessly and repetitively manipulate their input parameters in a flow chart-like working procedure, and simultaneously have real-time feedback as well as integrated post-processing platforms. Thanks to these features, together with two-way data streaming (looping) plugins, e.g., Hoopsnake and Anemone, parametric analyses of regenerative urban design with multiple iterations have become viable (Natanian & Auer, 2020). More interestingly, using the Rhino Common Software Development Kit (SDK), Grasshopper integrates such common scripting platforms as Python, C# and VB .NET, giving the designers the opportunity to develop their own components or rather modify an existing one. Furthermore, Grasshopper includes components for single (Galapagos) and multi-objective (Octopus) evolutionary optimisation (Rutten, 2021). Undoubtedly, the use of open-source plugins in Grasshopper makes it popular amongst designers and facilitates the application of optimisation studies in practice.

5.3.2 *Research Problem and Objectives*

Egypt is racing against overwhelming population growth and striving to contain slums and urban sprawl within and around its metropolis, Cairo. There has been an extensive campaign for expanding existing cities as well as planning for new communities. However, the governmental endeavours to reduce energy consumption (MHUUC, 2005) were confined to the building scale taking no account of the morphological relationship with neighbouring buildings. Furthermore, The Egyptian Unified Construction Act (MHUUC, 2008) stipulates mainly spatial rather than climate-based design criteria. The fact that the total final energy consumption in Egypt has nearly doubled between 2000 and 2020 with the building sector responsible for 42% of this consumption (IEA, 2021) necessitates a paradigm shift in both research and practice, but most importantly, linking the gap between them. However, to the best of the authors' knowledge, there are no multi-dimensional studies of Egypt that investigate energy efficiency together with outdoor thermal comfort, despite the urgent need for them.

This paper addresses the need of urban planners and designers to bring energy performance and thermal comfort together to acquire a multi-criteria performance-driven decision support in the early design stages. The paper does so by investigating the impact of different typologies and their associated morphological parameters, namely, the distance between buildings, building heights, orientation, FAR and BCR on the outdoor thermal comfort and building energy consumption. The study capitalises on the parametric capabilities of Grasshopper and its environmental analysis plugins, Ladybug tools to highlight the trade-offs between different performance criteria through an iterative simulation workflow. The study is conducted in the hot-arid climate of Cairo, Egypt, where Cairo accommodates almost 50% of Egypt's urban residents and accounts for at least 32% of the current residential constructions, and around 44% of the residential apartments with air conditioning (CAPMAS, 2019). The objective of this study is to define the optimum design parameters on an urban block scale that simultaneously maximise outdoor thermal comfort and minimise energy consumption. Design guidelines are presented to help design experts achieve more liveable and sustainable urban communities.

5.4 Methodology

A simulation approach for hypothetical case studies is applied in this study. This approach is appropriate in parametric studies aiming to support stakeholders in the planning stage, where the use of abstracted building typologies and standardised design parameters reduces the complexity of parametric combinations, hence the simulation of a higher number of case studies, whose results can be easily interpreted by designers.

5.4.1 Case Study Modelling

A hypothetical urban block comprising of arrays of residential buildings, 21×21 m each was parametrically modelled in Grasshopper within a 3×3 identical surrounding context. Each building is 441 m^2 per floor, which comprises four residential apartments. Floor heights were set to 3 m to match the step size of the building heights in Table 5.2 (a single floor higher per each building height increment). Unlike parametric studies using the same approach (Vartholomaios, 2017; Natanian *et al.*, 2019a), a generic Python script was used in this study to automatically switch back and forth between different building typologies (Figure 5.4-top), based on the distance between buildings (see Supplementary Materials). Scattered layouts are simulated with distances between buildings ranging between 6 m and 18 m, where the distances between blocks are kept at half of this distance (as illustrated in Figure 5.4). Distances 21 m and 24 m trigger the creation of an intermediate building that transforms scattered layouts into linear forms (one axis triggered) or courtyard forms (both axes triggered). Distances 24 m on both axes were set to create a courtyard form with 6 m rather than 12 m distance between blocks in order to have a comparative analysis of the same distances throughout the different typologies.

This number of permutations resulted in a simulation of 3430 cases in a single run. Since linear forms could be generated in both NS and EW directions, maximum orientation was set to 90° . Maximum and minimum thresholds of the simulated parameters (Table 5.2) were limited in accordance with the Egyptian Construction Act (MHUUC, 2008), with the exception that the minimum distances between buildings were one step lower, recommended based on a previous study by the authors (Ibrahim *et al.*, 2021b). This dynamic parametrisation of buildings' geometry has generated a wide range of density indicators; BCR ranging from 0.33 to 0.64 and FAR ranging from 1.00 to 7.65. The ground surface was further

subdivided into a number of sub-surfaces proportional to the number of points of interest (Figure 5.4-bottom row) for outdoor comfort calculation in a way that balances the accuracy of shading variation and computation time.

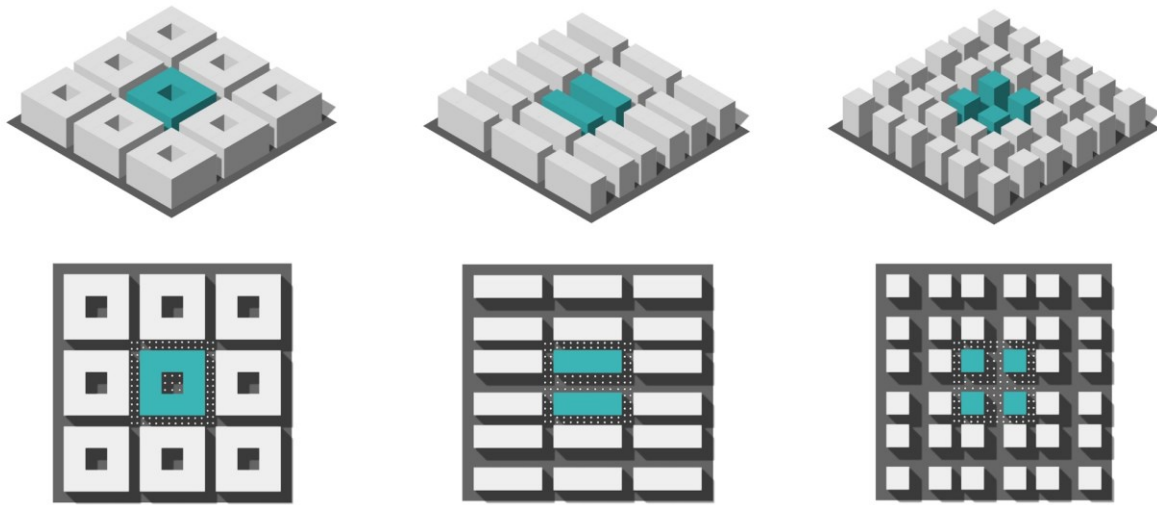


Figure 5.4: Three archetypes exemplified in this study as a 3D View (top) and plan view showing the points of interest in outdoor comfort studies (Bottom).

Table 5.2: Minimum, maximum and step size of each dynamic parameter simulated.

Design parameter	Min.	Step Size	Max.	Iterations
Distance between building (<i>X</i> -axis (EW))	6 m	3 m	24 m	7
Distance between building (<i>Y</i> -axis (NS))	6 m	3 m	24 m	7
Building heights	9 m	3 m	36 m	10
Orientation (CCW from North)	0°	15°	90°	7

5.4.2 Simulation Workflow

The simulation workflow applies an aggregated bottom-up approach by chaining the inputs and outputs of validated software engines, i.e., EnergyPlus (Crawley *et al.*, 2001) and UWG (Bueno *et al.*, 2013), by means of the Ladybug tools (Roudsari *et al.*, 2013), the plugins of Grasshopper. EnergyPlus, the BEM interface, was validated with ASHRAE 1052RP test and verified against the BESTEST (Witte *et al.*), as such was proven to be suitable for small district-scale analyses similar to the study in hand. The UWG uses an algorithm that combines a variety of geometrical parameters, such as average building heights, footprints, surface roughness and thermal properties to reflect the UHI effect induced by the built environment. This happens by morphing the hourly air temperatures and relative humidity within the “rural” weather data file and generating a new “urban” weather file.

Moreover, the validation of the algorithm with field measurements in various climates (Bueno *et al.*, 2013; Bueno *et al.*, 2014; Salvati *et al.*, 2019) has shown its reliability in homogeneous urban contexts as in this study. Figure 5.5 depicts how the input and output data are streamed between the Ladybug tools and different simulation engines. Simulation parameters (see Section 5.4.4) and climatic data (Section 5.4.5) are kept fixed in this study. The iteration of the dynamic parameters (Section 5.4.1) triggers the simulation engines via the Ladybug tools (see Supplementary Materials); Dragonfly links Grasshopper to the UWG to generate an urban weather file where; Honeybee links Grasshopper to EnergyPlus to calculate the energy loads and the outside surface temperatures. View factors between the points of interest (representing a standing mannequin) and the sky or surrounding surfaces are calculated using the raytracing capabilities of Rhino. View factors are further passed through a Python component dedicated to accounting for the absorbed sky longwave and solar shortwave radiation by a human body, following, respectively the equations of the MENEX (Błazejczyk) and SolarCal (ASHRAE, 2017a) models. The aggregate amount, together with the longwave radiation from surrounding surfaces constitute the MRT, which in turn is combined with the urban climatic data from UWG to estimate the outdoor thermal comfort. Ladybug components are used for the visualisation of environmental data and the results.

A full description of the equations governing the model can be found in Ibrahim *et al.* (2020a), where detailed graphical representations of the Grasshopper components used were shown by Evola *et al.* (2020). The workflow described above was validated against the ENVI-met software, which in turn was validated against field measurements in Cairo (Elnabawi *et al.*, 2013). The results showed considerable agreement between the two models in terms of the MRT and the Universal Thermal Climate Index (UTCI) with ($R^2 = 0.94$ and 0.96 respectively) over a whole day, and even more precise during daytime hours (Ibrahim *et al.*, 2020b). Furthermore, the workflow was validated with field measurements in a Mediterranean climate as well as a hot-arid climate similar to the current study, showing a good agreement with regards to both MRT and the Physiological Equivalent Temperature (PET) with $R^2 = 0.92$. This qualifies the workflow to be sufficiently appropriate for the purpose of this study.

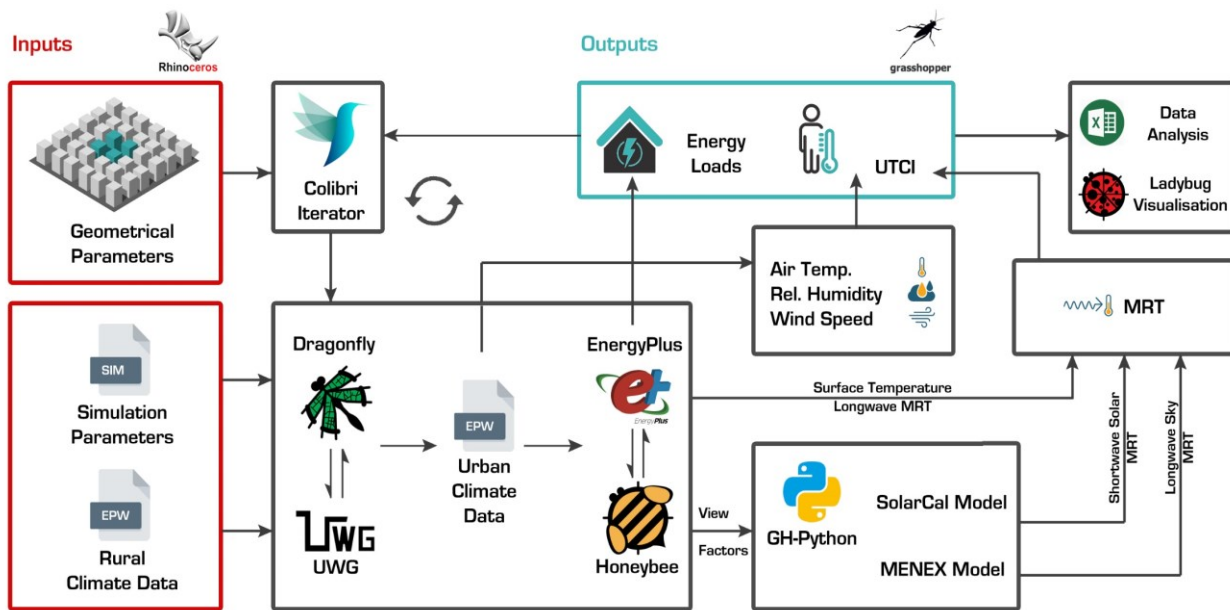


Figure 5.5: Simulation workflow showing the streaming of data between different Grasshopper components.

5.4.3 Performance Evaluation

In this study, the performance of different typologies and their corresponding morphological parameters are evaluated based on two environmental indicators, energy consumption and outdoor thermal comfort. Energy consumption is accounted for by the Energy Use Intensity (EUI) metric; the total energy loads due to cooling, heating, lighting and electric equipment normalised by the total floor area. Note that the courtyard form is exemplified here as a group of residential buildings, also known as a perimeter urban block, rather than a single courtyard building. This is accounted for by dividing the total EUI by the number of buildings in the typology to estimate the EUI in a single building, following (Taleghani *et al.*, 2013). The Universal Thermal Climate Index (UTCI) (Bröde *et al.*, 2012) was adopted to indicate outdoor thermal comfort for several reasons. UTCI has widely been applied across all climatic contexts and validated against field surveys and other thermal indices. Additionally, UTCI presents a detailed categorisation of thermal sensation for extreme cold and hot conditions, in which the equivalent temperature for sensation is provided in degrees Celsius, which makes it more perceptible by designers. On a grid size of 6 m, receptor points were distributed in and around each geometrical iteration (Figure 5.4-bottom), 1.1 m above ground level, to denote the thermal sensation of a standing person.

Outputs of the UTCI are recorded during daytime hours (5 am to 7 pm) and averaged across all the receptor points. UTCI results are further averaged across a typical hot month, July (see Section 5.4.5) to provide a basic value for comparison, while EUI results are presented as monthly aggregate.

5.4.4 Parameterisation

In each case, the analysed buildings were vertically subdivided into EnergyPlus thermal zones, respective to the number of building floors, where the surrounding blocks were defined as shading contexts, and the solar distribution module “Full interior and exterior with reflections” was used. An EnergyPlus thermal zone with no wind exposure nor internal loads was defined as a ground zone, where the upper surface represents the ground floor surface. Heat, Ventilation and Air Conditioning (HVAC), activities, schedules, as well as the thermal properties of construction materials were set following the study of Mahdy and Nikolopoulou (2014), based on the Egyptian Residential Energy Code (MHUUC, 2005). Cooling setpoint was set as the upper temperature bound calculated according to the adaptive comfort model by ASHRAE 55–2013 with 90% of occupants comfortable and using the weighted running mean temperature of the previous week in hybrid (air-conditioned/naturally ventilated) buildings, as a common practice for energy saving in energy modelling studies (Bienvenido-Huertas *et al.*, 2020). A fixed schedule for HVAC and occupation template (weekdays, working hours, etc.) was used in all scenarios, based on the common lifestyle of Egyptian residents (Mahdy & Nikolopoulou, 2014), where the default “EnergyPlus Ideal Air Loads” HVAC algorithm was used. Window-to-Wall ratios (WWRs) were set as 12% for Eastern and Western facades, 15.6% for Northern façades and 15% for Southern façades, according to the Egyptian Residential Energy Code (MHUUC, 2005). Table 5.3 lists the different simulation parameters as used in this study, while the physical and thermal properties of the construction materials can be found in Appendix A.

Based on a preliminary study by the authors, coupling the simulation workflow with OpenFOAM for CFD analyses using the wind factors method had minimal impact on the output UTCI. The sensitivity analysis of Natanian *et al.* (2020) using the same workflow in a hot desert climate confirmed our inference and showed the MRT to be the most dominant factor. Consequently, weather file 10 m-high wind speeds were converted into 2 m-high wind speeds and based on the wind profile power law by using a dedicated Ladybug component.

Table 5.3: Fixed simulation parameters used in the study.

Parameter		Value			
HVAC	Cooling setpoint	29°, otherwise natural ventilation is used			
	Schedule	All day			
Zone Loads	Equipment	4 W/m ²			
	People	0.04 People/m ²			
	Schedule	Weekdays: 00:00 (50%)-06:00 (75%)-08:00 (25%)-16:00 (75%)-18:00 (100%)-23:00 (75%)			
		Weekends: 00:00 (50%)-11:00 (75%)-21:00 (100%)-23:00 (75%)			
Lighting	3 W/m ²				
	Schedule	Weekdays: 00:00 (25%)-06:00 (40%)-08:00 (15%)-16:00 (40%)-18:00 (150%)-23:00 (40%)			
Weekends: 00:00 (50%)-11:00 (75%)-21:00 (100%)-23:00 (75%)					
Materials	Walls	Thickness	27 cm	U-Value	1.058 W/m ² K
	Roofs	Thickness	29 cm	U-Value	0.627 W/m ² K
	Floors	Thickness	20 cm		3.785 W/m ² K
	Windows (6 mm Clear)	SHGC	0.71	U-Value	5.76 W/m ² K
Infiltration		0.003 m ³ /s-m ²			

5.4.5 Climate Context

Egypt encompasses a diversity of climatic conditions, ranging from extreme hot to extreme cold conditions. However, it is generally categorised as a hot-desert climate (BWh), according to the Köppen Geiger classification. The climate is characterised by very high solar radiation intensity most of the year, with the highest average temperatures recorded in July and the lowest in January.

Figure 5.6 shows the highest average hourly air temperatures, direct normal radiation as well as cooling degree-days occurring in July. Accordingly, this study is conducted in July to represent the worst-case scenario. Cairo, the governorate of Egypt, is selected for this study since, in addition to the aforementioned reasons, it represents a typical hot-arid climate in Egypt, and also suffers from the UHI phenomenon. The International Weather for Energy Calculations (IWEC) weather file for Cairo was obtained from the official webpage of the U.S Department of Energy (DoE, 2020) and used as input for the simulation.

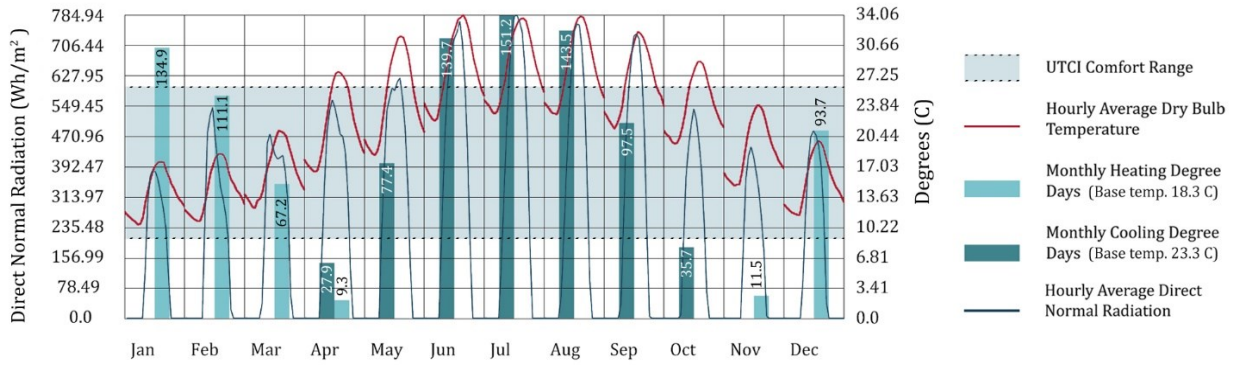


Figure 5.6: Average hourly air temperatures and direct normal radiation (lines) plotted against the UTCI comfort range and the monthly cooling and heating degree-days (bars) in Cairo. Calculated and graphically represented by Ladybug (Roudsari *et al.*, 2013).

5.5 Results and Discussion

In this section, the impact of typologies and their corresponding design parameters and density indicators on environmental performance is discussed. Design parameters are compared against 2 performance indicators, see section 5.4.3, as well as a combined fitness function that refers to the joint dimensionless quality of both the average UTCI (Av. UTCI) and EUI together. The lower the fitness value, the higher the environmental performance. The following formula was used after (Konis *et al.*, 2016) to represent the fitness function (y):

$$y = (\text{Av.UTCI}_i - \text{Av.UTCI}_{\min}) \cdot C_1 + (\text{EUI}_i - \text{EUI}_{\min}) \cdot C_2 \quad \text{Equation 5.1}$$

$$C_1 = \frac{100}{\text{Av.UTCI}_{\max} - \text{Av.UTCI}_{\min}}, \quad C_2 = \frac{100}{\text{EUI}_{\max} - \text{EUI}_{\min}}$$

where the subscripts (i) is the result of an iteration, (min) is the minimum value of all iterations, and (max) is the maximum value of all iterations. In order to present a perceptible interpretation for the fitness function as the percentage improvement over the lowest fitness, the following formula was used:

$$\text{Combined fitness} = \left(1 - \frac{y}{y_{\max}}\right) \times 100 \quad \text{Equation 5.2}$$

where (y_{\max}) is the worst fitness. The higher the combined fitness, the greater the improvement over the lowest fitness.

5.5.1 *Typology and Environmental Performance*

The performance of each typology varied across each of the fitness criteria. Figure 5.7 shows the frequency distribution for each performance criterion, recorded across the different typologies. In Figure 5.7-a, the courtyard and scattered forms shared higher percentages of the lowest Av.UTCI. Linear forms exceeded the other two typologies around mid-range Av.UTCI, while scattered forms shared with the latter most of the highest Av.UTCI. This indicates a tendency of courtyards to maintain lower Av.UTCI as opposed to linear forms with higher values. Scattered forms are more distributed along the whole range with a mean value similar to that of the whole sample of 32.2 °C. This is also confirmed in Figure 5.7-b, with courtyards possessing higher shares of lower maximum UTCI values recorded and the opposite for linear and scattered forms in mid and higher maxima. This implies that compact high-density scattered forms can perform as well as courtyards due to the shading they cast in both street directions. Figure 5.7-c shows the courtyards and linear forms sharing the lowest EUI due to the larger shades they pose on blocks' surfaces and lower percentage area of intermediate buildings' envelopes exposed to solar radiation, especially when facing cardinal directions, keeping the indoor temperatures lower, and accordingly with a lower EUI. Scattered forms dominated the highest EUI, and again with a mean value slightly above the whole sample of 46 kWh/m². A similar trend is noticed in Figure 5.7-d where scattered forms are two units below average, while linear and courtyards are one and four units, respectively, above the average combined fitness of 40. This comes in agreement with the study of Natanian and Auer (2020) in a hot Mediterranean climate.

5.5.2 *The Effect of Design Parameters*

A series of linear and multiple regression analyses were run to check for the interdependency and correlation between design and morphological parameters and the performance criteria. To avoid misleading regressions due to the definition of changing typologies based on the distance between buildings, the latter was replaced by the distance between blocks. Although the first set of regressions show a statistically significant correlation with combined fitness ($F(5, 3424) = 3032, p < 0.001, R^2 = 0.84$), they also exhibit multicollinearity, for instance between building heights and FAR, or distances and BCR. Consequently, density parameters' regressions were made separately.

A strong correlation was found between both Av. UTCI and EUI and the design parameters' model with $R^2 = 0.73$ and 0.97 , respectively, albeit with weak to moderate individual correlations (Table 5.4). As a single orientation comprises a variety of other design parameters, it exhibited insignificant correlations ($p > 0.05$) in different analyses, although the effect of orientation is well pronounced as discussed in the next section.

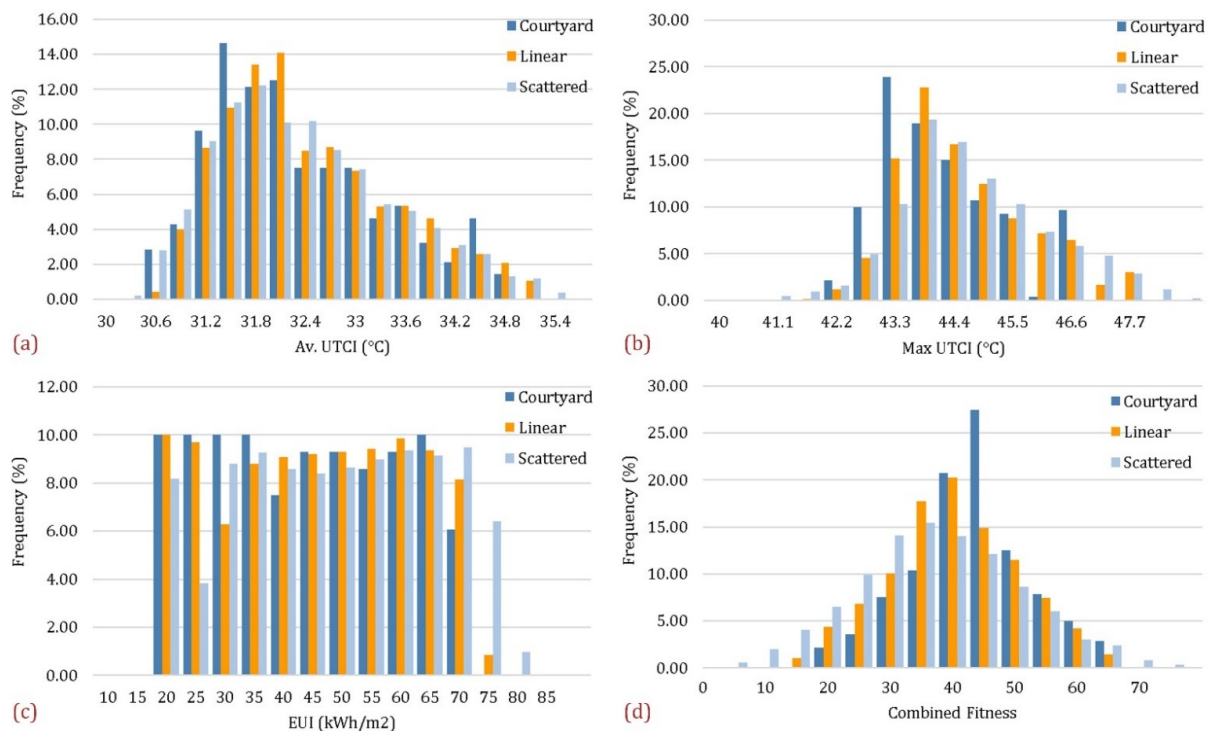


Figure 5.7: Frequency distribution of (a) Av.UTCI, (b) max UTCI, (c) EUI, and (d) combined fitness, over the three typologies.

Table 5.4: Correlation coefficients (R) between design parameters and performance criteria. The strongest correlations are highlighted.

Criterion	Dist. Blocks (EW)	Dist. Blocks (NS)	Heights	Orientation
Av. UTCI	0.2282	0.2103	-0.7990	0.0079
EUI	-0.0156	-0.0166	0.9874	0.0079
Comb. fitness	-0.2580	-0.2341	-0.5875	-0.0092

5.5.2.1 Orientation

With solar altitude reaching as high as 83° in July, NS streets are shaded during the morning and late afternoon, while being fully exposed to higher solar radiation intensities at noon. EW streets are exposed during almost all daytime hours with minimal shading at noon due to the high solar altitude. This makes ordinal orientations preferred for lower Av.UTCI as they provide shading in both directions

as shown in Figure 5.8-a. Courtyards tend to exhibit slightly lower Av.UTCI than scattered forms, while both appear to be lower than linear forms. On the other hand, EW-facing building walls (NS streets) tend to be more exposed to solar radiation than NS-facing walls. Again, courtyards and linear elongated built forms have higher mutual or courtyard self-shading between building walls. This is clear in Figure 5.8-b, where courtyards and linear forms appear to have less EUI than scattered forms. Although cardinal orientations entail less EUI than ordinal ones, the variations are more pronounced due to changing typology. On aggregate, as in Figure 5.8-c, courtyards with intermediate orientations appear to be favoured, followed by linear and then scattered forms. This makes orientation alone responsible for almost 15% and 10% difference in Av.UTCI and EUI, respectively. Vartholomaios (2017) reported that orientation and surface-to-volume ratio exerted the greatest influence on annual energy loads in a Mediterranean climate. Our results come into agreement with studies in temperate climates with regards to EUI (Taleghani *et al.*, 2013; Allegrini *et al.*, 2016), as well as in a hot-arid climate with regards to thermal comfort (Galal *et al.*, 2020).

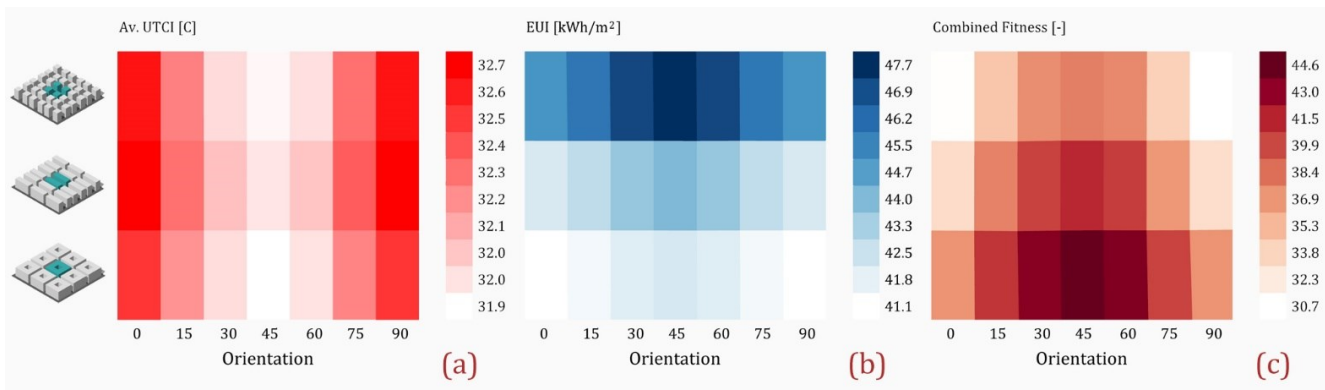


Figure 5.8: Performance evaluation of the three typologies in different orientations in terms of (a) AV.UTCI, (b) EUI, and (c) combined fitness.

5.5.2.2 Distance between Buildings

The effect of the distance between buildings on the EW axis is similar to that on the NS axis. Accordingly, EW distances were plotted against different orientations in Figure 5.9 to highlight their impact on the performance of each typology. It should be noted that a single EW distance comprises the average of all other NS distances. This is exemplified in linear forms, where distances 21 and 24 represent linear EW canyons with different (NS) street widths (6–18 m) and vice versa. It can clearly be noticed that increasing distances entails higher Av.UTCI and

EUI, due to the lack of shading on streets and building walls Figure 5.9-a. The effect of orientation overpasses that of the distances, where NS canyons orientated 90° (into EW) with 18 m distances are shown to maintain higher Av.UTCI, while the lowest Av.UTCI were recorded in scattered and linear forms orientated 45° and 6 m apart. The effect also applies to the EUI with a constant increase in cooling energy as the distances increase and the shading on building walls decreases. Figure 5.9-b shows courtyards, linear NS with minimum distances or linear EW canyons to have yielded the lowest EUI. It also reveals that NS canyons can be as energy efficient as EW canyons if streets are kept 6 m wide. This is useful in cases where both outdoor thermal comfort and energy efficiency are of equal priority in the design process. As it might seem, however, with regards to the combined fitness (Figure 5.9-c) that linear and scattered forms with 6 m streets (3 m alleys between blocks) are the most favourable, these arrangements are not always achievable from a practical point of view.

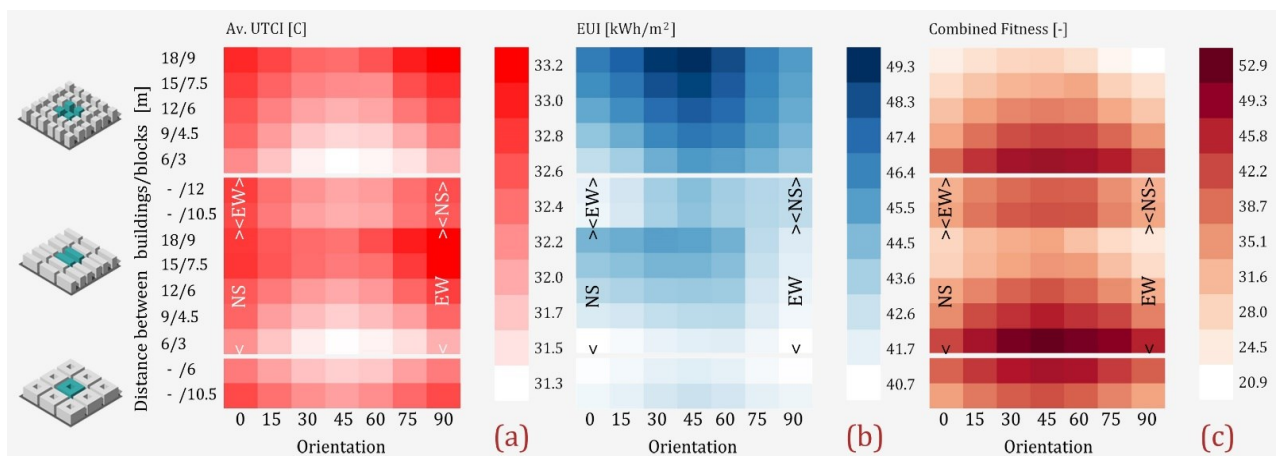


Figure 5.9: Distances between buildings/blocks on the East–West axis across different orientations (shown as deviation from starting position), plotted against the performance indicators, (a) AV.UTCI, (b) EUI, and (c) combined fitness. A single EW distance comprises the average of all other North–South distances.

5.5.2.3 Building Heights

Buildings' heights are shown to have the strongest correlation with thermal and energy performance. Figure 5.10 shows the trendlines indicating the variations in performance as building heights change. The effect of changing building heights appears to be more significant than changing the typology. In Figure 5.10-a, As building heights increase, Av.UTCI decreases by 2.5 °C, due to improved shading, thereby improving thermal comfort.

The relationship, however, between the Av.UTCI and building heights is polynomial, and so is the relationship with FAR as discussed in the next section, indicating a near-constant Av.UTCI above a certain height (33 m in this study), after which the streets become fully shaded and do not benefit from any further increase in building heights. Differences between typologies seem to be negligible, showing the courtyards slightly lower in Av.UTCI. Conversely, taller buildings with larger floor spaces resulted in higher EUIs, increasing by as much as 50 kWh/m² (Figure 5.10-b). The impact of changing the heights is more significant on EUI than on Av.UTCI, and so are the variations between typologies. This is well explained by the linear relationship between EUI and the building heights. The effect is more pronounced in the combined fitness with larger differences between taller buildings (Figure 5.10-c). On aggregate, the overall fitness improves with increasing building heights until the effect of shading becomes marginal (height 24 m) and then declines due to higher EUI. Similar inferences were reported by Martins *et al.* (2016) in hot-humid conditions, who concluded that albedo, H/W ratio and distance between buildings account for almost 80% of the variation in solar radiation exposure.

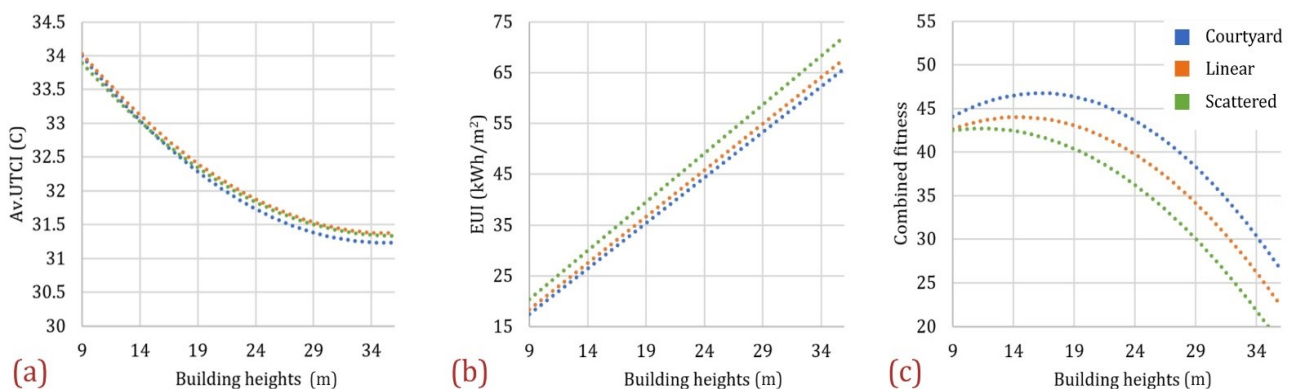


Figure 5.10: Trendlines of heights-based performance for the three typologies in terms of (a) AV.UTCI, (b) EUI, and (c) combined fitness.

5.5.3 The Effect of Density

A multi-regression analysis of density parameters, i.e., FAR and BCR, has revealed a significant correlation with performance indicators, such that 70% and 95% of the variation of Av.UTCI and EUI, respectively, can be explained by FAR and BCR together. However, BCR showed an insignificant *p*-value against Av.UTCI (*p* = 0.06). Simple linear regression analyses have shown that BCR has moderate correlations with Av.UTCI, while EUI and Av.UTCI, as anticipated following the

effect of building heights, are strongly dependent on FAR (Table 5.5). A 2nd order polynomial regression shows a stronger correlation with Av.UTCI (Figure 5.11), showing marginal reductions in Av.UTCI within the highest FARs. Furthermore, the correlation between FAR and the combined fitness was higher for a single building height (15 m) with $R = 0.74$, and for a single distance (9 m) with $R = 0.92$. This indicates that, although FAR exhibits a strong impact on both AV.UTCI and EUI, it cannot be used alone as an indicator for density, yet rather have to be associated with the horizontal density (compactness) parameters as shown below.

Table 5.5: Correlation coefficients (R) between density parameters and performance Criteria. The strongest correlations are highlighted.

Criterion	BCR	FAR
Av. UTCI	-0.3058	-0.8385
EUI	-0.1329	0.8434
Combined fitness	0.5918	-0.3084

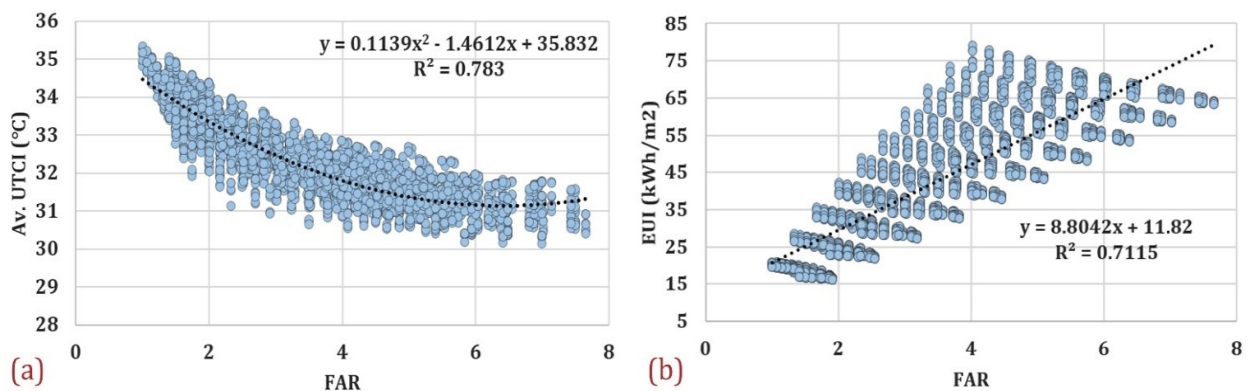


Figure 5.11: Relationship between FAR and (a) Av.UTCI, and (b) EUI.

Intriguingly, the categorisation of FAR into BCRs has shown distinct insights. Figure 5.12 shows the relationship between the performance indicators and FAR in each BCR. Fitness values were averaged for each FAR, e.g., $1 \leq \text{FAR} < 2$, and then averaged for each BCR, e.g., $0.3 \leq \text{BCR} < 0.35$. As FAR increases as high as 3, shading over ground increases and brings about lower Av.UTCI. As it continues to increase, the amount of longwave radiation from building walls increases and causes the Av.UTCI to rise up to a limit (FAR = 5), after which the effect of overshadowing surpasses that of the longwave heat exchange and lower Av.UTCI values ensue (Figure 5.12-a). Conversely, the first few increments in FAR induce higher EUI, followed by a decline due to shading over building walls and then a constant increase as of FAR = 4 (Figure 5.12-b).

Quan *et al.* (2014) found similar trends in their analysis of annual energy loads in a mixed humid climate. It can also be noticed that, for a constant FAR, higher BCR results in 1.5 °C lower Av.UTCI on average and up to 10 kWh/m² lower EUI. Wei *et al.* (2016) recommended similar configurations for lower ambient and radiant temperatures when they performed a cross-evaluation of FAR and BCR in a humid subtropical climate. Moreover, in a similar hot-arid climate, Krüger *et al.* (2010) reported that for a constant FAR, increasing H/W (thereby increasing BCR) does reduce cooling demand when they investigated 32 hypothetical cases from January to August. Again, where both lower Av.UTCI and EUI are acquired, a combined fitness would qualify a compact (BCR ≥ 60%), medium-density (2 ≤ FAR < 4) configuration to be the best trade-off (Figure 5.12 c).

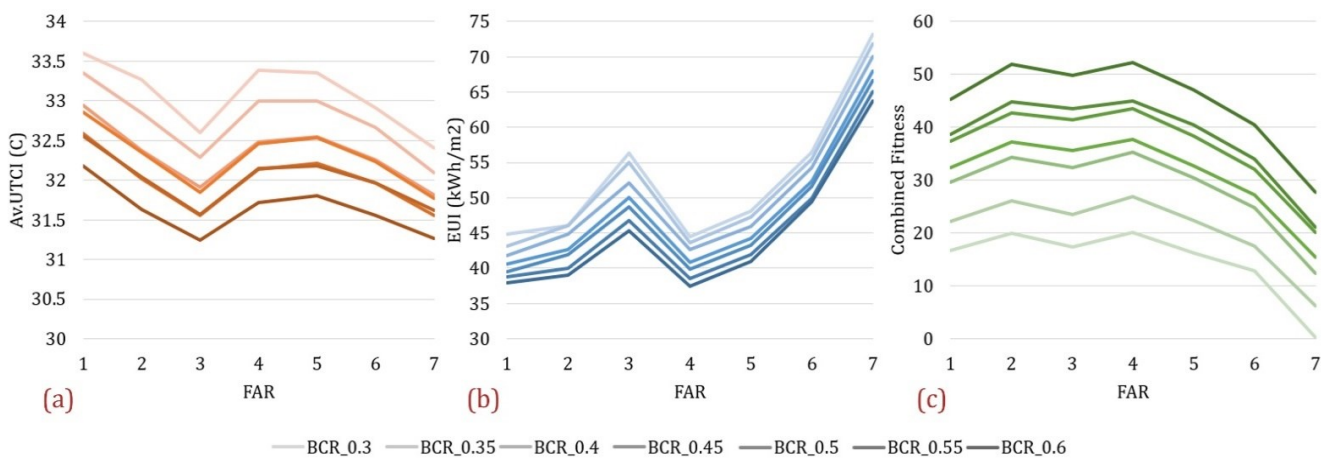


Figure 5.12: Relationship between FAR, BCR and performance indicators, (a) Av.UTCI, (b) EUI, and (c) combined fitness.

5.6 Selective Cases and Urban Design Implications

Using Core Studio Design explorer ("Core Studio, Design Explorer," 2021), a web-based design exploration interface, we were able to visualise the multivariate relationship between all the design parameters and the fitness criteria. As shown previously, some typologies outperformed the others with regards to a specific fitness criterion, for instance, the scattered in Av.UTCI and the courtyards in EUI. Accordingly, in Figure 5.13–15, the best performing case within each typology is selected, rather than the optimum cases. Each column of these figures represents a different parameter used in the optimisation. The first (leftmost) six columns plot the values of the six input parameters, and the last (rightmost) two plot the values of the output being measured. Each line running left to right plots the values for an

individual geometric case being analysed. On each figure, the lines representing the best performing courtyard, linear and scattered form for the output being studied are coloured in blue, green and red, respectively. Distances in these figures refer to the distance between buildings rather than blocks. For instance, linear forms with an NS distance of 21 m have an NS distance between blocks of 10.5 m. Courtyards with distances of 24 m have a 6 m distance between blocks in both directions (see sections 5.4.1 and 5.5.2.2). Figure 5.13 depicts the optimum configurations required to achieve the lowest Av.UTCI, where the selected cases confirm the results obtained regarding each design parameter. Compact and highly dense scattered forms orientated 45° appear to possess the lowest Av.UTCI. In fact, these configurations might not seem applicable in practice in Egypt, although they are extensively found in North African countries with similar climates, such as Morocco (Johansson, 2006) and Algeria (Bourbia & Boucheriba, 2010). Figure 5.13 also shows a variety of design thresholds that can deliver a moderate heat stress Av.UTCI of <32 °C; building heights ≥ 21; BCR ≥ 50% and; FAR ≥ 4, preferably orientated between 30 and 60°.

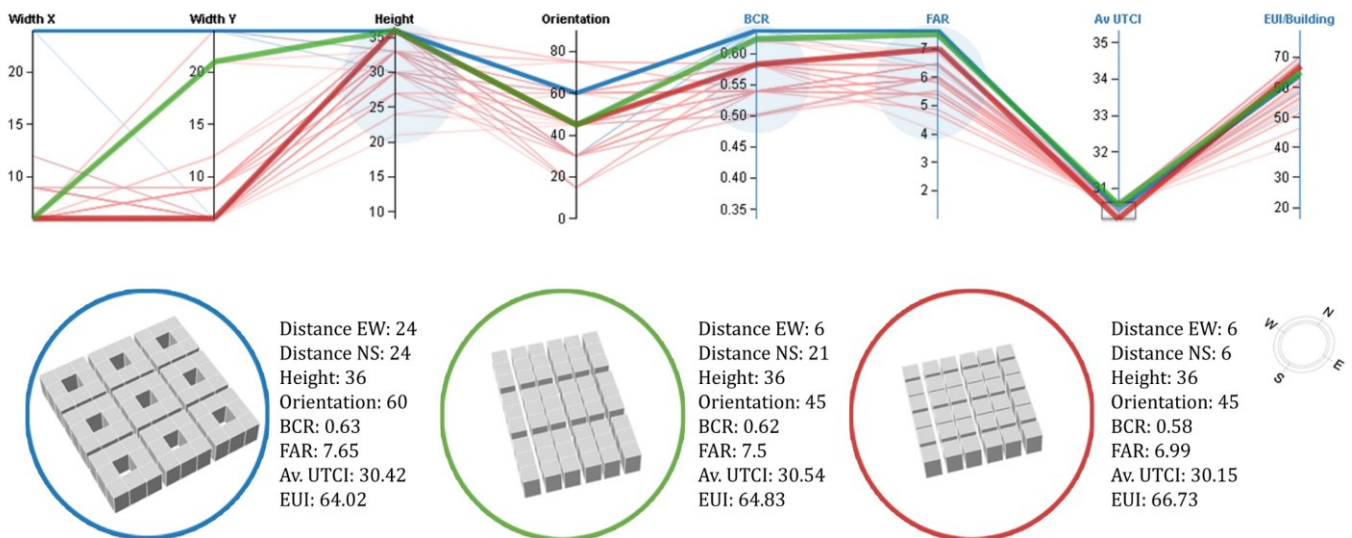


Figure 5.13: Parallel coordinates showing the selective cases for the minimum Av.UTCI.

In Figure 5.14, the three best performing typologies share approximate design parameters to attain EUI lower than ~32 kWh/m² which is only ~40% of the highest consumption recorded. Courtyards and linear forms dominated the objective space for EUI; however, the common features of low energy urban forms are the same in all typologies; higher BCR and lower FAR are the most predominant (Section 5.5.3), followed by orientating blocks to the South.

Despite the large number of design parameters that bring forth the lowest 40% EUI, cases with lower building heights and BCR bring about higher AV.UTCI due to the lack of shadowing on streets.

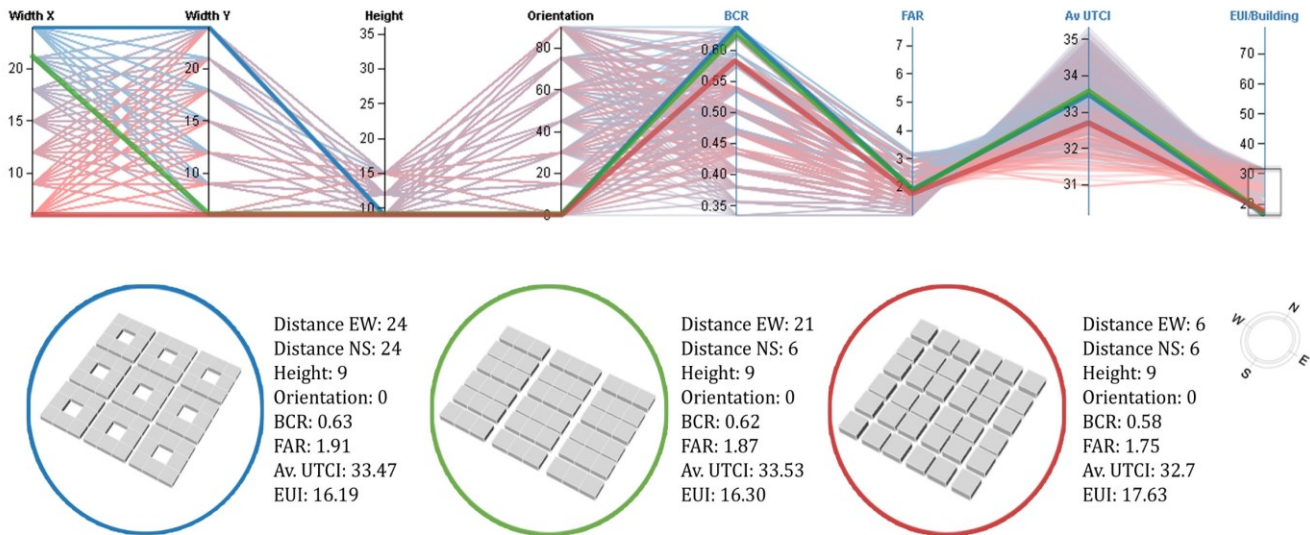


Figure 5.14: Parallel coordinates showing the selective cases for the minimum EUI.

Our results are partially congruent with the recommendations of Olgyay in (Taleghani *et al.*, 2013) and Dekay and Brown in (Vartholomaios, 2017) for hot-arid regions. The latter, however, recommended designing for wide EW streets to allow for winter sun but narrow NS streets to maximise shading. Such street configurations in extreme hot conditions as in Egypt will bring about intolerable heat stress in summer.

Figure 5.15 depicts the optimum case in each typology achieving moderate heat stress AV.UTCI of <32 as well as the lowest 40% EUI. The optimum cases tend to have lower building heights ≤ 15 , and FAR below ~ 3.3 and higher BCR $\geq 50\%$. Under these configurations, orientation does not seem to have a strong impact on the overall performance of courtyards and scattered forms, whereas the shading potential of linear forms remains a function of street orientation (also see Section 5.5.2.1).

Our results support the recommendation of Galal *et al.* (2020) for designing perimeter blocks in ordinal directions for best thermal conditions. They are shown here as candidates for the best overall performance. For online access to the data analysis and visualisation on Design Explorer, see Supplementary Materials.

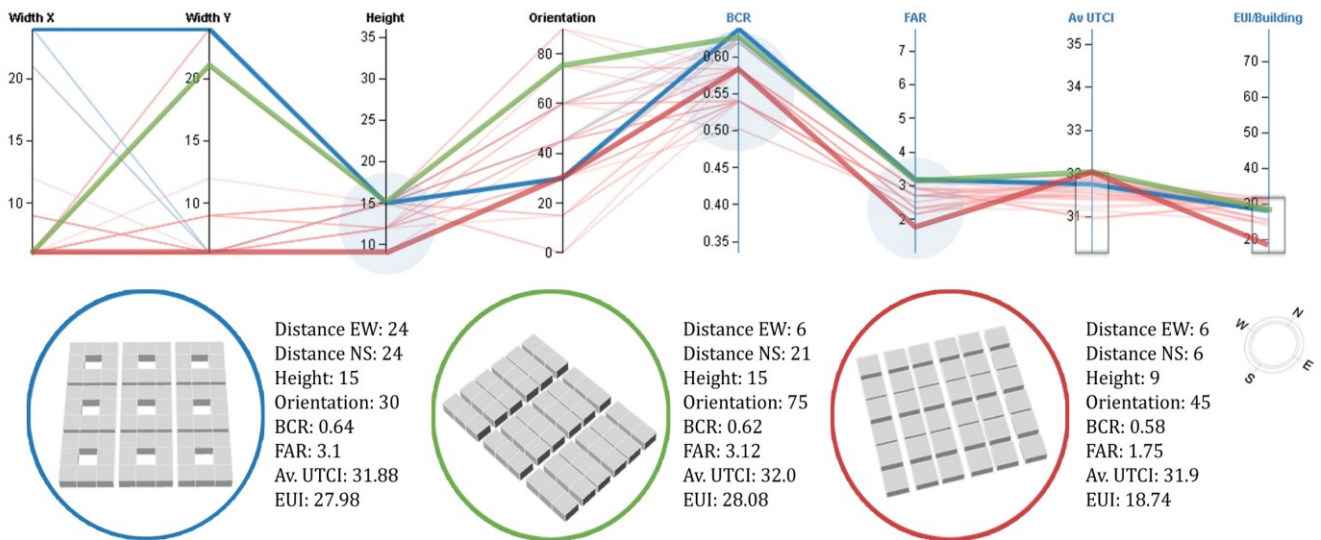


Figure 5.15: Selective cases for moderate heat stress Av.UTCI and the lowest 40% EUI.

Based on the results and implications presented above, Table 5.6 lists the optimum design thresholds in each typology that can be interpreted as design guidelines towards achieving pedestrian-friendly but also resource-efficient urban built environments which conform to the sustainable development goals.

Table 5.6: Design recommendations for the optimum design thresholds in each typology.

Typology	Configuration				
	St. Widths	Heights	Orientation	BCR	FAR
Courtyard	<10 m	<15 m	30–60°	≥60%	2–4
Linear	NS 12–18 m EW 6–9 m	<15 m	0–30°	≥60%	2–3
Scattered	6–8 m	<9 m	45°	≥50%	1–2

5.7 Conclusions

This study harnessed the capabilities of the Ladybug tools simulation workflow via Grasshopper/Rhino3D to highlight the relationship between urban form design parameters and energy performance together with outdoor thermal comfort in summer, in the hot-arid climate of Cairo, Egypt. The workflow was capable of assessing the multi-aspect performance of various typological and morphological configurations. Presenting such results using open-source simulation engines is just one of the many reasons which qualify this workflow to be widely applicable in practice. Another reason is the possibility of extending this methodology by linking the current workflow with multi-objective evolutionary algorithms, allowing for the investigation of complicated parametric combinations.

The results presented here are for the hot-arid climate of Cairo, Egypt, however, the methodology used in this study can easily be applied to other climatic contexts. It is anticipated that the optimum geometric forms will vary with location and background climatic conditions. For instance, scattered forms might be a better trade-off in hot-humid areas, where ventilation is most needed (Golany, 1996). Moreover, the scalability of this workflow is associated with exponential computation time, depending on the spatial resolution of the area investigated. This study was limited by using uniform building heights over the whole quarter, however, while simulating each building height independently may result in more rigorous performative insights, under the same number of parameters examined in this study, it would result in billions of parametric combinations that even evolutionary algorithms would find unwieldy to be solved, also known as the “curse of dimensionality” (Vartholomaios, 2017).

Our results have shown a statistically significant correlation between the design parameters and the performance indicators, Av. UTCI and EUI, such that 70% and 95% of the variations in each respective metric can be explained by the density parameters, FAR and BCR. The design parameters exhibited such impacts on the different typologies that seemed similar in nature, but disparate in magnitude. Compact and dense scattered forms were shown to be as good as (or slightly better than) courtyard typologies, outperforming linear configurations when accounting for outdoor thermal comfort. On the other hand, courtyards and linear forms surpassed the scattered forms regarding their energy performance owing to their ability to deliver adequate self and mutual shading to the building walls. Moreover, it was shown that orientation possesses a decisive impact on the overall performance, but also that their impact on typological differences is less absolute. From an environmental and practical point of view, compact ($BCR \geq 60\%$) and medium-density ($4 \geq FAR > 2$) courtyards orientated 45° , not only offer a satisfying thermal versus energy performance trade-off, but also exhibit a greater potential for achieving net-zero energy urban communities. The results of this study present performance-driven insights in the pre-design process to urban planners, designers and stakeholders aiming to create healthy, liveable and resource-efficient urban communities now, but will also increase the resilience of urban environments to the increasing temperatures projected as a result of climatic change.

Future work will include integrating the workflow with multi-objective evolutionary algorithms to investigate the impact of non-uniform building densities on the overall performance. This should include minimising the number of design parameters to a limit, below which the complexity of the search space can be appropriately managed.

Supplementary Materials

The following are available online at <https://researchdata.bath.ac.uk/1021>, Video S1: Iteration of different typologies based on the distance between buildings. Video S2: Simulation sample showing the calculation of performance indicators for different cases (Ibrahim, 2021b). Access to the data visualisation on design explorer at:

http://tt-acm.github.io/DesignExplorer/?ID=BL_3o1ZHVX (27 May, 2021).

Data Availability Statement

Data available in a publicly accessible repository; The data presented in this study are openly available in [University of Bath Research Data Archive] at [<https://doi.org/10.15125/BATH-01021>] (Ibrahim, 2021b).

Appendix A

Table A. 1: Thermal and Physical properties of the construction materials used in the study.

Construction	Thickness (cm)	U-Value (W/m ² K)	Material-outer to Inner face ↓	Thickness (cm)	Density (kg/m ³)	Thermal Conductivity (W/m.K)	Specific Heat (J/kg.K)	Thermal Resistance (m ² K/W)
Full red-brick wall with expanded polystyrene insulation	32	1.058	Plaster	0.5	600	0.16	1000	0.031
			Mortar	2	1570	0.9	896	0.022
			polystyrene	2	35	0.034	1400	0.588
			Full Brick	25	1950	1	829	0.25
			Mortar	2	1570	0.9	896	0.022
			Plaster	0.5	600	0.16	1000	0.031
Standard reinforced concrete roof	29	0.627	Tiles	1	2100	1.4	1000	0.007
			Mortar	2	1570	0.9	896	0.022
			Sand	5	1520	0.33	800	0.152
			Polystyrene	4	35	0.034	1400	1.176
			Damp proof	2	1055	0.15	1000	1.333
			R. concrete	15	2460	1.44	1000	0.104
Standard reinforced concrete floor	20	3.785	Tiles	1	2100	1.4	1000	0.007
			Mortar	2	1570	0.9	896	0.022
			Sand	5	1520	0.33	800	0.152
			R. concrete	12	2460	1.44	1000	0.083
Clear Glass	Thickness: 0.6		U-value: 5.76		SHGC: 0.71		Transmissivity: 0.65	

5.8 References

- Ali-Toudert, F. (2005). Dependence of Outdoor Thermal Comfort on Street Design in Hot and Dry Climate. (PhD). Institutes der Universität Freiburg, Freiburg, Germany. (15)
- Ali-Toudert, F., Djenane, M., Bensalem, R., & Mayer, H. (2005). Outdoor thermal comfort in the old desert city of Beni-Isguen, Algeria. *Climate Research*, 28(3), 243-256. doi: <http://doi.org/10.3354/cr028243>.
- Allegrini, J., Dorer, V., & Carmeliet, J. (2015). Influence of morphologies on the microclimate in urban neighbourhoods. *Journal of Wind Engineering and Industrial Aerodynamics*, 144, 108-117. doi: <https://doi.org/10.1016/j.jweia.2015.03.024>.
- Allegrini, J., Dorer, V., & Carmeliet, J. (2016). Impact of radiation exchange between buildings in urban street canyons on space cooling demands of buildings. *Energy and Buildings*, 127, 1074-1084. doi: <http://dx.doi.org/10.1016/j.enbuild.2016.06.073>.
- ASHRAE. (2017). ANSI/ASHRAE Standard 55-2017: Thermal environmental conditions for human occupancy. In (pp. 22-29). Atlanta, GA: American Society of Heating, Refrigerating and Air-Conditioning Engineers, .
- Attia, S., Evrard, A., & Gratia, E. (2012). Development of benchmark models for the Egyptian residential buildings sector. *Applied Energy*, 94, 270-284. doi: <https://doi.org/10.1016/j.apenergy.2012.01.065>.
- Bienvenido-Huertas, D., Sánchez-García, D., Pérez-Fargallo, A., & Rubio-Bellido, C. (2020). Optimization of energy saving with adaptive setpoint temperatures by calculating the prevailing mean outdoor air temperature. *Building and Environment*, 170(106612). doi: <https://doi.org/10.1016/j.buildenv.2019.106612>.
- Blazejczyk, K. MENEX: the man-environment heat exchange model and its applications in bioclimatology. In *Proceedings of The Fifth International Conference on Environmental Ergonomics*.
- Bourbia, F., & Awbi, H. B. (2004). Building cluster and shading in urban canyon for hot dry climate Part 2: Shading simulations *Renewable energy*, 29(2), 291-301 doi: [https://doi.org/10.1016/S0960-1481\(03\)00171-X](https://doi.org/10.1016/S0960-1481(03)00171-X).
- Bourbia, F., & Boucheriba, F. (2010). Impact of street design on urban microclimate for semi arid climate (Constantine). *Renewable energy*, 35(2), 343-347. doi: <https://doi.org/10.1016/j.renene.2009.07.017>.
- Bröde, P., Fiala, D., Błażejczyk, K., Holmér, I., Jendritzky, G., Kampmann, B., Tinz, B., & Havenith, G. (2012). Deriving the operational procedure for the Universal Thermal Climate Index (UTCI). *International journal of biometeorology*, 56(3), 481-494. doi: <https://doi.org/10.1007/s00484-011-0454-1>.
- Bruse, M. (2020). ENVI-met. Retrieved from <https://www.envi-met.com/>
- Bueno, B., Norford, L., Hidalgo, J., & Pigeon, G. (2013). The urban weather generator. *Journal of Building Performance Simulation*, 6(4), 269-281. doi: <https://doi.org/10.1080/19401493.2012.718797>.
- Bueno, B., Roth, M., Norford, L., & Li, R. (2014). Computationally efficient prediction of canopy level urban air temperature at the neighbourhood scale. *Urban Climate*, 9, 35-53. doi: <http://dx.doi.org/10.1016/j.uclim.2014.05.005>.

- CAPMAS. (2019). Bulletin of Housing in Egypt. (71-21123-2019). Cairo, Egypt: Central Agency for Public Mobilization & Statistics Retrieved from https://www.capmas.gov.eg/Pages/Publications.aspx?page_id=5104&Year=23415
- Chatzidimitriou, A., & Yannas, S. (2017). Street canyon design and improvement potential for urban open spaces; the influence of canyon aspect ratio and orientation on microclimate and outdoor comfort. *Sustainable Cities and Society*, 33, 85-101. doi: <https://doi.org/10.1016/j.scs.2017.05.019>.
- Cities, L. (2014). *Cities and Energy: Urban Morphology and Heat Energy Demand*. London, UK Core Studio, Design Explorer. (2021). Retrieved from <http://tt-acm.github.io/DesignExplorer/>
- Crawley, D. B., Lawrie, L. K., Winkelmann, F. C., Buhl, W. F., Huang, Y. J., Pedersen, C. O., Strand, R. K., Liesen, R. J., Fisher, D. E., & Witte, M. J. (2001). EnergyPlus: creating a new-generation building energy simulation program. *Energy and Buildings*, 33(4), 319-331. doi: [https://doi.org/10.1016/S0378-7788\(00\)00114-6](https://doi.org/10.1016/S0378-7788(00)00114-6).
- DoE. (2020). Weather Data. Retrieved from <https://energyplus.net/weather>
- Elnabawi, M. H., Hamza, N., & Dudek, S. (2013). Use and evaluation of the ENVI-met model for two different urban forms in Cairo, Egypt: measurements and model simulations. In *13th Conference of International Building Performance Simulation Association, Chambéry, France*.
- Elnahas, M. (2003). The effects of urban configuration on urban air temperatures. *Architectural Science Review*, 46(2), 135-138. doi: <https://doi.org/10.1080/00038628.2003.9696975>.
- Evola, G., Costanzo, V., Magri, C., Margani, G., Marletta, L., & Naboni, E. (2020). A novel comprehensive workflow for modelling outdoor thermal comfort and energy demand in urban canyons: results and critical issues. *Energy and Buildings*, 216(109946), 1-19. doi: <https://doi.org/10.1016/j.enbuild.2020.109946>.
- Fahmy, M. (2010). Interactive urban form design of local climate scale in hot semi-arid zone. (PhD). The University of Sheffield,
- Fletcher, J. A., Kershaw, T., & Mills, G. (2013). Urban form and function as building performance parameters. *Building and Environment*, 62, 112-123. doi: <https://doi.org/10.1016/j.buildenv.2013.01.021>.
- Galal, O. M., Sailor, D. J., & Mahmoud, H. (2020). The impact of urban form on outdoor thermal comfort in hot arid environments during daylight hours, case study: New Aswan. *Building and Environment*, 184(107222), 1-15. doi: <https://doi.org/10.1016/j.buildenv.2020.107222>.
- Giannopoulou, K., Santamouris, M., Livada, I., Georgakis, C., & Caouris, Y. (2010). The impact of canyon geometry on intra urban and urban: suburban night temperature differences under warm weather conditions. *Pure and applied geophysics*, 167(11), 1433-1449. doi: <https://doi.org/10.1007/s00024-010-0099-8>.
- Golany, G. S. (1996). Urban design morphology and thermal performance. *Atmospheric Environment*, 30(3), 455-465. doi: [https://doi.org/10.1016/1352-2310\(95\)00266-9](https://doi.org/10.1016/1352-2310(95)00266-9).
- Gupta, V. (1987). Thermal efficiency of building clusters: an index for non air-conditioned buildings in hot climates. In D. Hawkes, J. Owers, P. Rickaby, & P. Steadman (Eds.), *Energy and urban built form* (pp. 133-145). London: Butterworths.
- Gupta, V. K. (1984). Solar radiation and urban design for hot climates. *Environment and Planning B: Planning and Design*, 11(4), 435-454.

-
- Holmer, B. (1992). A simple operative method for determination of sky view factors in complex urban canyons from fisheye photographs. *Meteorologische Zeitschrift*, 1(5), 236-239.
- Ibrahim, Y. (2021). Dataset for "On the optimisation of urban form design, energy consumption and outdoor thermal comfort using a parametric workflow in a hot arid zone". Retrieved from: <https://researchdata.bath.ac.uk/1021/>
- Ibrahim, Y., Kershaw, T., & Shepherd, P. (2020a). Improvement of the Ladybug-tools microclimate workflow: A verification study. In *Building Simulation and Optimization 2020*, Loughborough University, Loughborough, UK.
- Ibrahim, Y., Kershaw, T., & Shepherd, P. (2020b). A methodology For Modelling Microclimate: A Ladybug-tools and ENVI-met Verification Study. In *35th PLEA Conference. Sustainable Architecture and Urban Design: Planning Post Carbon Cities*, A Coruña, Spain, 1-3 September.
- Ibrahim, Y., Kershaw, T., Shepherd, P., & Elwy, I. (2021). A parametric optimisation study of urban geometry design to assess outdoor thermal comfort. *Sustainable Cities and Society*, 75(103352), 1-18. doi: <https://doi.org/10.1016/j.scs.2021.103352>.
- IEA. (2020). Energy technology perspectives 2020. OECD Publishing. Paris, France
- IEA, International Energy Agency. (2021). IEA Energy Atlas. Retrieved from <http://energyatlas.iea.org>
- Jamei, E., Rajagopalan, P., Seyedmahmoudian, M., & Jamei, Y. (2016). Review on the impact of urban geometry and pedestrian level greening on outdoor thermal comfort. *Renewable and Sustainable Energy Reviews*, 54, 1002-1017. doi: <http://dx.doi.org/10.1016/j.rser.2015.10.104>.
- Javanroodi, K., Mahdavejad, M., & Nik, V. M. (2018). Impacts of urban morphology on reducing cooling load and increasing ventilation potential in hot-arid climate. *Applied Energy*, 231, 714-746. doi: <https://doi.org/10.1016/j.apenergy.2018.09.116>.
- Jin, H., Cui, P., Wong, N. H., & Ignatius, M. (2018). Assessing the effects of urban morphology parameters on microclimate in Singapore to control the urban heat island effect. *Sustainability*, 10(206), 1-18. doi: <https://doi.org/10.3390/su10010206>.
- Johansson, E. (2006). Influence of urban geometry on outdoor thermal comfort in a hot dry climate: A study in Fez, Morocco. *Building and Environment*, 41(10), 1326-1338. doi: <https://doi.org/10.1016/j.buildenv.2005.05.022>.
- Johansson, E., & Emmanuel, R. (2006). The influence of urban design on outdoor thermal comfort in the hot, humid city of Colombo, Sri Lanka. *International journal of biometeorology*, 51(2), 119-133. doi: <http://dx.doi.org/10.1007/s00484-006-0047-6>.
- Konis, K., Gamas, A., & Kensek, K. (2016). Passive performance and building form: An optimization framework for early-stage design support. *Solar Energy*, 125, 161-179. doi: <https://doi.org/10.1016/j.solener.2015.12.020>.
- Krüger, E., Pearlmutter, D., & Rasia, F. (2010). Evaluating the impact of canyon geometry and orientation on cooling loads in a high-mass building in a hot dry environment. *Applied Energy*, 87(6), 2068-2078. doi: <https://doi.org/10.1016/j.apenergy.2009.11.034>.
- Mahdy, M. M. (2014). Applying architecture simulation tools to assess building sustainable design: Adapting the Egyptian residential energy code for climate change. (PhD). University of Kent, Retrieved from <https://books.google.co.uk/books?id=2mDjvgEACAAJ>
- Mahdy, M. M., & Nikolopoulou, M. (2014). Evaluation of fenestration specifications in Egypt in terms of energy consumption and long term cost-effectiveness. *Energy and Buildings*, 69, 329-343. doi: <http://dx.doi.org/10.1016/j.enbuild.2013.11.028>.

- Mahmoud, H., Ghanem, H., & Sodoudi, S. (2021). Urban geometry as an adaptation strategy to improve the outdoor thermal performance in hot arid regions: Aswan University as a case study. *Sustainable Cities and Society*, 71(102965). doi: <https://doi.org/10.1016/j.scs.2021.102965>.
- March, L., & Martin, L. (1972). *Urban space and structures*. Cambridge, UK: University Press Cambridge.
- Martins, T., Adolphe, L., Bastos, L., & Martins, A. (2016). Sensitivity analysis of urban morphology factors regarding solar energy potential of buildings in a Brazilian tropical context. *Solar Energy*, 137, 11-24. doi: <http://dx.doi.org/10.1016/j.solener.2016.07.053>.
- Matzarakis, A., Rutz, F., & Mayer, H. (2007). Modelling radiation fluxes in simple and complex environments—application of the RayMan model. *International journal of biometeorology*, 51(4), 323-334. doi: <https://doi.org/10.1007/s00484-006-0061-8>.
- McNeel, R. (2021). Rhinoceros 3D. Retrieved from <https://www.rhino3d.com/>
- McRae, I., Freedman, F., Rivera, A., Li, X., Dou, J., Cruz, I., Ren, C., Dronova, I., Fraker, H., & Bornstein, R. (2020). Integration of the WUDAPT, WRF, and ENVI-met models to simulate extreme daytime temperature mitigation strategies in San Jose, California. *Building and Environment*, 184(107180). doi: <https://doi.org/10.1016/j.buildenv.2020.107180>.
- MHUUC, Ministry of Housing Utilities & Urban Communities. (2005). Egyptian Code for Improving the Efficiency of Energy Use in Buildings (306/2005). In *Part 1: Residential Buildings (306/1)* (pp. 152). Cairo, Egypt: National Housing & Building Research Centre, HBRC.
- MHUUC, Ministry of Housing Utilities & Urban Communities. (2008). The Executive Regulations for the Egyptian Unified Construction Act. In (pp. 163). Cairo, Egypt: General Organisation for Physical Planning.
- Naboni, E., Natanian, J., Brizzi, G., Florio, P., Chokhachian, A., Galanos, T., & Rastogi, P. (2019). A digital workflow to quantify regenerative urban design in the context of a changing climate. *Renewable and Sustainable Energy Reviews*, 113(109255). doi: <https://doi.org/10.1016/j.rser.2019.109255>.
- Nakamura, Y., & Oke, T. R. (1988). Wind, Temperature and Stability Conditions in an East-West Oriented Urban Canyon. *Atmospheric Environment*, 22(12), 2691-2700. doi: [https://doi.org/10.1016/0004-6981\(88\)90437-4](https://doi.org/10.1016/0004-6981(88)90437-4).
- Natanian, J., Aleksandrowicz, O., & Auer, T. (2019a). A parametric approach to optimizing urban form, energy balance and environmental quality: The case of Mediterranean districts. *Applied Energy*, 254, 113637. doi: <https://doi.org/10.1016/j.apenergy.2019.113637>.
- Natanian, J., & Auer, T. (2020). Beyond nearly zero energy urban design: A holistic microclimatic energy and environmental quality evaluation workflow. *Sustainable Cities and Society*, 56(102094), 1-11. doi: <https://doi.org/10.1016/j.scs.2020.102094>.
- Natanian, J., Kastner, P., Dogan, T., & Auer, T. (2020). From energy performative to livable Mediterranean cities: An annual outdoor thermal comfort and energy balance cross-climatic typological study. *Energy and Buildings*, 224(110283). doi: <https://doi.org/10.1016/j.enbuild.2020.110283>.
- Natanian, J., Maiullari, D., Yezioro, A., & Auer, T. (2019b). Synergetic urban microclimate and energy simulation parametric workflow. In *Journal of Physics: Conference Series*.
- Nikolopoulou, M., & Steemers, K. (2003). Thermal comfort and psychological adaptation as a guide for designing urban spaces. *Energy and Buildings*, 35(1), 95-101. doi: [https://doi.org/10.1016/S0378-7788\(02\)00084-1](https://doi.org/10.1016/S0378-7788(02)00084-1).

-
- Nunez, M., & Oke, T. R. (1977). The Energy Balance of an Urban Canyon. *Journal of Applied Meteorology*, 16(1), 11-19.
- Oke, T. R. (1981). Canyon geometry and the nocturnal heat island: comparison of scale model and field observations. *Journal of Climatology*, 1(3), 237-254. doi: <https://doi.org/10.1002/joc.3370010304>.
- Oke, T. R. (1988). Street Design and Urban Canopy Layer Climate. *Energy and Buildings*, 11(3), 103-113. doi: [https://doi.org/10.1016/0378-7788\(88\)90026-6](https://doi.org/10.1016/0378-7788(88)90026-6).
- Oke, T. R. (1995). The heat island of the urban boundary layer: characteristics, causes and effects. In *Wind climate in cities* (pp. 81-107). Berlin/Heidelberg, Germany: Springer.
- Oke, T. R. (2006). Initial guidance to obtain representative meteorological observations at urban sites. World Meteorological Organization: Geneva, Switzerland
- Okeil, A. (2010). A holistic approach to energy efficient building forms. *Energy and Buildings*, 42(9), 1437-1444. doi: <https://doi.org/10.1016/j.enbuild.2010.03.013>.
- Oliveira, V. M. A. d. (2016). *Urban Morphology - An Introduction to the Study of the Physical Form of Cities*. Switzerland: Springer.
- Perini, K., Chokhachian, A., Dong, S., & Auer, T. (2017). Modeling and simulating urban outdoor comfort: Coupling ENVI-Met and TRNSYS by grasshopper. *Energy and Buildings*, 152, 373-384. doi: <https://doi.org/10.1016/j.enbuild.2017.07.061>.
- Qaid, A., & Ossen, D. R. (2015). Effect of asymmetrical street aspect ratios on microclimates in hot, humid regions. *International journal of biometeorology*, 59(6), 657-677. doi: <https://doi.org/10.1007/s00484-014-0878-5>.
- Quan, S. J., Economou, A., Grasl, T., & Yang, P. P.-J. (2014). Computing energy performance of building density, shape and typology in urban context. *Energy Procedia*, 61, 1602-1605. doi: <http://doi.org/10.1016/j.egypro.2014.12.181>.
- Ratti, C., Baker, N., & Steemers, K. (2005). Energy consumption and urban texture. *Energy and Buildings*, 37(7), 762-776. doi: <http://doi.org/10.1016/j.enbuild.2004.10.010>.
- Ratti, C., Raydan, D., & Steemers, K. (2003). Building form and environmental performance: archetypes, analysis and an arid climate. *Energy and Buildings*, 35(1), 49-59. doi: [https://doi.org/10.1016/S0378-7788\(02\)00079-8](https://doi.org/10.1016/S0378-7788(02)00079-8).
- Recast, E. (2010). Directive 2010/31/EU of the European Parliament and of the Council of 19 May 2010 on the energy performance of buildings (recast). *Official Journal of the European Union*, 18(06), 2010.
- Robinson, D., Haldi, F., Leroux, P., Perez, D., Rasheed, A., & Wilke, U. (2009). CitySim: Comprehensive micro-simulation of resource flows for sustainable urban planning. In *Proceedings of the Eleventh International IBPSA Conference*.
- Rode, P., Keim, C., Robazza, G., Viejo, P., & Schofield, J. (2014). Cities and energy: urban morphology and residential heat-energy demand. *Environment and Planning B: Planning and Design*, 41(1), 138-162. doi: <https://doi.org/10.1068/b39065>.
- Rodler, A., Lauzet, N., Musy, M., Azam, M.-H., Guernouti, S., Mauree, D., & Colinart, T. (2021). Urban Microclimate and Building Energy Simulation Coupling Techniques. In M. Palme & A. Salvati (Eds.), *Urban Microclimate Modelling for Comfort and Energy Studies*. Glasgow, UK: Springer Nature Switzerland AG.

- Roudsari, M. S., Pak, M., & Smith, A. (2013). Ladybug: a parametric environmental plugin for grasshopper to help designers create an environmentally-conscious design. In *Proceedings of the 13th international IBPSA conference*, Lyon, France, 25-30 August.
- Rutten, D. (2021). Grasshopper3D. Retrieved from <https://www.grasshopper3d.com/>
- Salvati, A., Coch, H., & Morganti, M. (2017). Effects of urban compactness on the building energy performance in Mediterranean climate. *Energy Procedia*, 122, 499-504. doi: <https://doi.org/10.1016/j.egypro.2017.07.303>.
- Salvati, A., Monti, P., Roura, H. C., & Cecere, C. (2019). Climatic performance of urban textures: Analysis tools for a Mediterranean urban context. *Energy and Buildings*, 185, 162-179. doi: <https://doi.org/10.1016/j.enbuild.2018.12.024>.
- Santamouris, M., Papanikolaou, N., Koronakis, I., Livada, I., & Asimakopoulos, D. (1999). Thermal and air flow characteristics in a deep pedestrian canyon under hot weather conditions. *Atmospheric Environment*, 33, 4503-4521. doi: [https://doi.org/10.1016/S1352-2310\(99\)00187-9](https://doi.org/10.1016/S1352-2310(99)00187-9).
- Seto, K. C., Dhakal, S., Bigio, A., Blanco, H., Delgado, G. C., Dewar, D., Huang, L., Inaba, A., Kansal, A., & Lwasa, S. (2014). Human settlements, infrastructure and spatial planning. In *Climate Change 2014: Mitigation of Climate Change. Contribution of Working Group III to the Fifth Assessment Report of the Intergovernmental Panel on Climate Change*; Cambridge University Press: Cambridge, UK, 2014.
- Sharmin, T., Steemers, K., & Matzarakis, A. (2017). Microclimatic modelling in assessing the impact of urban geometry on urban thermal environment. *Sustainable Cities and Society*, 34, 293-308. doi: <http://dx.doi.org/10.1016/j.scs.2017.07.006>.
- Shashua-Bar, L., & Hoffman, M. E. (2004). Quantitative evaluation of passive cooling of the UCL microclimate in hot regions in summer, case study: urban streets and courtyards with trees. *Building and Environment*, 39(9), 1087 - 1099. doi: <https://doi.org/10.1016/j.buildenv.2003.11.007>.
- Stewart, I. D., & Oke, T. R. (2012). Local climate zones for urban temperature studies. *Bulletin of the American Meteorological Society*, 93(12), 1879-1900. doi: <https://doi.org/10.1175/BAMS-D-11-00019.1>.
- Taleghani, M., Kleerekoper, L., Tenpierik, M., & Van Den Dobbelsteen, A. (2015). Outdoor thermal comfort within five different urban forms in the Netherlands. *Building and Environment*, 83, 65-78. doi: <http://dx.doi.org/10.1016/j.buildenv.2014.03.014>.
- Taleghani, M., Tenpierik, M., Van Den Dobbelsteen, A., & De Dear, R. (2013). Energy use impact of and thermal comfort in different urban block types in the Netherlands. *Energy and Buildings*, 67, 166-175. doi: <http://dx.doi.org/10.1016/j.enbuild.2013.08.024>.
- Tereci, A., Ozkan, S. T. E., & Eicker, U. (2013). Energy benchmarking for residential buildings. *Energy and Buildings*, 60, 92-99. doi: <http://dx.doi.org/10.1016/j.enbuild.2012.12.004>.
- Thermal Energy System Specialists, TESS. (2021). TRNSYS-Transient System Simulation Tool. Retrieved from <http://www.trnsys.com/>
- United Nations, Department of Economic and Social Affairs Population Division. (2018). *World Urbanization Prospects: The 2018 Revision*. New York: United Nations
- Vallati, A., Grignaffini, S., Romagna, M., Mauri, L., & Colucci, C. (2016). Influence of street Canyon's microclimate on the energy demand for space cooling and heating of buildings. *Energy Procedia*, 101, 941-947. doi: <http://doi.org/10.1016/j.egypro.2016.11.119>.

-
- Vartholomaios, A. (2017). A parametric sensitivity analysis of the influence of urban form on domestic energy consumption for heating and cooling in a Mediterranean city. *Sustainable Cities and Society*, 28, 135-145. doi: <http://dx.doi.org/10.1016/j.scs.2016.09.006>.
- Wei, R., Song, D., Wong, N. H., & Martin, M. (2016). Impact of urban morphology parameters on microclimate. *Procedia Engineering*, 169, 142-149. doi: <http://doi.org/10.1016/j.proeng.2016.10.017>.
- Witte, M. J., Henninger, R. H., Glazer, J., & Crawley, D. B. Testing and validation of a new building energy simulation program. In *7th IBSPA Conference*.
- Wortmann, T., & Natanian, J. (2020). Multi-objective Optimization for Zero-Energy Urban Design in China: A Benchmark. In *SimAUD2020*.
- Xu, Y., Ren, C., Ma, P., Ho, J., Wang, W., Lau, K. K.-L., Lin, H., & Ng, E. (2017). Urban morphology detection and computation for urban climate research. *Landscape and Urban Planning*, 167, 212-224. doi: <http://dx.doi.org/10.1016/j.landurbplan.2017.06.018>.
- Zhang, J., Xu, L., Shabunko, V., Tay, S. E. R., Sun, H., Lau, S. S. Y., & Reindl, T. (2019). Impact of urban block typology on building solar potential and energy use efficiency in tropical high-density city. *Applied Energy*, 240, 513-533. doi: <https://doi.org/10.1016/j.apenergy.2019.02.033>.

5.9 Epilogue

In this work, energy loads per unit floor area was used, which drew similar implications as though the absolute energy loads is used. The decision to use this metric (section 3.2) was to inform urban planners about the absolute impact of urban form on energy loads. Also, it allows for a sector by sector approach of how energy is used, which is most needed in decision making. In a preliminary analysis of the data obtained in this study, it was found that using normalised energy loads resulted in slight differences with respect to the effect of orientation and distance between buildings on energy loads, as well as on combined fitness; however, the effect of building heights and FAR, as expected, drew different insights with respect to both performance criteria. This leaves such a relationship open for future investigations, though it is not included as part of this thesis' scope.

This chapter expanded the scope of the previous chapter to include urban scale design parameters of urban block typologies in a multi-objective simulation workflow. In accounting of outdoor thermal comfort, energy loads as well as a combined metric, the study revealed that compact ($BCR \geq 60\%$) and moderately-dense ($4 > FAR > 2$) courtyards provide the best performance when they are oriented diagonally with regards to the summer solar path. Overall, it can be deduced that courtyards are preferable in residential areas where energy consumption is prioritised over the design for outdoor spaces. It can also be implied that compact scattered forms are a feasible option if more outdoor spaces are required. This comes from their ability to offer an intelligible public realm with spatially permeable street networks, and if deliberately heightened, they can offer adequate shading whilst inducing lower energy loads.

This study also highlights the urgent need for integrating coupling studies within a parametric workflow in Egypt, and other hot-arid zones, to further scrutinise the relationship between the outdoor thermal conditions and the indoor energy performance. In line with the aims of this thesis, the discussion in this chapter presented design guidelines, the application of which in practice promises enhanced environmental performance, not only for courtyards but also the other typologies. Qualitative studies are still needed to check the acceptability of the optimised built forms in reality, in Egypt. Based on the results and conclusion of this study, the next chapter investigates the environmental performance of courtyard urban blocks with varying heights of their individual buildings.

6 Courtyard Blocks Algorithmic Optimisation

6.1 Preface

The study of solar access (or shading) in residential clusters (blocks) as a climate responsive design strategy in hot-arid deserts started decades ago (Rahamimoff, 1984), building upon the seminal work by Ralph Knowles (Knowles, 1981). In his work, Knowles developed the Solar Envelope, “a construct of space and time... the solar envelope avoids unacceptable shadows above designated boundaries called shadow fences... the envelope provides the largest volume within time constraints, called cut-off times,” Knowles articulated (Knowles, 2003), to provide solar access and cross-ventilation for each residential unit (Figure 6.1). Okeil (2010) adopted the concept, however, with special focus on the open spaces between buildings than the neighbouring buildings. At latitude 48°, his proposed model, the Residential Solar Block (RSB) (Figure 6.1), was compared to conventional courtyard blocks to gauge its efficacy of minimising heat gain and enhancing heat loss in summer, and vice versa in winter. The two concepts (Knowles, 1981; Okeil, 2010), together constituted a basis for recent studies as well as signifies a great potential of parametric studies on the passive solar design of courtyard urban blocks.

Vartholomaios (2015) proposed the RSB Envelope - a hybrid strategy to improve the passive solar heating through the increase of exposed southern façades of blocks, rather than single units, with the aim to minimise heating energy. His model proved to outperform the reference case, increasing the percentage of southern surfaces receiving maximum insolation to 21% (Figure 6.2). Natanian *et al.* (2021) proposed the Solar Block Generator (SBG) to account for a set of exposure and shading indices simultaneously, with the aim to double the existing density of the site (Figure 6.2). Most, if not all, of these studies focus on the solar exposure/daylighting aspects of the urban configuration. In the context of Cairo's hot-arid climate, a holistic approach which, besides guaranteeing winter insolation, accounts for summer pedestrian thermal comfort together with energy consumption of courtyard blocks becomes imperative, and promises to bring this inherent vernacular design strategy back into practice after its demise in favour of the contemporary low and mid-rise dispersed urban forms.

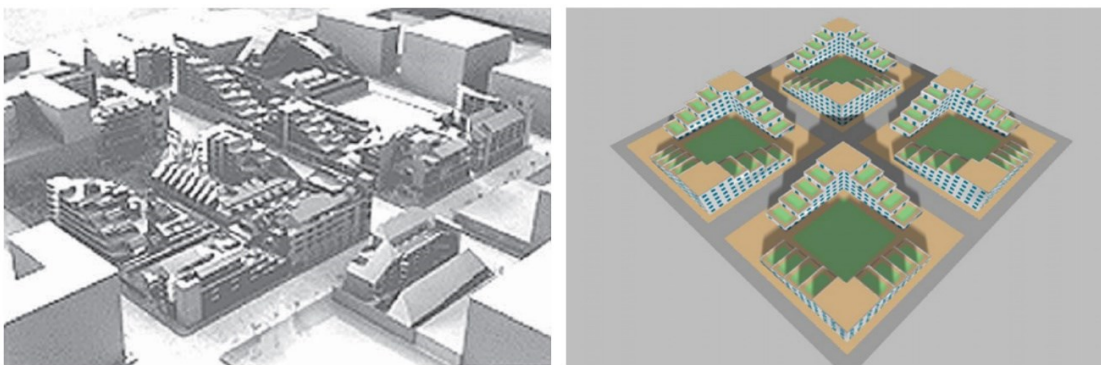


Figure 6.1: Residential units under the solar envelope, adapted from Knowles (2003) (left), and Okeil's Residential Solar Block (2010) (right).

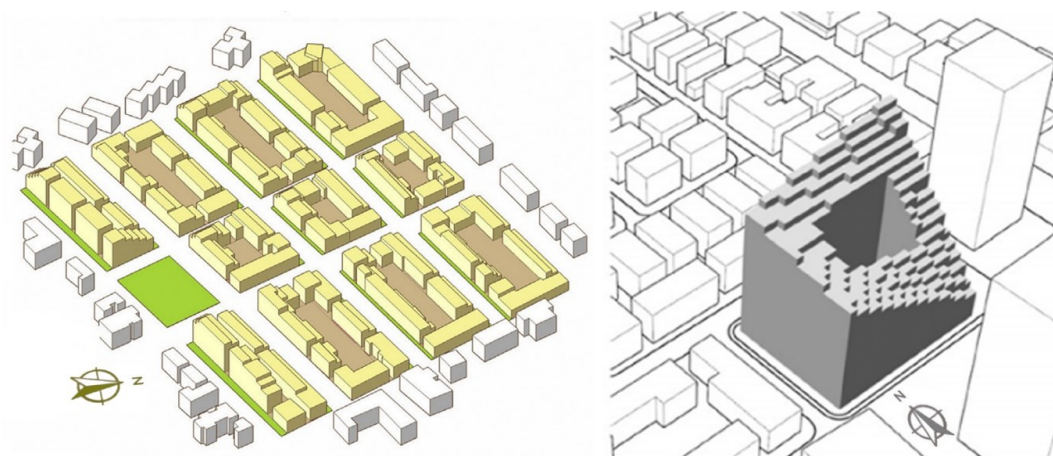


Figure 6.2: The RSB Envelope applied in a Mediterranean Climate (Vartholomaios, 2015) (left), and the SBG applied in a hot-Mediterranean climate (Natanian *et al.*, 2021) (right).

This chapter addresses the third research question “*To what extent could the urban scale design parameters improve the thermal and energy performance of courtyard urban blocks?*” by assessing the performance of courtyard blocks in a multi-objective simulation workflow. As a cluster of residential buildings, this work considers the orientation, distance between buildings (interspaces), and the individual height of each building – as a reconceptualisation of Okeil’s RSB – to maximise outdoor thermal comfort in terms of UTCI and minimise energy consumption in summer. This enhances the current study as outdoor thermal comfort was not addressed in any of the above mentioned two studies. Since both lighting energy and electrical equipment loads are not comparable to those of cooling energy, only the latter is accounted for in this study. This was also based on the premise that including lighting and electrical loads would not alter the ranking of the results, but rather only shift the distribution. With the parameterisation of the design variables entailing millions of permutations, genetic algorithms (GAs) become indispensable in this context.

Among other GAs, the Hypervolume Estimation (HypE) is one of the best performing search algorithms, for solving multi-objective problems, in terms of convergence and robustness (Wortmann & Natanian, 2021). Convergence refers to the ability to explore the entire search space to find the optimum solutions, while robustness is the ability to maintain its convergence performance throughout the search process. Design variables are stored within solutions (individuals) as strings of binary bits. HypE, like most GAs, applies selection, mutation, and crossover, inspired by the process of natural evolution, where a population of individuals is evolved iteratively based on the fittest solutions in the previous iteration (generation). Fitness values are assigned to solutions based on their hypervolume contribution with regard to the overall hypervolume - the area bounded by the orthogonal domains of a set of solutions and a reference point in the objective space (Figure 6.3). Selection is done following a Tournament selection, which implies, for several rounds, picking two random candidate solutions, and selecting the fittest to be a parent candidate for the next generation. Offspring are generated by applying genetic operators, crossover and mutation. For crossover, bits of two parent strings are swapped at randomly chosen location(s) on the strings to generate two offspring candidates. Using mutation, bits are flipped within one parent string (from zero to one and vice versa) to generate a new offspring (Figure 6.3) (Back, 2000; Bader & Zitzler, 2011).

This chapter is based on the paper “Multi-objective optimisation of urban courtyard blocks in hot arid zones,” submitted to the journal Solar Energy in 2022 in collaboration with a researcher in Cairo. The collaboration included the conceptualisation and formulation of the methodology. Details of authorship of this paper are given in Table 6.1.

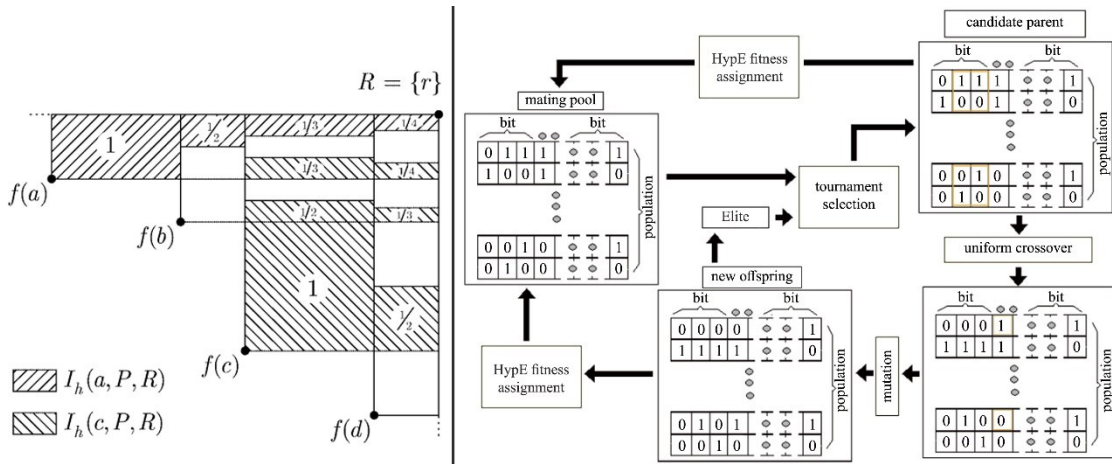


Figure 6.3: Illustration of the basic fitness assignment (left) (details in Bader & Zitzler, 2011), and the basic operations in HypE (adapted from Chiu, 2010).

Table 6.1: Declaration of authorship.

This declaration concerns the article entitled:	
Multi-objective optimisation of urban courtyard blocks in hot arid zones.	
Publication status (tick one):	
Draft manuscript <input type="checkbox"/> Submitted <input type="checkbox"/> In review <input type="checkbox"/> Accepted <input type="checkbox"/> Published <input checked="" type="checkbox"/>	
Publication details (reference):	
Ibrahim, Y. , Kershaw, T., Shepherd, P., & ElKady, H. (2022). Multi-objective optimisation of urban courtyard blocks in hot arid zones. <i>Solar Energy</i> , 240 (July 2022), pp: 104-120. DOI: https://doi.org/10.1016/j.solener.2022.05.024 .	
Copyright status (tick the appropriate statement):	
<ul style="list-style-type: none"> • I hold the copyright for this material <input type="checkbox"/> • Copyright is retained by the publisher, but I have been given permission to replicate the material here <input checked="" type="checkbox"/> 	
Candidate's contribution to the paper (%):	
The candidate has predominantly contributed to: <ul style="list-style-type: none"> • Formulation of ideas (70%): Y. Ibrahim developed the ideas, in consultations with the co-authors. • Design of methodology (90%): Y. Ibrahim developed the methodology, in consultation with T. Kershaw. • Data analysis (100%): Y. Ibrahim conducted the data analysis. • Presentation of data in journal format (80%): Y. Ibrahim wrote and submitted the paper. T. Kershaw and P. Shepherd provided their valuable feedback for improvements. 	
Statement from Candidate:	
This paper reports on original research I conducted during the period of my Higher Degree by Research candidature.	
Signed:	Date: September 2022

6.2 Abstract

Courtyard blocks are well known for their tempering potential of the thermal conditions in various climates. In this paper, the building heights, orientation and interspaces of courtyard blocks are optimised for the hot-arid climate of Cairo, Egypt. Simulations are conducted using an evolutionary search algorithm within the Grasshopper parametric design environment for Rhino 3D. The Ladybug-tools, plugins of Grasshopper were used to calculate the objective functions, the summer weekly cooling loads and the weekly average Universal Thermal Climate Index (UTCI). For three courtyard block types elongated 1, 2 and 3-fold the width of the inner court, the Pareto optimal sets of the three types all comprised solutions with the minimum interspaces. Orientation 45° was predominant in the square type, whilst orientation 135° was predominant in the elongated types ($W/L = 2, 3$). Pareto optimal solutions were ranked using the weighted sum method, with the optimised cases reducing cooling loads by up to 31.7% and reducing UTCI by up to 1.6°C , as compared to a reference case. Solar radiation analysis showed that the optimised cases have great potential to increase the percentage of exposed surfaces by 4% to reduce the heating loads in winter.

6.3 Introduction

Currently, cities consume around 76% of the global primary energy demand, with the building sector responsible for almost 30% of it (Seto *et al.*, 2014; IEA, 2020). About half of the world's population live in urban areas, but the number of urban residents is expected to grow to almost two thirds of the global population by 2050 (United Nations, 2018). The recent report from the Intergovernmental Panel on Climate Change (IPCC) declares that the human influence on warming the climate system is “unequivocal”, evoking further negative consequences on human health and well-being (IPCC, 2021). The interactions between the built form geometry and surface properties under a specific climate generate microclimates (Taleghani *et al.*, 2014b), and the impact of warming microclimates on public health has already been documented (Kovats & Hajat, 2008). Urban areas are often warmer than their sub-urban/rural surroundings, due to the transformation of the land use/land cover as well as the terrain roughness, leading to modifications to the surface-atmosphere radiative and convective interactions, known as Urban Heat Island (UHI) (Oke, 1976). In this concern, the potential of urban geometry to regulate the microclimate, as well as to affect the building sector energy

consumption, has been well established (Taleghani *et al.*, 2013). Of the housing typologies being widely recognised across the globe, not just in hot climates, courtyard buildings have long been of significant interest to many researchers. A courtyard is an open space bounded by buildings on all sides, which serves as a passive architectural design strategy to provide stabilising thermal conditions for people in different climates (Apolonio Callejas *et al.*, 2020). Besides natural lighting, courtyard buildings allow for greater cross-ventilation in humid climates, shading and protection from dust in hot climates, and protection against winds in cold climates (Taleghani *et al.*, 2014a). In hot areas, a courtyard's thermal performance mostly depends on the solar access to the internal envelope (Martinelli & Matzarakis, 2017).

The temperature difference between exposed versus shaded surfaces creates heat transfer via radiation and convection between the air and the surfaces. Warm air rises and the difference in air density promotes natural ventilation to the sky above the courtyard (Zamani *et al.*, 2018). The tempering potential of courtyards, however, depends on their geometrical proportions (height-to-width ratio and orientation), material properties and the presence of any natural elements (trees and water spaces), the latter being particularly necessary for people's well-being through contact with nature (Diz-Mellado *et al.*, 2021). The geometrical proportions of courtyards differ from one region to another, based on various environmental, social, and cultural aspects. This paper deals with urban courtyard blocks typically defined as a multi-story residential building delimitating an open space.

6.3.1 Background

A courtyard house is one of the oldest housing typologies, dating back to 5000 years ago. Particularly found in the Middle East and China, courtyards were built as a shelter from severe weather conditions and unfriendly neighbours (Soflaei *et al.*, 2017). This is clear in ancient civilisations, where the protective features of underground courtyard houses are evident, for instance, the simplest underground settlement in Honan, China is similar to Troglodyte villages in Tunisia, having the most primitive underground courtyard houses in the world (Zamani *et al.*, 2018). Besides their thermal performance, courtyards were also built for various cultural and philosophical aspects. For instance, the concept of the courtyards surrounded by multipurpose enclosed spaces meets the principle of unity, fulfils the privacy features of Islamic culture, while also encourages the use of outdoor space (Soflaei *et al.*, 2017; Zamani *et al.*, 2018).

Courtyards can provide greater aesthetic values if properly furnished with the green and/or water spaces typically found in Persian architecture, which resemble the English country garden found in the UK (Malekzadeh & Loveday, 2008). In Mediterranean climates, courtyards are considered part of the living spaces (Diz-Mellado *et al.*, 2021), and are believed to have inherited their features during the Islamic reign in the Iberian Peninsula (around 8th century), later dubbed the Spanish Mudéjar style (Ernest & Ford, 2012), which has further spread to many European countries. During the Spanish colonisation of the Americas (15th century), the architectural style of the courtyards suitable for warm climates has appeared in some Caribbean regions; Cuba is an example, albeit without taking account of the humid conditions of the Caribbean islands (Tablada *et al.*, 2009). During the last two centuries, courtyard buildings have appeared on the West Coast of North America, with the influence of the Spanish Colonial Revival Movement in Southern California (19th century) (Zamani *et al.*, 2018). Although the tempering potential of courtyards has been realised since ancient times, it has only been quantified in the last few decades.

6.3.2 *Microclimatic and energy performance of courtyards*

March and Martin (1972) suggested six archetypal building forms representing different shapes of pavilions, slabs and courtyards, in their investigation of density, surface coverage and daylighting. These archetypes have been further adopted in several lines of research. In a hot-arid climate, Gupta (1987) studied the solar radiation exposure over three of these archetypes, while Ratti *et al.* (2003) analysed the thermal performance of all six archetypes in terms of their shadow density and daylight distribution. Both studies have acknowledged the higher performance of the courtyard form. In a series of studies by Muhaisen and Gadi, a tool to calculate the shaded versus sunlit areas in circular (Muhaisen & Gadi, 2005), and polygonal courtyards (Muhaisen & Gadi, 2006) was presented. Their results showed that shallow courtyards provide a better trade-off between summer shading and winter exposure than the deep ones. Moreover, Muhaisen (2006) studied annual shading patterns of rectangular courtyards in four different climates. Notably, he found that the maximum sunlit area in winter monitored in Cairo is at the same orientation (60°) as that which produces the greatest shading in summer. Further, he recommended using proportions of courtyard perimeter-to-height of 4-8 to keep the shading reduction in winter in Cairo below 50%.

The existing literature on the microclimatic performance of courtyard forms often deals with the indoor thermal comfort or the temperature gap between the ambient air temperatures and those inside the courtyard, due to several factors. For instance, the effect of a courtyard's proportions, height (H), width (W), length (L) (Aldawoud, 2008; Soflaei *et al.*, 2017), H/W or aspect ratio (Yezioro *et al.*, 2006; Yaşa & Ok, 2014; Martinelli & Matzarakis, 2017), orientation and block elongation (Taleghani *et al.*, 2014a); openings and glazing ratio (Aldawoud, 2008; Guedouh & Zemmouri, 2017), change of climate zone (Aldawoud, 2008; Martinelli & Matzarakis, 2017; Rojas-Fernández *et al.*, 2017), and pavements and roofs materials (Taleghani *et al.*, 2014a; Chatzidimitriou & Yannas, 2016). Etzion (1990) reported 1 to 2 hours of lag between the daily temperature profile inside the courtyard of a hot arid climate, relative to the ambient temperature, due to the heat capacity of the walls and floor. Diz-Mellado *et al.* (2021) supported the existing literature claiming that courtyards perform better when the ambient temperatures are the highest. They reported a thermal gap of 13.9 °C between the courtyard and the ambient temperature during a “heat wave” summer week in the Mediterranean climate of Cordoba, Spain. Al-Masri and Abu-Hijleh (2012) found that an optimised courtyard could save around 11% of annual energy consumption compared to a conventional building in the hot-arid climate of Dubai, UAE. Moreover, a study in the temperate climate of Amsterdam underlined the potential of covered courtyards (atriums) to reduce heating demand by up to 11 kW/m², albeit making the indoor environment warmer in this case (Taleghani *et al.*, 2014a).

There have also been studies of the thermal and energy performance of courtyard blocks at an urban scale. Malekzadeh and Loveday (2008) coupled ENVI-met and TRNSYS to investigate the annual heating and cooling loads, as well as the thermal comfort in Physiological Equivalent Temperature (PET), in Asfahan, Iran. Among six typologies investigated, the courtyard form had the highest percentage of comfortable hours. A study of 3 urban typologies in the Mediterranean climate of Thessaloniki, Greece, recommended using elongated urban blocks along the East-West (EW) axis, with minimum distances between buildings as the best configuration for lower annual energy loads (Vartholomaios, 2017). In a series of studies in different cities characterised by a Mediterranean hot climate, Natanian and others emphasised the higher performance of the courtyard typology against pavilion, slab, and high-rise typologies, in terms of their outdoor thermal comfort, cooling loads, and daylighting potential (Natanian *et al.*, 2019b; Natanian *et al.*, 2019c; Natanian & Auer, 2020).

In another study of the humid subtropical climate of Shanghai, Wortmann and Natanian (2020) showed that L-shaped and square courtyards represented 33% of the optimum cases using evolutionary Multi-Objective Optimisation (MOO) algorithms. Moreover, a recent study of the hot-arid climate of Cairo, Egypt, concluded that compact and medium-density courtyard forms, orientated 45° from North, exhibit the best trade-off between outdoor thermal comfort and energy use in summer (Ibrahim *et al.*, 2021a).

Notwithstanding the above-mentioned benefits, courtyard forms are often typified in the literature as uniformly extruded urban blocks. Okeil (2010) criticised the mutual overshadowing and the uneven distribution of the solar energy across the external and internal facades for a conventional courtyard block in winter in the hot-humid climate of UAE. A Residential Solar Block (RSB) was derived from a conventional block orientated 45° to North, by cutting solar profiles in winter for a specific latitude so that the resulting shadows could fit exactly in the central courtyard. The RSB was shown to have higher winter solar exposure, lower exposure on the roofs and improved airflow in summer (Okeil, 2010). A recent study reported that, of the relevant literature, only 20% of the studies considered the thermal and microclimatic performance of courtyards simultaneously (Zamani *et al.*, 2018).

Hence, this paper reconceptualises Okeil's RSB, in summer, in the hot-arid climate of Cairo, Egypt. Starting from the premise that urban shading is the most effective heat mitigation strategy in hot-arid areas, this study investigates both the microclimatic and energy performance of non-uniform courtyard blocks using an urban scale parametric optimisation workflow. By using the parametric features of Grasshopper for Rhinoceros 3D (Rutten, 2021), its environmental plugins the Ladybug-tools (Roudsari & Mackey, 2022), and an evolutionary MOO plugin Octopus (Vierlinger, 2021), courtyard blocks' elongation, orientation, interspaces, and the various heights of their buildings are simulated to find the best geometrical configuration of a courtyard block.

6.4 Methodology

A common approach to building performance simulation is removing the complexities of real urban forms, which allows building forms to be represented as straightforward design parameters. This helps to establish performative relationships between urban forms and their environmental impacts in the

predesign stage. In practice, multi-zone urban building energy simulations are often more time consuming than simple optimisation problems (Dogan & Reinhart, 2017). Moreover, in parametric optimisation, the number of solutions increases exponentially with the number of design parameters, also known as the “curse of dimensionality”. Hence, one should consider the number of possible solutions that arises from such dimensionality. In this study, the authors sought to investigate the microclimatic and energy performance of three courtyard geometries with different elongations, comprising 8, 10 and 12 buildings, as shown as courtyard block types A, B and C respectively, in Figure 6.4.

Table 6.2 lists the range, step size and number of iterations for each design parameter as well as the total number of permutations for each courtyard type. Minimum and maximum thresholds of building heights and interspaces were kept in accordance with the Executive Regulations of the Egyptian Construction Act (MHUUC, 2008). Indeed, the number of potential combinations of design parameters that could be simulated is in the hundreds of thousands. Heuristic optimisation approaches exhibit a significant potential to balance the trade-off between the computational burden and the ability to find a good approximation of the best set of solutions (Evins, 2013). Examples of MOO using heuristic approaches in the architectural domain are abundant; for instance, those considering building envelopes (Kämpf & Robinson, 2009), building form (Kämpf *et al.*, 2010), as well as the design of Heating, Cooling and Air Conditioning (HVAC) systems (Stanescu *et al.*, 2012).

Table 6.2: Range, step size and number of iterations of each design parameter, and the total number of permutations in each case.

Design parameter	Range		Step size	# Iterations
	Minimum	Maximum		
Orientation (CCW from N)	0°	135°	45°	4
Interspaces	12m	24m	6m	3
Building heights	12m	36m	12m	3 ⁿ
n is the number of buildings in one type of courtyard blocks				
# Permutations Type A (8 buildings)				78732
# Permutations Type B (10 buildings)				708588
# Permutations Type C (12 buildings)				6377292

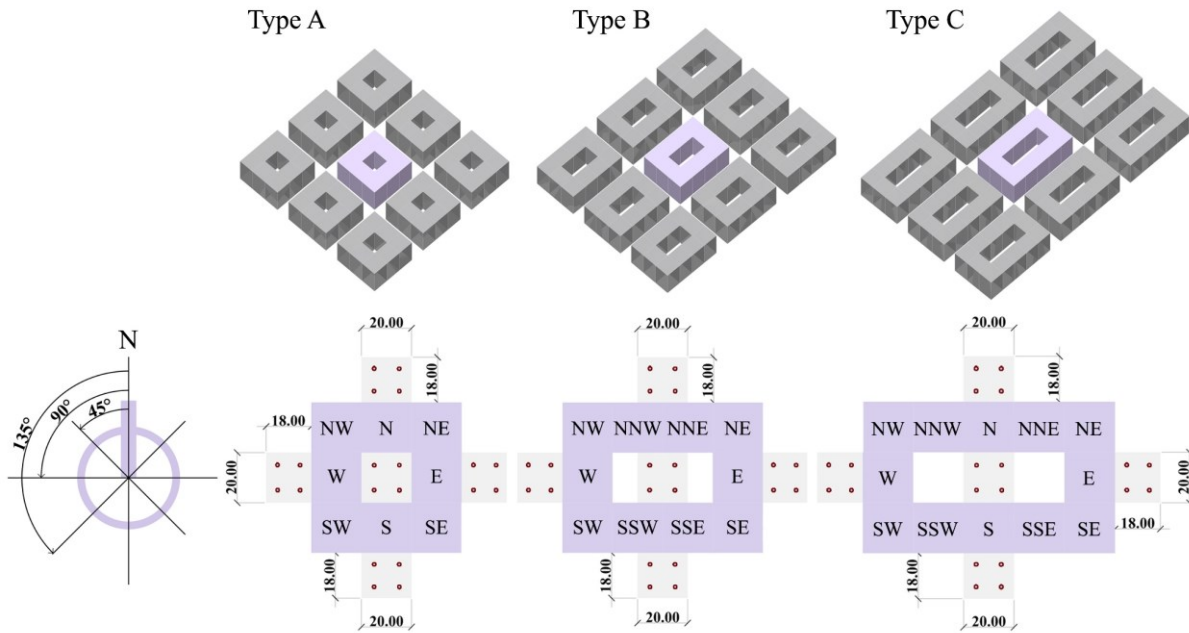


Figure 6.4: Types of courtyards investigated in this study. The upper row shows the courtyard block under investigation within a 3×3 grid. The bottom row shows an example of the dimensions of the ground zones within 18 m interspaces showing the locations of the receptor points for UTCI calculations. Buildings are referred to as their directions in a 0° orientation, and rotated CCW from N as shown in the left compass.

6.4.1 Experimental approach

Parametric optimisation is performed in this study within Rhinoceros 3D (Rhino) (McNeel, 2021). Rhino is a 3D modelling environment with advanced parametric and algorithmic design capabilities via its platform, Grasshopper. The latter supports multi-objective evolutionary optimisations by means of its plugin, Octopus. In MOO, design candidates that achieve the best trade-off between multiple conflicting objectives are visually represented on a Pareto front. In this case, the best set of points is the set comprising, preferably diverse, non-dominated points, i.e., it is impossible to improve one objective without degrading others. With a large number of design candidates, a true Pareto front is often difficult to find, and an optimisation algorithm thus aims to find the best approximation of the true Pareto front.

6.4.1.1 Evolutionary algorithms

Evolutionary Algorithms (EAs) are common meta-heuristic optimisation algorithms which apply the principles of natural evolution. Solutions are represented by individuals (chromosomes) comprising all the design variables as binary bits. Each group of individuals forms a population (generation), where new generations are produced based on the fittest individuals in the previous generation (Back, 2000; Emmerich & Deutz, 2018). EAs can exhibit excellent search capabilities due to their sampling of the design space (all candidate solutions) (Vierlinger, 2015). Of the different strategies of EAs, Genetic Algorithms (GAs) have been shown to require less computational time than other optimisation techniques (e.g., Particle Swarm Optimisation), particularly in high dimensional problems (Tuhus-Dubrow & Krarti, 2009; Bichiou & Krarti, 2011).

Typically, GAs build an initial population of individuals, evaluate their fitness, and select the fittest individuals for reproduction in the next generation. New individuals are bred by applying genetic operators, i.e., crossover and mutation. The fitness of the new offspring is evaluated such that, in case new non-dominated solutions exist, part of the population (with relatively lower fitness) is truncated to fit the desired new population size. The paradigm used to define the selection procedure distinguishes one algorithm from the other. A general categorisation of these paradigms is (1) Pareto based, applied in e.g., SPEA-2, (2) Decomposition based, applied in e.g., NSGA-III, and (3) Indicator based MOEA, applied in e.g., HypE (Emmerich & Deutz, 2018). Currently, Octopus allows the use of two multi-objective evolutionary algorithms (MOEA), namely the Strength Pareto (SPEA-2) (Zitzler *et al.*, 2001), and the Hypervolume Estimation (HypE) (Bader & Zitzler, 2011) evolutionary algorithms. HypE outperformed six other search algorithms in an optimisation problem to maximise density without affecting the solar exposure of roofs, southern facades and outdoor surfaces on the winter solstice (Wortmann & Natanian, 2021).

6.4.1.2 Algorithm settings

Given the high dimensionality of the search space in this work, and since SPEA-2 is reported to lack a robust mechanism to exploit the entire range of possible solutions (Vierlinger, 2015), therefore, it was concluded that HypE was the most suitable to the study conducted here, as implemented in the Octopus plugin.

HypE depends on the calculation of the hypervolume indicator, which indicates the n -dimensional space bounded by the orthogonal domains of a set of points (solutions) and a reference point; according to the number of objectives (n), the area of the space for 2 objectives, the volume for 3 objectives, or the hypervolume for 4 or more objectives. The hypervolume indicator thus measures the size of the space that is dominated by a set of solutions (Bader & Zitzler, 2010). A population size of 2-6 times the number of design variables was recommended by Ascione *et al.* (2016). Accordingly, a population size of 50 solutions is used in this study.

In Octopus, the first generation is twice as big as the population size in order to create the mating pool, from which the individuals are selected as parent candidates for reproduction. An elitism ratio, which indicates a percentage of new solutions to be bred out of the elite solutions from the previous generation rather than out of the mating pool was set to 0.2 (10 solutions).

Fitness value is assigned to one solution according to its contribution to the overall hypervolume (Bader & Zitzler, 2011). Offspring are generated by applying two main operators, crossover (recombination) and mutation (Back, 2000; Chiu, 2010). In Octopus, mutation and crossover are governed by a given probability and a rate applied to a parent string which define the amount of change in a single design variable. Normally, higher probabilities hinder convergence towards the Pareto front, nonetheless, they help to avoid premature convergence. Thus, a value of 0.8 was used for the crossover and mutation rates to allow greater exploration of the search space.

6.4.2 *Objective function evaluation*

Objective functions are evaluated using a parametric simulation workflow (Mackey *et al.*, 2017), using the environmental analysis plugins of Grasshopper, the Ladybug-tools. The plugins include Ladybug which analyses and visualises climate data, Honeybee which runs and visualises energy models using EnergyPlus, and Dragonfly which enables district-scale UHI modelling using the Urban Weather Generator (UWG) (Roudsari & Mackey, 2022). The workflow is based on the integration of valid software engines dedicated to calculating the energy and microclimatic components governing the outdoor thermal comfort; EnergyPlus (Crawley *et al.*, 2001) to calculate the cooling loads and external surface temperatures, and Urban Weather Generator (UWG) (Bueno *et al.*, 2013) to estimate the effect of UHI on air temperature and relative humidity.

Surface temperatures are used as part of the mean radiant temperature (MRT) calculation, along with other Honeybee components for view factor calculations and human-sky heat exchange. MRT is combined with the other meteorological parameters estimated by the UWG (urban air temperatures and relative humidity), along with wind speeds from the weather file, to calculate the Universal Thermal Climate Index (UTCI) (Bröde et al., 2012), an indicator for outdoor thermal comfort (see Ibrahim *et al.*, 2020a). In a precursor study, the simulation workflow was validated against field measurements, showing a congruent performance in terms of the UTCI with $R^2 = 0.91$ (Ibrahim *et al.*, 2021b).

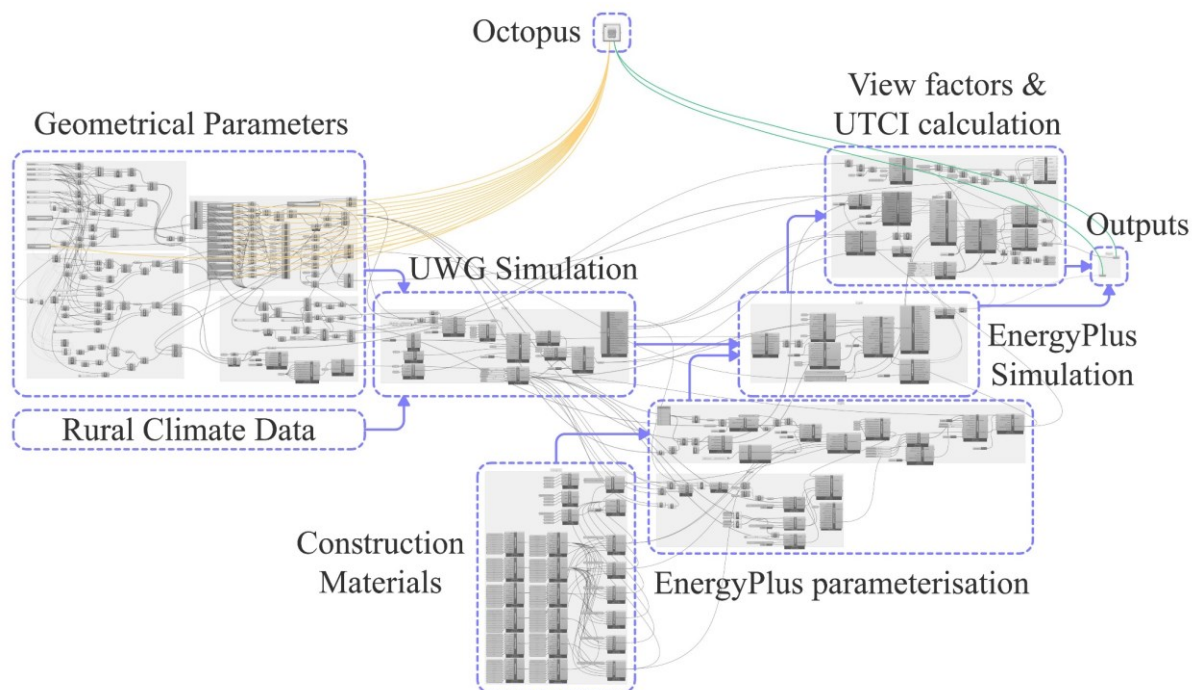


Figure 6.5: Graphical Abstract showing the simulation workflow, highlighted on the Grasshopper GUI.

Figure 6.5 shows the simulation workflow within the Grasshopper GUI, highlighting the connection between the optimisation component, Octopus, and both the design parameters and objectives. Once the search process is initiated in Octopus, the design variables, orientation, interspaces and individual building heights, change and trigger the simulation workflow, where the objective functions are recorded by Octopus for fitness evaluation. The process runs iteratively for each design individual until the search stops. Cooling loads are estimated as the weekly aggregate of each building of a courtyard type.

UTCI is presented as the average of all receptor points, recorded 1.2 m above the ground, and distributed around and inside the central courtyard (Figure 6.4 bottom). Further, UTCI results are averaged over the daytime hours (6 am to 7 pm) for a week, to provide a single value for comparison between courtyards. This average is referred to as the Av. UTCI throughout the rest of the paper.

6.4.3 Climate context

The hot and arid climatic conditions of Cairo, Egypt (30.13°N, 31.40°E) are represented by using an International Weather for Energy Calculation (IWEC) file, obtained from the U.S. DoE (2020). Cairo is defined as a hot desert climate (BWh) under the Köppen-Geiger classification. The climate is characterised by very high solar radiation intensities throughout the year, with an average of 2600 kWh/m²/year; relatively high daily average maximum air temperatures of 35 °C in June, and average minimum of 10 °C in January with annual average of 22 °C; and relative humidity of an average of 58% with very low precipitation levels, typically occurring in January. Winds are North-Westerly most of the year, with some South-Westerly sand storms in April with an average wind speed of 3.5 m/s. Given the high computational time required for fitness evaluation, and since the worst thermal conditions are experienced in summer, also typified with a significant use of air conditioning, a representative hot week (5th - 11th June) is chosen as the analysis period for performance evaluation. Figure 6.6 shows the weather data in Cairo in the typical hot week as retrieved from the IWEC file and used in this study.

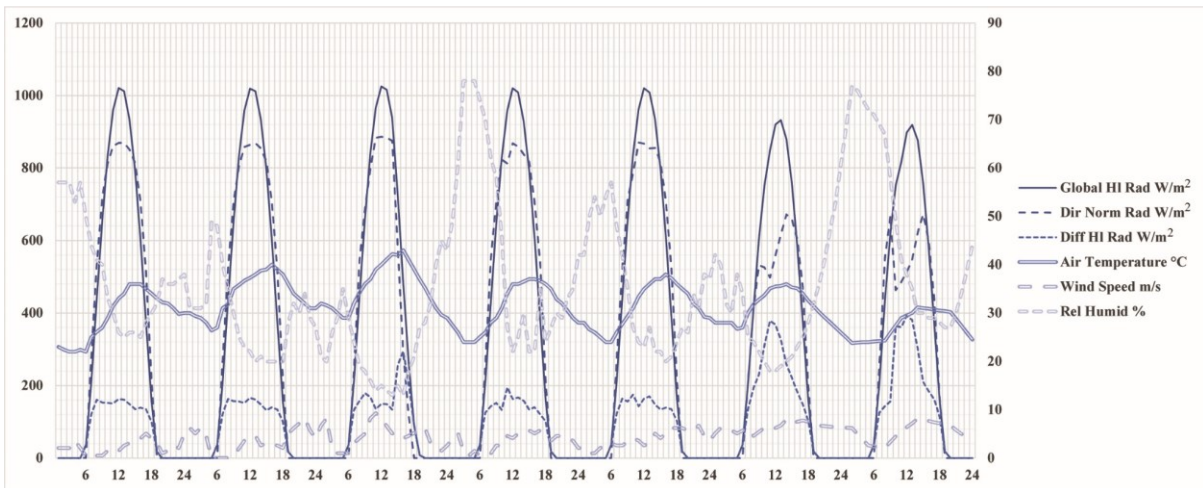


Figure 6.6: Cairo's weather data in the typical hot week (5th - 11th June), as extracted from the IWEC file. Radiation data are plotted against the primary axis, while the others are plotted against the secondary axis.

6.4.4 Case study modelling

Courtyards were modelled as groups of buildings, 20×20 m² each, representing approximately three residential apartments. Floor to ceiling heights were set to 3 m such that a single step size of building heights (Table 6.2) corresponds to four floors. Each courtyard was surrounded by an identical context within a 3×3 grid. Distances between courtyards in both North-South and East-West directions had the same value in each iteration. The ground was modelled as EnergyPlus thermal zones, where the upper surfaces represent the ground to account for the ground surface temperature and the associated contribution to mean radiant temperatures for the UTCI calculation.

In each courtyard type, these ground zones were modelled in the middle of the inner court ($20 \text{ m} \times 20 \text{ m}$) as well as the middle of each of the surrounding streets ($20 \text{ m} \times \text{interspaces m}$) (Figure 6.4-bottom row). This ensures an even comparison between the different types of courtyards. Ground zones were further subdivided into four zones each with a receptor point each separated 10 m apart, corresponding to a total of 20 receptor points. Moreover, the central block was modelled as multiple EnergyPlus thermal zones, respective to the number of floors, while the other eight surrounding courtyards were defined as shading objects. As for the former, window-to-wall ratios were set as 15% for Northern and Southern façades, and 12% for Eastern and Western façades, within the thresholds of the Egyptian Residential Energy Code (MHUUC, 2005).

6.4.5 Simulation setup

Simulation parameters were kept fixed for all the simulations herein. For the UWG setup, streets' albedo was set to 0.2, while walls and roofs albedo were set to 0.4 and 0.3, respectively. A value of 4 W/m^2 was used as the sensible anthropogenic heat generated in urban canyons, typical of a residential area. The default values governing the height of the urban boundary layer were used; 1000 m and 50 m during the daytime and night-time, respectively, while the inversion height was set to 150 m. For EnergyPlus parameters, the solar distribution module, "full interior and exterior with reflections", was used, while "Ideal Air Loads" used for HVAC. The thermal properties of the construction materials (Appendix A, Table A. 2) were set according to the Egyptian Residential Energy Code (MHUUC, 2005).

The HVAC and occupation schedules were set following the study of Mahdy and Nikolopoulou (2014), considering the common lifestyle of Egyptian residents. HVAC, zone loads, and infiltration input parameters for EnergyPlus as used in this study can be found in Appendix A, Table A. 3.

6.5 Results

For courtyard types A, B and C, the search process was stopped upon the end of generation 52, 54 and 100, respectively, in conjunction with the convergence towards the Pareto optimal non-dominated solutions and where further improvements on the Pareto front cannot be noticed (Zhao & Du, 2020). Given the nature of heuristic search techniques, some solutions, as selected randomly, were re-evaluated several times in comparison to other solutions. It is worth mentioning that the Ladybug-tools workflow is deterministic, in other words, several simulations of one case (specific height, width, and orientation) entail identical results (objective function values) each time. This allowed duplicate solutions to be removed using the explicit components of Octopus during the post-processing of the results. Hence, a total of 1129, 1856 and 2848 discrete geometrical cases were investigated in each type, respectively. Throughout the rest of this paper, the 1129, 1856 and 2848 solutions are referred to as the entire sample of types A, B and C, respectively. Figure 6.7 shows the output solutions for each type, plotted on the objective space, with the Pareto front optimal solutions highlighted. For the Pareto fronts, a hypervolume of 0.83, 0.81 and 0.83 was recorded for types A, B and C, respectively, which indicates high dominance of the Pareto set. Similar hypervolume measures were reported by Wortmann and Natanian (2021) when investigating the optimisation of courtyards and high rise buildings.

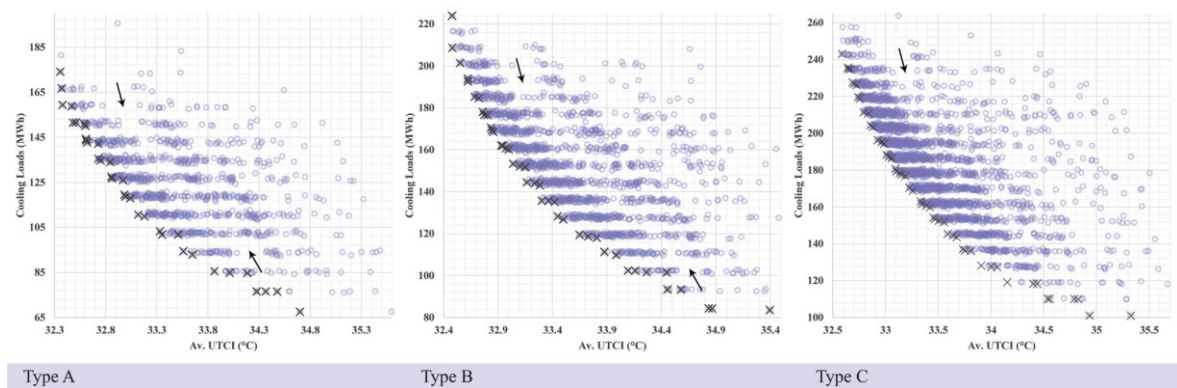


Figure 6.7: Solutions on the objective space for each courtyard type. Pareto front optimal solutions are marked with black crosses.

From Figure 6.7, it can be seen that the conflicting relationship between cooling loads and the Av. UTCI differs for each courtyard type. In type A, cooling loads gradually decrease as Av. UTCI increases until 33.3 °C, after which the conflict increases. In type B and C, the conflict point changes to 33.1 °C and 33.4 °C, respectively. Furthermore, Av. UTCI appears to be more distributed than cooling loads in the three types, due to the setting of a single step size of building heights corresponding to four building floors. This has also resulted in UTCI blind spots which are indicated by arrows in Figure 6.7 in each cooling loads category. These spots, however, are less evident in type C due to greater variability of building heights in this type. Upon the final generation of type A, B and C, the numbers of Pareto optimal solutions obtained were 35, 42 and 52, respectively. The three Pareto optimal sets are compared in Figure 6.8-c, where type A outperforms both types B and C regarding Av. UTCI, since the inner court is more exposed to solar radiation in the latter two, but also regarding cooling loads due to having smaller floor area.

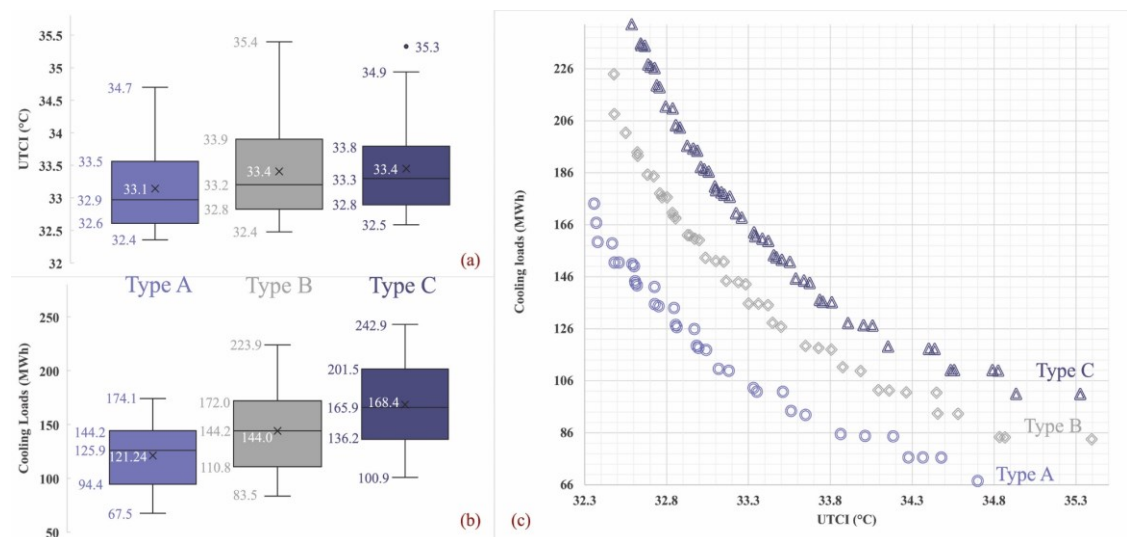


Figure 6.8: Distribution of the Pareto front solutions, in terms of (a) Av. UTCI, (b) Cooling loads and (c) both objectives.

This is further demonstrated in Figure 6.8-a and Figure 6.8-b, where type A shows the lowest minimum, lower quartile, upper quartile, and maximum values of Av. UTCI. Type B and C have a similar average of 33.4 °C UTCI, even though type C has slightly lower 3rd quartile and maximum, potentially due to being run for 100 generations, and hence, converging around the solutions with the best trade-off. Av. UTCI ranges of 2.34, 2.92 and 2.34 °C were covered by the Pareto sets for types A, B and C, respectively, excluding a single outlier in type C.

The corresponding ranges for cooling energy were 106.62, 140.41 and 142.04 MWh. The lowest cooling energy is achieved in the solutions with the shortest buildings, in which the trade-off becomes a function of orientation and interspaces, whose effect cannot compensate for the increase in Av. UTCI due to the lack of shading. This explains the relatively higher conflict between the two objectives in the lower ~30% of cooling energy.

6.5.1 *The effect of design parameters*

A series of multiple regression analyses for the entire samples revealed that the design parameters exhibit significant correlations with the objective functions; type C is the strongest regarding Av. UTCI ($F(14, 2832) = 905, p < 0.0001, R^2 = 0.81$), followed by type B and type A; type B is the strongest regarding cooling loads ($F(12, 1843) = 137227, p < 0.0001, R^2 = 0.998$), followed by type C and type A. Nevertheless, interspaces and orientation showed insignificant individual correlations ($p > 0.05$). It was found that all the Pareto optimal solutions have the same interspaces (12 m), and most of them have the same orientation (45° in case of type A, and 135° in case of types B and C). Therefore, the effect of interspaces and orientation is discussed below for the entire sample.

6.5.1.1 Interspaces and orientation

Figure 6.9-a shows that interspaces of 12 m exhibit an incomparable predominance over the other interspaces in all courtyard types. This indicates that 12 m interspaces always yield lower values for both objective functions, and therefore was the most investigated by the search algorithm. Moreover, with wider interspaces, the more courtyards are elongated, receptor points receive more longwave radiation from building surfaces. This explains the larger differences between interspaces in types B and C. As mentioned, orientations 45° and 135° appear to be dominant in all types. The performance of courtyards is subject to several processes: the amount of shading on the streets and the buildings, thereby improving the Av. UTCI, and the amount of solar heat gain, increasing cooling loads, but also increasing the outside surface temperatures, thereby deteriorating the Av. UTCI. Given the asymmetry of the microclimatic parameters over the course of a day (Figure 6.6), where higher solar radiation and air temperatures are evident in the afternoon, orientation 135° becomes favourable for type C for lower cooling loads, provided there is adequate shading from the context geometry, while orientation 45° decreases the Av. UTCI. The opposite is true for type B.

The frequency distribution of the orientation is shown in Figure 6.9-b, with orientations 45° and 135° being predominant in types B and C. The preponderance of orientation 45° , compared to the supposedly equivalent, 135° , in type A can only be explained by the performance difference due to the positioning of higher buildings. For instance, in 12 m interspaces, a total of 150 cases simulated in orientation 135° , compared to 547 cases in orientation 45° ; having the Floor Area Ratio (FAR) -the ratio between the blocks' ground floor area multiplied by the number of floors, and the lot area- as an indication for building heights, the 150 cases have an average FAR of 4.29 compared to 4.16 for the 547 cases, albeit with higher Av. UTCI and cooling loads. This indicates that, most of the 150 cases had higher buildings positioned where they contribute less to shading (following section). Therefore, in mating selection, the algorithm selected orientation 45° in preference to orientation 135° .

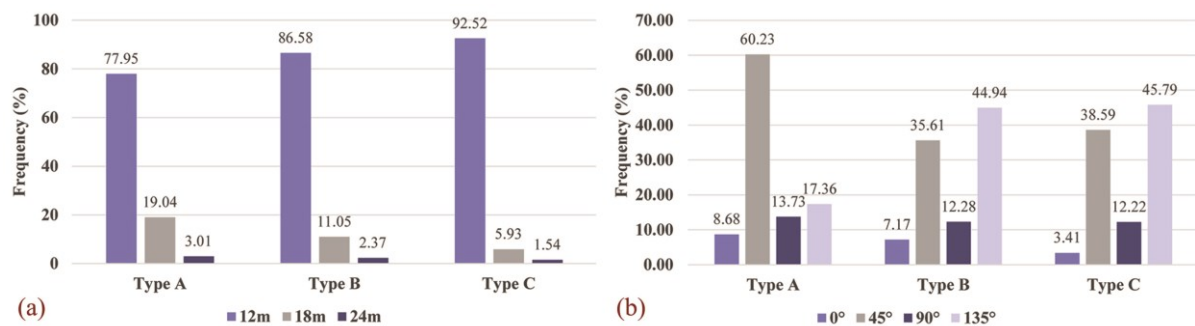


Figure 6.9: Frequency distribution of (a) interspaces, and (b) orientation, over the entire samples.

The performance of all courtyards comprising various building heights, but having the same orientation and interspaces, is averaged to further demonstrate the effect of orientation and interspaces on each objective. Figure 6.10 demonstrates the Av. UTCI performance, and Figure 6.11 demonstrates the cooling loads, where each grid cell in the figures is scaled with a percentage of average FAR reduction relative to the highest average FAR (4.31 in type A, 12 m interspaces, and rotated 90°). As shown in Figure 6.10, orientations 45° and 135° appear to be favourable for all types, especially within 12 m interspaces.

The differences between orientations 45° and 135° and between orientations 0° and 90° are attributed to the FAR; lower FAR (lower building heights) yields higher Av. UTCI. This is clearly seen in type A orientated 0° and type B orientated 90° within 24 m interspaces, and in type C orientated 0° within 18 m interspaces.

This also implies that FAR has a decisive impact on the Av. UTCI in orientations 0° and 90°. For both types B and C, the surrounding streets perform as urban canyons, and hence maintain comfortable thermal conditions in NS direction (90°) with narrower interspaces, while EW direction (0°) becomes favourable in wider interspaces, as elaborated in Ibrahim *et al.* (2021b).

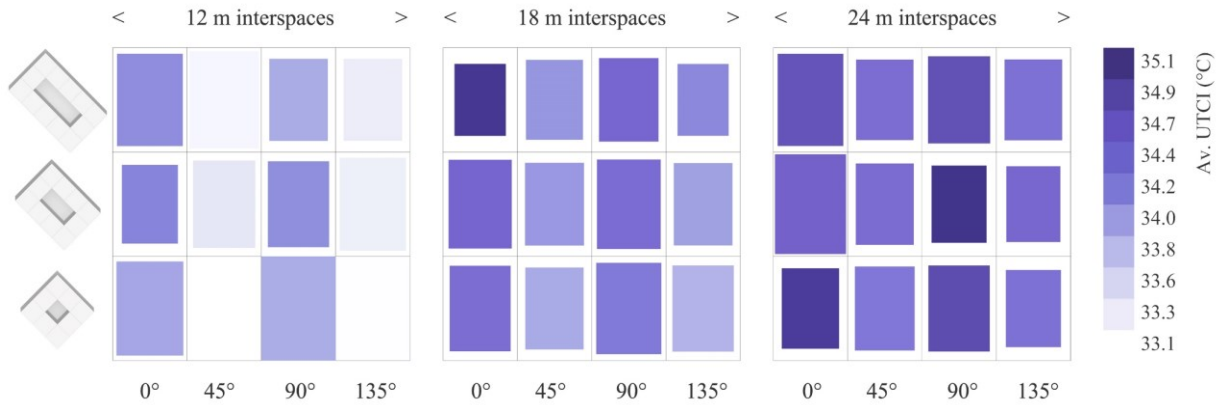


Figure 6.10: Performance of different courtyard types in different orientations and interspaces regarding Av. UTCI. Grid cells are scaled with regard to FAR reduction relative to the highest FAR, recorded in type A, 12 m interspaces and rotated 90°.

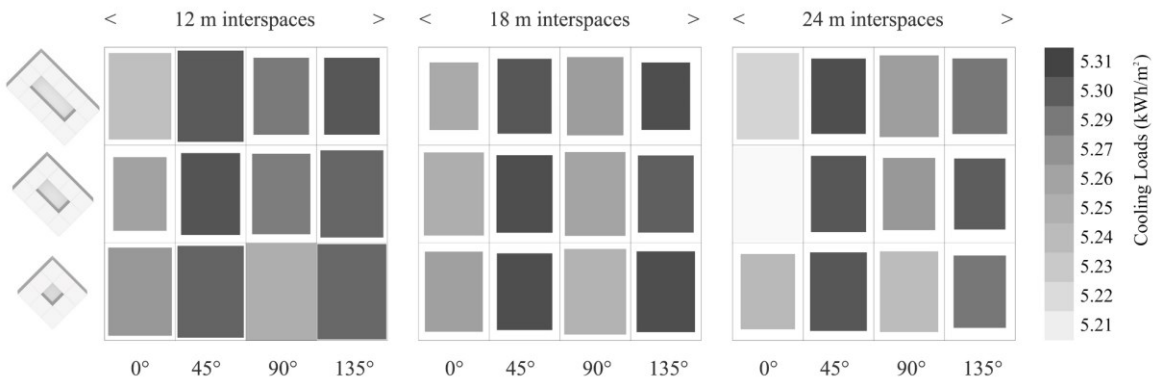


Figure 6.11: Performance of different courtyard types in different orientations and interspaces regarding the cooling loads. Grid cells are scaled with regard to FAR reduction relative to the highest FAR, recorded in type A, 12 m interspaces and rotated 90°.

Figure 6.11 shows the cooling loads normalised by the total floor area. Orientations 0° and 90° appear to be favourable for all types; Types B and C perform slightly better in orientation 0° when the long axis is mostly exposed during midday with solar altitude of 82°, than in orientation 90° where the long axis is exposed during the early and afternoon hours. Again, some differences between orientations 45° and 135° and between orientations 0° and 90° are attributed to the

FAR; higher FAR yields lower normalised cooling loads, where FAR has a stronger impact in orientations 45° and 135° . Although wider interspaces yield higher cooling loads, there are few instances with lower cooling loads in 12 m interspaces; after a sensitivity analysis, the difference is attributed to the number of cases with lower cooling loads before averaging, not to mention the difference in FAR.

6.5.1.2 Building heights

The effects of building heights on the performance of the Pareto optimal sets are represented by the frequency distribution of each building height in the Figure 6.12-16. Figure 6.12 shows that, in a 45° orientation, buildings in the SW, W, NE and S directions are crucial for providing shading both on the inner court and on the streets, but also on the other buildings' roofs, therefore they possess the greatest number of instances of 36 m height. Note that the heights of surrounding context are identical to those of the central block, thus are no less important for mutual shading. Following in importance are the buildings in the N and E directions, casting shade on the streets in the morning and afternoon hours, respectively, therefore they possess the greatest number of instances of 24 m height. The buildings in the SE and NW contribute the least to shading, thus they possess the greatest number of instances of 12 m height to balance the cooling loads.

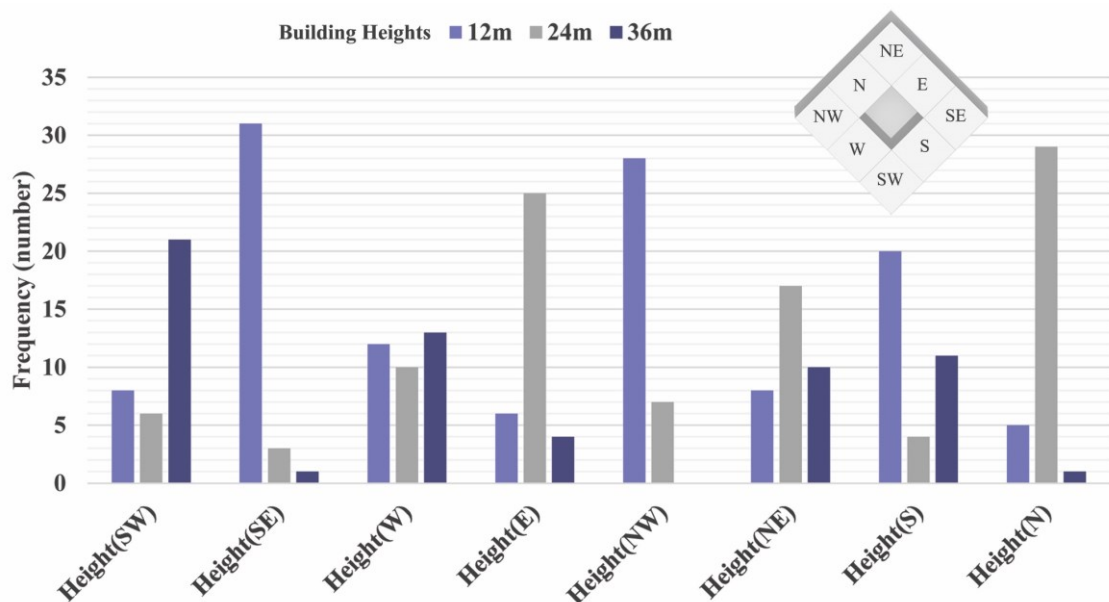


Figure 6.12: Frequency distribution of building heights in each direction of the courtyard in the Pareto optimal set of type A. The guiding key in the top right corner exemplifies an instance rotated 45° , as it appears most often in the set. Guiding keys for other orientations can be found in Appendix B, Figure B. 1.

. Table 6.3 lists the correlation of building heights with both objectives. Building heights with the greatest number of instances of 24 m together with 36 m exhibit the strongest correlation with both objectives. The buildings with the greatest number of instances of 12 m together with the fewest instances of 36 m exhibit the weakest correlation.

Table 6.3: Correlation coefficients (R) of building heights in each direction of the courtyard type A with both objectives.

Objective/Height	SW	SE	W	E	NW	NE	S	N
Cooling loads	0.77	0.42	0.84	0.79	0.43	0.71	0.77	0.55
Av. UTCI	-0.81	-0.34	-0.78	-0.82	-0.35	-0.69	-0.64	-0.66

In an 135° orientation of type B, as shown in Figure 6.13, buildings in the NNW and SSE directions cast shade on the inner court, on the streets and the roofs of the other buildings, therefore they possess the greatest number of instances of 36 m height. Following in significance are the buildings in the SE, E, W and SSW directions, which provide shade on the streets. The effect of the former two directions is critical in the morning hours, whilst that of the latter two is critical in the afternoon hours. Notably, these four buildings share the greatest number of instances of 24 m height, or instances of 24 m height together with 36 m height.

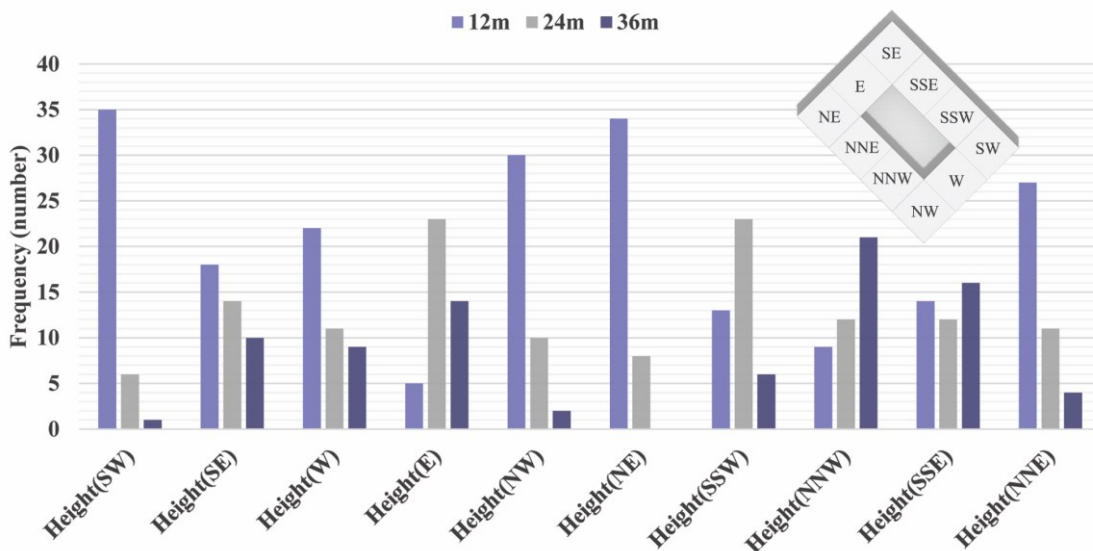


Figure 6.13: Frequency distribution of building heights in each direction of the courtyard in the Pareto optimal set of type B. The guiding key in the top right corner exemplifies an instance rotated 135° as it appears most often in the set. Guiding keys for other orientations can be found in Appendix B, Figure B. 1.

The buildings in the SW, NW, SE and NNE contribute the least to shading, thus they possess the greatest number of instances of 12 m height to reduce the cooling loads. Table 6.4 confirms these findings, where building heights with the greatest number of instances of 24 m together with 36 m in Figure 6.13 exhibit the strongest correlation with both objectives. The buildings with the greatest number of instances of 12 m together with the fewest instances of 36 m exhibit the weakest correlation.

Table 6.4: Correlation coefficients (R) of building heights in each direction of the courtyard type B with both objectives.

Objective/Height	SW	SE	W	E	NW	NE	SSW	NNW	SSE	NNE
Cooling loads	0.16	0.82	0.74	0.84	0.70	0.06	0.75	0.85	0.82	0.44
Av. UTCI	-0.18	-0.73	-0.64	-0.84	-0.58	-0.08	-0.77	-0.88	-0.80	-0.33

In the case of type C, the search algorithm converged towards the cases with the fewest number of taller buildings, but also the cases with a gradient of heights in one direction (e.g., the Northern) which opposes the gradient of heights in the other direction (the Southern). Within an orientation of 45° or 135° , these taller buildings are the ones in the SW, E, NE, S, N and NNE directions (Figure 6.14). Again, these building exhibit the strongest correlation with both objectives (Table 6.5).

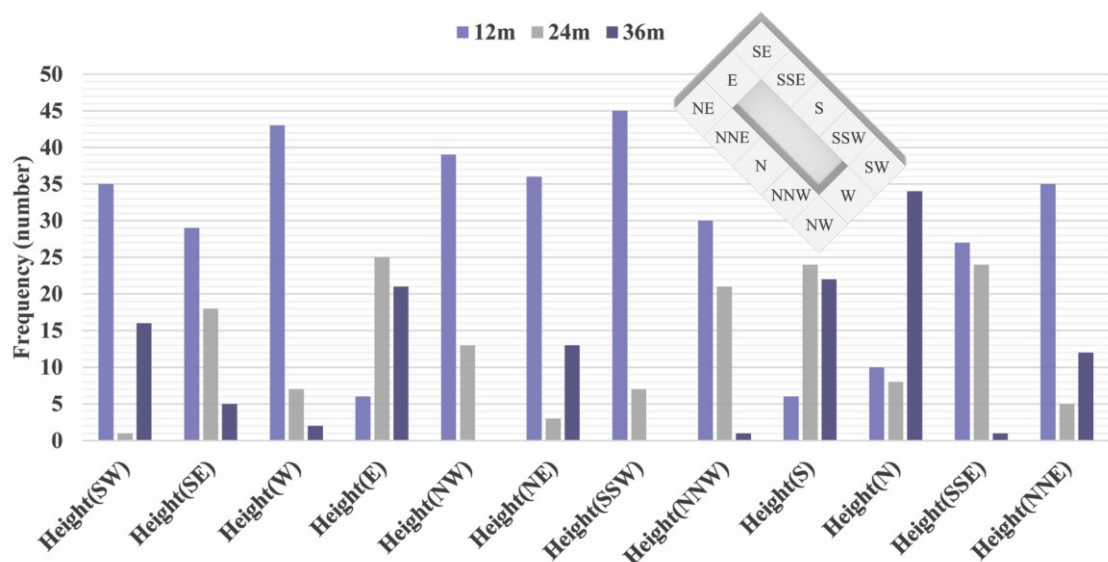


Figure 6.14: Frequency distribution of building heights in each direction of the courtyard in the Pareto optimal set of type C. The guiding key in the top right corner exemplifies an instance rotated 135° as it exists the most in the set. Guiding keys for other orientations can be found in Appendix B, Figure B. 1.

The next most significant are the buildings which contribute less to the shading of the inner court, and hence maintain a balance between mutual shading of streets and the inner court on one hand, and the cooling loads on the other. These are the ones in the W, SSW, NNW and SSE directions, which possess a combination of 12 m and 24 m height and exhibit moderate correlations with the objectives. An exception is the buildings in the SE and NW directions, which exhibit the weakest correlations. These buildings maintain a 12 m height in the instances with lower Av. UTCI, orientated 45°, however, maintain a 24 m height within those with lower cooling loads, orientated 135°.

Table 6.5: Correlation coefficients (R) of building heights in each direction of the courtyard type C with both objectives.

Obj./Height	SW	SE	W	E	NW	NE	SSW	NNW	S	N	SSE	NNE
Cooling loads	0.77	-0.08	0.60	0.88	0.09	0.81	0.58	0.45	0.88	0.79	0.41	0.82
Av. UTCI	-0.65	-0.10	-0.45	-0.89	-0.21	-0.65	-0.43	-0.47	-0.90	-0.87	-0.35	-0.66

6.6 Discussion

Some solutions offer the best performance in one objective, but the worst performance in the other objective. Other solutions offer a trade-off between the different objectives. It is then the choice of urban planners and designers in the pre-design stages to define the best solution(s) according to the design requirements. A common approach in multi-objective decision-making is the weighted sum method, where each objective $f_i(x)$ is assigned a weight coefficient according to its priority in the decision-making process. The calculation of the weighted sum $F(x)$ is as follows (Delgarm *et al.*, 2016):

$$F(x) = \alpha_i \sum_{i=1}^{i=n} \frac{f_i(x) - f_i(x_{min})}{f_i(x_{max}) - f_i(x_{min})} \tag{Equation 6.1}$$

Where α_i is the weight coefficient of one objective and the sum of all coefficients equals 1. The subscripts min and max denote the minimum and maximum values in the set, respectively, and n is the number of objectives.

In order to define a threshold for the optimum performance in both objectives, a reference case is assigned in each type, which results in the worst performance in both objectives simultaneously. These are the cases with 24 m interspaces, 36 m height of all buildings, and orientated 0°. Using the weighted sum method, and using equal weights for both objectives (0.5), the best performing 12

solutions outperforming the reference case in each respective type are depicted in the Figure 6.15-19, where the lower left legend shows the position of the solution on the pareto front, with Av. UTCI on the x-axis and cooling loads on the y-axis.

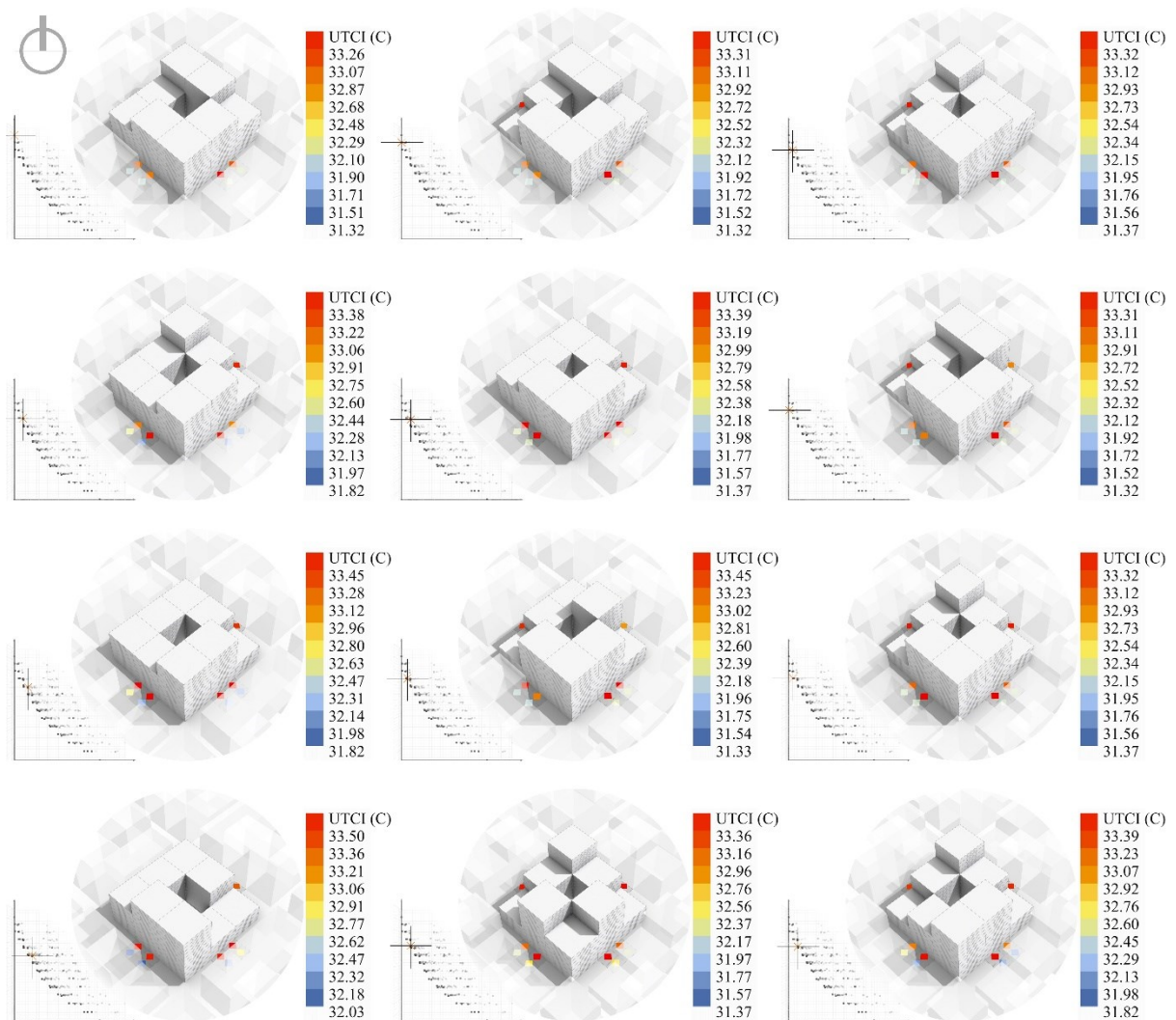


Figure 6.15: The best 12 cases of type A which outperform the reference case in both objectives.

It should be noticed that the optimised cases in all types fall within the part of the Pareto front, which prioritise the Av. UTCI over the cooling loads. This is due to the large difference between the maximum and minimum cooling loads, which in turn has, to some extent, diminished its weight. Other weight coefficients can be used to counterbalance such difference. However, given that cooling loads in this study are calculated for the entire floor space, they represent a worst-case scenario, thus weighting coefficients which prioritise the Av. UTCI were chosen. For type A, all the optimised cases are rotated 45° with 12 m interspaces.

Buildings are the highest at the SW and NE directions and slope down to the SE and NW directions (Figure 6.15). Natanian *et al.* (2021) optimised the outdoor shading index (ratio between exposed and shaded streets) for a courtyard building, in a hot Mediterranean climate at 32° N latitude, similar to the present study, having a W/L ratio of ~ 1.5 in an EW orientation. The optimum case was also shown to have the highest voxels in the NE direction, sloping down towards the NW direction.

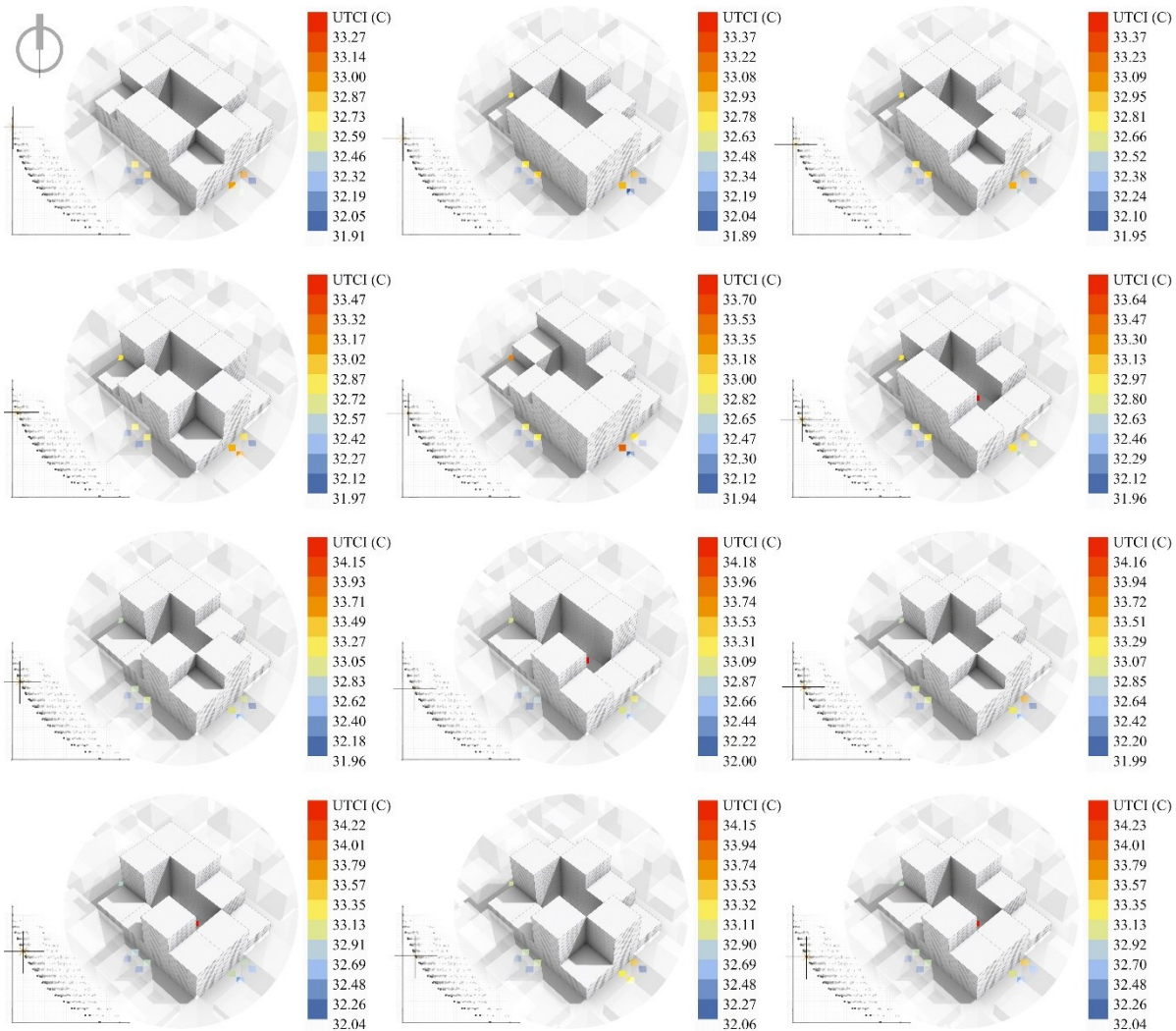


Figure 6.16: The best 12 cases of type B which outperform the reference case in both objectives.

For type B, all the optimised cases are rotated 135° with 12 m interspaces. Buildings are the highest at the NNW, SSE, E and W directions and slope down towards the NE and SW directions (Figure 6.16). Yezioro *et al.* (2006) recommended using H/W of 0.5 in the case of NW-SE courtyards at 32° N latitude with W/L of 2 (type B in this study) to maximise the ratio of exposed surface area to the total area in winter. These criteria are met in most cases of type B in the NE and

SW directions of the courtyard. This indicates that the optimum cases of type B receive adequate insolation at least in the morning and the afternoon in winter.

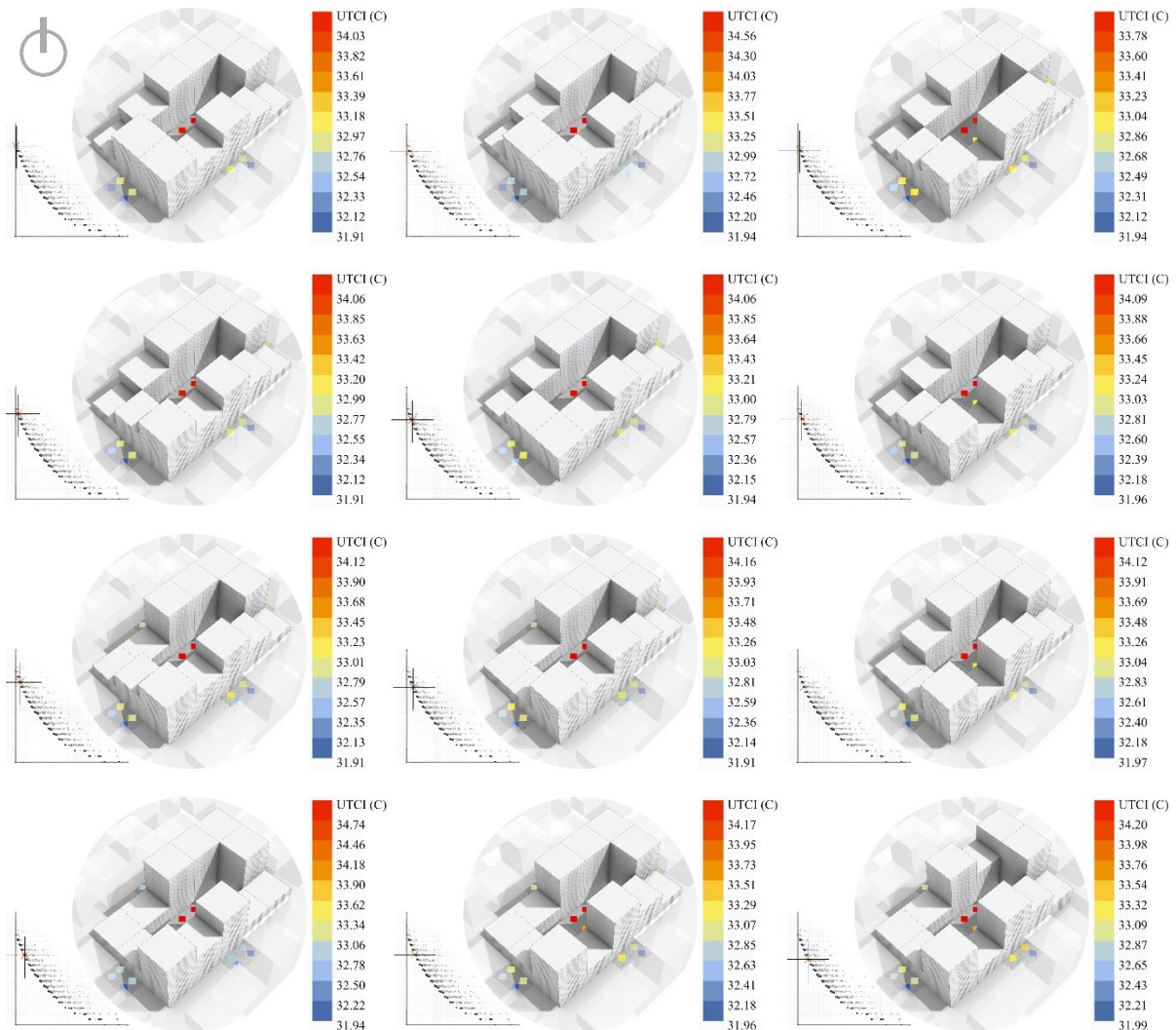


Figure 6.17: The best 12 cases of type C which outperform the reference case in both objectives.

For type C, all the optimised cases are rotated 45° with 12 m interspaces. Buildings are the highest at the SW direction and slope down towards the SE direction, as opposed to the declination of the buildings in the NE direction towards the NW direction of the courtyard. The optimum cases almost appear in the shape of 2 opposing L-shapes, in agreement with the conceptualisation proposed in Galal *et al.* (2020) for the mitigation of heat stress in extreme hot environments in Egypt.

The performance of the optimum solutions relative to the reference case in both objectives are presented in Table 6.6. The optimum cases appear to be capable of improving the cooling loads in types A, B and C by up to 31.7, 30.9 and 30.8%, respectively, and improving the Av. UTCI by 1.5, 1.6 and 1.6 °C respectively.

Table 6.6: Comparisons between the optimal solutions in each type and the respective reference case.

	Type A				Type B				Type C			
	cooling loads (MWh)	Av. UTCI (°C)	Cooling Diff (%)	UTCI Diff (°C)	cooling loads (MWh)	Av. UTCI (°C)	Cooling Diff (%)	UTCI Diff (°C)	cooling loads (MWh)	Av. UTCI (°C)	Cooling Diff (%)	UTCI Diff (°C)
Ref	196.2	33.87	-	-	245.1	34.07	-	-	293.8	34.23	-	-
1	174.1	33.26	-11.3	-1.5	223.9	32.48	-8.6	-1.6	243.0	32.59	-17.3	-1.6
2	166.8	32.37	-15	-1.5	208.6	32.48	-14.9	-1.6	234.8	32.67	-20.1	-1.6
3	158.8	32.47	-19.1	-1.4	201.4	32.55	-17.9	-1.5	235.6	32.64	-19.8	-1.6
4	150.9	32.59	-23.1	-1.3	193.9	32.62	-20.9	-1.5	235.0	32.65	-20.0	-1.6
5	150.1	32.60	-23.5	-1.3	192.6	32.62	-21.4	-1.4	226.2	32.73	-23.0	-1.5
6	159.4	32.38	-18.8	-1.5	184.6	32.72	-24.7	-1.3	227.6	32.69	-22.5	-1.5
7	142.1	32.73	-27.6	-1.1	185.3	32.68	-24.4	-1.4	226.8	32.70	-22.8	-1.5
8	151.5	32.51	-22.8	-1.4	176.5	32.8	-28.0	-1.3	218.8	32.76	-25.5	-1.5
9	151.5	32.48	-22.8	-1.4	178.1	32.76	-27.4	-1.3	219.6	32.74	-25.3	-1.5
10	134.0	32.85	-31.7	-1.0	176.6	32.77	-27.9	-1.3	210.7	32.84	-28.3	-1.4
11	144.3	32.61	-26.5	-1.3	170.6	32.84	-30.4	-1.2	211.4	32.79	-28.0	-1.4
12	143.6	32.61	-26.8	-1.3	169.3	32.84	-30.9	-1.2	203.3	32.88	-30.8	-1.4

To study the insolation performance of the optimal solutions in winter, a case of type B was compared to the same case with maximum building heights. The latter meets the criteria recommended by Muhaisen (2006); having a perimeter-to-height ratio of 7.7, which maintains the reduction in sunlit area in winter below 50% from a reference case with the maximum solar exposure. Radiation analysis was conducted in a typical cold week, 6th to 12th of December, with heating set point equal to 18°C to study their performance with respect to heating loads. Both cases have shown Av. UTCI within the neutral range with no thermal stress, thus the Av. UTCI is not shown here. Figure 6.18 depicts the radiation analysis of the two cases, showing the optimal case of type B improving the insolation of the surfaces. The difference in insolation was 188 kWh/m² with an increase in the percentage of exposed surfaces by 4%. Moreover, the optimum case of type B has 4.2 W/m² lower heating loads due to increased solar heat gain.

Based on the design attributes of the optimal cases presented above, Figure 6.19 shows the range of building heights of the best performing 12 cases in each courtyard type. The optimum design attributes for each type according to the best performing 12 cases presented above were interpreted into design guidelines in

Table 6.7. The recommended design guidelines offer a wide range of building heights in each direction of the courtyard block, especially where the height of the building does not significantly contribute to shading. This offers a great flexibility for urban designers aiming to retain the benefits of urban compactness, without degrading other environmental qualities such as urban daylighting.

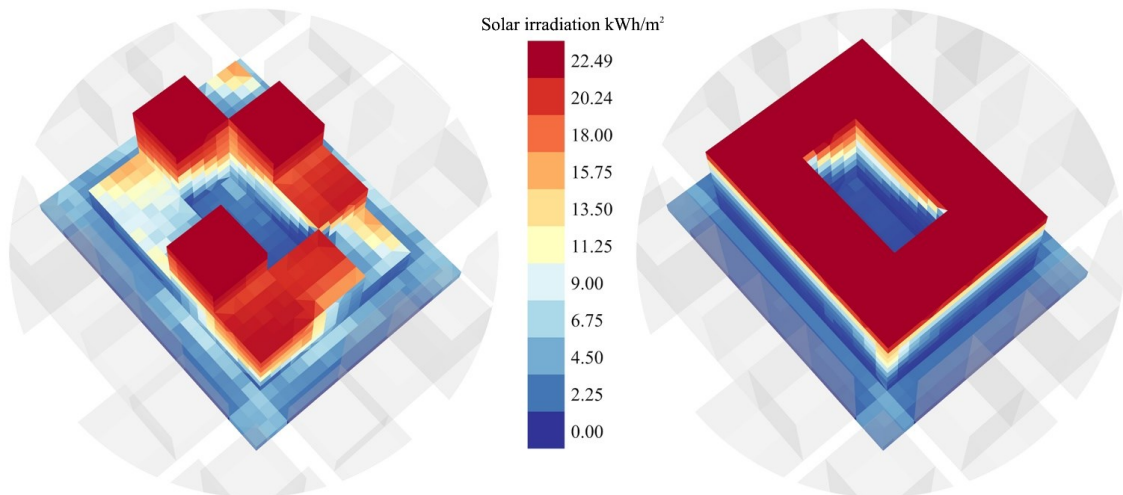


Figure 6.18: Solar radiation analysis of (left) a selected case of type B and (right) a reference case as recommended in Muhaisen (2006).

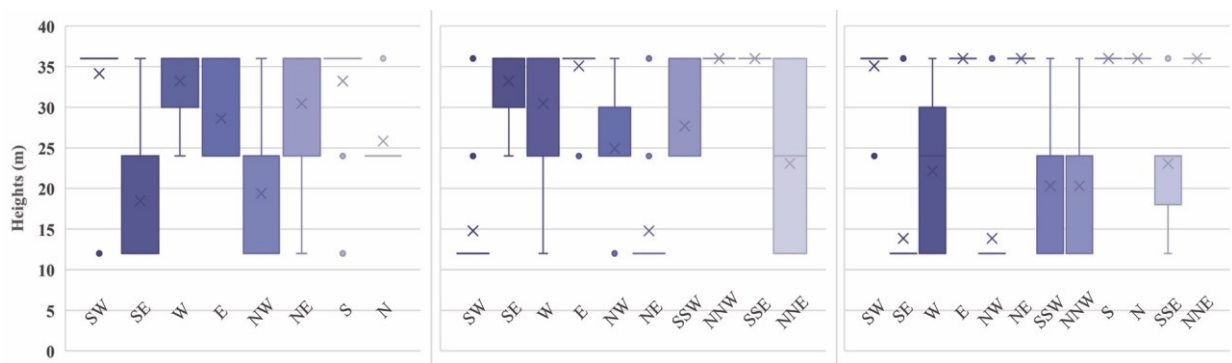


Figure 6.19: Range of building heights of the best 12 cases (figures 6.17-19) in type A (left), type B (middle) and type C (right).

Table 6.7: Design guidelines for each courtyard type based on the results of the study.

Type	Inter-spaces	Orient.	Building heights (m)											
			SW	SE	W	E	NW	NE	S	N	SSW	NNW	SSE	NNE
A	12 m	45°	34-36	12-24	30-36	24-36	12-24	24-36	33-36	24-26				
B	12 m	135°	12-15	30-36	24-36	35-36	24-30	12-15			24-36	36	36	12-36
C	12 m	45°	35-36	12-14	12-30	36	12-14	36	36	36	12-24	12-24	18-24	36

Furthermore, with the inner courtyards having greater openness to the sky, the design schemes could harness the benefits of shading inside the courtyard, but also improve the air flow within the inner court and hence reducing the thermal isolation from the ambient temperatures. Additionally, the design schemes support the concept of mixed-use developments, where lower buildings could serve as a commercial podium, in which case, higher buildings could be designed with greater variability in household sizes and economic levels, for instance, designing other buildings' roofs as private outdoor spaces. Based on the general characteristics of the Pareto optimal sets, the following remarks can be deduced:

- Square courtyard blocks provide better thermal and energy performance than elongated ones, since building and ground surfaces of the former receive less radiation.
- Minimum interspaces of 12 m, which correspond to compact configurations with Building Coverage Ratio (BCR) of almost 55-60%, yield the best thermal and energy performance in all courtyard types.
- Orientations 45° and 135° provide the best trade-off between solar shading to reduce the UTCI, and solar heat gain to reduce the cooling loads, in all courtyard types.
- For square courtyard blocks, as in a 45° rotation (Figure B. 1 - annotations omitted), the best thermal and energy performance can be achieved when the southern and northern parts have a FAR of almost 8, and the eastern and western parts have a FAR of 4.5.
- For two-fold elongated courtyards, as in a 135° rotation (Figure B. 1 - annotations omitted), the best thermal and energy performance can be achieved when the southern and northern parts have a FAR of almost 7-8, and the eastern and western parts have a FAR of 5-6.
- For three-fold elongated courtyards, the best thermal performance can be achieved in a 45° rotation (Figure B. 1 - annotations omitted), provided the southern and northern parts have FAR's of almost 8 and 11, respectively, and the eastern and western parts have a FAR of almost 7.5.
- The best energy performance in the latter type can be achieved in a 135° rotation (Figure B. 1 - annotations omitted), provided the southern and northern parts have FAR's of almost 5 and 7, respectively, and the eastern and western parts have a FAR of almost 3.5.

This study was limited by the number of parametric combinations shaped by the design variables investigated. Nevertheless, the obtained results have shed the light on the range of optimum design attributes of energy efficient and thermally comfortable courtyard blocks. This helps to guide future research in this particular field, but also in other fields of climate-based and responsive design of the urban built environments. Also, the methodology used in this paper could be applied in other climatic zones.

6.7 Conclusion

This paper reconceptualised the Residential Solar Block (RSB) proposed by Okeil (2010) to find the optimum design attributes of courtyard blocks in the hot-arid climate of Cairo, Egypt. For doing so, a methodology was presented to simulate the orientation, interspaces and building heights of three courtyard blocks to find the best performing cases with respect to cooling loads and the average UTCI in summer. Given the huge number of permutations to be simulated, which exceeded hundreds of thousands, an evolutionary algorithm was used to search for the optimal set of solutions. After only 3% of the simulation runs that would be required for a brute force approach, the optimised cases were found to outperform conventional courtyard blocks in both design objectives, but also with respect to the solar heat gain in winter. This is in agreement with Okeil's proposal, albeit with different proportions for the optimised cases. The methodology presented paves the way for future optimisation studies aiming to scrutinise the relationship between design parameters and passive solar design. For instance, to focus the simulations around the optimum values obtained in this study (10 and 14 m interspaces, 30 and 60° orientation, and 3 m higher or lower the optimum height of each building). Integrating building design parameters, such as glazing materials, window-to-walls ratio, and occupancy schedules into the optimisation process is another potential future extension to this study. To this end, with the number of design parameters significantly increased, Machine Learning techniques could also be integrated in tandem with evolutionary algorithms, which are also available in the Octopus plugin in Grasshopper. The optimised design attributes provide urban designers with a variety of compact and potentially mixed-use design schemes, promoting the creation of socially, economically, and environmentally sustainable built environments.

Data Availability Statement

Data available in a publicly accessible repository. The data presented in this study are openly available in University of Bath Research Data Archive at <https://doi.org/10.15125/BATH-01137> (Ibrahim, 2022).

Appendix A

Table A. 2: Thermal and physical properties of the construction materials used in this study.

Construction	Thickness (cm)	U-value (W/m ² K)	Material - outer to inner face ↓	Thickness (cm)	Density (kg/m ³)	Thermal conductivity (W/m.K)	Specific heat (J/kg.K)	Thermal Resistance (m ² K/W)
Full red-brick wall with expanded polystyrene insulation	32	1.058	Plaster	0.5	600	0.16	1000	0.031
			Mortar	2	1570	0.9	896	0.022
			polystyrene	2	35	0.034	1400	0.588
			Full Brick	25	1950	1	829	0.25
			Mortar	2	1570	0.9	896	0.022
			Plaster	0.5	600	0.16	1000	0.031
Standard reinforced concrete roof	29	0.627	Tiles	1	2100	1.4	1000	0.007
			Mortar	2	1570	0.9	896	0.022
			Sand	5	1520	0.33	800	0.152
			Polystyrene	4	35	0.034	1400	1.176
			Damp proof	2	1055	0.15	1000	1.333
			R. concrete	15	2460	1.44	1000	0.104
Standard reinforced concrete floor	20	3.785	Tiles	1	2100	1.4	1000	0.007
			Mortar	2	1570	0.9	896	0.022
			Sand	5	1520	0.33	800	0.152
			R. concrete	12	2460	1.44	1000	0.083
Clear Glass	Thickness: 0.6		U-value: 5.76		SHGC: 0.71		Transmissivity: 0.65	

Table A. 3: The simulation parameters used in the study.

Parameter	Value	
HVAC	Cooling setpoint	25°
	Schedule	All day
Zone Loads	Equipment	4 W/m ²
	People	0.04 People/m ²
	Schedule	Weekdays: 00:00 (50%) - 06:00 (75%) - 08:00 (25%) - 16:00 (75%) - 18:00 (100%) - 23:00 (75%) Weekends: 00:00 (50%) - 11:00 (75%) - 21:00 (100%) - 23:00 (75%)
	Lighting	3 W/m ²
	Schedule	Weekdays: 00:00 (25%) - 06:00 (40%) - 08:00 (15%) - 16:00 (40%) - 18:00 (150%) - 23:00 (40%) Weekends: 00:00 (50%) - 11:00 (75%) - 21:00 (100%) - 23:00 (75%)
Infiltration	0.003 m ³ /s-m ²	

Appendix B

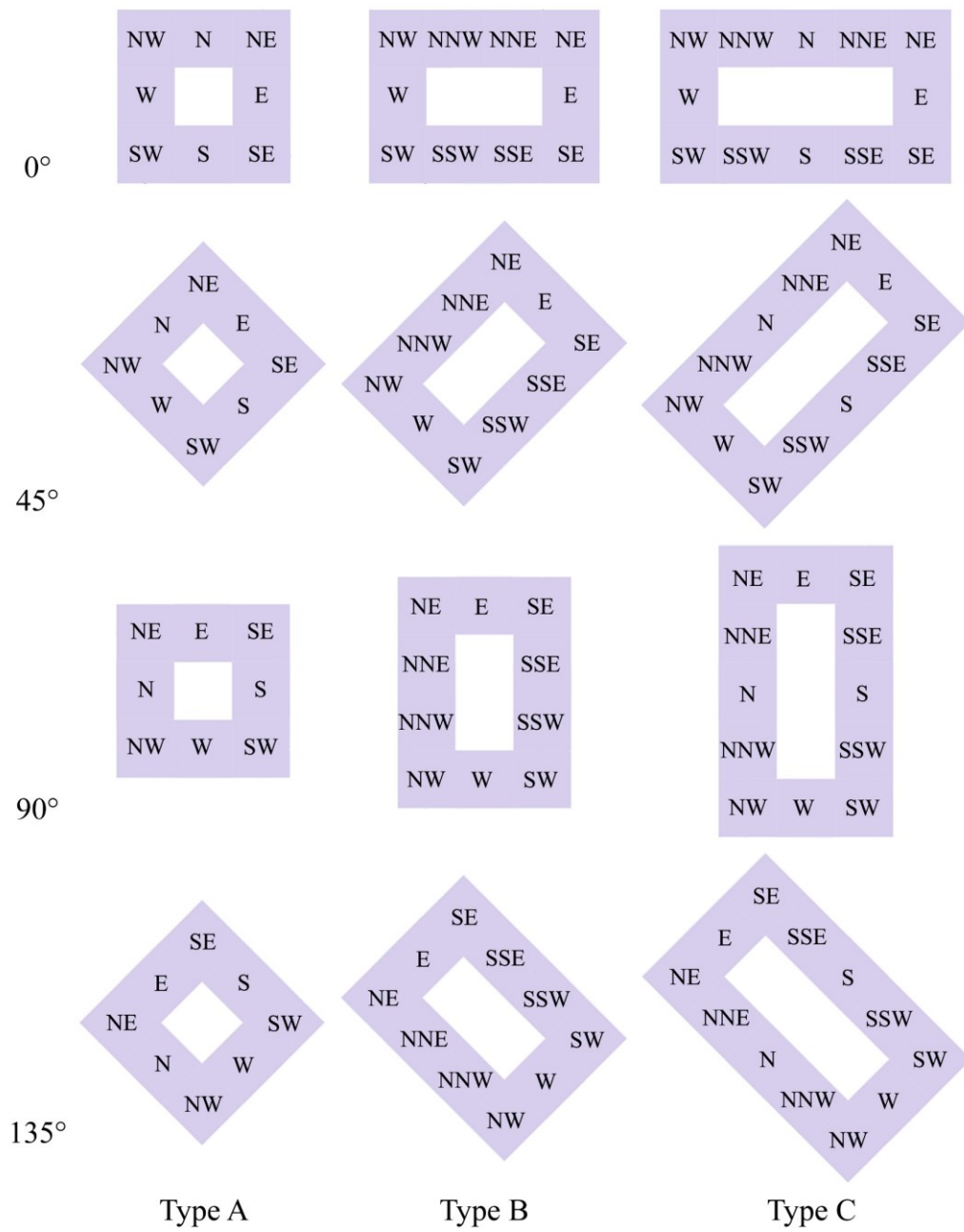


Figure B. 1: Locations of buildings in different orientations

6.8 References

- Al-Masri, N., & Abu-Hijleh, B. (2012). Courtyard housing in midrise buildings: An environmental assessment in hot-arid climate. *Renewable and Sustainable Energy Reviews*, 16(4), 1892-1898. doi: <https://doi.org/10.1016/j.rser.2012.01.008>.
- Aldawoud, A. (2008). Thermal performance of courtyard buildings. *Energy and Buildings*, 40(5), 906-910. doi: <https://doi.org/10.1016/j.enbuild.2007.07.007>.
- Apolonio Callejas, I. J., Cleonice Durante, L., Diz-Mellado, E., & Galán-Marín, C. (2020). Thermal sensation in courtyards: Potentialities as a passive strategy in tropical climates. *Sustainability*, 12(15), 6135. doi: <https://doi.org/10.3390/su12156135>.
- Ascione, F., Bianco, N., De Stasio, C., Mauro, G. M., & Vanoli, G. P. (2016). Multi-stage and multi-objective optimization for energy retrofitting a developed hospital reference building: A new approach to assess cost-optimality. *Applied Energy*, 174, 37-68. doi: <https://doi.org/10.1016/j.apenergy.2016.04.078>.
- Back, T. (2000). *Evolutionary Computation 1. Basic Algorithms and Operators*. Bristol and Philadelphia: Institute of Physics Publishing.
- Bader, J., & Zitzler, E. (2010). A hypervolume-based optimizer for high-dimensional objective spaces. In *New Developments in Multiple Objective and Goal Programming* (pp. 35-54): Springer.
- Bader, J., & Zitzler, E. (2011). HypE: An algorithm for fast hypervolume-based many-objective optimization. *Evolutionary computation*, 19(1), 45-76. doi: https://doi.org/10.1162/EVCO_a_00009.
- Bichiou, Y., & Krarti, M. (2011). Optimization of envelope and HVAC systems selection for residential buildings. *Energy and Buildings*, 43(12), 3373-3382. doi: <https://doi.org/10.1016/j.enbuild.2011.08.031>.
- Bröde, P., Fiala, D., Błażejczyk, K., Holmér, I., Jendritzky, G., Kampmann, B., Tinz, B., & Havenith, G. (2012). Deriving the operational procedure for the Universal Thermal Climate Index (UTCI). *International journal of biometeorology*, 56(3), 481-494. doi: <https://doi.org/10.1007/s00484-011-0454-1>.
- Bueno, B., Norford, L., Hidalgo, J., & Pigeon, G. (2013). The urban weather generator. *Journal of Building Performance Simulation*, 6(4), 269-281. doi: <https://doi.org/10.1080/19401493.2012.718797>.
- Chatzidimitriou, A., & Yannas, S. (2016). Microclimate design for open spaces: Ranking urban design effects on pedestrian thermal comfort in summer. *Sustainable Cities and Society*, 26, 27-47. doi: <http://dx.doi.org/10.1016/j.scs.2016.05.004>.
- Chiu, M.-C. (2010). The numerical assessment of optimal equipment allocation and acoustical barrier shape in a multi-noise plant by using the genetic algorithm method. *Journal of Marine Science and Technology*, 18(1), 56-68. doi: <https://doi.org/10.1080/02522667.2009.10699930>.
- Crawley, D. B., Lawrie, L. K., Winkelmann, F. C., Buhl, W. F., Huang, Y. J., Pedersen, C. O., Strand, R. K., Liesen, R. J., Fisher, D. E., & Witte, M. J. (2001). EnergyPlus: creating a new-generation building energy simulation program. *Energy and Buildings*, 33(4), 319-331. doi: [https://doi.org/10.1016/S0378-7788\(00\)00114-6](https://doi.org/10.1016/S0378-7788(00)00114-6).
- Delgarm, N., Sajadi, B., Kowsary, F., & Delgarm, S. (2016). Multi-objective optimization of the building energy performance: A simulation-based approach by means of particle swarm optimization (PSO). *Applied Energy*, 170, 293-303. doi: <https://doi.org/10.1016/j.enbuild.2016.09.003>.

- Diz-Mellado, E., López-Cabeza, V. P., Rivera-Gómez, C., Galán-Marín, C., Rojas-Fernández, J., & Nikolopoulou, M. (2021). Extending the adaptive thermal comfort models for courtyards. *Building and Environment*, 203, 108094. doi: <https://doi.org/10.1016/j.buildenv.2021.108094>.
- DoE. (2020). Weather Data. Retrieved from <https://energyplus.net/weather>
- Dogan, T., & Reinhart, C. (2017). Shoeboxer: An algorithm for abstracted rapid multi-zone urban building energy model generation and simulation. *Energy and Buildings*, 140, 140-153. doi: <https://doi.org/10.1016/j.enbuild.2017.01.030>.
- Emmerich, M. T., & Deutz, A. H. (2018). A tutorial on multiobjective optimization: fundamentals and evolutionary methods. *Natural computing*, 17(3), 585-609. doi: <https://doi.org/10.1007/s11047-018-9685-y>.
- Ernest, R., & Ford, B. (2012). The role of multiple-courtyards in the promotion of convective cooling. *Architectural Science Review*, 55(4), 241-249. doi: <http://dx.doi.org/10.1080/00038628.2012.723400>.
- Etzion, Y. (1990). The Thermal Behaviour of Non-Shaded Closed Courtyards in Hot-Arid Zones [1]. *Architectural Science Review*, 33(3), 79-83. doi: <https://doi.org/10.1080/00038628.1990.9696677>.
- Evins, R. (2013). A review of computational optimisation methods applied to sustainable building design. *Renewable and Sustainable Energy Reviews*, 22, 230-245. doi: <http://dx.doi.org/10.1016/j.rser.2013.02.004>.
- Galal, O. M., Sailor, D. J., & Mahmoud, H. (2020). The impact of urban form on outdoor thermal comfort in hot arid environments during daylight hours, case study: New Aswan. *Building and Environment*, 184(107222), 1-15. doi: <https://doi.org/10.1016/j.buildenv.2020.107222>.
- Guedouh, M. S., & Zemmouri, N. (2017). Courtyard building's morphology impact on thermal and luminous environments in hot and arid region. *Energy Procedia*, 119, 153-162. doi: <https://doi.org/10.1016/j.egypro.2017.07.063>.
- Gupta, V. (1987). Thermal efficiency of building clusters: an index for non air-conditioned buildings in hot climates. In D. Hawkes, J. Owers, P. Rickaby, & P. Steadman (Eds.), *Energy and urban built form* (pp. 133-145). London: Butterworths.
- Ibrahim, Y., Kershaw, T., & Shepherd, P. (2020). Improvement of the Ladybug-tools microclimate workflow: A verification study. In *Building Simulation and Optimization 2020*, Loughborough University, Loughborough, UK.
- Ibrahim, Y., Kershaw, T., Shepherd, P., & Coley, D. (2021a). On the Optimisation of Urban form Design, Energy Consumption and Outdoor Thermal Comfort Using a Parametric Workflow in a Hot Arid Zone. *Energies*, 14(4026), 22. doi: <https://doi.org/10.3390/en14134026>.
- Ibrahim, Y., Kershaw, T., Shepherd, P., & Elwy, I. (2021b). A parametric optimisation study of urban geometry design to assess outdoor thermal comfort. *Sustainable Cities and Society*, 75(103352), 1-18. doi: <https://doi.org/10.1016/j.scs.2021.103352>.
- IEA. (2020). *Energy technology perspectives 2020*. OECD Publishing. Paris, France
- IPCC. (2021). *Summary for Policymakers. Climate Change 2021: The Physical Science Basis*. Contribution of Working Group I to the Sixth Assessment Report of the Intergovernmental Panel on Climate Change. V. Masson-Delmotte, P. Zhai, A. Pirani, S. L. Connors, C. Péan, S. Berger, N. Caud, Y. Chen, L. Goldfarb, M. I. Gomis, M. Huang, K. Leitzell, E. Lonnoy, J. B. R. Matthews, T. K. Maycock, T. Waterfield, O. Yelekçi, R. Yu, & B. Zhou. Cambridge University Press In Press.

- Kämpf, J. H., Montavon, M., Bunyesc, J., Bolliger, R., & Robinson, D. (2010). Optimisation of buildings' solar irradiation availability. *Solar Energy*, 84(4), 596-603. doi: <https://doi.org/10.1016/j.solener.2009.07.013>.
- Kämpf, J. H., & Robinson, D. (2009). Optimisation of urban energy demand using an evolutionary algorithm. In *Proceedings of the Eleventh International IBPSA Conference*.
- Knowles, R. (1981). *Sun Rhythm Form*. Cambridge, MA: MIT Press.
- Knowles, R. (2003). The solar envelope: its meaning for energy and buildings. *Energy and Buildings*, 35(1), 15-25. doi: [https://doi.org/10.1016/S0378-7788\(02\)00076-2](https://doi.org/10.1016/S0378-7788(02)00076-2).
- Kovats, R. S., & Hajat, S. (2008). Heat stress and public health: a critical review. *Annu. Rev. Public Health*, 29, 41-55. doi: <https://doi.org/10.1146/annurev.publhealth.29.020907.090843>.
- Mackey, C., Galanos, T., Norford, L., Roudsari, M. S., & Architects, P. (2017). Wind, sun, surface temperature, and heat island: critical variables for high-resolution outdoor thermal comfort. In *Proceedings of the 15th International conference of Building Performance Simulation Association. San Francisco, USA*.
- Mahdy, M. M., & Nikolopoulou, M. (2014). Evaluation of fenestration specifications in Egypt in terms of energy consumption and long term cost-effectiveness. *Energy and Buildings*, 69, 329-343. doi: <http://dx.doi.org/10.1016/j.enbuild.2013.11.028>.
- Malekzadeh, M., & Loveday, D. (2008). Towards the integrated thermal simulation of indoor and outdoor building spaces. In *Proceedings of Conference: Air Conditioning and the Low Carbon Cooling Challenge, Cumberland Lodge, Windsor, UK*.
- March, L., & Martin, L. (1972). *Urban space and structures*. Cambridge, UK: University Press Cambridge.
- Martinelli, L., & Matzarakis, A. (2017). Influence of height/width proportions on the thermal comfort of courtyard typology for Italian climate zones. *Sustainable Cities and Society*, 29, 97-106. doi: <http://dx.doi.org/10.1016/j.scs.2016.12.004>.
- McNeel, R. (2021). Rhinoceros 3D. Retrieved from <https://www.rhino3d.com/>
- MHUUC, Ministry of Housing Utilities & Urban Communities. (2005). Egyptian Code for Improving the Efficiency of Energy Use in Buildings (306/2005). In *Part 1: Residential Buildings (306/1)* (pp. 152). Cairo, Egypt: National Housing & Building Research Centre, HBRC.
- MHUUC, Ministry of Housing Utilities & Urban Communities. (2008). The Executive Regulations for the Egyptian Unified Construction Act. In (pp. 163). Cairo, Egypt: General Organisation for Physical Planning.
- Muhaisen, A. S. (2006). Shading simulation of the courtyard form in different climatic regions *Building and Environment*, 41(12), 1731-1741 doi: <https://doi.org/10.1016/j.buildenv.2005.07.016>.
- Muhaisen, A. S., & Gadi, M. B. (2005). Mathematical model for calculating the shaded and sunlit areas in a circular courtyard geometry. *Building and Environment*, 40(12), 1619-1625. doi: <https://doi.org/10.1016/j.buildenv.2004.12.018>.
- Muhaisen, A. S., & Gadi, M. B. (2006). Shading performance of polygonal courtyard forms. *Building and Environment*, 41(8), 1050-1059. doi: <https://doi.org/10.1016/j.buildenv.2005.04.027>.
- Natanian, J., Aleksandrowicz, O., & Auer, T. (2019a). A parametric approach to optimizing urban form, energy balance and environmental quality: The case of Mediterranean districts. *Applied Energy*, 254(113637), 1-17. doi: <https://doi.org/10.1016/j.apenergy.2019.113637>.

- Natanian, J., & Auer, T. (2020). Beyond nearly zero energy urban design: A holistic microclimatic energy and environmental quality evaluation workflow. *Sustainable Cities and Society*, 56(102094), 1-11. doi: <https://doi.org/10.1016/j.scs.2020.102094>.
- Natanian, J., De Luca, F., Wortmann, T., & Capeluto, G. (2021). The Solar Block Generator: an additive parametric method for solar driven urban block design. In *Journal of Physics: Conference Series*.
- Natanian, J., Maiullari, D., Yezioro, A., & Auer, T. (2019b). Synergetic urban microclimate and energy simulation parametric workflow. In *Journal of Physics: Conference Series*.
- Oke, T. R. (1976). The distinction between canopy and boundary-layer heat islands. *Atmosphere* 14, 268-277. doi: <https://doi.org/10.1080/00046973.1976.9648422>.
- Okeil, A. (2010). A holistic approach to energy efficient building forms. *Energy and Buildings*, 42(9), 1437-1444. doi: <https://doi.org/10.1016/j.enbuild.2010.03.013>.
- Rahamimoff, A. (1984). Residential Cluster Based on Climate and Energy Considerations. *Energy and Buildings*, 7(2), 89 - 107. doi: [https://doi.org/10.1016/0378-7788\(84\)90032-X](https://doi.org/10.1016/0378-7788(84)90032-X).
- Ratti, C., Raydan, D., & Steemers, K. (2003). Building form and environmental performance: archetypes, analysis and an arid climate. *Energy and Buildings*, 35(1), 49-59. doi: [https://doi.org/10.1016/S0378-7788\(02\)00079-8](https://doi.org/10.1016/S0378-7788(02)00079-8).
- Rojas-Fernández, J., Galán-Marín, C., Roa-Fernández, J., & Rivera-Gómez, C. (2017). Correlations between GIS-based urban building densification analysis and climate guidelines for Mediterranean courtyards. *Sustainability*, 9(12), 2255. doi: <https://doi.org/10.3390/su9122255>.
- Roudsari, M. S., & Mackey, C. (2022). Ladybug-tools. Retrieved from <https://www.ladybug.tools/>
- Rutten, D. (2021). Grasshopper3D. Retrieved from <https://www.grasshopper3d.com/>
- Seto, K. C., Dhakal, S., Bigio, A., Blanco, H., Delgado, G. C., Dewar, D., Huang, L., Inaba, A., Kansal, A., & Lwasa, S. (2014). Human settlements, infrastructure and spatial planning. In *Climate Change 2014: Mitigation of Climate Change. Contribution of Working Group III to the Fifth Assessment Report of the Intergovernmental Panel on Climate Change*; Cambridge University Press: Cambridge, UK, 2014.
- Soflaei, F., Shokouhian, M., Abraveshdar, H., & Alipour, A. (2017). The impact of courtyard design variants on shading performance in hot-arid climates of Iran. *Energy and Buildings*, 143, 71-83. doi: <http://dx.doi.org/10.1016/j.enbuild.2017.03.027>.
- Stanescu, M., Kajl, S., & Lamarche, L. (2012). Evolutionary algorithm with three different permutation options used for preliminary HVAC system design. In *Proceedings of the building simulation and optimization conference*.
- Tablada, A., De Troyer, F., Blocken, B., Carmeliet, J., & Verschure, H. (2009). On natural ventilation and thermal comfort in compact urban environments-the Old Havana case. *Building and Environment*, 44(9), 1943-1958. doi: <https://doi.org/10.1016/j.buildenv.2009.01.008>.
- Taleghani, M., Tenpierik, M., & van den Dobbela, A. (2014a). Indoor thermal comfort in urban courtyard block dwellings in the Netherlands. *Building and Environment*, 82, 566-579. doi: <http://dx.doi.org/10.1016/j.buildenv.2014.09.028>.
- Taleghani, M., Tenpierik, M., Van Den Dobbela, A., & De Dear, R. (2013). Energy use impact of and thermal comfort in different urban block types in the Netherlands. *Energy and Buildings*, 67, 166-175. doi: <http://dx.doi.org/10.1016/j.enbuild.2013.08.024>.
- Taleghani, M., Tenpierik, M., van den Dobbela, A., & Sailor, D. J. (2014b). Heat in courtyards: A validated and calibrated parametric study of heat mitigation strategies for urban courtyards in

- the Netherlands. *Solar Energy*, 103, 108-124. doi: <http://dx.doi.org/10.1016/j.solener.2014.01.033>.
- Tuhus-Dubrow, D., & Krarti, M. (2009). Comparative analysis of optimization approaches to design building envelope for residential buildings. *ASHRAE Transactions*, 115(2), 554-563.
- United Nations, Department of Economic and Social Affairs Population Division. (2018). World Urbanization Prospects: The 2018 Revision. New York: United Nations
- Vartholomaios, A. (2015). The residential solar block envelope: A method for enabling the development of compact urban blocks with high passive solar potential. *Energy and Buildings*, 99, 303-312. doi: <https://www.doi.org/10.1016/j.enbuild.2015.04.046>.
- Vartholomaios, A. (2017). A parametric sensitivity analysis of the influence of urban form on domestic energy consumption for heating and cooling in a Mediterranean city. *Sustainable Cities and Society*, 28, 135-145. doi: <http://dx.doi.org/10.1016/j.scs.2016.09.006>.
- Vierlinger, R. (2015). Multi Objective Design Interface. (Masters). Technischen Universität Wien, Vienna.
- Vierlinger, R. (2021). Octopus - Multi-Objective Evolutionary Optimizer. Retrieved from <https://www.food4rhino.com/en/app/octopus>
- Wortmann, T., & Natanian, J. (2020). Multi-objective Optimization for Zero-Energy Urban Design in China: A Benchmark. In *SimAUD2020*.
- Wortmann, T., & Natanian, J. (2021). Optimizing solar access and density in Tel Aviv: Benchmarking multi-objective optimization algorithms. In *Journal of Physics: Conference Series*.
- Yaşa, E., & Ok, V. (2014). Evaluation of the effects of courtyard building shapes on solar heat gains and energy efficiency according to different climatic regions. *Energy and Buildings*, 73, 192-199. doi: <http://dx.doi.org/10.1016/j.enbuild.2013.12.042>.
- Yezioro, A., Capeluto, I. G., & Shaviv, E. (2006). Design guidelines for appropriate insolation of urban squares. *Renewable energy*, 31(7), 1011-1023. doi: <https://www.doi.org/10.1016/j.renene.2005.05.015>.
- Zamani, Z., Heidari, S., & Hanachi, P. (2018). Reviewing the thermal and microclimatic function of courtyards. *Renewable and Sustainable Energy Reviews*, 93, 580-595. doi: <https://doi.org/10.1016/j.rser.2018.05.055>.
- Zhao, J., & Du, Y. (2020). Multi-objective optimization design for windows and shading configuration considering energy consumption and thermal comfort: A case study for office building in different climatic regions of China. *Solar Energy*, 206, 997-1017. doi: <https://doi.org/10.1016/j.solener.2020.05.090>.
- Zitzler, E., Laumanns, M., & Thiele, L. (2001). SPEA2: Improving the strength Pareto evolutionary algorithm. *TIK-report*, 103. doi: <https://doi.org/10.3929/ethz-a-004284029>.

6.9 Addendum

This study used an evolutionary algorithm to find the best set of optimum solutions. In this process, the selection of the best solution in one generation evolved based on the fittest solution of the preceding one. Consequently, the process does not effectively simulate the entire design space, comprising all design candidates. Since the results of this study represent the optimum solutions in the objective space of the last generation, as expected, differences between the entire sample were minimised. Not only this was reason for the small differences in Figure 6.10, but also presenting the UTCI as the average of UTCI values over the daytime hours, and then across all the grid points. Although maximum UTCI of some 50 °C and minimum UTCI of 20 °C were recorded in certain hours (see supplementary data in section 6.7), the average in Figure 6.10 spanned only 2 °C UTCI. On the other hand, differences in cooling loads reached almost 20 MWh, 40 MWh and 50 MWh in types A, B and C, respectively (Figure 6.20). As shown in the same figure, differences in cooling loads are more driven by the variations in FAR (i.e., total floor area), than by interspaces and orientation; a single building height increment entails 4 building floors higher, corresponding to around 8100 kWh. Given this strong correlation, normalising the cooling loads by total floor area has entailed minor differences as in Figure 6.11, albeit has emphasised the effect of interspaces and orientation on cooling loads.

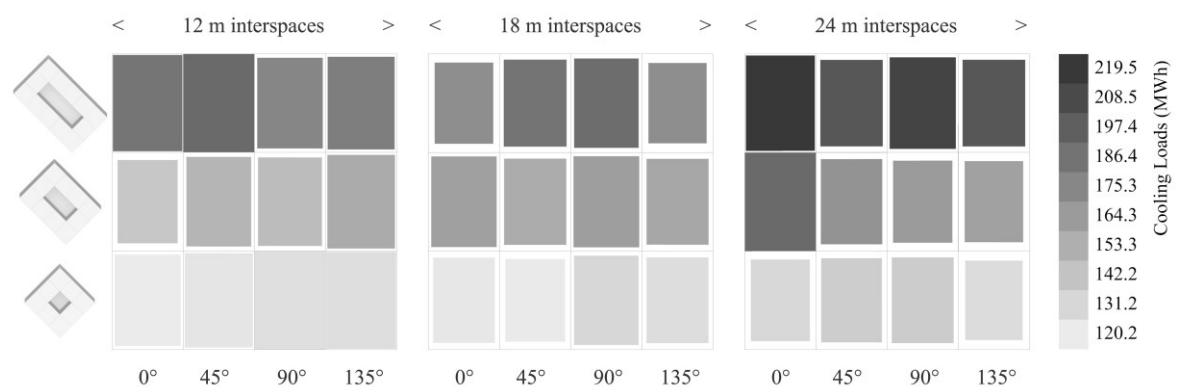


Figure 6.20: Performance of different courtyard types in different orientations and interspaces regarding the cooling loads. Grid cells are scaled with regard to FAR reduction relative to the highest FAR in each type; in type A, 12 m interspaces and orientation 90°; in type B, 24 m interspaces and orientation 0°; and in type C, 12 m interspaces and orientation 45°.

6.10 Epilogue

This study revealed that a deliberate passive solar design could improve the thermal and energy performance of courtyard blocks. Urban densification as an impeccable design strategy in hot-arid climates is a fallacy, this study highlights this by providing a variety of moderately dense courtyard blocks offering a trade-off between outdoor thermal comfort and cooling energy in summer. Moreover, the outperformance of the optimal design schemes, compared to the -supposedly optimal- conventional courtyards with uniform building heights suggested by Muhaisen (2006) with regard to the winter insolation proves the latter to be a futile design option. The results of this chapter bestowed a new perspective of the parameterisation of courtyard's proportions on those of the previous chapter, though conformed therein with respect to the orientation and interspaces. It should be noted, however, that the UTCI range obtained here was slightly higher, due to the sampling of interspaces, i.e. the minimum is 12 m, compared to 6 m in the previous chapter. Even so, improvements in the UTCI performance could be attained in specific locations with moderate heat stress (26 - 32° C). The study did not account for the cooling loads per unit area since increasing FAR, in some (deceptive) solutions, decreased both cooling loads and UTCI - a direct opposition to the nature of dual-objective optimisations. With the scope of the design variables narrowed down by the results obtained, this can now be overcome through detailed modelling of the thermal zones (rather than cooling the whole floor space), as the computational overhead can be remarkably reduced. Likewise, modelling UTCI could be significantly improved with regard to the sampling of the ground surface to further demonstrate the UTCI spatial differences across the street section. The implications of this study with regards to the aims of the thesis introduce a new approach for quantitative research on courtyard blocks in Egypt, but also necessitates its integration in practice. The study reported on the best 12 performing design schemes in each courtyard type ranked by the weighted sum method. In practice, these can be adjusted to match the design requirements for a specific context. Also, the implementation of the search algorithm, HypE has proven more than efficient in the context of sustainable urban design, where the integration of other environmental qualities - as design objectives - in the simulation workflow is a viable option, for instance urban daylighting and energy supply potential which are out of the scope of this thesis.

7 Conclusions

This thesis revolved around the unexplored aspects of the relationship between urban form design and environmental sustainability in the hot-arid climate of Cairo, Egypt. The thesis investigated the impact of manipulating the urban design parameters on both outdoor thermal comfort and energy consumption at different scales. Myriad configurations of urban canyons, typologies and courtyard blocks were evaluated using a parametric simulation workflow, which highlighted the contrasting relationship between outdoor thermal comfort and energy consumption, and hence portray the trade-off between urban densification and environmental performance. Although most of the design parameters investigated in the quantitative studies ranged within the local construction and energy codes in Egypt, exceptions had to be made to explore the potential improvements in environmental criteria beyond the thresholds of these codes. What's more, the refinement of the design parameters, and the decision to include/exclude a certain typology in the analysis have evolved as this thesis progressed. The following subsections summarise the findings, answer the research questions, and draw conclusions and recommendations with regards to the aims and objectives of this thesis.

7.1 Research findings

Chapter 4 investigated the impact of a combination of various building heights, street widths, and orientations, which entailed 7716 simulations, on the thermal performance (UTCI) of symmetrical and asymmetrical urban canyons. The study compared the resultant UTCI from using both the optimised design thresholds and those of the Egyptian Construction Act to set a benchmark for the reduction in thermal stress.

The results showed that following the design regulations of the Egyptian Construction Act, using a H/W of 1.5 could reduce the UTCI by 3.7 and 2.6 °C in symmetrical and asymmetrical street canyons, respectively, compared to the highest UTCI obtained. However, in a worst-case condition, using higher H/W ratios increases the potential to reduce the UTCI by up to 6 °C in NS, NE-SW and NW-SE ($3 < H/W < 6$), and up to 4 °C in EW symmetrical canyons ($4.5 < H/W < 6$). In asymmetrical canyons, the potential reaches up to 3 °C and 2 °C, respectively. The results also showed that H/W alone is not an accurate indicator of the spatial configuration of an urban canyon; for instance, an urban canyon, 6 m high and 12 m wide registered 1.2 °C lower UTCI than that 9 m high and 18 m wide in a NW-SE orientation. Moreover, in asymmetrical canyons, the impact of changing the height seemed negligible compared to changing the street width. The study recommended design guidelines for minimum H/W thresholds for achieving the 3.7 and 2.6 °C reduction in UTCI, addressing the fourth objective. In the extreme conditions studied in this stage, the UTCI category (strong heat stress) did not change with optimising the design parameters; however, since UTCI is *per se* perceptible, i.e., describes how the pedestrians feel, the optimum thresholds correspond to pedestrians feeling 6 °C and 3 °C lower in symmetrical and asymmetrical canyons, respectively.

Chapter 5 investigated the impact of the combination of 7 street widths in both directions, 10 building heights, 7 orientations, accounting for 3430 simulations, on the thermal and energy performance of 3 building typologies. The study analysed the relationship between the design parameters, along with the urban scale density parameters, and the performance criteria for the three typologies. The study highlighted the optimum design thresholds for achieving the best performance in each criterion, and then for achieving the best combined performance.

The results showed that changing orientation could reduce the UTCI by 0.8 °C and reduce the energy loads by up to 1.3 MWh/building. When the effects of both orientation and interspaces were combined, ordinal orientations (30-60°) seemed to be the best if minimum interspaces (9-10.5 m) are used, reducing the UTCI by almost 1.7 °C and the energy loads by up to 2.1 MWh/building. Building heights brought about a contradicting impact on the UTCI and energy loads, with building heights of 15-20 m being a turning point on the combined fitness curve. As these configurations are interpreted as density parameters, it was found that for a constant Floor Area Ratio (FAR), increasing Building Coverage Ratio (BCR) from 30% to 60% reduced the UTCI by 1.5 °C, and the energy loads by 4.11 MWh/building. Moreover, compact (BCR = 60%) and medium density ($2 < \text{FAR} < 4$) configurations seemed to be the best trade-off between both performance criteria. Design guidelines were recommended based on the design attributes of urban typologies achieving lower UTCI than 32 °C (moderate heat stress), and simultaneously achieving 60% reduction in energy loads, relative to the highest obtained, addressing the fourth objective.

Chapter 6 investigated the impact of 3 interspaces, 4 orientations and 3 heights of each building, on the thermal and energy performance of 3 courtyard block typologies of different elongations, corresponding to different numbers of buildings (8, 10 and 12). The total number of permutations exceeded 7 million, therefore a genetic algorithm was used to find the optimum cases. These were compared to those recommended in the literature, to highlight the improvements in both performance criteria, as well as in solar exposure in winter.

The results showed that, using minimum interspaces of 12 m, courtyard blocks performed better when their long axes were directed NE-SW and NW-SE, regardless of the building heights, reducing the UTCI by almost 1.5 °C, and reducing the cooling loads by almost 15%. Within a NW-SE configuration, a courtyard block with W/L of 1 performs best when the buildings in the S, SW and NE directions are the highest; those with W/L of 2 performs best when the buildings in the SW, NE, N and NW directions are the highest; and those with W/L of 3 performs best when buildings in the NW, W, NE, SW and SWW directions are the highest. By highest, they are meant to be at least 33 m high. As compared to a reference case with 24 m interspaces, 36 m height of all buildings, and aligned to the EW axis, the best performing 12 cases in all courtyard types were shown to reduce the UTCI by up to 1.6 °C and reduce the cooling loads by up to 31.7%.

Moreover, a selected case with W/L of 2 was shown to increase solar exposure by 188 kWh/m², as such the percentage of exposed surfaces by 4% in a typical cold week, as compared to a reference case recommended in a previous study in Cairo. Design guidelines were recommended based on the design attributes of the best performing 12 cases in each courtyard type, addressing the fourth objective.

7.2 Interpretation of the findings: answers to research questions

Findings of this thesis attested the research hypotheses by showing that optimising the urban geometry design parameters could improve outdoor thermal comfort to a higher extent than what resulted from using the local design regulations. This was also shown on an urban block scale, where narrower streets and higher BCR (higher H/W ratios) were recommended to improve both thermal comfort and energy consumption. Furthermore, it was shown that courtyard blocks are the best performing typology in hot-arid climates, and that by optimising their design parameters, they could outperform conventional courtyard blocks.

Chapter 4: *What are the canyon scale optimum design parameters for improving outdoor thermal comfort?*

As compared to the highest UTCI obtained in all phases, in symmetrical canyons, thermal comfort could be improved in NS, NE-SW and NW-SE canyons by using H/W ratios of as low as 3, whereas in EW canyons a H/W ratio of as low as 4.5 is required. In asymmetrical canyons, NS canyons could be designed with one flank having a H/W of 2.6, provided the other flank has at least a H/W of 4. The decision of which flank should be higher in NS canyons does not affect the UTCI. In ordinal orientations, a H/W ratio of 3 is recommended for the flanks facing SE and SW, given the opposing flanks facing NE and NW have at least a H/W of 5. In EW canyons, northern flanks should have a H/W of at least 4, whereas the southern should be as high as possible. Comparing the performance of all orientations, NS canyons showed the lowest UTCI, followed by NE-SW and NW-SE canyons, then EW canyons were the highest.

Chapter 5: *What are the optimum design parameters which yield the best thermal and energy performance for urban block typologies?*

In typical hot conditions studied in the second stage, optimising the design parameters could change the UTCI category from “strong” to “moderate heat stress”; however, the magnitude of reduction from the highest UTCI is lower than the first stage, due to considering both street directions. To achieve the best thermal and energy performance, street widths should be minimised, and BCR maximised, implying higher H/W ratio, though not as high as in the first stage, with the energy criterion being considered. For scattered forms, the optimum design thresholds are $BCR > 50\%$, $1 < FAR < 2$ and orientated 45° ; linear forms should be designed at $BCR > 60\%$, $2 < FAR < 3$ and orientated $0-30^\circ$ from NS-axis; and courtyards should be designed at $BCR > 60\%$, $2 < FAR < 4$, and orientated $30-60^\circ$.

Chapter 6: *To what extent could the urban-scale design parameters improve the thermal and energy performance of courtyard urban blocks?*

Courtyard blocks with minimum interspaces of 12 m, BCR of almost 55–60%, and orientated NE-SW or NW-SE had almost 2.5°C lower average UTCI and 34% lower cooling loads, compared to the highest values obtained. In the hot conditions of a typical week, the UTCI category did not change, considering the average of all grid points. However, moderate heat stress was achieved in certain points. In comparison with conventional courtyards studied in the second stage, optimising the building heights could achieve 1.6°C lower UTCI and 31.7% lower cooling loads. An optimum square courtyard block would be orientated NE-SW, with a FAR of 8 at the northern and southern parts, and FAR of 4.5 at the eastern and western parts. These ratios change to 7-8 and 5-6, respectively, for two-fold elongated courtyards. For three-fold elongated courtyards, FAR of 5 for southern, 7 for northern, and 3.5 for eastern and western parts are the best.

7.3 Bringing all together

The findings of this thesis have shown that urban form design *per se* exhibits significant potential to enhance the energy efficiency and the thermal comfort at different scales. In reality, this comes in conjunction with a series of mitigation and adaptation measures. As aforementioned, in the hot-arid climate context of Cairo, recent studies have shown that using green roofs, tree lines, high reflectivity pavements and shading structures could reduce the ambient air temperatures by almost 2.5 °C, which corresponds to approximately 4 °C UTCI (Fahmy *et al.*, 2018). Another study has also shown that using green roofs and façades at a neighbourhood scale could potentially reduce the summer monthly energy consumption by almost 7.7 MWh, corresponding to 16% lower energy consumption than the base case neighbourhood (Fahmy *et al.*, 2017). Moreover, the reductions in energy consumption, obtained by manipulating the urban scale design parameters, are comparable to those potentially obtained by manipulating the building envelope (Mahdy & Nikolopoulou, 2014). These findings reveal that the potential of urban form design to alleviate hot thermal conditions and reduce energy consumption approximates, or arguably surpasses, those of other strategies. In fact, in light of the current environmental challenges, a sustainable design will have to integrate both approaches, to take advantage of the synergies between them.

The findings have also shed light on the variations of thermal and energy performance from one scale to another, and in different design conditions. As these change from extreme to typical hot conditions, the potential of urban form design to improve outdoor thermal comfort decreases, albeit with a potential to alleviate pedestrian thermal sensation from strong to moderate heat stress. Urban street canyons are seldom found isolated from their surrounding contexts. In reality, they constitute linear typologies and interspaces of perimeter urban blocks. That said, the decision whether to follow the guidelines specified in chapter 4, chapter 5, or a combination of both, depends on the designer's interest. For instance, guidelines of chapter 4 should be used when the goal is to design for extreme conditions, where thermal comfort is prioritised, whereas those of chapter 5 could be used in typical conditions, when the thermal performance of both street directions could be described by an average value, as balanced with energy loads. Summer UHI intensity is higher within denser (vertically high) urban textures, whereas winter UHI is higher within compact textures (Salvati *et al.*, 2019).

The guidelines specified in chapter 5 and 6 could, therefore, be used to mitigate the UHI, accordingly. Conventional courtyard blocks (chapter 5) could be designed in high density areas, while residential solar blocks (chapter 6) could be designed in compact areas (Figure 7.1), increasing the aerodynamic roughness, and hence promoting ventilation.



Figure 7.1: Recommendations for using courtyard block types. Conventional courtyard blocks are to be used in high-density areas (left), while residential solar blocks are to be used in compact areas (right).

7.4 Contribution to knowledge

This thesis has defined environmental performance driven design guidelines for urban built forms in hot-arid climates, which can help shift design regulations from being density-oriented towards being climate-oriented. Simulating a multitude of geometrical configurations that has not been previously assessed in hot-arid zones, the thesis has contributed new correlations between urban geometry parameters and environmental performance. For instance, in chapter 4, variations in thermal performance were found to be more dependent on H/W ratios and SVF than previously reported. Moreover, the study emphasised the importance of considering the H/W ratio of each canyon side in asymmetrical configurations. Recalling the ‘better’ urban density by Carmona *et al.* (2010), chapter 5 investigated the balance between urban density and the contradicting performance of both outdoor thermal comfort and energy loads – a seldom explored relationship in hot-arid climates. The study provided detailed insights on the correlation between the density parameters and the performance criteria.

For instance, FAR and BCR together were found to be responsible for 70% and 95% of the variations in thermal comfort and energy loads, respectively. Achieving better density was also sought through the reconceptualisation of the Residential Solar Block, in chapter 6 – another unexplored potential in hot-arid zones. The study provided the attributes of moderately dense courtyard blocks offering a trade-off between outdoor thermal comfort and cooling loads, while also outperforming conventional courtyard blocks, highlighting the role passive solar design could play in improving the performance of courtyard blocks.

Another contribution of this thesis is presenting a methodology for modelling and simulating outdoor thermal comfort and energy loads in a parametric workflow, providing a comprehensive body of knowledge on the environmental performance of urban built forms. This methodology can be replicated to inform urban designers, planners and architects of how sustainable their design schemes are. Findings of this thesis were discussed in graphical representations which could be readily interpreted and replicated – the UTCI rose in section 4.6, the parallel coordinates in section 5.6, and the Pareto front optimal cases in section 6.6 are all examples. The versatility of embedding this research within the Ladybug-tools also expands the designers' ability to explore other performance criteria, such as renewable energy potentials and urban daylighting, or other criteria using different plugins which can be easily integrated in Grasshopper. Given the ever-increasing popularity of Grasshopper in education and research, this thesis, hence, can serve as a future reference for both educational and research studies.

The implications drawn in this thesis can be significantly correlated to the mitigation of the canopy layer UHI in several ways. Chapter 4 presented the optimum H/W ratios of asymmetrical urban canyons, with lower building heights in the northern direction and increased SVF, which in turn facilitate convective cooling to reduce the UHI. This also helps in reducing the UHI through decreased surface area, and thus reduced reflections of shortwave radiation and increased longwave radiation loss. The reported best typologies in chapter 5, with medium density, on the one hand, are characterised by relatively higher SVF, and hence facilitate the above mentioned thermal processes, and on the other, maintain lower building energy consumption, and hence contribute to reducing the anthropogenic heat from buildings. Likewise, the reported optimum courtyard blocks in chapter 6 are featured with higher SVF and lower energy loads, and therefore are another mitigation strategy of the canopy layer UHI.

In light of Egypt's Vision 2030, the findings of this thesis can help attain its goals, however, only in tandem with a concerted effort from policy makers, practitioners, and the research community. The Egyptian MHUUC will have a key role to play in amending the local codes, and most importantly, in enforcing them. Moreover, Raising the awareness of practitioners and urban designers of the new technological approaches to urban planning is a key task, entrusted to the Egyptian Green Building Council (EGBC). Also, while the Housing and Building National Research Centre (HBRC) is entrusted to support innovative solutions for the construction sector, the integration of parametric design techniques facilitates, if not guarantees, achieving that.

7.5 Research limitations

This research was limited by using simplified building typologies with replicated urban contexts, through the standardisation of design parameters. On a neighbourhood scale, urban form is characterised by heterogeneous spatial configurations, both horizontally and vertically, that need to be further considered in detail. However, the scalability of this workflow is limited by the number of design parameters included, which corresponds to exponential computational cost. Another limitation with regards to the computational cost was the decision not to include wind simulation. Although wind speed was shown to have marginal effect on the UTCI in the context of this thesis, including their effect helps deliver rigor insights on the thermal performance of urban built forms, and hence more robust decision making. This could be soon attainable, given that computational cost will continue to decrease over time.

Furthermore, validation of the simulation workflow in a street canyon has shown variations of almost 3 °C compared with field measurements. These variations have been attributed to uncertainties of the weather data, and the heat transfer module, specially with respect to the radiative heat transfer with the ground surface. Also, the difference in spatial resolution from reality suggests validating the workflow within various geometrical configurations. Although the variations were consistent over the hypothetical cases in this research, further improvements are needed for running detailed analyses.

Another limitation of this research is using the standard UTCI categories. Although the scale has been extensively validated in several climatic zones, qualitative studies have shown that the human subjective sensation might shift the categories by a few degrees (Potchter *et al.*, 2018). Given the extremely hot conditions in summer in Cairo - reaching up to 45 °C - people are adapted to higher temperatures, and thus adapting the UTCI categories to their subjective sensation should better highlight the potential of optimising the urban geometry parameters to achieve the neutral range.

Finally, this research has dealt with the urban form design from an environmental perspective, which in some cases, recommended very high aspect ratios. In light of a human scale approach to urban design, qualitative measures considering the pedestrian level dynamic perception of how urban spaces could be utilised and how the shape of cities impact human lives, need to be further investigated. That is to say, the applicability of these configurations in Egypt remains dependent on the cognitive and socio-cultural factors affecting people's perception of density, which should be reflected in policy making.

7.6 Future work

Starting from the research limitations, future work includes further modifications to the Python source code to achieve a rigorous quantification of the heat storage within a surface, and the human-sky heat exchange processes, and thus achieve a more reliable assessment of the human thermal comfort.

Although this research did not consider the impact of vegetation on the environmental performance, interventions to the code are extended to integrate the full spectrum of the heat exchange with vegetation (shortwave and longwave). This is meant to be a significant addition to the Ladybug-tools, where the optimisation of urban fabric, together with vegetation should add new perspectives to the sustainable design of urban communities.

Validating the UTCI thermal stress categories against human subjective thermal sensation in Egypt would, on the one hand, inform future studies on thermal comfort in hot-arid climates, and on the other hand, reinforce the accuracy of the Ladybug-tools model, through better interpretations of the results.

Finally, generative models are promising computational tools aiming at the evolution of urban masses (cellular automata), street networks (L-systems) or both (space syntax), following bottom-up and/or top-down spatial rules. These tools are becoming popular in the field of computational urban planning and their full integration in Grasshopper is only a matter of time; currently some features of cellular automata and L-systems are available in Grasshopper through the *Rabbit* plugin, while space syntax is available through the *Decoding-Spaces* plugin. Coupling these generative models with climate-based simulation workflows (Figure 7.2), such as the one presented in this thesis to inform the evolution of urban masses on a city-scale is a promising approach towards climate-sensitive city planning.

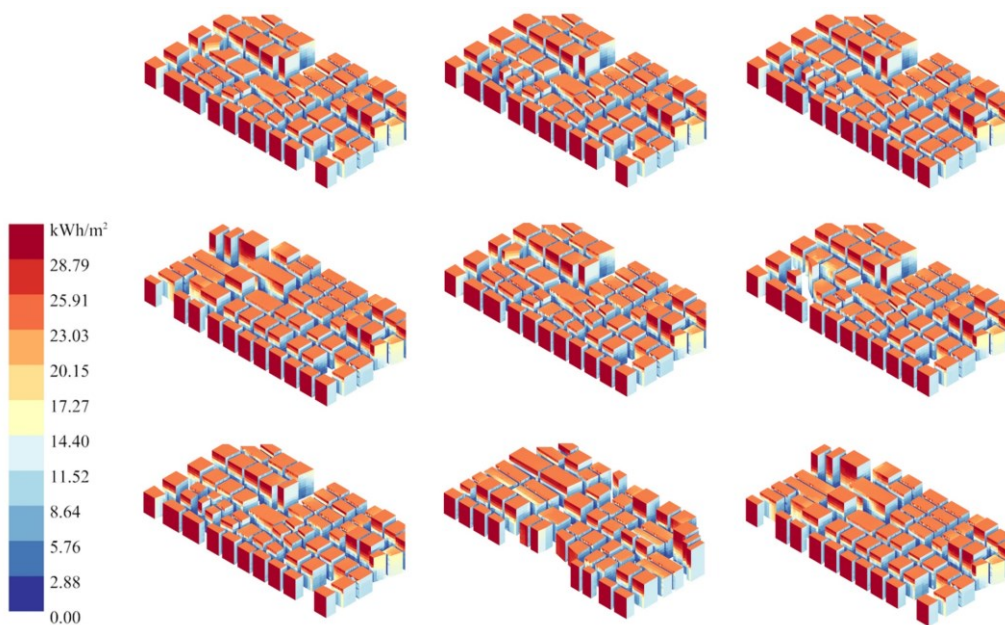


Figure 7.2: Surface radiation analysis of nine design alternatives generated using Decoding-Spaces (by the author).

7.7 Concluding remarks

This thesis underlined the extensive capabilities of Ladybug-tools within Grasshopper, to highlight the differences in urban geometry configurations and their impact on outdoor thermal comfort and building energy consumption. The study has reaffirmed some of the previous findings in hot-arid regions - urban shading, mostly created by building heights, is the most effective strategy for alleviating extreme thermal conditions in summer; the courtyard typology exhibits significant microclimatic and energy benefits.

The study, however, has done so by scrutinising detailed geometry configurations, which has resulted in new insights on the effectiveness of urban shading with regards to the H/W ratio of each canyon side. The study has presented the results in a discernible way through the parametric nature of Grasshopper.

Optimisation of urban form has been shown to have significantly improved the environmental performance of urban areas. In this respect, parametric design techniques will have a key role to play in the design of future urban environments, and hence are indispensable in decision support and policy making. Recent technological developments are now considering social and economic aspects of sustainability, e.g., contact with nature, visual and acoustic quality, street connectivity and accessibility to buildings, Life Cycle Assessment (LCA), and Net Zero Energy Districts (NZED). Having these sustainability indicators coupled together in a parametric design environment will likely be recognised within a few years, and integrating such versatile techniques in the design process seems to be the only way to cope with an emerging set of environmental qualities. To this end, it can be concluded that the deductions of Williams *et al.* (2000) that there is no definitive sustainable urban form, but rather a variety of 'more sustainable' urban forms than others, still hold true. The tendency for achieving sustainable urban form will continue to evolve, as the number of environmental qualities continues to do so, and the question will shift to whether or not a certain performance criterion should be considered, under which circumstances, to achieve which goal.

References

- Abreu-Harbach, L. V., Labaki, L. C., & Matzarakis, A. (2014). Thermal bioclimate in idealized urban street canyons in Campinas, Brazil. *Theoretical and Applied Climatology*, 115(1-2), 333-340.
- Ahmed, K. (1994). A comparative analysis of the outdoor thermal environment of the urban vernacular and the contemporary development: case studies in Dhaka. In *Proceedings of the 11 th PLEA International Conference*, Dead Sea.
- Akbari, H. (2009). *Cooling our communities. A guidebook on tree planting and light-colored surfacing*. Lawrence Berkeley Laboratory.
- Akbari, H., & Konopacki, S. (2005). Calculating energy-saving potentials of heat-island reduction strategies. *Energy Policy*, 33(6), 721-756. doi: <https://doi.org/10.1016/j.enpol.2003.10.001>.
- Akbari, H., Matthews, H. D., & Seto, D. (2012). The long-term effect of increasing the albedo of urban areas. *Environmental Research Letters*, 7(2), 1-10.
- Akbari, H., Rose, L. S., & Taha, H. (1999). Characterizing the fabric of the urban environment: a case study of Sacramento, California.
- AKDC, Aga Khan Documentation Center at MIT. (2021). Archnet. Retrieved from <https://www.archnet.org/>
- Al-Masri, N., & Abu-Hijleh, B. (2012). Courtyard housing in midrise buildings: An environmental assessment in hot-arid climate. *Renewable and Sustainable Energy Reviews*, 16(4), 1892-1898. doi: <https://doi.org/10.1016/j.rser.2012.01.008>.
- Aldawoud, A. (2008). Thermal performance of courtyard buildings. *Energy and Buildings*, 40(5), 906-910. doi: <https://doi.org/10.1016/j.enbuild.2007.07.007>.
- Ali-Toudert, F. (2005). Dependence of Outdoor Thermal Comfort on Street Design in Hot and Dry Climate. (PhD). Institutes der Universität Freiburg, Freiburg, Germany. (15)
- Ali-Toudert, F., Djenane, M., Bensalem, R., & Mayer, H. (2005). Outdoor thermal comfort in the old desert city of Beni-Isguen, Algeria. *Climate Research*, 28(3), 243-256. doi: <http://doi.org/10.3354/cr028243>.
- Ali-Toudert, F., & Mayer, H. (2006). Numerical study on the effects of aspect ratio and orientation of an urban street canyon on outdoor thermal comfort in hot and dry climate. *Building and Environment*, 41(2), 94-108. doi: <https://doi.org/10.1016/j.buildenv.2005.01.013>.
- Ali-Toudert, F., & Mayer, H. (2007a). Effects of asymmetry, galleries, overhanging fac, ades and vegetation on thermal comfort in urban street canyons. *Solar Energy*, 81(6), 742-754. doi: <https://doi.org/10.1016/j.solener.2006.10.007>.
- Ali-Toudert, F., & Mayer, H. (2007b). Thermal comfort in an east-west oriented street canyon in Freiburg (Germany) under hot summer conditions. *Theoretical and Applied Climatology*, 87(1-4), 223-237. doi: <https://doi.org/10.1007/s00704-005-0194-4>.
- Allegrini, J., Dorer, V., & Carmeliet, J. (2015). Influence of morphologies on the microclimate in urban neighbourhoods. *Journal of Wind Engineering and Industrial Aerodynamics*, 144, 108-117. doi: <https://doi.org/10.1016/j.jweia.2015.03.024>.
- Allegrini, J., Dorer, V., & Carmeliet, J. (2016). Impact of radiation exchange between buildings in urban street canyons on space cooling demands of buildings. *Energy and Buildings*, 127, 1074-1084. doi: <http://dx.doi.org/10.1016/j.enbuild.2016.06.073>.
- Ampatzidis, P., & Kershaw, T. (2020). A review of the impact of blue space on the urban microclimate. *Science of the total environment*, 730, 1-18. doi: <https://doi.org/10.1016/j.scitotenv.2020.139068>.

-
- Andreou, E. (2013). Thermal comfort in outdoor spaces and urban canyon microclimate. *Renewable energy*, 55, 182-188. doi: <http://dx.doi.org/10.1016/j.renene.2012.12.040>.
- Apolonio Callejas, I. J., Cleonice Durante, L., Diz-Mellado, E., & Galán-Marín, C. (2020). Thermal sensation in courtyards: Potentialities as a passive strategy in tropical climates. *Sustainability*, 12(15), 6135. doi: <https://doi.org/10.3390/su12156135>.
- Arens, E., Hoyt, T., Zhou, X., Huang, L., Zhang, H., & Schiavon, S. (2015). Modeling the comfort effects of short-wave solar radiation indoors. *Building and Environment*, 88, 3-9. doi: <http://dx.doi.org/10.1016/j.buildenv.2014.09.004>.
- Arnfield, A. (2003). Two Decades of Urban Climate Research: A review of Turbulence, Exchange of Energy, Water and the urban heat islands. *International Journal of Climatology*, 23(1), 1-26. doi: <https://doi.org/10.1002/joc.859>.
- Ascione, F., Bianco, N., De Stasio, C., Mauro, G. M., & Vanoli, G. P. (2016). Multi-stage and multi-objective optimization for energy retrofitting a developed hospital reference building: A new approach to assess cost-optimality. *Applied Energy*, 174, 37-68. doi: <https://doi.org/10.1016/j.apenergy.2016.04.078>.
- ASHRAE. (2014). Measurement of Energy and Demand Savings. In (pp. 16-17). Atlanta: American Society of Heating, Refrigerating and Air-Conditioning Engineers.
- ASHRAE. (2017a). ANSI/ASHRAE Standard 55-2017: Thermal environmental conditions for human occupancy. In (pp. 22-29). Atlanta, GA: American Society of Heating, Refrigerating and Air-Conditioning Engineers, .
- ASHRAE. (2017b). ASHRAE HandBook of Fundamentals (SI Edition). In. Atlanta: American Society of Heating, refrigerating, and Air-Conditioning Engineers Inc.
- Attia, S., Evrard, A., & Gratia, E. (2012). Development of benchmark models for the Egyptian residential buildings sector. *Applied Energy*, 94, 270-284. doi: <https://doi.org/10.1016/j.apenergy.2012.01.065>.
- Auliciems, A. (1981). Towards a psycho-physiological model of thermal perception. *International journal of biometeorology*, 25(2), 109-122. doi: <https://doi.org/10.1007/BF02184458>.
- Auliciems, A., & Szokolay, S. V. (2007). Thermal Comfort. In (2nd ed.). Brisbane: PLEA in association with Department of Architecture, The University of Queensland.
- Back, T. (2000). Evolutionary Computation 1. Basic Algorithms and Operators. Bristol and Philadelphia: Institute of Physics Publishing.
- Bader, J., & Zitzler, E. (2010). A hypervolume-based optimizer for high-dimensional objective spaces. In *New Developments in Multiple Objective and Goal Programming* (pp. 35-54): Springer.
- Bader, J., & Zitzler, E. (2011). HypE: An algorithm for fast hypervolume-based many-objective optimization. *Evolutionary computation*, 19(1), 45-76. doi: https://doi.org/10.1162/EVCO_a_00009.
- Baker, L., Brazel, A., & Westerhoff, P. (2004). Environmental consequences of rapid urbanization in warm, arid lands: case study of Phoenix, Arizona (USA). *WIT Transactions on Ecology and the Environment*, 72, 155-164. doi: <http://doi.org/10.2495/SC040161>.
- Bayomi, N., Elkholy, M., Rakha, T., & Fernandez, J. E. (2021). Passive survivability under extreme heat events: The case of AlDarb Al Ahmar, Cairo. *Science and Technology for the Built Environment*, 27(8), 1144-1163. doi: <https://doi.org/10.1080/23744731.2021.1953356>.
- Bichiou, Y., & Krarti, M. (2011). Optimization of envelope and HVAC systems selection for residential buildings. *Energy and Buildings*, 43(12), 3373-3382. doi: <https://doi.org/10.1016/j.enbuild.2011.08.031>.

- Bidarmaghz, A., Choudhary, R., Soga, K., Terrington, R. L., Kessler, H., & Thorpe, S. (2020). Large-scale urban underground hydro-thermal modelling—A case study of the Royal Borough of Kensington and Chelsea, London. *Science of the total environment*, 700, 134955. doi: <https://doi.org/10.1016/j.scitotenv.2019.134955>.
- Bienvenido-Huertas, D., Sánchez-García, D., Pérez-Fargallo, A., & Rubio-Bellido, C. (2020). Optimization of energy saving with adaptive setpoint temperatures by calculating the prevailing mean outdoor air temperature. *Building and Environment*, 170(106612). doi: <https://doi.org/10.1016/j.buildenv.2019.106612>.
- Binarti, F., Koerniawan, M. D., Triyadi, S., Utami, S. S., & Matzarakis, A. (2020). A review of outdoor thermal comfort indices and neutral ranges for hot-humid regions. *Urban Climate*, 31(100531). doi: <https://doi.org/10.1016/j.uclim.2019.100531>.
- Blazejczyk, K. MENEX: the man-environment heat exchange model and its applications in bioclimatology. In *Proceedings of The Fifth International Conference on Environmental Ergonomics*.
- Blazejczyk, K. (2005). MENEX_2005. The Updated Version of Man-Environment Heat Exchange Model.
- Blazejczyk, K., Epstein, Y., Jendritzky, G., Staiger, H., & Tinz, B. (2012). Comparison of UTCI to selected thermal indices. *International journal of biometeorology*, 56(3), 515-535. doi: <https://doi.org/10.1007/s00484-011-0453-2>.
- Bornstein, R. D. (1968). Observations of the urban heat island effect in New York City. *Journal of Applied Meteorology*, 7(4), 575-582.
- Bourbia, F., & Awbi, H. B. (2004). Building cluster and shading in urban canyon for hot dry climate Part 2: Shading simulations *Renewable energy*, 29(2), 291-301 doi: [https://doi.org/10.1016/S0960-1481\(03\)00171-X](https://doi.org/10.1016/S0960-1481(03)00171-X).
- Bourbia, F., & Boucheriba, F. (2010). Impact of street design on urban microclimate for semi arid climate (Constantine). *Renewable energy*, 35(2), 343-347. doi: <https://doi.org/10.1016/j.renene.2009.07.017>.
- Bröde, P., Fiala, D., Blazejczyk, K., Holmér, I., Jendritzky, G., Kampmann, B., Tinz, B., & Havenith, G. (2012). Deriving the operational procedure for the Universal Thermal Climate Index (UTCI). *International journal of biometeorology*, 56(3), 481-494. doi: <https://doi.org/10.1007/s00484-011-0454-1>.
- Brody, J. S. (2010). Constructing professional knowledge: The neighborhood unit concept in the community builders handbook. (PhD). University of Illinois at Urbana-Champaign,
- Bruse, M. (2020). ENVI-met. Retrieved from <https://www.envi-met.com/>
- BSI, British Standards Institution. (2001). Ergonomics of the thermal environment—Instruments for measuring physical quantities (BS EN ISO 7726:2001). In (pp. 51).
- Bueno, B., Norford, L., Hidalgo, J., & Pigeon, G. (2013). The urban weather generator. *Journal of Building Performance Simulation*, 6(4), 269-281. doi: <https://doi.org/10.1080/19401493.2012.718797>.
- Bueno, B., Roth, M., Norford, L., & Li, R. (2014). Computationally efficient prediction of canopy level urban air temperature at the neighbourhood scale. *Urban Climate*, 9, 35-53. doi: <http://dx.doi.org/10.1016/j.uclim.2014.05.005>.
- Burgess, R., & Jenks, M. (2000). Compact cities: sustainable urban forms for developing countries. London: Taylor & Francis.
- CAPMAS. (2019). Bulletin of Housing in Egypt. (71-21123-2019). Cairo, Egypt: Central Agency for Public Mobilization & Statistics Retrieved from https://www.capmas.gov.eg/Pages/Publications.aspx?page_id=5104&Year=23415

-
- Caprotti, F. (2014). Critical research on eco-cities? A walk through the Sino-Singapore Tianjin Eco-City, China. *Cities*, 36(Feb), 10-17. doi: <https://doi.org/10.1016/j.cities.2013.08.005>.
- Carmona, M., Tiesdell, S., Heath, T., & Oc, T. (2010). *Public Places - Urban Spaces: The Dimensions of Urban Design* (Second ed.). Oxford, UK: Architectural Press.
- Chakraborty, T., & Lee, X. (2019). A simplified urban-extent algorithm to characterize surface urban heat islands on a global scale and examine vegetation control on their spatiotemporal variability. *International Journal of Applied Earth Observation and Geoinformation*, 74, 269-280. doi: <https://doi.org/10.1016/j.jag.2018.09.015>.
- Chandler, T. J. (1965). *The climate of London* Hutchinson.
- Changnon, S. (2003). Urban modification of freezing-rain events. *Journal of Applied Meteorology and Climatology*, 42(6), 863-870.
- Charalampopoulos, I., Tsiros, I., Chronopoulou-Sereli, A., & Matzarakis, A. (2013). Analysis of thermal bioclimate in various urban configurations in Athens, Greece. *Urban Ecosystems*, 16(2), 217-233. doi: <https://doi.org/10.1007/s11252-012-0252-5>.
- Chatzidimitriou, A., & Yannas, S. (2016). Microclimate design for open spaces: Ranking urban design effects on pedestrian thermal comfort in summer. *Sustainable Cities and Society*, 26, 27-47. doi: <http://dx.doi.org/10.1016/j.scs.2016.05.004>.
- Chatzidimitriou, A., & Yannas, S. (2017). Street canyon design and improvement potential for urban open spaces; the influence of canyon aspect ratio and orientation on microclimate and outdoor comfort. *Sustainable Cities and Society*, 33, 85-101. doi: <https://doi.org/10.1016/j.scs.2017.05.019>.
- Cheng, V. (2009). Understanding density and high density. In *Designing high-density cities* (pp. 37-51): Routledge.
- Chinazzo, G., Rastogi, P., & Andersen, M. (2015). Assessing robustness regarding weather uncertainties for energy-efficiency-driven building refurbishments. *Energy Procedia*, 78, 931-936. doi: <https://doi.org/10.1016/j.egypro.2015.11.021>.
- Chiu, M.-C. (2010). The numerical assessment of optimal equipment allocation and acoustical barrier shape in a multi-noise plant by using the genetic algorithm method. *Journal of Marine Science and Technology*, 18(1), 56-68. doi: <https://doi.org/10.1080/02522667.2009.10699930>.
- Cities, L. (2014). *Cities and Energy: Urban Morphology and Heat Energy Demand*. London, UK
- Coccolo, S., Kämpf, J., Scartezzini, J.-L., & Pearlmutter, D. (2016). Outdoor human comfort and thermal stress: A comprehensive review on models and standards. *Urban Climate*, 18, 33-57. doi: <http://dx.doi.org/10.1016/j.uclim.2016.08.004>.
- Conzen, M. R. G. (1960). *Alnwick, Northumberland: a study in town-plan analysis*. London, UK: Wiley.
- CoP, Conference of the Parties. (2015). Paris agreement. In *Report of the Conference of the Parties to the United Nations Framework Convention on Climate Change* (pp. 36). Paris.
- Corbusier, L., & Eardley, A. (1973). *The athens charter*. New York: Grossman Publishers
- Core Studio, Design Explorer. (2021). Retrieved from <http://tt-acm.github.io/DesignExplorer/>
- Crawley, D. B., Lawrie, L. K., Winkelmann, F. C., Buhl, W. F., Huang, Y. J., Pedersen, C. O., Strand, R. K., Liesen, R. J., Fisher, D. E., & Witte, M. J. (2001). EnergyPlus: creating a new-generation building energy simulation program. *Energy and Buildings*, 33(4), 319-331. doi: [https://doi.org/10.1016/S0378-7788\(00\)00114-6](https://doi.org/10.1016/S0378-7788(00)00114-6).
- Cullen, G. (1961). *The Concise Townscape*. London: The Architectural Press.
- Dantzig, G., & Saaty, T. (1973). *Compact city: a plan for a livable urban environment*. San Francisco: W. H. Freeman and company.

- de-Dear, R. J., & Brager, G. S. (1998). Developing an Adaptive Model of Thermal Comfort and Preference. *ASHRAE Transactions*, 104 (1), 145-167. doi: <https://escholarship.org/uc/item/4qq2p9c6>.
- De Freitas, C. R., & Grigorieva, E. A. (2017). A comparison and appraisal of a comprehensive range of human thermal climate indices. *International journal of biometeorology*, 61(3), 487-512. doi: <https://doi.org/10.1007/s00484-016-1228-6>.
- DeKay, M., & Brown, G. Z. (1985). *Sun, Wind & Light: Architectural Design Strategies* (1st ed.). New Jersey, US: Wiley.
- Delgarm, N., Sajadi, B., Kowsary, F., & Delgarm, S. (2016). Multi-objective optimization of the building energy performance: A simulation-based approach by means of particle swarm optimization (PSO). *Applied Energy*, 170, 293-303. doi: <https://doi.org/10.1016/j.enbuild.2016.09.003>.
- Dimoudi, A., & Nikolopoulou, M. (2003). Vegetation in the Urban Environments: Microclimatic Analysis and Benefits. *Energy and Buildings*, 35(1), 69-76. doi: [https://doi.org/10.1016/S0378-7788\(02\)00081-6](https://doi.org/10.1016/S0378-7788(02)00081-6).
- Diz-Mellado, E., López-Cabeza, V. P., Rivera-Gómez, C., Galán-Marín, C., Rojas-Fernández, J., & Nikolopoulou, M. (2021). Extending the adaptive thermal comfort models for courtyards. *Building and Environment*, 203, 108094. doi: <https://doi.org/10.1016/j.buildenv.2021.108094>.
- DoE. (2019). Engineering reference: EnergyPlus version 9.2.0. In (pp. 58-167).
- DoE. (2020). Weather Data. Retrieved from <https://energyplus.net/weather>
- Dogan, T., & Reinhart, C. (2017). Shoeboxer: An algorithm for abstracted rapid multi-zone urban building energy model generation and simulation. *Energy and Buildings*, 140, 140-153. doi: <https://doi.org/10.1016/j.enbuild.2017.01.030>.
- Duany, A., Plater-Zyberk, E., & Speck, J. (2001). *Suburban nation: The rise of sprawl and the decline of the American dream* Macmillan.
- DuBois. (1916). A formula to estimate the approximate surface area if height and body mass be known. *Archives of internal medicine*, 17, 863-871.
- Edeisy, M. (2020, 15-18 September). Environmental Analysis of the Residential Sector in Cairo. In *Proceedings of REAL CORP 2020: Shaping Urban Change*, Aachen, Germany.
- Edeisy, M., & Cecere, C. (2018). Energy Efficiency for Egyptian Housing: Code Compliance and Enforcement. *International Journal of the Constructed Environment*, 9(3), 1-19. doi: <http://doi.org/10.18848/2154-8587/CGP/v09i03/1-15>.
- EEAA, Egyptian Environmental Affairs Agency. (2018). Egypt's first Biennial Update Report to the United Nations Framework Convention on Climate Change.
- EGBC, Egypt Green Building Council. (2022). Retrieved from <https://www.egyptgbc.org/>
- Elnabawi, M. H., Hamza, N., & Dudek, S. (2013). Use and evaluation of the ENVI-met model for two different urban forms in Cairo, Egypt: measurements and model simulations. In *13th Conference of International Building Performance Simulation Association, Chambéry, France*.
- Elnahas, M. (2003). The effects of urban configuration on urban air temperatures. *Architectural Science Review*, 46(2), 135-138. doi: <https://doi.org/10.1080/00038628.2003.9696975>.
- Elshahed, M. M. K. (2007). *Facades of modernity: Image, performance, and transformation in the Egyptian metropolis*. (Masters). Massachusetts Institute of Technology, Retrieved from <http://hdl.handle.net/1721.1/39305>
- Elwy, I., Ibrahim, Y., Fahmy, M., & Mahdy, M. (2018). Outdoor microclimatic validation for hybrid simulation workflow in hot arid climates against ENVI-met and field measurements. *Energy Procedia*, 153, 29-34. doi: <https://doi.org/10.1016/j.egypro.2018.10.009>.

-
- Emmanuel, R. (1993). A hypothetical 'shadow umbrella' for thermal comfort enhancement in the Equatorial urban outdoors. *Architectural Science Review*, 36(4), 173-184. doi: <https://doi.org/10.1080/00038628.1993.9696759>.
- Emmanuel, R., Rosenlund, H., & Johansson, E. (2007a). Urban shading—a design option for the tropics? A study in Colombo, Sri Lanka. *International Journal of Climatology: A Journal of the Royal Meteorological Society*, 27(14), 1995-2004. doi: <https://doi.org/10.1002/joc.1609>.
- Emmanuel, R., Rosenlund, H., & Johansson, E. (2007b). Urban shading—a design option for the tropics? A study in Colombo, Sri Lanka. *International Journal of Climatology*, 27(14), 1995-2004. doi: <https://doi.org/10.1002/joc.1609>.
- Emmanuel, R., & Steemers, K. (2018). Connecting the realms of urban form, density and microclimate. 46(8), 804-808. doi: <https://doi.org/10.1080/09613218.2018.1507078>.
- Emmerich, M. T., & Deutz, A. H. (2018). A tutorial on multiobjective optimization: fundamentals and evolutionary methods. *Natural computing*, 17(3), 585-609. doi: <https://doi.org/10.1007/s11047-018-9685-y>.
- Engineering-ToolBox. (2001). Engineering ToolBox. Retrieved from <https://www.engineeringtoolbox.com/>
- Ernest, R., & Ford, B. (2012). The role of multiple-courtyards in the promotion of convective cooling. *Architectural Science Review*, 55(4), 241-249. doi: <http://dx.doi.org/10.1080/00038628.2012.723400>.
- Etzion, Y. (1990). The Thermal Behaviour of Non-Shaded Closed Courtyards in Hot-Arid Zones [1]. *Architectural Science Review*, 33(3), 79-83. doi: <https://doi.org/10.1080/00038628.1990.9696677>.
- Evins, R. (2013). A review of computational optimisation methods applied to sustainable building design. *Renewable and Sustainable Energy Reviews*, 22, 230-245. doi: <http://dx.doi.org/10.1016/j.rser.2013.02.004>.
- Evola, G., Costanzo, V., Magri, C., Margani, G., Marletta, L., & Naboni, E. (2020). A novel comprehensive workflow for modelling outdoor thermal comfort and energy demand in urban canyons: results and critical issues. *Energy and Buildings*, 216(109946), 1-19. doi: <https://doi.org/10.1016/j.enbuild.2020.109946>.
- Extech. (2021). Extech HT30: Heat Stress WBGT (Wet Bulb Globe Temperature) Meter. Retrieved from <http://www.extech.com/ht30/>
- Fahmi, W., & Sutton, K. (2008). Greater Cairo's housing crisis: Contested spaces from inner city areas to new communities. *Cities*, 25(5), 277-297. doi: <https://doi.org/10.1016/j.cities.2008.06.001>.
- Fahmy, M. (2010). Interactive urban form design of local climate scale in hot semi-arid zone. (PhD). The University of Sheffield,
- Fahmy, M., El-Hady, H., Mahdy, M., & Abdelalim, M. F. (2017). On the green adaptation of urban developments in Egypt; predicting community future energy efficiency using coupled outdoor-indoor simulations. *Energy and Buildings*, 153, 241-261. doi: <http://dx.doi.org/10.1016/j.enbuild.2017.08.008>.
- Fahmy, M., Ibrahim, Y., Hanafi, E., & Barakat, M. (2018). Would LEED-UHI greenery and high albedo strategies mitigate climate change at neighborhood scale in Cairo, Egypt? *Building Simulation*, 11(6), 1273-1288. doi: <https://doi.org/10.1007/s12273-018-0463-7>.
- Fanger, P. O. (1970). Thermal comfort; Analysis and applications in environmental engineering. New York: McGraw-Hill, first published in 1970, Danish Technical Press, Copenhagen.

- Fathy, F., Mansour, Y., Sabry, H., Abdelmohsen, S., & Wagdy, A. (2015). Cellular Automata for Efficient Daylighting Performance: Optimized Façade Treatment. In *Proceedings of the 14th Conference of the International Building Performance Simulation Association (IBPSA)*.
- Fathy, H. (1973). *Architecture for the Poor: An Experiment in Rural Egypt*. Chicago: University of Chicago Press
- Fathy, H. (1986). *Natural Energy and Vernacular Architecture*. Chicago: The University of Chicago Press.
- Fiala, D., Havenith, G., Bröde, P., Kampmann, B., & Jendritzky, G. (2012). UTCI-Fiala multi-node model of human heat transfer and temperature regulation. *International journal of biometeorology*, 56(3), 429-441. doi: <https://doi.org/10.1007/s00484-011-0424-7>.
- Fiala, D., Lomas, K. J., & Stohrer, M. (2001). Computer prediction of human thermoregulatory and temperature responses to a wide range of environmental conditions. *International journal of biometeorology*, 45(3), 143-159. doi: <https://doi.org/10.1007/s004840100099>.
- Folk Jr, G. (1974). *Textbook of environmental physiology*. Philadelphia PA: Lea and Febiger.
- Forouzandeh, A. (2018). Numerical modeling validation for the microclimate thermal condition of semi-closed courtyard spaces between buildings. *Sustainable Cities and Society*, 36, 327-345. doi: <https://doi.org/10.1016/j.scs.2017.07.025>.
- Futcher, J. A., Kershaw, T., & Mills, G. (2013). Urban form and function as building performance parameters. *Building and Environment*, 62, 112-123. doi: <https://doi.org/10.1016/j.buildenv.2013.01.021>.
- Gagge, A., Nishi, Y., & Gonzalez, R. (1972). Standard Effective Temperature Index of temperature sensation and thermal discomfort. In *Proceedings of the CIB Commission W45 Symposium on Human Requirements*, Building Research Station, UK.
- Gagge, A. P. (1936). The linearity criterion as applied to partitional calorimetry. *American Journal of Physiology-Legacy Content*, 116(3), 656-668. doi: <https://doi.org/10.1152/ajplegacy.1936.116.3.656>.
- Gagge, A. P., Burton, A. C., & Bazett, H. C. (1941). A practical system of units for the description of the heat exchange of man with his environment. *Science*, 94(2445), 428-430. doi: <https://doi.org/10.1126/science.94.2445.428>.
- Gagge, A. P., Fobelets, A. P., & Berglund, L. G. (1986). Standard Predictive Index of Human Response to the Thermal Environment. *ASHRAE Transactions*, 92 (2), 709-731.
- Galal, O. M., Sailor, D. J., & Mahmoud, H. (2020). The impact of urban form on outdoor thermal comfort in hot arid environments during daylight hours, case study: New Aswan. *Building and Environment*, 184(107222), 1-15. doi: <https://doi.org/10.1016/j.buildenv.2020.107222>.
- Giannopoulou, K., Santamouris, M., Livada, I., Georgakis, C., & Caouris, Y. (2010). The impact of canyon geometry on intra urban and urban: suburban night temperature differences under warm weather conditions. *Pure and applied geophysics*, 167(11), 1433-1449. doi: <https://doi.org/10.1007/s00024-010-0099-8>.
- Gillette Jr, H. (2011). *Civitas by design: Building better communities, from the garden city to the new urbanism* University of Pennsylvania Press.
- Giridharan, R., & Emmanuel, R. (2018). The impact of urban compactness, comfort strategies and energy consumption on tropical urban heat island intensity: A review. *Sustainable Cities and Society*, 40, 677-687. doi: <https://doi.org/10.1016/j.scs.2018.01.024>.
- Givoni, B. (1998). *Climate consideration in urban and building design* (2nd Ed.). New York: Van Nostrand Reinhold.

-
- Golany, G. S. (1996). Urban design morphology and thermal performance. *Atmospheric Environment*, 30(3), 455-465. doi: [https://doi.org/10.1016/1352-2310\(95\)00266-9](https://doi.org/10.1016/1352-2310(95)00266-9).
- Grant, J. L. (2009). Theory and practice in planning the suburbs: Challenges to implementing new urbanism, smart growth, and sustainability principles 1. *Planning Theory & Practice*, 10(1), 11-33. doi: <https://doi.org/10.1080/14649350802661683>.
- Grimmond, C., Roth, M., Oke, T. R., Au, Y., Best, M., Betts, R., Carmichael, G., Cleugh, H., Dabberdt, W., & Emmanuel, R. (2010). Climate and more sustainable cities: climate information for improved planning and management of cities (producers/capabilities perspective). *Procedia Environmental Sciences*, 1, 247-274. doi: <https://doi.org/10.1016/j.proenv.2010.09.016>.
- Guedouh, M. S., & Zemmouri, N. (2017). Courtyard building's morphology impact on thermal and luminous environments in hot and arid region. *Energy Procedia*, 119, 153-162. doi: <https://doi.org/10.1016/j.egypro.2017.07.063>.
- Guo, H., Aviv, D., Loyola, M., Teitelbaum, E., Houchois, N., & Meggers, F. (2019). On the understanding of the mean radiant temperature within both the indoor and outdoor environment, a critical review. *Renewable and Sustainable Energy Reviews*, 117(2020), 1-15. doi: <https://doi.org/10.1016/j.rser.2019.06.014>.
- Gupta, V. (1987). Thermal efficiency of building clusters: an index for non air-conditioned buildings in hot climates. In D. Hawkes, J. Owers, P. Rickaby, & P. Steadman (Eds.), *Energy and urban built form* (pp. 133-145). London: Butterworths.
- Gupta, V. K. (1984). Solar radiation and urban design for hot climates. *Environment and Planning B: Planning and Design*, 11(4), 435-454.
- Hall, P. (1988). *Cities of tomorrow: An intellectual history of urban planning and design since 1880* Basil Blackwell Ltd.
- Havenith, G., Fiala, D., Błazejczyk, K., Richards, M., Bröde, P., Holmér, I., Rintamaki, H., Benschabat, Y., & Jendritzky, G. (2012). The UTCI-clothing model. *International journal of biometeorology*, 56(3), 461-470. doi: <https://doi.org/10.1007/s00484-011-0451-4>.
- HBRC. (2008). *Egyptian code for reducing energy consumption in residential buildings*. Cairo: Egyptian Ministry of Housing, Utilities and Urban Communities; Housing and Building Research Centre.
- He, B.-J., Ding, L., & Prasad, D. (2019). Enhancing urban ventilation performance through the development of precinct ventilation zones: A case study based on the Greater Sydney, Australia. *Sustainable Cities and Society*, 47(101472), 14. doi: <https://doi.org/10.1016/j.scs.2019.101472>.
- Hirt, S. (2007). The compact versus the dispersed city: history of planning ideas on Sofia's urban form. *Journal of Planning History*, 6(2), 138-165. doi: <https://doi.org/10.1177/1538513206301327>.
- Holmer, B. (1992). A simple operative method for determination of sky view factors in complex urban canyons from fisheye photographs. *Meteorologische Zeitschrift*, 1(5), 236-239.
- Höppe, P. (1999). The physiological equivalent temperature—a universal index for the biometeorological assessment of the thermal environment. *International journal of biometeorology*, 43(2), 71-75. doi: <https://doi.org/10.1007/s004840050118>.
- Houghton, F., & Yaglou, C. (1923). Determination of the Comfort Zone. *Journal of ASHVE*, 29, 361.
- Howard, E. (1902). *Garden Cities of To-morrow* (second ed.). Cambridge, MA: MIT Press
- Howard, L. (1833). *The climate of London: deduced from meteorological observations made in the metropolis and at various places around it* (2nd ed.). London: International Association for Urban Climate.

- Hu, J., & Yu, X. (2013). Experimental study of sustainable asphalt binder: Influence of thermochromic materials. *Transportation Research Record: Journal of the Transportation Research Board*(2372), 108-115. doi: <https://doi.org/10.3141/2372-12>.
- Hu, Y., White, M., & Ding, W. (2016). An urban form experiment on urban heat island effect in high density area. *Procedia Engineering*, 169, 166-174. doi: <https://doi.org/10.1016/j.proeng.2016.10.020>.
- Huang, J., Cedeno-Laurent, J. G., & Spengler, J. D. (2014). CityComfort+: A simulation-based method for predicting mean radiant temperature in dense urban areas. *Building and Environment*, 80, 84-95. doi: <https://doi.org/10.1016/j.buildenv.2014.05.019>.
- Humphreys, M. A. (1975). Field studies of indoor thermal comfort and the progress of the adaptive approach. *The Building Services Engineer*, 44(27), 5-23.
- Huttner, S. (2012). Further development and application of the 3D microclimate simulation ENVI-met. (PhD). Mainz University, Germany,
- Ibrahim, Y. (2021a). Dataset for "A parametric optimisation study of urban geometry design to assess outdoor thermal comfort". Retrieved from: <https://researchdata.bath.ac.uk/1045>
- Ibrahim, Y. (2021b). Dataset for "On the optimisation of urban form design, energy consumption and outdoor thermal comfort using a parametric workflow in a hot arid zone". Retrieved from: <https://researchdata.bath.ac.uk/1021/>
- Ibrahim, Y. (2022). Dataset for "Multi-objective optimisation of urban courtyard blocks in hot arid zones". Retrieved from: <https://researchdata.bath.ac.uk/id/eprint/1137>
- Ibrahim, Y., Kershaw, T., & Shepherd, P. (2020a). Improvement of the Ladybug-tools microclimate workflow: A verification study. In *Building Simulation and Optimization 2020*, Loughborough University, Loughborough, UK.
- Ibrahim, Y., Kershaw, T., & Shepherd, P. (2020b). A methodology For Modelling Microclimate: A Ladybug-tools and ENVI-met Verification Study. In *35th PLEA Conference. Sustainable Architecture and Urban Design: Planning Post Carbon Cities*, A Coruña, Spain, 1-3 September.
- Ibrahim, Y., Kershaw, T., Shepherd, P., & Coley, D. (2021a). On the Optimisation of Urban form Design, Energy Consumption and Outdoor Thermal Comfort Using a Parametric Workflow in a Hot Arid Zone. *Energies*, 14(4026), 22. doi: <https://doi.org/10.3390/en14134026>.
- Ibrahim, Y., Kershaw, T., Shepherd, P., & Elwy, I. (2021b). A parametric optimisation study of urban geometry design to assess outdoor thermal comfort. *Sustainable Cities and Society*, 75(103352), 1-18. doi: <https://doi.org/10.1016/j.scs.2021.103352>.
- IEA. (2020). Energy technology perspectives 2020. OECD Publishing. Paris, France
- IEA, International Energy Agency. (2021). IEA Energy Atlas. Retrieved from <http://energyatlas.iea.org>
- IPCC. (2021). Summary for Policymakers. Climate Change 2021: The Physical Science Basis. Contribution of Working Group I to the Sixth Assessment Report of the Intergovernmental Panel on Climate Change. V. Masson-Delmotte, P. Zhai, A. Pirani, S. L. Connors, C. Péan, S. Berger, N. Caud, Y. Chen, L. Goldfarb, M. I. Gomis, M. Huang, K. Leitzell, E. Lonnoy, J. B. R. Matthews, T. K. Maycock, T. Waterfield, O. Yelekçi, R. Yu, & B. Zhou. Cambridge University Press In Press.
- ISO. (2005). Ergonomics of the Thermal Environment: Analytical Determination and Interpretation of Thermal Comfort Using Calculation of the PMV and PPD Indices and Local Thermal Comfort Criteria. In (pp. 52): International Organization for Standardization.
- Jabareen, Y. (2006). Sustainable Urban Forms: Their Typologies, Models, and Concepts. *Journal of Planning Education and Research*, 26(1), 38-52. doi: <https://doi.org/10.1177/0739456X05285119>.

-
- Jacobs, J. (1961). *The death and life of great American cities* Vintage.
- Jamei, E., & Rajagopalan, P. (2019). Effect of street design on pedestrian thermal comfort. *Architectural Science Review*, 62(2), 92-111. doi: <https://doi.org/10.1080/00038628.2018.1537236>.
- Jamei, E., Rajagopalan, P., Seyedmahmoudian, M., & Jamei, Y. (2016). Review on the impact of urban geometry and pedestrian level greening on outdoor thermal comfort. *Renewable and Sustainable Energy Reviews*, 54, 1002-1017. doi: <http://dx.doi.org/10.1016/j.rser.2015.10.104>.
- Jänicke, B., Meier, F., Hoelscher, M.-T., & Scherer, D. (2015). Evaluating the effects of façade greening on human bioclimate in a complex urban environment. *Advances in Meteorology*, 2015. doi: <https://doi.org/10.1155/2015/747259>.
- Javanroodi, K., Mahdavinnejad, M., & Nik, V. M. (2018). Impacts of urban morphology on reducing cooling load and increasing ventilation potential in hot-arid climate. *Applied Energy*, 231, 714-746. doi: <https://doi.org/10.1016/j.apenergy.2018.09.116>.
- Jendritzky, G. (1990). Regional bioclimatological assessment procedure using meso-scale bioclimate maps as example. In G. Jendritzky, H. Schirmer, G. Menz, & W. Schmidt-Kessen (Eds.), *Method of a region-oriented assessment of the thermal component of human bioclimate (Updated Klima-Michel model)* (1st ed., Vol. 114, pp. 7-69). Hannover: Academy for Spatial Research and Regional Planning.
- Jendritzky, G., de Dear, R., & Havenith, G. (2012). UTCI—why another thermal index? *International journal of biometeorology*, 56(3), 421-428. doi: <https://doi.org/10.1007/s00484-011-0513-7>.
- Jenks, M. (2000). The acceptability of urban intensification. In *Achieving sustainable urban form* (pp. 242-250).
- Jenks, M., Burton, E., & Williams, K. (1996). *The Compact city: a sustainable urban form?* Oxford: Taylor & Francis
- Jin, H., Cui, P., Wong, N. H., & Ignatius, M. (2018). Assessing the effects of urban morphology parameters on microclimate in Singapore to control the urban heat island effect. *Sustainability*, 10(206), 1-18. doi: <https://doi.org/10.3390/su10010206>.
- Johansson, E. (2006). Influence of urban geometry on outdoor thermal comfort in a hot dry climate: A study in Fez, Morocco. *Building and Environment*, 41(10), 1326-1338. doi: <https://doi.org/10.1016/j.buildenv.2005.05.022>.
- Johansson, E., & Emmanuel, R. (2006). The influence of urban design on outdoor thermal comfort in the hot, humid city of Colombo, Sri Lanka. *International journal of biometeorology*, 51(2), 119-133. doi: <http://dx.doi.org/10.1007/s00484-006-0047-6>.
- Joss, S., & Molella, A. P. (2013). The eco-city as urban technology: Perspectives on Caofeidian international eco-city (China). *Journal of Urban Technology*, 20(1), 115-137. doi: <https://doi.org/10.1080/10630732.2012.735411>.
- Kämpf, J. H., Montavon, M., Bunyesc, J., Bolliger, R., & Robinson, D. (2010). Optimisation of buildings' solar irradiation availability. *Solar Energy*, 84(4), 596-603. doi: <https://doi.org/10.1016/j.solener.2009.07.013>.
- Kämpf, J. H., & Robinson, D. (2009). Optimisation of urban energy demand using an evolutionary algorithm. In *Proceedings of the Eleventh International IBPSA Conference*.
- Karlessi, T., Santamouris, M., Apostolakis, K., Synnefa, A., & Livada, I. (2009). Development and testing of thermochromic coatings for buildings and urban structures. *Solar Energy*, 83(4), 538-551. doi: <https://doi.org/10.1016/j.solener.2008.10.005>.
- Kershaw, T. (2017). *Climate Change Resilience in the Urban Environment* IOP Publishing.

- Knowles, R. (1981). *Sun Rhythm Form*. Cambridge, MA: MIT Press.
- Knowles, R. (2003). The solar envelope: its meaning for energy and buildings. *Energy and Buildings*, 35(1), 15-25. doi: [https://doi.org/10.1016/S0378-7788\(02\)00076-2](https://doi.org/10.1016/S0378-7788(02)00076-2).
- Kolokotroni, M., & Giridharan, R. (2008). Urban heat island intensity in London: An investigation of the impact of physical characteristics on changes in outdoor air temperature during summer. *Solar Energy*, 82(11), 986-998. doi: <https://doi.org/10.1016/j.solener.2008.05.004>.
- Konis, K., Gamas, A., & Kensek, K. (2016). Passive performance and building form: An optimization framework for early-stage design support. *Solar Energy*, 125, 161-179. doi: <https://doi.org/10.1016/j.solener.2015.12.020>.
- Kovats, R. S., & Hajat, S. (2008). Heat stress and public health: a critical review. *Annu. Rev. Public Health*, 29, 41-55. doi: <https://doi.org/10.1146/annurev.publhealth.29.020907.090843>.
- Krüger, E., Pearlmutter, D., & Rasia, F. (2010). Evaluating the impact of canyon geometry and orientation on cooling loads in a high-mass building in a hot dry environment. *Applied Energy*, 87(6), 2068-2078.
- Kyriakodis, G., & Santamouris, M. (2017). Using reflective pavements to mitigate urban heat island in warm climates-Results from a large scale urban mitigation project. *Urban Climate*. doi: <https://doi.org/10.1016/j.uclim.2017.02.002>.
- Labib, R., & Beltran, L. (2015). Optimized Street Design to Balance Outdoor Thermal Comfort And Indoor Daylighting Performance Within Large Scale Urban Settings in Hot Arid Climates.
- Lai, J., Zhan, W., Huang, F., Quan, J., Hu, L., Gao, L., & Ju, W. (2018). Does quality control matter? Surface urban heat island intensity variations estimated by satellite-derived land surface temperature products. *ISPRS Journal of Photogrammetry and Remote Sensing*, 139, 212-227. doi: <https://doi.org/10.1016/j.isprsjprs.2018.03.012>.
- Lin, P., Gou, Z., Lau, S. S.-Y., & Qin, H. (2017). The impact of urban design descriptors on outdoor thermal environment: A literature review. *Energies*, 10(12), 2151. doi: <https://doi.org/10.3390/en10122151>.
- Lindberg, F., Holmer, B., & Thorsson, S. (2008). SOLWEIG 1.0-Modelling spatial variations of 3D radiant fluxes and mean radiant temperature in complex urban settings. *International journal of biometeorology*, 52(7), 697-713. doi: <https://doi.org/10.1007/s00484-008-0162-7>.
- Lindberg, F., Onomura, S., & Grimmond, C. (2016). Influence of ground surface characteristics on the mean radiant temperature in urban areas. *International journal of biometeorology*, 60(9), 1439-1452. doi: <https://doi.org/10.1007/s00484-016-1135-x>.
- Low, M. (2013). Eco-cities in Japan: past and future. *Journal of Urban Technology*, 20(1), 7-22. doi: <https://doi.org/10.1080/10630732.2012.735107>.
- Lynch, K. (1960). *The image of the city*. Cambridge, MA: MIT press.
- Mackey, C. (2015). *Pan climatic humans: shaping thermal habits in an unconditioned society*. (PhD). Massachusetts Institute of Technology,
- Mackey, C., Galanos, T., Norford, L., Roudsari, M. S., & Architects, P. (2017). Wind, sun, surface temperature, and heat island: critical variables for high-resolution outdoor thermal comfort. In *Proceedings of the 15th International conference of Building Performance Simulation Association*. San Francisco, USA.
- MacLeod, G. (2013). New urbanism/smart growth in the Scottish Highlands: Mobile policies and post-politics in local development planning. *Urban studies*, 50(11), 2196-2221. doi: <https://doi.org/10.1177/0042098013491164>.

-
- Mahdy, M. M. (2014). Applying architecture simulation tools to assess building sustainable design: Adapting the Egyptian residential energy code for climate change. (PhD). University of Kent, Retrieved from <https://books.google.co.uk/books?id=2mDjvgEACAAJ>
- Mahdy, M. M., & Nikolopoulou, M. (2014). Evaluation of fenestration specifications in Egypt in terms of energy consumption and long term cost-effectiveness. *Energy and Buildings*, 69, 329-343. doi: <http://dx.doi.org/10.1016/j.enbuild.2013.11.028>.
- Mahmoud, H., Ghanem, H., & Sodoudi, S. (2021). Urban geometry as an adaptation strategy to improve the outdoor thermal performance in hot arid regions: Aswan University as a case study. *Sustainable Cities and Society*, 71(102965). doi: <https://doi.org/10.1016/j.scs.2021.102965>.
- Malekzadeh, M., & Loveday, D. (2008). Towards the integrated thermal simulation of indoor and outdoor building spaces. In *Proceedings of Conference: Air Conditioning and the Low Carbon Cooling Challenge, Cumberland Lodge, Windsor, UK*.
- March, L., & Martin, L. (1972). Urban space and structures. Cambridge, UK: University Press Cambridge.
- Martinelli, L., & Matzarakis, A. (2017). Influence of height/width proportions on the thermal comfort of courtyard typology for Italian climate zones. *Sustainable Cities and Society*, 29, 97-106. doi: <http://dx.doi.org/10.1016/j.scs.2016.12.004>.
- Martins, T., Adolphe, L., Bastos, L., & Martins, A. (2016). Sensitivity analysis of urban morphology factors regarding solar energy potential of buildings in a Brazilian tropical context. *Solar Energy*, 137, 11-24. doi: <http://dx.doi.org/10.1016/j.solener.2016.07.053>.
- Matzarakis, A., & Amelung, B. (2008). Physiological equivalent temperature as indicator for impacts of climate change on thermal comfort of humans. In *Seasonal forecasts, climatic change and human health* (pp. 161-172): Springer.
- Matzarakis, A., Mayer, H., & Iziomon, M. G. (1999). Applications of a universal thermal index: physiological equivalent temperature. *International journal of biometeorology*, 43(2), 76-84. doi: <https://doi.org/10.1007/s004840050119>.
- Matzarakis, A., Rutz, F., & Mayer, H. (2007). Modelling radiation fluxes in simple and complex environments—application of the RayMan model. *International journal of biometeorology*, 51(4), 323-334. doi: <https://doi.org/10.1007/s00484-006-0061-8>.
- Matzarakis, A., Rutz, F., & Mayer, H. (2010). Modelling radiation fluxes in simple and complex environments: basics of the RayMan model. *International journal of biometeorology*, 54(2), 131-139. doi: <https://doi.org/10.1007/s00484-009-0261-0>.
- Mauree, D., Naboni, E., Coccolo, S., Perera, A. T. D., Nik, V. M., & Scartezzini, J.-L. (2019). A review of assessment methods for the urban environment and its energy sustainability to guarantee climate adaptation of future cities. *Renewable and Sustainable Energy Reviews*, 112, 733-746. doi: <https://doi.org/10.1016/j.rser.2019.06.005>.
- McNeel, R. (2021). Rhino3D. Retrieved from <https://www.rhino3d.com/>
- McRae, I., Freedman, F., Rivera, A., Li, X., Dou, J., Cruz, I., Ren, C., Dronova, I., Fraker, H., & Bornstein, R. (2020). Integration of the WUDAPT, WRF, and ENVI-met models to simulate extreme daytime temperature mitigation strategies in San Jose, California. *Building and Environment*, 184(107180). doi: <https://doi.org/10.1016/j.buildenv.2020.107180>.
- Mehaffy, M. W., Porta, S., & Romice, O. (2015). The “neighborhood unit” on trial: a case study in the impacts of urban morphology. *Journal of Urbanism: International Research on Placemaking and Urban Sustainability*, 8(2), 199-217. doi: <https://doi.org/10.1080/17549175.2014.908786>.

- Menberg, K., Blum, P., Schaffitel, A., & Bayer, P. (2013). Long-term evolution of anthropogenic heat fluxes into a subsurface urban heat island. *Environmental science & technology*, 47(17), 9747-9755. doi: <https://doi.org/10.1021/es401546u>.
- MFA, Ministry of Foreign Affairs. (2015). Egyptian Intended Nationally Determined Contribution as per UNFCCC. Retrieved from <https://www4.unfccc.int/sites/NDCStaging/Pages/All.aspx>
- MHUUC, Ministry of Housing Utilities & Urban Communities. (2005). Egyptian Code for Improving the Efficiency of Energy Use in Buildings (306/2005). In *Part 1: Residential Buildings (306/1)* (pp. 152). Cairo, Egypt: National Housing & Building Research Centre, HBRC.
- MHUUC, Ministry of Housing Utilities & Urban Communities. (2008). The Executive Regulations for the Egyptian Unified Construction Act. In (pp. 163). Cairo, Egypt: General Organisation for Physical Planning.
- Mills, G., Ching, J., See, L., Bechtel, B., & Foley, M. (2015). An introduction to the WUDAPT project. In *Proceedings of the 9th International Conference on Urban Climate*, Toulouse, France.
- MoEE, Ministry of Environment of Egypt. (2021). Egypt Pavilion: Road to CoP 27. CoP 26, Glasgow
- Mohamed, N. A. G., & Ali, W. H. (2014). Traditional residential architecture in Cairo from a green architecture perspective. *Arts and Design Studies*, 16, 6-26.
- MoL, Mayor of London. (2022). London Heat Map. Retrieved from <https://maps.london.gov.uk/heatmap>
- Morris, K. I., Chan, A., Morris, K. J. K., Ooi, M. C., Oozeer, M. Y., Abakr, Y. A., Nadzir, M. S. M., Mohammed, I. Y., & Al-Qrimli, H. F. (2017). Impact of urbanization level on the interactions of urban area, the urban climate, and human thermal comfort. *Applied Geography*, 79, 50-72. doi: <https://doi.org/10.1016/j.apgeog.2016.12.007>.
- Muhaisen, A. S. (2006). Shading simulation of the courtyard form in different climatic regions *Building and Environment*, 41(12), 1731-1741 doi: <https://doi.org/10.1016/j.buildenv.2005.07.016>.
- Muhaisen, A. S., & Gadi, M. B. (2005). Mathematical model for calculating the shaded and sunlit areas in a circular courtyard geometry. *Building and Environment*, 40(12), 1619-1625. doi: <https://doi.org/10.1016/j.buildenv.2004.12.018>.
- Muhaisen, A. S., & Gadi, M. B. (2006). Shading performance of polygonal courtyard forms. *Building and Environment*, 41(8), 1050-1059. doi: <https://doi.org/10.1016/j.buildenv.2005.04.027>.
- Naboni, E., Meloni, M., Coccolo, S., Kaempf, J., & Scartezzini, J.-L. (2017). An overview of simulation tools for predicting the mean radiant temperature in an outdoor space. *Energy Procedia*, 122, 1111-1116. doi: <https://doi.org/10.1016/j.egypro.2017.07.471>.
- Naboni, E., Meloni, M., Mackey, C., & Kaempf, J. (2019a). The simulation of mean radiant temperature in outdoor conditions: A review of software tools capabilities. In *Proceedings of the 16th IBPSA Conference*, Rome, Italy, Sept. 2-4, 2019.
- Naboni, E., Natanian, J., Brizzi, G., Florio, P., Chokhachian, A., Galanos, T., & Rastogi, P. (2019b). A digital workflow to quantify regenerative urban design in the context of a changing climate. *Renewable and Sustainable Energy Reviews*, 113(109255). doi: <https://doi.org/10.1016/j.rser.2019.109255>.
- Naboni, E., Ofria, L., & Danzo, E. (2019c). A Parametric Workflow to Conceive Facades as Indoor and Outdoor Climate Givers. In *SimAUD 2019*, April 07-09: Atlanta, Georgia.
- Nakamura, Y., & Oke, T. R. (1988). Wind, Temperature and Stability Conditions in an East-West Oriented Urban Canyon. *Atmospheric Environment*, 22(12), 2691-2700. doi: [https://doi.org/10.1016/0004-6981\(88\)90437-4](https://doi.org/10.1016/0004-6981(88)90437-4).

-
- Natanian, J., Aleksandrowicz, O., & Auer, T. (2019a). A parametric approach to optimizing urban form, energy balance and environmental quality: The case of Mediterranean districts. *Applied Energy*, 254, 113637. doi: <https://doi.org/10.1016/j.apenergy.2019.113637>.
- Natanian, J., Aleksandrowicz, O., & Auer, T. (2019b). A parametric approach to optimizing urban form, energy balance and environmental quality: The case of Mediterranean districts. *Applied Energy*, 254(113637), 1-17. doi: <https://doi.org/10.1016/j.apenergy.2019.113637>.
- Natanian, J., & Auer, T. (2020). Beyond nearly zero energy urban design: A holistic microclimatic energy and environmental quality evaluation workflow. *Sustainable Cities and Society*, 56(102094), 1-11. doi: <https://doi.org/10.1016/j.scs.2020.102094>.
- Natanian, J., De Luca, F., Wortmann, T., & Capeluto, G. (2021). The Solar Block Generator: an additive parametric method for solar driven urban block design. In *Journal of Physics: Conference Series*.
- Natanian, J., Kastner, P., Dogan, T., & Auer, T. (2020). From energy performative to livable Mediterranean cities: An annual outdoor thermal comfort and energy balance cross-climatic typological study. *Energy and Buildings*, 224(110283). doi: <https://doi.org/10.1016/j.enbuild.2020.110283>.
- Natanian, J., Maiullari, D., Yezioro, A., & Auer, T. (2019c). Synergetic urban microclimate and energy simulation parametric workflow. In *Journal of Physics: Conference Series*.
- Niachou, K., Hassid, S., Santamouris, M., & Livada, I. (2008). Experimental performance investigation of natural, mechanical and hybrid ventilation in urban environment. *Building and Environment*, 43(8), 1373-1382. doi: <https://doi.org/10.1016/j.buildenv.2007.01.046>.
- Niang, I., Ruppel, O. C., Abdrabo, M. A., Essel, C., Lennard, C., Padgham, J., Urquhart, P., & Descheemaeker, K. (2014). Africa.Climate Change 2014: Impacts, Adaptation, and Vulnerability. Part B: Regional Aspects. Contribution of Working Group II to the Fifth Assessment.
- Nikolopoulou, M., Baker, N., & Steemers, K. (2001). Thermal comfort in outdoor urban spaces: Understanding the Human parameter. *Solar Energy*, 70(3), 227-235. doi: [https://doi.org/10.1016/S0038-092X\(00\)00093-1](https://doi.org/10.1016/S0038-092X(00)00093-1).
- Nikolopoulou, M., & Steemers, K. (2003). Thermal comfort and psychological adaptation as a guide for designing urban spaces. *Energy and Buildings*, 35(1), 95-101. doi: [https://doi.org/10.1016/S0378-7788\(02\)00084-1](https://doi.org/10.1016/S0378-7788(02)00084-1).
- Nishi, Y., & Gagge, A. (1970). Direct evaluation of convective heat transfer coefficient by naphthalene sublimation. *Journal of applied physiology*, 29(6), 830-838. doi: <https://doi.org/10.1152/jappl.1970.29.6.830>.
- Nouri, A. S., Costa, J. P., & Matzarakis, A. (2017). Examining default urban-aspect-ratios and sky-view-factors to identify priorities for thermal-sensitive public space design in hot-summer Mediterranean climates: The Lisbon case. *Building and Environment*, 126, 442-456. doi: <https://doi.org/10.1016/j.buildenv.2017.10.027>.
- Nunez, M., & Oke, T. R. (1977). The Energy Balance of an Urban Canyon. *Journal of Applied Meteorology*, 16(1), 11-19.
- O'Malley, C., Piroozfar, P., Farr, E. R., & Pomponi, F. (2015). Urban Heat Island (UHI) mitigating strategies: A case-based comparative analysis. *Sustainable Cities and Society*, 19(2), 222-235. doi: <https://doi.org/10.1016/j.scs.2015.05.009>.
- Oke, T., Mills, G., Christen, A., & Voogt, J. (2017). *Urban Climates*. Cambridge Cambridge University Press.
- Oke, T. R. (1973). City size and the urban heat island. *Atmospheric Environment*, 7(8), 769-779. doi: [https://doi.org/10.1016/0004-6981\(73\)90140-6](https://doi.org/10.1016/0004-6981(73)90140-6).

- Oke, T. R. (1976). The distinction between canopy and boundary-layer heat islands. *Atmosphere* 14, 268-277. doi: <https://doi.org/10.1080/00046973.1976.9648422>.
- Oke, T. R. (1981). Canyon geometry and the nocturnal heat island: comparison of scale model and field observations. *Journal of Climatology*, 1(3), 237-254. doi: <https://doi.org/10.1002/joc.3370010304>.
- Oke, T. R. (1982). The energetic basis of the urban heat island. *Quarterly Journal of the Royal Meteorological Society*, 108(455), 1-24.
- Oke, T. R. (1987). Boundary layer climates. London: Methuen.
- Oke, T. R. (1988). Street Design and Urban Canopy Layer Climate. *Energy and Buildings*, 11(3), 103-113. doi: [https://doi.org/10.1016/0378-7788\(88\)90026-6](https://doi.org/10.1016/0378-7788(88)90026-6).
- Oke, T. R. (1995). The heat island of the urban boundary layer: characteristics, causes and effects. In *Wind climate in cities* (pp. 81-107). Berlin/Heidelberg, Germany: Springer.
- Oke, T. R. (2006). Initial guidance to obtain representative meteorological observations at urban sites. World Meteorological Organization: Geneva, Switzerland
- Okeil, A. (2010). A holistic approach to energy efficient building forms. *Energy and Buildings*, 42(9), 1437-1444. doi: <https://doi.org/10.1016/j.enbuild.2010.03.013>.
- Olgay, V. (1963). *Design with climate; bioclimatic approach and architectural regionalism* (1st ed.). Princeton, NJ: Princeton University Press.
- Oliveira, V. M. A. d. (2016). *Urban Morphology - An Introduction to the Study of the Physical Form of Cities*. Switzerland: Springer.
- Onset. (2021). HOB0 U30 Data Loggers. Retrieved from <http://www.onsetcomp.com/products/data-loggers/U30-data-loggers>
- Parsons, K. (2006). *Human thermal environments: the effects of hot, moderate, and cold environments on human health, comfort and performance*. London: Taylor & Francis.
- Pearlmutter, D., Berliner, P., & Shaviv, E. (2007). Urban climatology in arid regions: current research in the Negev desert. *International Journal of Climatology*, 27(14), 1875-1885. doi: <https://doi.org/10.1002/joc.1523>.
- Pearlmutter, D., Jiao, D., & Garb, Y. (2014). The relationship between bioclimatic thermal stress and subjective thermal sensation in pedestrian spaces. *International journal of biometeorology*, 58(10), 2111-2127. doi: <https://doi.org/10.1007/s00484-014-0812-x>.
- Perini, K., Chokhachian, A., Dong, S., & Auer, T. (2017). Modeling and simulating urban outdoor comfort: Coupling ENVI-Met and TRNSYS by grasshopper. *Energy and Buildings*, 152, 373-384. doi: <https://doi.org/10.1016/j.enbuild.2017.07.061>.
- Perini, K., & Magliocco, A. (2014). Effects of vegetation, urban density, building height, and atmospheric conditions on local temperatures and thermal comfort. *Urban Forestry & Urban Greening*, 13(3), 495-506. doi: <http://dx.doi.org/10.1016/j.ufug.2014.03.003>.
- Perry, C. (1929). The neighborhood unit. *The urban design reader*, 54-65.
- Potchter, O., Cohen, P., Lin, T.-P., & Matzarakis, A. (2018). Outdoor human thermal perception in various climates: A comprehensive review of approaches, methods and quantification. *Science of the total environment*, 631, 390-406. doi: <https://doi.org/10.1016/j.scitotenv.2018.02.276>.
- Qaid, A., Lamit, H. B., Ossen, D. R., & Rasidi, M. H. (2018). Effect of the position of the visible sky in determining the sky view factor on micrometeorological and human thermal comfort conditions in urban street canyons. *Theoretical and Applied Climatology*, 131(3), 1083-1100. doi: <https://doi.org/10.1007/s00704-016-2023-3>.

-
- Qaid, A., & Ossen, D. R. (2015). Effect of asymmetrical street aspect ratios on microclimates in hot, humid regions. *International journal of biometeorology*, 59(6), 657-677. doi: <https://doi.org/10.1007/s00484-014-0878-5>.
- Qin, Y. (2015). A review on the development of cool pavements to mitigate urban heat island effect. *Renewable and Sustainable Energy Reviews*, 52, 445-459. doi: <https://doi.org/10.1016/j.rser.2015.07.177>.
- Quan, S. J., Economou, A., Grasl, T., & Yang, P. P.-J. (2014). Computing energy performance of building density, shape and typology in urban context. *Energy Procedia*, 61, 1602-1605. doi: <http://doi.org/10.1016/j.egypro.2014.12.181>.
- Rahamimoff, A. (1984). Residential Cluster Based on Climate and Energy Considerations. *Energy and Buildings*, 7(2), 89 - 107. doi: [https://doi.org/10.1016/0378-7788\(84\)90032-X](https://doi.org/10.1016/0378-7788(84)90032-X).
- Rajagopalan, P., Lim, K. C., & Jamei, E. (2014). Urban heat island and wind flow characteristics of a tropical city. *Solar Energy*, 107, 159-170. doi: <http://dx.doi.org/10.1016/j.solener.2014.05.042>.
- Rakha, T., Zhand, P., & Reinhart, C. (2017). A Framework for Outdoor Mean Radiant Temperature Simulation: Towards Spatially Resolved Thermal Comfort Mapping in Urban Spaces. In *Proceedings of the 15th IBPSA Conference*.
- Ratti, C., Baker, N., & Steemers, K. (2005). Energy consumption and urban texture. *Energy and Buildings*, 37(7), 762-776. doi: <http://doi.org/10.1016/j.enbuild.2004.10.010>.
- Ratti, C., Di Sabatino, S., & Britter, R. (2006). Urban texture analysis with image processing techniques: winds and dispersion. *Theoretical and Applied Climatology*, 84(1), 77-90. doi: <https://doi.org/10.1007/s00704-005-0146-z>.
- Ratti, C., Raydan, D., & Steemers, K. (2003). Building form and environmental performance: archetypes, analysis and an arid climate. *Energy and Buildings*, 35(1), 49-59. doi: [https://doi.org/10.1016/S0378-7788\(02\)00079-8](https://doi.org/10.1016/S0378-7788(02)00079-8).
- Recast, E. (2010). Directive 2010/31/EU of the European Parliament and of the Council of 19 May 2010 on the energy performance of buildings (recast). *Official Journal of the European Union*, 18(06), 2010.
- Rijal, H. B., Ooka, R., Huang, H., Katsuki, T., & Oh, B. (2010). Study on heat island mitigation effect of large-scale greenery using numerical simulation. In *10th REHVA WORLD CONGRESS, Clima*.
- Robinson, D., Haldi, F., Leroux, P., Perez, D., Rasheed, A., & Wilke, U. (2009). CitySim: Comprehensive micro-simulation of resource flows for sustainable urban planning. In *Proceedings of the Eleventh International IBPSA Conference*.
- Robinson, D., & Stone, A. (2004, 19 - 22 September 2004). Irradiation modelling made simple: the cumulative sky approach and its applications. In *21st PLEA Conference*, Eindhoven, The Netherlands.
- Rode, P., Keim, C., Robazza, G., Viejo, P., & Schofield, J. (2014). Cities and energy: urban morphology and residential heat-energy demand. *Environment and Planning B: Planning and Design*, 41(1), 138-162. doi: <https://doi.org/10.1068/b39065>.
- Rodler, A., Lauzet, N., Musy, M., Azam, M.-H., Guernouti, S., Mauree, D., & Colinart, T. (2021). Urban Microclimate and Building Energy Simulation Coupling Techniques. In M. Palme & A. Salvati (Eds.), *Urban Microclimate Modelling for Comfort and Energy Studies*. Glasgow, UK: Springer Nature Switzerland AG.

- Rodríguez-Álvarez, J. (2016). Urban Energy Index for Buildings (UEIB): A new method to evaluate the effect of urban form on buildings' energy demand. *Landscape and Urban Planning*, 148(2016), 170-187. doi: <http://dx.doi.org/10.1016/j.landurbplan.2016.01.001>.
- Rojas-Fernández, J., Galán-Marín, C., Roa-Fernández, J., & Rivera-Gómez, C. (2017). Correlations between GIS-based urban building densification analysis and climate guidelines for Mediterranean courtyards. *Sustainability*, 9(12), 2255. doi: <https://doi.org/10.3390/su9122255>.
- Roudsari, M., Mackey, C., & Armour, T. (2022). Ladybug-Tools forum. Retrieved from <https://discourse.ladybug.tools/>
- Roudsari, M. S., & Mackey, C. (2022). Ladybug-tools. Retrieved from <https://www.ladybug.tools/>
- Roudsari, M. S., Pak, M., & Smith, A. (2013). Ladybug: a parametric environmental plugin for grasshopper to help designers create an environmentally-conscious design. In *Proceedings of the 13th international IBPSA conference*, Lyon, France, 25-30 August.
- Ruefenacht, L., Sukma, A., Acero, J. A., & Nevat, I. (2020). Climate-responsive design guidelines: Urban design guidelines to improve outdoor thermal comfort in the southern shore area of singapore.
- Rutheiser, C. (1997). Beyond the radiant garden city beautiful: Notes on the New Urbanism. *City & Society*, 9(1), 117-133. doi: <https://doi.org/10.1525/ciso.1997.9.1.117>.
- Rutten, D. (2021). Grasshopper3D. Retrieved from <https://www.grasshopper3d.com/>
- Salvati, A., Coch, H., & Morganti, M. (2017). Effects of urban compactness on the building energy performance in Mediterranean climate. *Energy Procedia*, 122, 499-504. doi: <https://doi.org/10.1016/j.egypro.2017.07.303>.
- Salvati, A., Monti, P., Roura, H. C., & Cecere, C. (2019). Climatic performance of urban textures: Analysis tools for a Mediterranean urban context. *Energy and Buildings*, 185, 162-179. doi: <https://doi.org/10.1016/j.enbuild.2018.12.024>.
- Santamouris, M. (2013). Using cool pavements as a mitigation strategy to fight urban heat island—A review of the actual developments. *Renewable and Sustainable Energy Reviews*, 26, 224-240. doi: <https://doi.org/10.1016/j.rser.2013.05.047>.
- Santamouris, M., Gaitani, N., Spanou, A., Saliari, M., Giannopoulou, K., Vasilakopoulou, K., & Kardomateas, T. (2012). Using cool paving materials to improve microclimate of urban areas—Design realization and results of the flisvos project. *Building and Environment*, 53, 128-136. doi: <https://doi.org/10.1016/j.buildenv.2012.01.022>.
- Santamouris, M., Papanikolaou, N., Koronakis, I., Livada, I., & Asimakopoulos, D. (1999). Thermal and air flow characteristics in a deep pedestrian canyon under hot weather conditions. *Atmospheric Environment*, 33, 4503-4521. doi: [https://doi.org/10.1016/S1352-2310\(99\)00187-9](https://doi.org/10.1016/S1352-2310(99)00187-9).
- Seto, K. C., Dhakal, S., Bigio, A., Blanco, H., Delgado, G. C., Dewar, D., Huang, L., Inaba, A., Kansal, A., & Lwasa, S. (2014). Human settlements, infrastructure and spatial planning. In *Climate Change 2014: Mitigation of Climate Change. Contribution of Working Group III to the Fifth Assessment Report of the Intergovernmental Panel on Climate Change*; Cambridge University Press: Cambridge, UK, 2014.
- Shahidan, M. F. (2015). Potential of Individual and Cluster Tree Cooling Effect Performances through Tree Canopy Density Model Evaluation in Improving Urban Microclimate. *Current World Environment*, 10(2), 398.
- Shalaby, A. S., & Shafey, A. M. (2018). Optimizing the Thermal Performance of Street Canyons in New Cairo, Egypt, Using ENVI-met. 5(4), 5639-5654.

-
- Sharifi, A. (2016). From Garden City to Eco-urbanism: The quest for sustainable neighborhood development. *Sustainable Cities and Society*, 20, 1-16. doi: <https://doi.org/10.1016/j.scs.2015.09.002>.
- Sharmin, T., Steemers, K., & Matzarakis, A. (2017). Microclimatic modelling in assessing the impact of urban geometry on urban thermal environment. *Sustainable Cities and Society*, 34, 293-308. doi: <http://dx.doi.org/10.1016/j.scs.2017.07.006>.
- Shashua-Bar, L., & Hoffman, M. E. (2000). Vegetation as a climatic component in the design of an urban street: An empirical model for predicting the cooling effect of urban green areas with trees. *Energy and Buildings*, 31(3), 221-235. doi: [https://doi.org/10.1016/S0378-7788\(99\)00018-3](https://doi.org/10.1016/S0378-7788(99)00018-3).
- Shashua-Bar, L., & Hoffman, M. E. (2004). Quantitative evaluation of passive cooling of the UCL microclimate in hot regions in summer, case study: urban streets and courtyards with trees. *Building and Environment*, 39(9), 1087 - 1099. doi: <https://doi.org/10.1016/j.buildenv.2003.11.007>.
- Shi, Z., Fonseca, J. A., & Schlueter, A. (2021). A parametric method using vernacular urban block typologies for investigating interactions between solar energy use and urban design. *Renewable energy*, 165, 823-841. doi: <https://doi.org/10.1016/j.renene.2020.10.067>.
- Shi, Z., & Zhang, X. (2011). Analyzing the effect of the longwave emissivity and solar reflectance of building envelopes on energy-saving in buildings in various climates. *Solar Energy*, 85(1), 28-37. doi: <https://doi.org/10.1016/j.solener.2010.11.009>.
- Silver, C. (2006). New Urbanism and Planning History: Back to the Future. *Culture, urbanism and planning*, 179-193.
- Sini, J.-F., Anquetin, S., & Mestayer, P. G. (1996). Pollutant dispersion and thermal effects in urban street canyons. *Atmospheric Environment*, 30(15), 2659-2677. doi: [https://doi.org/10.1016/1352-2310\(95\)00321-5](https://doi.org/10.1016/1352-2310(95)00321-5).
- Soflaei, F., Shokouhian, M., Abraveshdar, H., & Alipour, A. (2017). The impact of courtyard design variants on shading performance in hot-arid climates of Iran. *Energy and Buildings*, 143, 71-83. doi: <http://dx.doi.org/10.1016/j.enbuild.2017.03.027>.
- Staiger, H., Laschewski, G., & Grätz, A. (2012). The perceived temperature—a versatile index for the assessment of the human thermal environment. Part A: scientific basics. *International journal of biometeorology*, 56(1), 165-176. doi: <https://doi.org/10.1007/s00484-011-0409-6>.
- Stanescu, M., Kajl, S., & Lamarche, L. (2012). Evolutionary algorithm with three different permutation options used for preliminary HVAC system design. In *Proceedings of the building simulation and optimization conference*.
- Steemers, K., Baker, N., Crowther, D., Dubiel, J., & Nikolopoulou, M. (1998). Radiation absorption and urban texture. *Building Research & Information*, 26(2), 103-112. doi: <https://doi.org/10.1080/096132198370029>.
- Stewart, I. D., & Oke, T. R. (2012). Local climate zones for urban temperature studies. *Bulletin of the American Meteorological Society*, 93(12), 1879-1900. doi: <https://doi.org/10.1175/BAMS-D-11-00019.1>.
- Sundborg, A. (1951). Climatological studies in Uppsala: With special regard to the temperature conditions in the urban area. *Geographica*, 22.
- Sutton, K., & Fahmi, W. (2001). Cairo's urban growth and strategic master plans in the light of Egypt's 1996 population census results. *Cities*, 18(3), 135-149. doi: [https://doi.org/10.1016/S0264-2751\(01\)00006-3](https://doi.org/10.1016/S0264-2751(01)00006-3).

- Szokolay, S. V. (2008). Introduction to architectural science: the basis of sustainable design. Oxford: Architectural Press.
- Tablada, A., De Troyer, F., Blocken, B., Carmeliet, J., & Verschure, H. (2009). On natural ventilation and thermal comfort in compact urban environments—the Old Havana case. *Building and Environment*, 44(9), 1943-1958. doi: <https://doi.org/10.1016/j.buildenv.2009.01.008>.
- Taleghani, M., Kleerekoper, L., Tenpierik, M., & Van Den Dobbelsteen, A. (2015). Outdoor thermal comfort within five different urban forms in the Netherlands. *Building and Environment*, 83, 65-78. doi: <http://dx.doi.org/10.1016/j.buildenv.2014.03.014>.
- Taleghani, M., Tenpierik, M., & van den Dobbelsteen, A. (2014a). Indoor thermal comfort in urban courtyard block dwellings in the Netherlands. *Building and Environment*, 82, 566-579. doi: <http://dx.doi.org/10.1016/j.buildenv.2014.09.028>.
- Taleghani, M., Tenpierik, M., Van Den Dobbelsteen, A., & De Dear, R. (2013). Energy use impact of and thermal comfort in different urban block types in the Netherlands. *Energy and Buildings*, 67, 166-175. doi: <http://dx.doi.org/10.1016/j.enbuild.2013.08.024>.
- Taleghani, M., Tenpierik, M., van den Dobbelsteen, A., & Sailor, D. J. (2014b). Heat in courtyards: A validated and calibrated parametric study of heat mitigation strategies for urban courtyards in the Netherlands. *Solar Energy*, 103, 108-124. doi: <http://dx.doi.org/10.1016/j.solener.2014.01.033>.
- Tereci, A., Ozkan, S. T. E., & Eicker, U. (2013). Energy benchmarking for residential buildings. *Energy and Buildings*, 60, 92-99. doi: <http://dx.doi.org/10.1016/j.enbuild.2012.12.004>.
- Thanh Hoan, N., Liou, Y.-A., Nguyen, K.-A., Sharma, R., Tran, D.-P., Liou, C.-L., & Cham, D. (2018). Assessing the effects of land-use types in surface urban heat islands for developing comfortable living in Hanoi City. *Remote Sensing*, 10(12), 1965. doi: <https://doi.org/10.3390/rs10121965>.
- Theeuwes, N., Steeneveld, G., Ronda, R., Heusinkveld, B., Van Hove, L., & Holtslag, A. (2014). Seasonal dependence of the urban heat island on the street canyon aspect ratio. *Quarterly Journal of the Royal Meteorological Society*, 140(684), 2197-2210. doi: <https://doi.org/10.1002/qj.2289>.
- Thermal Energy System Specialists, TESS. (2021). TRNSYS-Transient System Simulation Tool. Retrieved from <http://www.trnsys.com/>
- Thorsson, S., Lindberg, F., Eliasson, I., & Holmer, B. (2007). Different methods for estimating the mean radiant temperature in an outdoor urban setting. *International Journal of Climatology: A Journal of the Royal Meteorological Society*, 27(14), 1983-1993. doi: <http://dx.doi.org/10.1002/joc.1537>.
- Tomasetti, T. (2020). Core Studio. Retrieved from <http://core.thorntontomasetti.com/>
- Tong, Z., Baldauf, R. W., Isakov, V., Deshmukh, P., & Zhang, K. M. (2016). Roadside vegetation barrier designs to mitigate near-road air pollution impacts. *Science of the total environment*, 541, 920-927. doi: <https://doi.org/10.1016/j.scitotenv.2015.09.067>.
- Toparlar, Y., Blocken, B., Vos, P. v., Van Heijst, G., Janssen, W., van Hooff, T., Montazeri, H., & Timmermans, H. (2015). CFD simulation and validation of urban microclimate: A case study for Bergpolder Zuid, Rotterdam. *Building and Environment*, 83, 79-90. doi: <http://dx.doi.org/10.1016/j.buildenv.2014.08.004>.
- Tsilini, V., Papantoniou, S., Kolokotsa, D.-D., & Maria, E.-A. (2015). Urban gardens as a solution to energy poverty and urban heat island. *Sustainable Cities and Society*, 14, 323-333. doi: <https://doi.org/10.1016/j.scs.2014.08.006>.
- Tuhus-Dubrow, D., & Krarti, M. (2009). Comparative analysis of optimization approaches to design building envelope for residential buildings. *ASHRAE Transactions*, 115(2), 554-563.
- UN, United Nations. (2021). UN Climate Change Conference. Retrieved from <https://ukcop26.org/>

-
- UNCED, U. N. C. o. E. a. D. (1992). Agenda 21. Rio De Janerio
- Underwood, C., & Ward, E. (1966). The solar radiation area of man. *Ergonomics*, 9(2), 155-168. doi: <https://doi.org/10.1080/00140136608964361>.
- United Nations, Department of Economic and Social Affairs Population Division. (2018). World Urbanization Prospects: The 2018 Revision. New York: United Nations
- United Nations, D. o. E. a. S. A., Population Division. (2019). World Population Prospects 2019: Highlights. New York: United Nations
- USEPA. (2020). U.S Environmental Protection Agency (EPA). Retrieved from <https://www.epa.gov>
- Vallati, A., Grignaffini, S., Romagna, M., Mauri, L., & Colucci, C. (2016). Influence of street Canyon's microclimate on the energy demand for space cooling and heating of buildings. *Energy Procedia*, 101, 941-947. doi: <http://doi.org/10.1016/j.egypro.2016.11.119>.
- Vartholomaios, A. (2015). The residential solar block envelope: A method for enabling the development of compact urban blocks with high passive solar potential. *Energy and Buildings*, 99, 303-312. doi: <https://www.doi.org/10.1016/j.enbuild.2015.04.046>.
- Vartholomaios, A. (2017). A parametric sensitivity analysis of the influence of urban form on domestic energy consumption for heating and cooling in a Mediterranean city. *Sustainable Cities and Society*, 28, 135-145. doi: <http://dx.doi.org/10.1016/j.scs.2016.09.006>.
- Vernon, H., & Warner, C. (1932). The influence of the humidity of the air on capacity for work at high temperatures. *Epidemiology & Infection*, 32(3), 431-462. doi: <https://doi.org/10.1017/S0022172400018167>.
- Vierlinger, R. (2015). Multi Objective Design Interface. (Masters). Technischen Universität Wien, Vienna.
- Vierlinger, R. (2021). Octopus - Multi-Objective Evolutionary Optimizer. Retrieved from <https://www.food4rhino.com/en/app/octopus>
- Wagdy, A., Sherif, A., Sabry, H., Arafa, R., & Mashaly, I. (2017). Daylighting simulation for the configuration of external sun-breakers on south oriented windows of hospital patient rooms under a clear desert sky. *Solar Energy*, 149, 164-175. doi: <http://dx.doi.org/10.1016/j.solener.2017.04.009>.
- Watkins, R., Palmer, J., & Kolokotroni, M. (2007). Increased temperature and intensification of the urban heat island: implications for human comfort and urban design. *Built Environment*, 33(1), 85-96. doi: <https://doi.org/10.2148/benv.33.1.85>.
- WCED, United Nations World Commission on Environment and Development. (1987). Our common future. Oxford
- Wei, R., Song, D., Wong, N. H., & Martin, M. (2016). Impact of urban morphology parameters on microclimate. *Procedia Engineering*, 169, 142-149. doi: <http://doi.org/10.1016/j.proeng.2016.10.017>.
- Wheeler, S. (2004). Planning for Sustainability: Toward Livable, Equitable, and Ecological Communities. London and New York: Routledge.
- Williams, K., Burton, E., & Jenks, M. (2000). Achieving sustainable urban form. London: Taylor & Francis.
- Witte, M. J., Henninger, R. H., Glazer, J., & Crawley, D. B. Testing and validation of a new building energy simulation program. In *7th IBSPA Conference*.
- Wortmann, T., & Natanian, J. (2020). Multi-objective Optimization for Zero-Energy Urban Design in China: A Benchmark. In *SimAUD2020*.
- Wortmann, T., & Natanian, J. (2021). Optimizing solar access and density in Tel Aviv: Benchmarking multi-objective optimization algorithms. In *Journal of Physics: Conference Series*.

- Xu, X., Wu, Y., Wang, W., Hong, T., & Xu, N. (2019). Performance-driven optimization of urban open space configuration in the cold-winter and hot-summer region of China. In *Building Simulation*.
- Xu, Y., Ren, C., Ma, P., Ho, J., Wang, W., Lau, K. K.-L., Lin, H., & Ng, E. (2017). Urban morphology detection and computation for urban climate research. *Landscape and Urban Planning*, 167, 212-224. doi: <http://dx.doi.org/10.1016/j.landurbplan.2017.06.018>.
- Yaşa, E., & Ok, V. (2014). Evaluation of the effects of courtyard building shapes on solar heat gains and energy efficiency according to different climatic regions. *Energy and Buildings*, 73, 192-199. doi: <http://dx.doi.org/10.1016/j.enbuild.2013.12.042>.
- Yezioro, A., Capeluto, I. G., & Shaviv, E. (2006). Design guidelines for appropriate insolation of urban squares. *Renewable energy*, 31(7), 1011-1023. doi: <https://www.doi.org/10.1016/j.renene.2005.05.015>.
- Yow, D. M. (2007). Urban heat islands: observations, impacts, and adaptation. *Geography Compass*, 1(6), 1227-1251. doi: <https://doi.org/10.1111/j.1749-8198.2007.00063.x>.
- Zaitchik, B., Macalady, A., Bonneau, L., & Smith, R. (2006). Europe's 2003 heat wave: A satellite view of impacts and land-atmosphere feedbacks. *International Journal of Climatology*, 26(6), 743-769. doi: <https://doi.org/10.1002/joc.1280>.
- Zamani, Z., Heidari, S., & Hanachi, P. (2018). Reviewing the thermal and microclimatic function of courtyards. *Renewable and Sustainable Energy Reviews*, 93, 580-595. doi: <https://doi.org/10.1016/j.rser.2018.05.055>.
- Zhan, W., Ju, W., Hai, S., Ferguson, G., Quan, J., Tang, C., Guo, Z., & Kong, F. (2014). Satellite-derived subsurface urban heat island. *Environmental science & technology*, 48(20), 12134-12140. doi: <https://doi.org/10.1021/es5021185>.
- Zhang, J., Xu, L., Shabunko, V., Tay, S. E. R., Sun, H., Lau, S. S. Y., & Reindl, T. (2019). Impact of urban block typology on building solar potential and energy use efficiency in tropical high-density city. *Applied Energy*, 240, 513-533. doi: <https://doi.org/10.1016/j.apenergy.2019.02.033>.
- Zhao, C., Jensen, J., Weng, Q., & Weaver, R. (2018). A Geographically Weighted Regression Analysis of the Underlying Factors Related to the Surface Urban Heat Island Phenomenon. *Remote Sensing*, 10(9), 1428. doi: <https://doi.org/10.3390/rs10091428>.
- Zhao, J., & Du, Y. (2020). Multi-objective optimization design for windows and shading configuration considering energy consumption and thermal comfort: A case study for office building in different climatic regions of China. *Solar Energy*, 206, 997-1017. doi: <https://doi.org/10.1016/j.solener.2020.05.090>.
- Zhu, K., Bayer, P., Grathwohl, P., & Blum, P. (2015). Groundwater temperature evolution in the subsurface urban heat island of Cologne, Germany. *Hydrological processes*, 29(6), 965-978. doi: <http://doi.org/10.1002/hyp.10209>.
- Zitzler, E., Laumanns, M., & Thiele, L. (2001). SPEA2: Improving the strength Pareto evolutionary algorithm. *TIK-report*, 103. doi: <https://doi.org/10.3929/ethz-a-004284029>.